

Development of Peptide-Modified Gemini Nanoplexes for Gene Delivery to the Retina

by

Lokesh Narsineni

A thesis

presented to the University of Waterloo

in fulfillment of the

thesis requirement for the degree of

Doctor of Philosophy

in

Pharmacy

Waterloo, Ontario, Canada, 2020

©Lokesh Narsineni 2020

Examining Committee Membership

The following served on the Examining Committee for this thesis. The decision of the Examining Committee is by majority vote.

External Examiner	Dr. Adriana Di Polo Professor, Department of Neuroscience, University of Montreal Hospital Research Center (CRCHUM)
Supervisor	Dr. Marianna Foldvari Professor, School of Pharmacy and Waterloo Institute for Nanotechnology, University of Waterloo
Internal Member	Dr. Praveen P Nekkar Rao Associate Professor, School of Pharmacy University of Waterloo
Internal Member	Dr. Jeremy Sivak Associate Professor, Department of Laboratory Medicine and Pathobiology, University of Toronto Glaucoma Research Chair, Krembil Research Institute, University Health Network, Toronto
Internal-External Member	Dr. Juewen Liu Professor, Department of Chemistry University of Waterloo

Author's Declaration

I hereby declare that I am the sole author of this thesis. This is a true copy of the thesis, including any required final revisions, as accepted by my examiners.

I understand that my thesis may be made electronically available to the public.

Abstract

Glaucoma is a retinal neurodegenerative disease where the retinal ganglion cells (RGCs) suffer from damage and die over time due to multiple factors, including a persistently elevated intraocular pressure (IOP). Glaucoma is a leading cause of blindness worldwide, but with protective new treatments significant progress could be made to prevent and regenerate vision loss in patients. Current glaucoma management relies on reducing and maintaining IOP by pharmacological and invasive surgical treatments. Neuroprotective approaches have the potential to prevent RGC damage and could be essential to preserve vision in patients over time. Neurotrophic factors and other neuroprotective compounds have been shown to be useful, however, efficient and reliable delivery of these agents to the retina is still a major obstacle. One of the neurotrophic factors (NTFs), brain-derived neurotrophic factor (BDNF) has been shown to protect RGCs, but in glaucoma there is a local deficiency due to decreased retinal levels of both local and retrogradely transported NTFs.

Gene therapy with BDNF-encoding gene could be a suitable approach to locally express BDNF in the retina long-term. We designed multifunctional non-viral peptide-targeted gemini surfactant-based gene delivery systems to deliver BDNF-encoding plasmid to retinal cells *in vitro* and *in vivo*. **The main objective** was to develop a new generation of nanoplex (NPX) system based on cell adhesion peptide (CAP)-modified dicationic gemini surfactants (m-s(p)-m) ($m=C_{18}$) for targeted delivery of BDNF gene to the retina.

First, a new synthesis method was developed for second generation m-7NH-m ($m=C_{12}$ and C_{18}) gemini surfactants which were then used as building blocks for conjugation of selected CAPs at the amino group in the spacer. The modified synthesis protocol was developed with a solvent-free, 4-Dimethylaminopyridine (DMAP)-free, one-pot synthetic scheme to synthesize m-7NH-m gemini surfactants with Boc_2O protection, quaternization with 1-bromoalkanes and deprotection with

trifluoroacetic acid cocktail to improve the purity of the m-7NH-m gemini surfactant. The new synthesis method provides a two-fold improved yield and the production of a pure species of m-7NH-m without DMAP and trimeric m-7N(m)-m surfactants as impurities. Also, for the first time, a one-pot method for the synthesis of trimeric gemini surfactants (bis-quaternary trimeric (m-7N(m)-m) (m=16 and 18)) was developed.

Second, using m-7NH-m gemini surfactants as building blocks two integrin-binding (p₁₋₂) and three immunoglobulin superfamily (IgSF)-peptide (p₃₋₅) modified m-sN(p₁₋₅)-m gemini surfactants (m-alkyl tail [12-18C], s-spacer 7C with amino-peptide substitution) were synthesized and purified. Nanoplexes (NPXs), lipoplexes (LPXs), peptide-modified nanoplexes (pNPXs) and peptide-modified lipoplexes (pLPXs) of dimeric, trimeric second generation gemini surfactants and peptide-conjugated m-7N(p₁₋₅)-m third generation gemini surfactants with gWIZ-GFP plasmid were formulated and optimized with and without 1,2-dioleoyl-sn-glycero-3-phosphatidylethanolamine (DOPE) helper lipid, respectively, at various charge ratios and characterized for particle size, zeta potential, transfection efficiency and toxicity in A7 astrocytes using flow cytometry and confocal microscopy.

Third, the NPXs and LPXs were evaluated both *in vitro* and *in vivo*: for corneal interactions in MatTek EpiCorneal[®] tissue equivalent model, for transfection efficiency in a 3D environment using MiEye8 retinal neurospheres, and for delivery and transfection ability *in vivo*. In the *in vivo* CD1 mouse model 18-7N(p₃)-18 pNPXs administered by IVT injection delivered tdTomato/BDNF plasmid to retinal cells and produced higher gene expression than the 18-7N(p₁)-18 pNPXs, the parent 18-7NH-18 NPXs and Lipofectamine[®] 3000 as demonstrated by confocal microscopy of whole mount retinas. The BDNF gene expression, assessed by ELISA, showed significantly high levels of BDNF with 18-7N(p₃)-18 (422.60 ± 42.60pg/eye), followed by 18-7N(p₁)-18 pNPXs (230.62 ± 24.47pg/eye), 18-7NH-18 NPXs (245.90 ± 39.72pg/eye), Lipofectamine[®] 3000 (199.99 ± 29.90 pg/eye) and untreated controls (131.33

± 20.30 pg/eye). In summary, the 18-7N(p₃)-18 pNPXs induced 3.4-fold higher BDNF level compared to controls and 2-fold higher than 18-7N(p₁)-18 pNPXs.

Fourth, it was shown that A β colocalizes in the apoptotic RGCs in experimental glaucoma models and induces RGC apoptosis, targeting the A β pathway has resulted in reduction of RGC apoptosis and helped in the protection of RGCs from degeneration, previously it was reported that amphiphilic gemini surfactants have potential to inhibit A β aggregation. Hence, some complementary exploratory studies were carried out on the amyloid A β ₄₀ aggregation inhibition properties of some of the new peptide-gemini surfactants by a fluorescence kinetic assay and on the binding affinities of CAP-gemini surfactants by molecular modelling. *In vitro* A β ₄₀ peptide aggregation inhibition studies showed that 18-7N(p₃)-18 and 18-7N(p₁)-18 gemini surfactants have the potential to inhibit A β ₄₀ peptide aggregation and formation of higher order oligomers.

In conclusion, the novel multifunctional IgSF peptide and integrin-binding peptide conjugated gemini NPXs provide a promising non-viral *in vivo* gene delivery approach to retinal cells. The pNPXs with CAPs from the neural IgSF represent a novel approach to non-viral gene delivery to the retina. The IgSF peptides are known to elicit a cell adhesion and binding interaction between the neural IgCAMs and have potential to engage in homophilic and heterophilic interaction with other cell surface proteins. This property of IgSF CAPs was exploited to improve the adhesion and delivery of pNPXs to the retinal cells by conjugating them on to gemini surfactant gene vectors. The conjugation of peptides to the 18-7NH-18 gemini surfactant and the pNPXs prepared from the IgSF peptide-modified gemini surfactants have enhanced transfection efficiency with low toxicity.

Acknowledgements

It has been my life's biggest achievement and privilege working with few of the brightest minds and experts in the field of formulation science, chemistry and vision science for the past 6 years of my PhD program here at University of Waterloo. First, I would like to sincerely thank Prof. Marianna Foldvari for trusting, bringing me to Canada by offering a PhD position and providing me an unconditional support throughout my program, I will be grateful all my life for this opportunity provided. You have never failed to inspire and ignite my mind to think in a new direction in approaching a problem and solving the roadblocks in my research. Your passion and dedication for research is an inspiration to the younger generation. You will always remain as my role-model in improving the quality of life of the people through my research. I would also like to take this opportunity to thank Dr. Praveen P Nekkar Rao and Dr. Jeremy Sivak for their unmatched support as committee members and more as mentors throughout the program. Dr. Praveen, thank you for always keeping your doors open for me and for answering all the countless questions that I have asked, the support provided by you is matchless, you have essentially been my chemistry encyclopedia. I have gained a lot of knowledge talking to you and your humble nature inspires me to treat people with kindness. Dr. Jeremy Sivak, you are another super kind soul that I have in my committee, even though I don't see you often at school of Pharmacy, you have been an exceptional committee member and guided me in the right direction with my research whenever possible. Your valuable feedback and comments throughout my progress has helped me to direct myself towards proper planning of the experiments. Your guidance is invaluable and highly appreciated. I had chance to make some great lifetime friends, Dr. Ding-wen (Roger) Chen and Ms. Daniella Calderon who are more than just colleagues and provided me a greater amount of support emotionally and motivated me throughout the program, Roger, you are one of the best peer someone can have with immeasurable wisdom, thank you for being there whenever I needed support. To other

friends, colleagues and staff at school of pharmacy with special thanks to Dr. Deep Patel, Amy Pham, Amna-El-Shatshat, Arash Shakeri, Dr. Anil Maharaj, Dr. Gokul Raj Pullagura, Monica Hoang, Samantha Shortall, Paul Malik, Cindy Hoi Ting Yeung, Josephine Orso Simon and Dr. Monica Tudorancea for your friendship and invaluable guidance. I would also like to take this opportunity to say thank you and can't express how grateful I am, for the patience, support and love shown on me, by my family. Specially my parents, brother and grandmother who have loved and supported me unconditionally.

Dedication

*“To my family **Babu Naidu Narsineni, Vanaja Narsineni and Sahithya Narsineni** to honor the countless sacrifices made in their life, so, I could have a better tomorrow.”*

“To the people and the nation of Canada for their love and unconditional support over the duration of my PhD studies”

Table of Contents

Examining Committee Membership	ii
Author's Declaration	iii
Abstract.....	iv
Acknowledgements	vii
Dedication	ix
List of Figures.....	xvi
List of Tables	xix
List of Schemes	xxi
List of Abbreviations	xxii
Chapter 1 Introduction.....	1
1.1 Ocular anatomy, barriers, routes of delivery and treatments in glaucoma therapy	1
<i>1.1.1 Ocular barriers to treatments targeting the posterior segment</i>	<i>1</i>
<i>1.1.2 Routes of delivery to posterior segment of eye.....</i>	<i>6</i>
1.2 Glaucoma	11
<i>1.2.1 Pathophysiology and epidemiology of glaucoma</i>	<i>11</i>
<i>1.2.2 Neurotrophic factors and their role in glaucoma and optic nerve degeneration</i>	<i>14</i>
<i>1.2.3 Role of other retinal cells in neurotrophic support for the retina.....</i>	<i>16</i>
<i>1.2.4 Advances in ocular drug and gene delivery: from simple IOP lowering therapies to neuroprotective and regenerative therapies in glaucoma treatment</i>	<i>18</i>

1.3 Gene therapy: potential applications in the treatment of retinal neurodegenerative conditions	25
1.4 Non-viral gene therapy: materials, properties and NP systems	28
1.5 Lipid based nanomaterials in gene delivery	30
1.6 Surfactant based gene delivery.....	32
<i>1.6.1 Gemini Surfactants</i>	<i>33</i>
<i>1.6.2 Evolution of gemini surfactants</i>	<i>33</i>
<i>1.6.3 Classification and properties of amphiphilic gemini surfactants</i>	<i>34</i>
<i>1.6.4 CMC and surface-active properties</i>	<i>37</i>
<i>1.6.5 Effect of spacer, amino substitution and alkyl tail length on transfection properties of gemini surfactants</i>	<i>37</i>
<i>1.6.6 Self-assembly of gemini surfactants</i>	<i>39</i>
1.7 Multi-functionalization: An approach to build intelligent non-viral gene delivery systems	40
1.8 Mechanism of cellular interaction, uptake and processing of non-viral gene delivery systems.....	41
1.9 Peptide mediated ocular therapeutic cargo delivery	46
1.10 Cell adhesion molecules	51
<i>1.10.1 Integrins and integrin binding moieties in retinal gene delivery</i>	<i>51</i>
<i>1.10.2 IgSF CAMs and their role in the eye</i>	<i>52</i>
Chapter 2 Research Emphasis	54
2.1 Rationale.....	54
2.2 Hypothesis	55

2.2.1 Main hypothesis	55
2.2.2 Sub hypothesis.....	55
Chapter 3 Improved synthesis and formulation design of dimeric and trimeric gemini surfactants and their evaluation as gene delivery vectors	57
3.1 Background	57
3.1.1 Traditional methods of gemini synthesis and advantages of the one-pot reaction method.	58
3.1.2 DMAP-free, solvent-free technique for Boc-protection of NH group in m-7NH-m gemini surfactant synthesis	60
3.1.3 Effect of DOPE on nanoparticle formulations and non-viral gene delivery systems	60
3.2 Rationale and objective	61
3.3 Materials and Methods.....	62
3.3.1 Synthesis of m-7NH-m dimeric gemini surfactants by one-pot, DMAP- free technique	62
3.3.2 Synthesis of m-7N(m)-m trimeric gemini surfactants using one-pot method	65
3.3.3 Formulation of m-7NH-m and m-7N(m)-m gemini NPXs and LPXs	65
3.3.4 Characterization of gemini surfactants and nanoparticle systems	68
3.3.5 Transfection efficiency and viability studies by flow cytometry.....	70
3.3.6 Kinetics of gene expression in A7 astrocytes treated with NPXs.....	71
3.3.7 Assessment of helper lipid DOPE as a formulation component by flow cytometric and confocal microscopy	71
3.3.8 In vitro corneal penetration studies using the 3D EpiCorneal™ model	72
3.3.9 Cy5 labelling of pDNA for 3D EpiCorneal™ penetration studies.....	73
3.3.10 Statistical analysis.....	74
3.4 Results	75

3.4.1 Synthesis of dimeric and trimeric gemini surfactants.....	75
3.4.2 Physicochemical characterization of dimeric and trimeric gemini surfactant NPXs (<i>m</i> -7NH- <i>m</i> and <i>m</i> -7N(<i>m</i>)- <i>m</i>).....	78
3.4.3 <i>In vitro</i> studies of interaction of 18-7NH-18 and 16-7N(16)-16 NPXs with EpiCorneal tissue.....	95
3.5 Discussion.....	99
3.6 Conclusion.....	107
Chapter 4 Development of multifunctional gemini nanoplexes for non-viral neurotrophic factor gene delivery to the retina.....	108
4.1 Introduction.....	108
4.1.1 Functionalization of gemini surfactants with integrin-binding and IgSF cell adhesion peptides (CAPs).....	108
4.2 Rationale and Objective.....	110
4.2.1 Rationale.....	110
4.2.2 Objective.....	110
4.3 Materials and Methods.....	111
4.3.1 Synthesis, purification and characterization of peptide-modified <i>m</i> -7N(<i>p</i>)- <i>m</i> gemini surfactants.....	113
4.3.2 Formulation and characterization of <i>m</i> -7N(<i>p</i> ₁₋₅)- <i>m</i> (<i>m</i> =12 and 18) gemini surfactant pNPXs and pLPXs.....	115
4.3.3 Characterization of pNPXs and pLPXs.....	116
4.3.4 <i>In vitro</i> transfection efficiency and toxicity studies of pNPXs and pLPXs in A7 astrocytes.....	117

4.3.5 <i>In vitro</i> corneal penetration and toxicity studies using a 3D EpiCorneal tissue model ...	118
4.3.6 <i>In vitro</i> transfection studies in retinal stem cell-derived neurospheres	119
4.3.7 <i>In vivo</i> retinal gene transfer studies in a CD1 mice.....	121
4.3.8 BDNF expression in eyes treated with pNPXs in CD1 mice.....	123
4.4 Results	124
4.4.1 Synthesis, purification and characterization of peptide-modified di-cationic <i>m</i> -7N(<i>Pn</i>)- <i>m</i> gemini surfactants	124
4.4.2 Formulation and characterization of <i>m</i> -7N(<i>p</i> ₁₋₃)- <i>m</i> (<i>m</i> =12 and 18) gemini surfactant pNPXs and pLPXs.....	128
4.4.3 <i>In vitro</i> assessment of transfection efficiency and toxicity of pNPXs in A7 astrocytes using flow cytometry.....	132
4.4.4 <i>In vitro</i> EpiCorneal tissue penetration studies for NPXs and pNPXs.....	137
4.4.5 Transfection studies in 3D retinal neurospheres	142
4.4.6 Gene delivery to the retina <i>in vivo</i> in a CD1 mouse model.....	146
4.4.7 BDNF gene expression in the retina <i>in vivo</i> in mice treated with integrin and IgSF binding peptide modified gemini surfactant pNPXs.....	151
4.5 Discussion.....	152
4.6 Conclusion	158
Chapter 5 Investigation of amphiphilic gemini surfactants and peptide-modified gemini surfactants as potential Amyloid-β₁₋₄₀ self-aggregation inhibitors	160
5.1 Introduction.....	160
5.2 Amyloid-β hypothesis- A pathophysiology of glaucoma and IOP associated with Alzheimer’s disease.....	160

5.2.1 Amyloid- β implications in glaucoma and RGC neurodegeneration.....	161
5.2.2 Amyloid- β peptide: Structural characteristics.....	163
5.2.3 Amphiphilic surfactants in amyloid- β aggregation inhibition.....	165
5.3 Rationale and Objective.....	166
5.4 Materials and methods.....	167
5.4.1 $A\beta$ -aggregation inhibition studies	167
5.4.2 Molecular docking studies -binding interactions assessment of amphiphilic gemini surfactants, integrin, IgSF-peptides and peptide-modified gemini surfactants with $A\beta_{40}$ peptide	168
5.5 Results.....	169
5.5.1 $A\beta_{40}$ -aggregation inhibition studies.....	169
5.5.2 Molecular docking studies.....	175
5.6 Discussion	189
5.7 Conclusion.....	192
5.8 Acknowledgments.....	193
Chapter 6 Summary and future directions	195
6.1 Summary	195
6.2 Future directions	196
Letter of copyright permission	198
References	199
Appendices	219

List of Figures

Figure 1-1 Barriers, penetration pathways and target locations for gene therapy in the eye	10
Figure 1-2 Mediators of RGC apoptosis and NTF deprivation.....	14
Figure 1-3 Routes of administration for retinal delivery, retinal cross section showing various layers and cell types in the retina that are targets for gene delivery.....	18
Figure 1-4 Schematic examples of non-viral gene delivery systems made of lipid, surfactant and polymeric systems.....	32
Figure 1-5 General schematic structures of gemini surfactants	37
Figure 1-6 Schematic of self-assembly in gemini surfactants into higher order aggregates.....	40
Figure 1-7 Classification and mechanisms of cellular uptake process.....	42
Figure 1-8 Structure of some immunoglobulin superfamily CAMs	53
Figure 3-1 DOPE vesicles processing and nanoparticle assembly.....	67
Figure 3-2 General formulation steps and schematic models of compacted NPXs/pNPXs and LPXs/pLPXs.	68
Figure 3-3 MatTek Human EpiCorneal tissue model (COR-100)	73
Figure 3-4 Illustration of nanoparticle penetration studies in the 3D-EpiCorneal™ tissue model	74
Figure 3-5 ¹ H NMR spectrum of 18-7NH-18 gemini surfactant.....	77
Figure 3-6 Surface tension vs log concentration plot for 18-7NH-18 gemini surfactant.....	78
Figure 3-7 Physicochemical characterization of dimeric gemini surfactant NPXs and LPXs.....	79
Figure 3-8 Assessment of TE and viability on A7 astrocytes treated with 18-7NH-18 (OS) and 18-7NH-18 (NS).....	82
Figure 3-9 Particle size distribution (A) and zeta potential data (B) of 18-7N(18)-18 gemini NPXs.	84
Figure 3-10 Assessment of TE of 18-7N(18)-18 and 16-7N(16)-16 NPXs in A7 astrocytes.	85

Figure 3-11 Kinetics of gene expression and optimization of TE	88
Figure 3-12 Assessment of DOPE concentration in LPXs on TE	90
Figure 3-13 Confocal microscopic study of maximum gene expression time point assessment and DOPE inclusion effects on TE and viability	94
Figure 3-14 <i>In Vitro</i> 3D-EpiCorneal model penetration studies.....	97
Figure 3-15 <i>In Vitro</i> 3D-EpiCorneal model penetration studies for 16-7N(16)-16 NPXs- 0.5 and 1 hour	99
Figure 3-16 General schematic structures of bis- and tris-quaternary trimeric gemini surfactants...	101
Figure 4-1 Schematic for evaluation of the TE and toxicity of pNPXs and pLPXs in 3D retinal stem cell derived neurospheres	121
Figure 4-2 Physicochemical properties of 18-7NH-18 NPXs and LPXs and 18-7N(p ₁₋₅)-18 pNPXs and pLPXs.....	132
Figure 4-3 TE and toxicity of pNPXs and their physical mixtures in A7 astrocytes by flow cytometry	135
Figure 4-4 Confocal microscopic images of NPX interactions with 3D EpiCorneal tissue model ...	141
Figure 4-5 Transfection of MiEye8 3D retinal neurospheres with pNPXs.	145
Figure 4-6 Confocal microscopic images of whole mount retinas from CD1 mice treated with 18-7N(p)-18 pNPXs. Whole mount images of retina treated with 18-7N(p ₃)-18 5:1 pNPXs	149
Figure 4-7 Quantitative assessment of gene expression by cMFI analysis	150
Figure 4-8 BDNF gene expression in the eye in vivo after treatment with peptide-conjugated pNPXs	151
Figure 5-1 Schematic implications of amyloid-beta accumulation in retina on glaucoma and neurodegeneration	162

Figure 5-2 Hypothetical schematic of tau protein accumulation implications in retinal neurodegeneration.....	164
Figure 5-3 A β_{40} -peptide showing the hydrophobic regions	165
Figure 5-4 A β_{40} aggregation inhibition studies of peptide controls.....	172
Figure 5-5 A β_{40} aggregation inhibition studies of treatment groups.....	174
Figure 5-6 Molecular docking studies of 18-7NH-18 with 2LMN using CDOCKER algorithm.....	176
Figure 5-7 Molecular docking studies of 18-7N(p ₁)-18 with 2LMN using CDOCKER algorithm..	179
Figure 5-8 Molecular docking studies of 18-7N(p ₂)-18 with 2LMN using CDOCKER algorithm..	181
Figure 5-9 Molecular docking studies of 18-7N(p ₃)-18 with 2LMN using CDOCKER algorithm..	184
Figure 5-10 Molecular docking studies of 18-7N(p ₄)-18 with 2LMN using CDOCKER algorithm	187
Figure 5-11 Comparative graph of (-) CDOCKER energy and (-) CDOCKER interaction energy of peptides and peptide modified gemini surfactants with A β_{40} peptide	188

List of Tables

Table 1-1 Physicochemical properties of various barriers in eye	3
Table 1-2 Current and prospective treatments in glaucoma	21
Table 1-3 List of retinal gene therapies currently approved and in clinical trials	26
Table 1-4 Foldvari Lab classification of gemini surfactants and various gemini surfactants used in gene delivery.....	35
Table 3-1 ¹ H NMR analysis of 18-7NH-18 (NS) gemini surfactant.....	76
Table 4-1 Integrin-binding and neural IgSF-derived peptides used for gemini NP design	109
Table 4-2 Peptides used in the peptide-modified dicationic gemini surfactant synthesis and their properties.....	112
Table 4-3 Peptide-modified gemini conjugates produced using the HATU/DIPEA reaction scheme	126
Table 4-4 Particle size (Z-average diameter), PDI and zeta (ζ) potential data for pNPXs (5:1 P:G ratio) and pLPXs (5:1:0.5 P:G:L ratio)	130
Table 5-1 Top hits and non-bonding interactions from molecular docking studies of 18-7NH-18 gemini surfactant with 2LMN	175
Table 5-2 Top hit and non-bonding interactions from molecular docking studies of 18-7N(p ₁)-18 gemini surfactant with 2LMN	177
Table 5-3 Top hits of 18-7N(p ₂)-18, p ₂ peptide and non-bonding interactions of 18-7N(p ₂)-18 with 2LMN	180
Table 5-4 Top hits of 18-7N(p ₃)-18, p ₃ peptide and non-bonding interactions of 18-7N(p ₃)-18 with 2LMN	183

Table 5-5 Top hits of 18-7N(p₄)-18, p₄ peptide and non-bonding interactions of 18-7N(p₄)-18 with 2LMN..... 185

List of Schemes

Scheme 1 General and improved schemes for synthesis of m-7NH-m dimeric gemini surfactant.....	64
Scheme 2 General scheme for synthesis of m-7N(m)-m trimeric gemini surfactant.....	65
Scheme 3 General scheme for synthesis of integrin-binding and IgSF peptide functionalized m-7N(p ₁ - s)-m gemini surfactant	115
Scheme 4 Schematic of HATU/DIPEA mechanism to form amide bond	125

List of Abbreviations

Abbreviations

¹ H NMR: Proton Nuclear Magnetic Resonance Spectroscopy	61
AAV: Adeno-Associated Virus	26
AMD: Age-Related Macular Degeneration	6
ANOVA: Analysis of Variance	74
A β : Amyloid- β	160
BDNF: Brain Derived Neurotrophic Factor.....	1
bFGF: Basic-Fibroblast Growth Factor	119
Boc ₂ O: di-(terbutyl) decarbonate	60
CAM: Cell Adhesion Molecule	7
CAP: Cell Adhesion Peptide.....	55
CMC: Critical Micelle Concentration.....	33
CME: Clathrin Mediated Endocytosis	43
CNS: Central Nervous System.....	11
CNTF: Ciliary Neurotrophic Factor.....	14
CNV: Choroidal Neovascularization	52
CTP: Cell Targeting Peptide.....	49
DIPEA: <i>N,N</i> -diisopropylethylamine	124
DLS: Dynamic Light Scattering	68
DMEM: Dulbecco's Modified Eagle's Medium.....	70
DNA: Deoxyribonucleic Acid	25
DOPE: 1,2-dioleyl-sn-glycero-3-phosphoethanolamine.....	30

DOTMA: <i>N</i> -[1-(2, 3-dioleyloxy) propyl]- <i>N,N,N</i> -trimethylammoniumchloride	30
ECM: Extra Cellular Matrix	51
EGF: Epidermal Growth Factor	52
ELISA: Enzyme-Linked Immunosorbent Assay	111
ESI-MS: Electro Spray Ionization- Mass Spectrometry.....	68
FBS: Fetal Bovine Serum.....	70
FDA: Food and Drug Administration.....	26
GAGs: Glycosaminoglycans	4
GCL: Ganglion Cell Layer	18
GFAP: Glial Fibrillary Acidic Protein	12
GFP: Green Fluorescent Protein.....	28
GPL: Gemini-Plasmid-Lipid	39
GS: Gemini Surfactant	33
HATU: 1-[Bis(dimethylamino)methylene]-1 <i>H</i> -1,2,3-triazolo[4,5- <i>b</i>]pyridinium-3-oxid hexafluorophosphate	112
HFIP: Hexafluoroisopropanol	167
INL: Inner Nuclear Layer.....	18
IOP: Intraocular Pressure	11
IPL: Inner Plexiform Layer	18
LPXs: Lipoplexes	30
MRSC: Multipotent Retinal Stem Cell.....	119
NFL: Nerve Fiber Layer.....	11
NP-1: Neuropilin-1	242
NPs: Nanoparticles	1

NPX: Nanoplex.....	33
NTF: Neurotrophic Factor	1
ONH: Optic Nerve Head.....	15
PAMAM: Polyamidoamine	29
PBS: Phosphate Buffer Saline	120
pDNA: Plasmid DNA	45
PDT: Photo Dynamic Therapy.....	16
PEG: Poly Ethylene Glycol	29
PEI: Polyethylenimine	29
PLGA: Poly (D,L-lactide-co-glycolide)	29
pLPXs: Peptide-Modified Lipoplexes	v
pNPXs: Peptide-Modified Nanoplexes.....	v
RBPMS: RNA-Binding Protein with Multiple Splicing.....	120
RFU: Relative Fluorescence Units.....	168
RGC: Retinal Ganglion Cells.....	6
RGD: Arginine-Glycine-Aspartic acid	7
RPE: Retinal Pigment Epithelium.....	6
RSCM-1: Retinal Stem Cell Media 1	119
RSCM-2: Retinal Stem Cell Media 2	119
RSCM-3: Retinal Stem Cell Media 3	119
SC: Superior Colliculus	13
siRNA: Small Interfering Ribonucleic Acid.....	27
TE: Transfection Efficiency.....	31
TEM: Transmission Electron Microscopy.....	197

TFA: Trifluoroacetic Acid.....	47
ThT: Thioflavin T.....	165
TM: Trabecular Meshwork.....	2
Trf: Transferrin.....	7
TrKB: Tropomyosin Receptor Kinase B.....	15
ULA: Ultra-Low Attachment	119

Chapter 1 Introduction

The primary goal of drug delivery research is to preserve or improve health by developing new treatment modalities by designing effective delivery systems for both old and new therapeutic agents. This is achieved either by targeting or circumventing various barriers that act as hindrance through physical and chemical modifications for safer and more effective delivery of therapeutic agents to the designated target. Our current research also focuses on a similar long-standing problem in ophthalmology for the treatment of glaucoma by developing a non-viral gene delivery system. The design and development of these systems especially become more complicated when considering the *in vivo* structural and physicochemical barriers faced by the gene medicine intended to reach the posterior segment of eye, that is the location of neurodegenerative processes. Work carried out and embodied in this thesis focuses on the development of a non-viral system for neurotrophic factor (more specifically brain derived neurotrophic factor (BDNF)) (NTF) gene therapy to the back-of-eye. The thesis presents the design, formulation and evaluation of peptide-targeted gemini nanoparticles (NPs) as gene delivery systems to the retina.

1.1 Ocular anatomy, barriers, routes of delivery and treatments in glaucoma therapy

1.1.1 Ocular barriers to treatments targeting the posterior segment

The cornea and conjunctiva represent the outermost layers of the eye. Both structures are covered by an approximately 10- μ m-thick film of tear fluid, that is produced by the lachrymal gland. Tear fluid is the first barrier encountered when a formulation is administered into the eye as a topical formulation. This film consists of an outer lipid layer (mostly sterol esters, phospholipids, triglycerides, free fatty acids and free sterols), an aqueous layer (salts, glucose, urea, and various proteins), and an inner mucus layer (mostly mucin [MUC1], a high-molecular-weight transmembrane glycoprotein), and it provides a barrier between the air and the hydrophilic surface of the cornea. Some of the physicochemical

properties of various barriers are shown in Table 1-1. The osmolality (310-350 mOsm/kg), surface tension (44 mN/m), pH (7.4), rheological behavior (non-Newtonian), polarity (negatively charged) and anti-adhesive properties (caused by glycosyl and sialic acid moieties on MUC1; pKa=2.6) of the tear film have been established in detail (1). The tear film is produced by the nasolacrimal drainage system, which has multiple functions, including the lubrication and protection of the eye, as well as the clearance of foreign bodies that enter the eye. This latter function constitutes the second major barrier affecting drug and macromolecule delivery into the eye. In humans, the normal tear production rate is 0.5–2.2 $\mu\text{L}/\text{min}$. This rate increases to approximately 300 $\mu\text{L}/\text{min}$ upon mechanical or chemical irritation, including drug administration, resulting in the removal of most foreign materials (2, 3). The dose volume, pH, electrolyte concentration, lipid and surfactant composition of a drug molecule may affect tear stability and result in adverse reactions. Altering the pH from physiological levels (e.g., from 6.5 to 7.6) (4) stimulates the production of excess tear fluid, which may cause drainage of ocular therapeutics via the trabecular meshwork (TM), resulting in the elimination of these therapeutics from the ocular cavity. Indeed, lacrimation and tear drainage limit the delivery of therapeutic molecules to the intraocular layers, to the extent where less than 3% of administered dose may pass into these layers. Furthermore, interactions between biomolecules and tear proteins also reduce the effective concentrations of therapeutics delivered to the eye (5).

Table 1-1 Physicochemical properties of various barriers in eye

Barriers	Properties	
Tear film	Thickness	<ul style="list-style-type: none"> Thickness between 7.0-7.5 μm (6)
	Outer lipid layer (Hydrophobic)	<ul style="list-style-type: none"> Sterol esters, phospholipids, triglycerides, free fatty acids and free sterols
	Aqueous layer (Hydrophilic)	<ul style="list-style-type: none"> Salts, glucose, urea and various proteins (7)
	Mucus layer	<ul style="list-style-type: none"> Mucin (MUC1), acts as barrier between air and hydrophilic surface of cornea (7, 8)
	pH	<ul style="list-style-type: none"> 7.4
	Osmolality	<ul style="list-style-type: none"> 310-350 mOsm/kg
	Surface tension	<ul style="list-style-type: none"> 44 mN/m
	Charge	<ul style="list-style-type: none"> Negatively charged
	Anti-adhesive	<ul style="list-style-type: none"> Glycosyl and sialic acid moieties on MUC 1 provide anti-adhesive property of tear film
	Tear volume	<ul style="list-style-type: none"> 0.5-2.2 $\mu\text{L}/\text{min}$ increases to 300 $\mu\text{L}/\text{min}$ after mechanical or chemical irritation which is a major barrier for delivery of therapeutics (2, 3)
Cornea	Thickness	<ul style="list-style-type: none"> 500-700μm (9)
	Surface area	<ul style="list-style-type: none"> 1.04 cm^2
	Charge	<ul style="list-style-type: none"> Negatively charged
	Epithelium	
	Thickness	<ul style="list-style-type: none"> 50 μm (6)
	Lipophilicity/Composition	<ul style="list-style-type: none"> Lipophilic, Tight junction cells 5-6 cell layers, Bowman's layer 15 μm below the epithelium.
	Stroma	<ul style="list-style-type: none"> Cornea is composed of 85% stroma, mostly made of water other connective tissue such as fibroblasts and collagen are present. Despite of its hydrophilic nature

		this layer does not act as a barrier for lipophilic compounds.
	Endothelium	
	Thickness	<ul style="list-style-type: none"> • 15 μm (10)
	Nature	<ul style="list-style-type: none"> • Lipophilic, hexagonal arrangement of cells.
Vitreous	pH	<ul style="list-style-type: none"> • 7.0-7.4
	Nature	<ul style="list-style-type: none"> • Composed of 80% water, glycosaminoglycans (GAGs), proteoglycans, hyaluronan and chondroitin sulfate. Acts as a potential barrier for cationic systems, can precipitate nucleic acids due to charge interactions. (11, 12) •
Conjunctiva	Thickness	<ul style="list-style-type: none"> • $240.1 \pm 29.8 \mu\text{m}$ (13)
	Nature	<ul style="list-style-type: none"> • Composed of mucus cells, tight junction cells are present beneath the apical cells, vascularized.
	Lipophilicity	<ul style="list-style-type: none"> • Hydrophilic; helps in permeation of hydrophilic moieties and large molecules (14). Drug delivery through conjunctival-sclera is a potential pathway that can be explored for delivery of large molecules (15).
Sclera	Thickness	<ul style="list-style-type: none"> • 550-850 μm
	Nature	<ul style="list-style-type: none"> • Composed of tight junction cells, connected by fibrin, elastin and collagen which act as a barrier for movement of ocular therapeutics.
	Charge	<ul style="list-style-type: none"> • Negatively charged (due to scleral proteoglycans), molecules possessing negative charge are highly permeable compared to cationic compounds due to reduced interactions with scleral proteoglycans (16).

Choroid	Thickness	<ul style="list-style-type: none"> • 100-200 μm
	Nature	<ul style="list-style-type: none"> • Fenestrated epithelium allows small molecules to pass. • Sclera and choroid are effective barriers to lipophilic delivery systems, which tend to be transported through non-corneal routes (17). • A thin, pigmented, vascular network that supplies blood to outer layers of the retina and RPE. • Also contains other cells such as melanocytes, fibroblasts and smooth muscles (18).
	Lipophilicity	<ul style="list-style-type: none"> • Hydrophilic • Conjunctiva-sclera-choroid is a potential permeation pathway for ocular therapeutics.
Retina	Thickness	<ul style="list-style-type: none"> • 150 μm (19)
	Nature	<ul style="list-style-type: none"> • Non-fenestrated RPE, acts as blood-retinal barrier. A layer composed of RGCs, Müller cells, astrocytes, glial cells, photoreceptor cells and oligodendrocytes.
	Lipophilicity	<ul style="list-style-type: none"> • Lipophilic, mostly allows highly lipophilic molecules to pass through the blood retinal barrier, large molecules cannot permeate through this barrier (20, 21).

Other relevant structural elements worth mentioning are that the cornea is continuous with the sclera, whereas the iris is continuous with the choroid at the posterior segment, and the innermost layer at the back of the eye is termed the retina. Suspensory ligaments in the iris hold the lens in a position that helps it to adjust to incoming light. The sclera, composed of tight junction-connected cellular barriers, contains a fiber matrix composed of elastin and collagen that acts as a potential barrier to the penetration of therapeutics. In addition, the transport of a compound across the sclera is dependent on the compound's molecular weight and charge. Molecules with negatively charged surfaces are more

capable of permeating these membranes than those with positively charged surfaces due to their reduced interactions with negatively charged scleral proteoglycans (16).

The retina is a complex, multi-layered tissue that comprises retinal ganglion cells (RGCs), glial cells, astrocytes, oligodendrocytes, Muller cells and photoreceptor cells. The mean thickness of the retina is approximately 150 μm as determined by optical coherence tomography or 107 μm as determined by retinal thickness analyzer measurements (19). It includes a non-fenestrated retinal pigment epithelium (RPE), which restricts the movement of therapeutic molecules (20, 21). The RPE also acts as a blood-retinal barrier by preventing systemically administered drugs from reaching retina by inhibiting blood flow into the retinal segment (22). Unlike the RPE, the choroid epithelium is fenestrated, allowing the passage of small molecules (23, 24).

1.1.2 Routes of delivery to posterior segment of eye

Administration into the eye includes topical, intravitreal, subconjunctival, subretinal and periocular delivery routes. Topical application is frequently used for front-of-the eye delivery, while injectable methods are necessary to reach the retina. Intravitreal administration provides a depot effect and sustained drug levels within ocular tissues (25), but it is not without risks. For example, the current method used for administering LUCENTIS[®] (ranibizumab injection) for neovascular (wet) age-related macular degeneration (AMD) involves a monthly intravitreal injection through the sclera into the vitreous using a 30G needle under local anesthesia following pretreatment with a broad-spectrum microbicide. Complications may include endophthalmitis, rhegmatogenous retinal detachment and iatrogenic traumatic cataracts. Other methods for delivering drugs to the back of the eye include systemic, subconjunctival, subretinal and periocular injections. Subconjunctival delivery has gained prominence in recent years due to higher permeability compared to the sclera after injection irrespective of the lipophilicity of the drug molecules (26). Also, this route allows subsequent passage of large

molecules through the sclera, which, unlike cornea, stands as a tough barrier to molecules with low lipophilicity and high molecular weight. Transscleral delivery of Immunoglobulin Cell Adhesion Molecule-1 (Ig CAM-1) through the sclera into choroid and retina was achieved by an implanted osmotic pump of an infusion kit with the tip placed to face the sclera. High levels of Ig complex found in the choroid and retina indicate that scleral delivery of large molecules is possible and may be explained by the low number of cells in sclera which provide high surface area (16.3 cm²) for permeation of larger molecules (27).

Periocular routes, such as sub-tenon and retrobulbar, could serve as alternative administration routes for bioactives to the deeper layers of the eye. Sub-tenon injections are given into tenon's capsule, whereas retrobulbar injections are administered into the rectus muscle and intermuscular septa. The latter can cause serious traumatic injuries to the optic nerve and is therefore the least preferred route of delivery for ocular bioactives.

Following intravenous delivery, drug levels in ocular tissues may reach therapeutic concentrations due to vascular perfusion. For example, intravenous delivery of anti-VEGF antibodies functionalized with transferrin (Trf) and arginine-glycine-aspartic acid (RGD) peptides enables these antibodies to reach RPE photoreceptors and endothelial cells, facilitating their delivery to the back of the eye and thereby aiding their targeting of choroidal neovascularization lesions . However, this type of intravenous delivery strategy increases the likelihood of systemic adverse reactions, due to the large doses that need to be delivered to attain therapeutic concentrations in the posterior segment of the eye. Blood perfusion into RPE cells and choroidal tissues also facilitates the delivery of bioactives to the posterior segment of the eye, and their delivery appears to be enhanced when bioactives are functionalized with peptides and targeting moieties (28). Sub-retinal route of delivery has gained more prominence in recent years with the approval of Luxturna[®] (voretigene neparvovec-rzyl), injected by subretinal route to treat retinal dystrophy characterized by the genetic mutation in the alleles of RPE65 leading to rod mediated retinal

dystrophies. The sub-retinal injection is performed by adapting all vitreoretinal techniques and successful gene transfer was achieved with this route of delivery as shown by the expression and visual field improvement in the human subjects (29). Despite the chances of complications related to endophthalmitis, cataract and retinal detachment this injection method is preferred in order to achieve therapeutic levels in the posterior segment of the eye.

Topically applied drugs can reach the retina through several possible penetration pathways, including via conjunctiva-sclera-choroid-RPE, cornea-posterior chamber-vitreous-retina and conjunctiva-orbital-optic nerve head routes (30)

The potential penetration pathways and barriers encountered along the way in the eye were also postulated for topically applied therapeutic formulations (Figure 1-1). For example, one pathway to the posterior chamber is through the complex 5-layered cornea of approximately 500–700 μm thickness (31). In general, drugs and delivery systems that include cationic components bind to the negatively charged membranes of corneal cells, and provide increased residence time and sustained drug release within the precorneal chamber (32-36). Tight junctions prevent the passive movement of hydrophilic and ionized compounds, whereas the diffusion of highly lipophilic compounds through the stroma, which accounts for 85% of total corneal thickness, is relatively uninhibited (37). The outermost epithelium is approximately 50 μm thick (6, 38), while the Bowman's layer, just beneath the epithelium, measures 15 μm and helps maintain the position of the endothelium. The internal membrane lining the cornea, also about 15 μm thick, is composed of hexagonal cells arranged in an ordered matrix (10). Despite being safe and well tolerated, the topical delivery route still faces many challenges related to drug bioavailability and residence time. The development of a satisfactory delivery method to the retina is important because newer strategies involve both promoting health of RGCs and providing neuroregenerative treatments for the optic nerve. Some drugs may penetrate through the vitreous, a large structural bulb filled with a jelly-like substance that is 80% water and includes a matrix of collagen

fibers and glycosaminoglycans, such as hyaluronan, proteoglycans, heparin and chondroitin sulfate, poses a significant barrier for ocular gene delivery. The GAGs present in the vitreous restrict the movement of cationic molecules and NPs, often preventing them from reaching the retinal layers by forming complexes with them (39).

Another potential permeation pathway is through the conjunctiva composed of mainly mucus cells. Drugs can be transported through the conjunctival layers by passage through the sclera and ciliary body into either the anterior chamber or the retinal segments of the eye (15). Hydrophilic molecules are transported through the conjunctiva to a greater extent compared to the cornea or sclera.

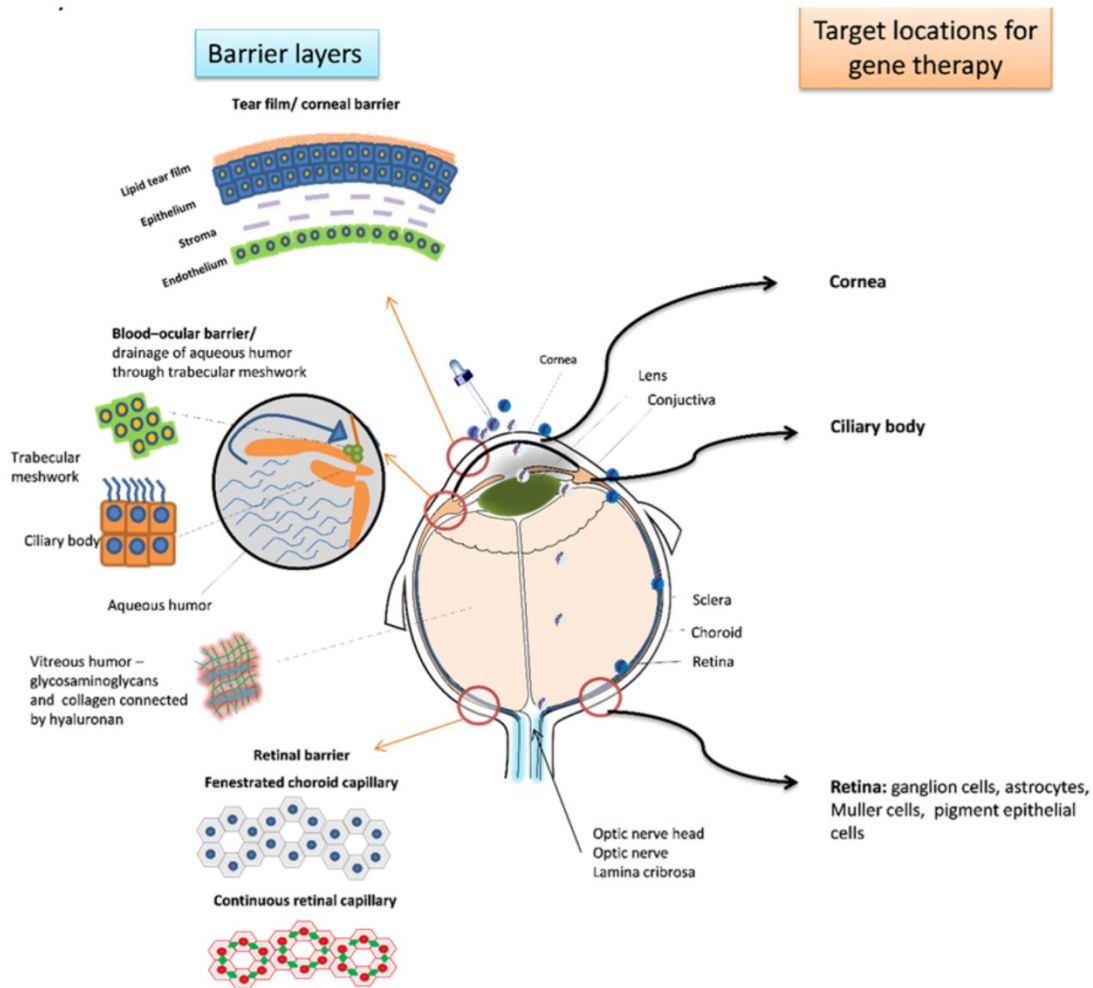


Figure 1-1 Barriers, penetration pathways and target locations for gene therapy in the eye, figure reprinted with permission from Foldvari et al. (Journal of Controlled Release (240), 165-190 (2016) (40)

1.2 Glaucoma

1.2.1 Pathophysiology and epidemiology of glaucoma

Glaucoma is characterized by progressive visual impairment, caused by the death of RGCs and degeneration of the optic nerve as a result of elevated intraocular pressure (IOP). Glaucoma is one of the most common causes of blindness in the world with figures reaching over 80 million people (41, 42), including 400,000 Canadians, affected by this disease. Patients lose their peripheral vision first followed by eventual complete loss of vision. High IOP does not produce any symptoms at the initial stages and patient can recognize the disorder only when they experience vision loss. Hence, it is difficult to identify it at earlier stages (43).

Regular IOP checkups can help in identifying the onset of this condition. Primary open angle glaucoma (POAG) and angle closure glaucoma are the two main glaucoma conditions. While the majority of the cases reported are of POAG, but both types of glaucoma cause potential loss of RGCs that help in transmitting visual signals to the central nervous system (CNS) by a bundle of axons joining to form optic nerve. In POAG the aqueous humor has free access to TM and Schlemm's canal. In secondary angle glaucoma there is an increased resistance to the outflow through the TM and Schlemm's canal due to conditions, such as exfoliative glaucoma and pigmentary glaucoma. In angle closure glaucoma the iris sticks to the cornea and is in contact with the TM, where the peripheral iris blocks the movement of aqueous humor movement from the peripheral chamber to anterior chamber thereby actively preventing its drainage through the TM (42).

Glaucoma is a result of multiple triggers, predispositions and activation of various inflammatory cascades. Characteristic signs include optic nerve head compression and cupping due to loss of the retinal nerve fiber layer (NFL) and ganglion cells contained in these fibers (44). Persistently elevated level of IOP is the major contributor to glaucoma progression, leading to substantial damage to the

optic nerve at the lamina cribrosa, that prevents the anterograde and retrograde transport of nutrition and NTFs causing the death of RGCs (42, 45). Molecular and cellular mechanisms of this specific death pattern are poorly understood. Obstruction of the TM that helps in regular outflow of aqueous humor from the anterior chamber, causes a raise in IOP above normal levels i.e. 10-21 mm Hg. This increased pressure is directly felt by the optic disc cupping or the optic nerve head at lamina cribrosa causing compression of optic nerve head and blocking the transport in either direction causing local ischemia leading to death of RGCs (46, 47). On the other hand, Howell et al. (2007) demonstrated that rodents lacking the collagenous plate in the lamina are also susceptible to glaucoma (48). The combination of increased IOP and mechanical stress on optic nerve head stimulates the production of tumor necrosis factor (TNF- α) and nitric oxide causing damage to the optic nerve (49). The deprivation of NTFs and nutritional supply to the cells trigger genes that regulate apoptosis due to metabolic stress and cause the death of cells in the optic nerve head (50). Reduced blood and nutrition supply also stimulate inflammatory and immune conditions that increase the presence of reactive astrocytes and increased glial fibrillary acidic protein (GFAP). The inflammatory process (51) and the reduced vascular access leads to hypoxic injuries in the retinal cells that trigger the activation of multiple cascades of inflammation leading to repair and apoptotic mechanisms. Some additional complex pathways that are involved in the glaucoma progression include astrogliosis, microglial activation, NTF deprivation, reactive oxygen species generation and mitochondrial dysfunction (52, 53). Astrocytes along with Müller glial cells help in supporting the functions of the RGCs and maintain homeostasis in the retinal cell layers. The trigger to form reactive astrocytes happens when there is an increased strain in the sclera, that surrounds the ONH. Reactive astrocytes are also involved in altering the ONH environment when activated by inflammatory mediators, they change the homeostasis in the ONH leading to axonal degeneration (54). Similarly, microglial activation was identified as another major trigger for degeneration of RGCs in a glaucomatous retina. When microglia are activated, they turn from quiescent

microglia to activated enlarged microglia which spread into the LC blood vessels, ONH and into the scleral interface (52, 55). NTF deprivation is another factor that triggers neurodegeneration by activating apoptotic pathways. NTFs normally promote the survival of the neurons by inhibiting the apoptotic pathways. Despite the local production of NTFs, it is equally important to have access to the distally produced NTFs from superior colliculus (SC). The local production helps in the temporary survival during deficits but cannot maintain long term survival. NTFs produced distally at SC are needed for maintaining health of RGC neurons in the retina (53, 56). Mitochondrial dysfunction is another pathway for neurodegeneration. The release of TNF- α induces mitochondrial dysfunction leading to the activation of the pathways and to apoptosis and cell death. The dysfunction also leads to excess production of reactive oxygen species that can trigger other inflammatory cascades and cell death. Factors such as aging, oxidative stress and genetic predisposition were considered as the promoters of mitochondrial dysfunction (57). Almasieh et al. (2012) and Alqawlaq et al. (2018) have extensively reviewed some contributing factors and pathways as discussed earlier in this section that were involved in the neurodegeneration in glaucoma. Summary of the mechanical triggers and common inflammatory cascades involved in RGC degeneration are shown in Figure 1-2 . It was also found that dendrites and synaptic terminals are the first to undergo degeneration before the reduction of the RGCs from the glaucomatous damage. (58). This stimulates a chain of manifestations in the extracellular matrix by forming a glial scar in the CNS or at damaged area making them unable to regenerate (59, 60). Nevertheless, the pathophysiology of neurodegeneration is still a widely debated topic and many groups are still working on elucidating the pathways of neural cell death

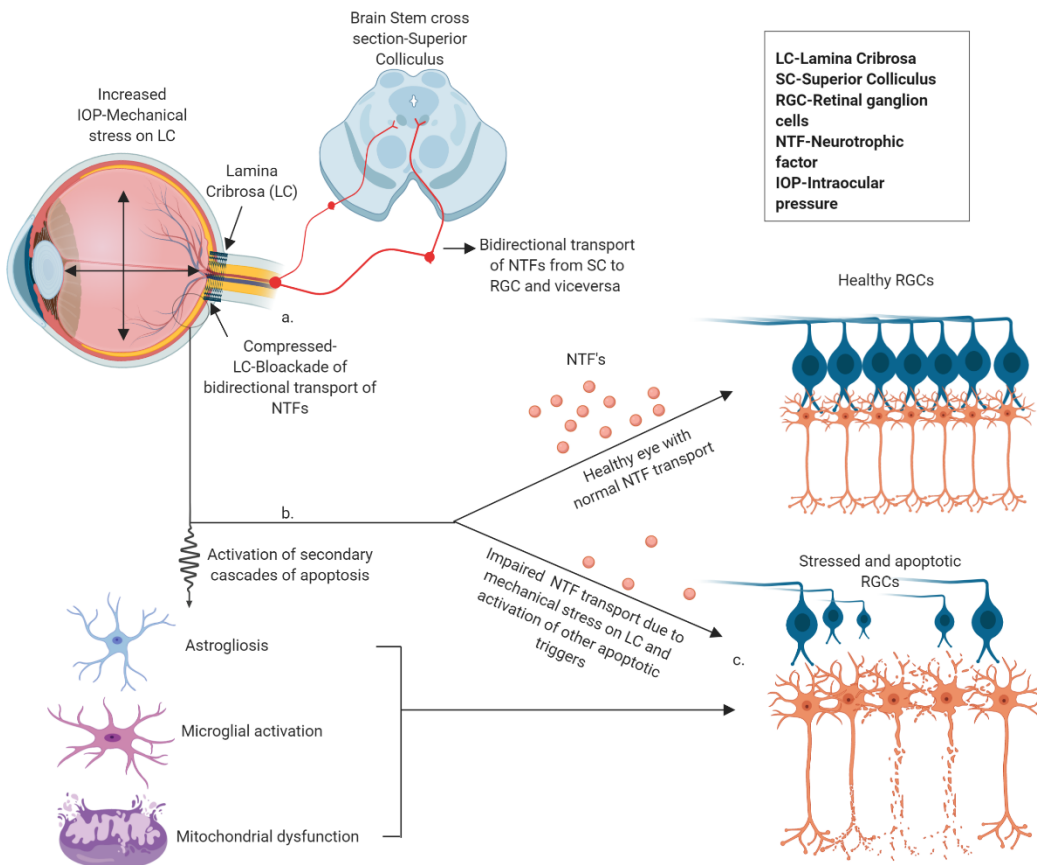


Figure 1-2 Mediators of RGC apoptosis and NTF deprivation. a. deprivation of bidirectional transport of NTFs, b. activation of secondary cascades of apoptosis and inflammation such as astrogliosis, microglial activation and mitochondrial dysfunction, and c. RGC cell death due to activation of inflammatory and secondary cascades of apoptosis (45, 53, 61). Figure generated by Lokesh Narsineni using BioRender.com.

1.2.2 Neurotrophic factors and their role in glaucoma and optic nerve degeneration

Neurotrophins are a class of small proteins that help in maintaining proper health and growth state of axons and RGCs. NTFs such as ciliary neurotrophic factor (CNTF) (62) and BDNF (63) when injected into the intraocular space and SC have shown improved growth of the axons and survival of RGCs. An increase in IOP interrupts the transport of BDNF which was identified as primary reason for the death

of RGCs (45). BDNF remains localized at the optic nerve head, as identified by immunolabelling tropomyosin receptor kinase B (TrkB) receptors, due to the mechanical compression at the optic nerve head (ONH) and this deprivation triggers the apoptosis of RGCs. BDNF deprivation is one of the primary reasons for glaucomatous degeneration of RGCs (64). Nerve growth factor (NGF) is a family of neurotrophins that can help in activation of both TrKA and p75^{NTR}. NGF can help in neuroprotection of RGCs by binding with the TrKA that are expressed in RGCs, while binding with the p75^{NTR} can trigger neuronal apoptosis (65). NGF is known to promote recovery of RGCs in the animal models that have been subjected to ischemia (66). Treatment with NGF eye drops twice daily for 7 weeks, prevented ischemia induced RGC apoptotic cell death in male Sprague-Dawley rats with induced glaucoma. NGF appeared to reach the back of the eye and helped prevent the decline of the RGC population by binding with NGF receptors and promoted survival and growth of RGCs (67). BDNF and CNTF treatments have shown good neuroprotective effects after optic nerve transection (68, 69). BDNF is expressed in the CNS and exerts its pro-survival effects by binding with TrkB receptors and upregulate the production of various pro-survival genes (70). BDNF also helps in activating the signaling pathways of phosphatidylinositol 3-kinase/Akt which deactivate the proapoptotic receptors (71). BDNF is considered as one of the factors responsible for maintaining the health of RGCs and as a powerful neuroprotective agent(72). As another evidence for the role of BDNF is that, a reduction in BDNF levels was noted prior to the death of RGCs and patients with POAG have low serum and tear fluid levels of BDNF compared to control subjects (73). The TrkB neurotrophin receptors in retinal glia were evaluated for their role in neural cell survival and neural regeneration. TrkB receptors are required to elicit the neuroprotective effects of BDNF. It is important to have both TrkB receptors expressed in the retinal glia and BDNF availability to show neuroprotective effects and to produce neural markers in the degenerating retina. The role of glial and neural cells in neurodegeneration was evaluated in a TrkB receptor knock out (KO) transgenic mice TrkB^{GFAP}(TrkB receptor is deleted in the retinal glia)

and TrkB^{c-kit} (TrkB receptor is deleted in the inner retinal neurons) in retinal glia. The retinal degeneration due to glutamate toxicity was found to be similar in both the TrkB^{GFAP} and TrkB^{c-kit} KO mice. When BDNF was supplied it did not protect the photoreceptor degeneration, Müller glial cell proliferation (which was identified in this study that BDNF-TrkB signalling stimulates proliferation and differentiation of Müller glial cells in the degenerating retina) and expression of neural markers in degenerating retina in TrkB^{GFAP} KO mice. The results demonstrated the potential of BDNF-TrkB glial cell signalling in neuroprotection and their role in the proliferation and differentiation of Müller glial cells to photoreceptors (74). Paskowitz et al. (2007) demonstrated the neuroprotective effect of BDNF and CNTF combination in photodynamic therapy (PDT). BDNF protected the retinal cells from PDT induced degeneration (75). Later it was shown that the combination therapy using BDNF and CNTF has shown better neuroprotection in PDT induced rats compared to the ones treated with only either CNTF or BDNF. Also, BDNF was found to have better neuroprotective activity compared to CNTF only treatment (76). Hence, NTFs, along with TrkB receptors are vital and play a major role in maintenance of normal health of the RGCs and promotion of neuroprotection.

1.2.3 Role of other retinal cells in neurotrophic support for the retina

NTF support is vital for maintaining the health and homeostasis of retinal cell population. It has been previously established that supply of BDNF through the SC and by local production in the retinal cells can help in protecting the RGCs from death (77, 78). However, selecting the right target cells for delivery of NTF gene and local production is necessary to supplement the lost NTF support, the local insufficiency due to elevated IOP and blockade of bidirectional transport through optic nerve makes it very difficult to deliver NTF through SC (79). Hence, in neurodegenerative conditions such as glaucoma other cell types in the retina are targeted to deliver therapeutics and make use of those cells in the retinal environment to produce NTFs. Cells that may be good targets for retinal therapy are

astrocytes or Müller cells (80), as these cells are known to increase in number in the retina when the inflammatory pathways are activated, for example after an episode of damage or injury (81). Our group showed that A7 astrocytes, transfected with nanoparticles carrying the BDNF gene expressed bioactive BDNF that promoted neurite outgrowth in the oxidatively stressed neuroblastoma cells in a two-layer contact-independent 3D neuronal co-culture model (82). Also, in a disease model where RGC's are declining in number it is not ideal to target RGCs and deliver the therapeutic gene, increased number of A7 astrocytes are mobilized to the retina during an episode of inflammation or injury. Hence, A7 astrocytes can be targeted in the retina to produce BDNF and supply to the dying RGCs inherently. Hence, A7 astrocytes were used in our *in vitro* studies to assess the efficiency of the NPXs to deliver reporter gene.

Retina is a key target for back-of-the-eye conditions, but as mentioned earlier it is highly challenging to reach retinal layers due to the complex and varying physicochemical issues in the eye, the various cell types in the retina (Figure 1-3) and the barriers involved (Figure 1-1). Administration routes such as intravitreal, sub-retinal and topical routes have shown positive gene expression in targeting the retinal layers by circumventing the barriers (83-86). Sanes and Masland in their review have shown the existence of 3 different types of photoreceptor cells, 12 types of bipolar cells, 40 amacrine cell types and 30 different types of RGC population which were classified based on morphology, gene expression, spacing and physiological properties (87), similarly, recent studies have shown the existence of more than 45 different subclasses of RGC's (88). Hence, targeting retinal cell populations is more complex with the presence of heterogenous populations of RGCs with varying protein expression capabilities. Various population of cells present in the retina that can be targeted for retinal delivery are shown under Figure 1-3.

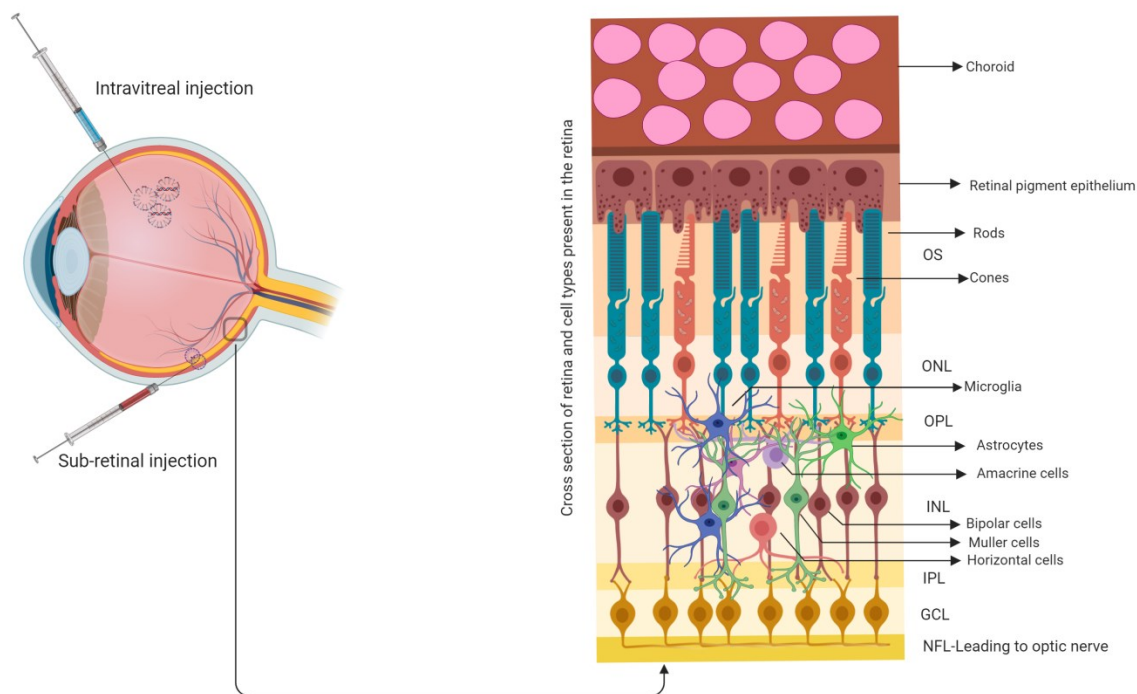


Figure 1-3 Routes of administration for retinal delivery, retinal cross section showing various layers and cell types in the retina that are targets for gene delivery. Outer segment (OS), Outer nuclear layer, outer plexiform layer (OPL), inner nuclear layer (INL), inner plexiform layer (IPL), ganglion cell layer (GCL) and NFL. Other targets in the retina such as astrocytes, bipolar cells, Müller cells, microglia and photoreceptor cells were present in the ONL and INL layers in the retina. Figure generated by Lokesh Narsineni using BioRender.com.

1.2.4 Advances in ocular drug and gene delivery: from simple IOP lowering therapies to neuroprotective and regenerative therapies in glaucoma treatment

Glaucoma therapeutics, current and under development, utilize IOP-lowering agents with various mechanisms of action e.g., miotics (β -blockers, α_2 agonists and prostaglandin analogs), aqueous outflow modulators, anti-angiogenic agents, neuroprotective agents (NTFs and all-trans retinoic acid), antioxidants, Rho-associated protein kinase (RhoA kinase or ROCK) inhibitors, β -secretase inhibitors, proteases, and antifibrotic agents (connective tissue growth factor inhibitors), to achieve clinical improvement (Table 1-2). β -blockers, such as timolol, levobunolol and betaxolol, and α_2 agonists, such

as brimonidine, help reduce the production of aqueous humor by acting locally on the ciliary body in the anterior segment of the eye (89, 90). However, β -blockers cannot provide prolonged protection compared with other lines of treatment, such as prostaglandins, over the nocturnal period (91).

A recent study found that brimonidine exerts neuroprotective effects by upregulating the expression of NTFs. Brimonidine achieves this up-regulation by acting on the excitatory amino acid carrier 1 (EAAC1) receptor, which removes excess glutamate (92, 93). ROCK inhibitors are a new class of molecules that have shown potential IOP-reducing effects. These effects are achieved via the inhibition of Rho kinase, which controls smooth muscle contraction and relaxation by phosphorylation and dephosphorylation (94, 95). Recent research on Rho kinase inhibitors has revealed their neuroprotective and neuroregenerative capacities through blocking the Rho kinase cascade. For example, administration of the ROCK inhibitor Y-39983 led to improved blood flow to the ONH (96), while the ROCK inhibitor Y-27632 has been shown to protect RGCs from apoptosis and ischemia-induced stress and can also increase RGC regeneration after optic nerve crush (97). Clinical trial data have suggested that ROCK inhibitors effectively improve neurite outgrowth and that these molecules may represent a promising approach for future glaucoma treatment and regenerative medicine (98-100). In the past decade research into neuroprotective and regenerative therapies has increased. Controlled release of NTF using a hydrogel system in the eye, where CNTF is complexed using affinity-based on the Src homology (SH-3) and its binding peptides CNTF is conjugated to SH-3 through affinity based interaction (CNTF-SH3) and is incorporated into hyaluronan and methyl cellulose (HAMC) hydrogel for a control release over 7 days to the retinal cells (101).

Apart from the treatments listed above in glaucoma, pharmacotherapies that focus on lowering the high IOP in the eye were widely used until today, various classes of drugs that possess distinct mechanism of action were employed in treating the increased IOP. Drug classes such as prostaglandins, beta-blockers, carbonic anhydrase inhibitors, α -agonists and miotics have been employed to treat the high

IOP in the eye. Second line therapies which include surgical treatments such as trabeculoplasty, micro-invasive glaucoma surgery and laser iridotomy were employed to relieve the high IOP. However, these treatments can only help delay the progression of the disease but cannot completely arrest the decline of the vision over time. Hence, new protective and regenerative therapeutics are necessary to protect from the vision loss in glaucoma. Prospective treatments such as Rho-kinase inhibitors, NTF therapies and anti-apoptotic therapies were in pre-clinical stages and few of them have entered clinical trials as potential therapeutics to treat glaucoma. Some, current and prospective treatments for glaucoma therapy are listed under Table 1-2 A and B.

Currently there are 25 gene therapies for ophthalmic conditions in pipeline undergoing phase I and II clinical trials such as for treating choroideremia (NCT02077361), achromatopsia (NCT03758404), Leber's congenital amaurosis, Leber's hereditary optic neuropathy (NCT03153293), retinitis pigmentosa (NCT02759952), X-linked retinitis pigmentosa (NCT03116113) and x-linked retinoschisis (NCT02317354) (102, 103).

Table 1-2 Current and prospective treatments in glaucoma

A) Small molecules and surgical treatments

Current treatments in glaucoma			
Pharmaceutical interventions (First line therapeutics)	Class of drugs	Therapeutic agent	Mechanism of action
	Prostaglandin analogues	• Latanoprost (Xalatan 0.005% Pfizer Inc.)	<ul style="list-style-type: none"> • Prostaglandin analogues (prodrugs of PGF2α) reduce the IOP of eye by improving the Uveo-scleral outflow of aqueous humor, relaxing ciliary muscles and remodelling the extracellular matrix in the ciliary body.
		• Travaprost (Travaton 0.004% Alcon Labs Inc.)	
• Brimatoprost (Lumigan 0.03%, Allergan Inc.)			
• Unoprostone (Rescula 0.15%, Novartis)			
Beta-blockers	• Timolol (Timoptic, Betimol 0.25% and 0.5%,)	<ul style="list-style-type: none"> • Beta-blockers help in reduction of aqueous humor production from ciliary by almost 20-50%. • Non-selective β blockers act both on β_1 and β_2 receptors. Selective β blockers target either β_1 or β_2 blockers 	
	• Levobunol (Betagen 0.25% and 0.5%, Allergan, Inc.)		
	• Cartelol (Ocupress 1%, CIBA Vision)		
	• Metipranolol (0.3%, OptiPranolol, Bausch& Lomb Inc.)		
	• Betaxolol- Selective β_1 antagonist (Betoptic 0.25%, Alcon Laboratories, Inc.)		

	Carbonic anhydrase inhibitors (CAIs)	Systemic CAIs <ul style="list-style-type: none"> • Acetazolamide-150 and 200 mg • Methazolamide- 25 and 50 mg 	<ul style="list-style-type: none"> • Carbonic anhydrase inhibitors are used in glaucoma therapy. • They decrease the aqueous humor production by acting as an antagonist on ciliary epithelium carbonic anhydrase.
		Topical CAIs <ul style="list-style-type: none"> • Dorzolamide HCl 2% (Trusopt-Merck Sharp& Dohme Corp) • Brinzolamide 1% (Azopt- Alcon Laboratories) 	
	Alpha-agonists	<ul style="list-style-type: none"> • Brimonidine tartrate 0.2% (Alphagen P-Allergan, Inc.) 	<ul style="list-style-type: none"> • Alpha-adrenergic agonists act by reducing the production of aqueous humor by modifying the ciliary body. • Promote the increase outflow of aqueous humor by uveoscleral outflow pathway.
		<ul style="list-style-type: none"> • Apraclonidine HCl 0.5% (Iopidine-Alcon Laboratories) 	
Miotics	<ul style="list-style-type: none"> • Pilocarpine HCl 0.5-4.0% (IsoptoCarpine and Pilocarpine gel-Alcon Laboratories) 	<ul style="list-style-type: none"> • Miotics reduce the IOP by contracting longitudinal ciliary muscles, opening of TM by scleral contraction and facilitate the movement of aqueous humor through TM. • Despite of reduced uveoscleral outflow of aqueous humor, increased TM outflow reduced the IOP in the eye 	
	<ul style="list-style-type: none"> • Carbachol (Isopto Carbachol-Alcon Laboratories) 		
Combination therapies	<ul style="list-style-type: none"> • Timolol 0.5% and dorzolamide 2% (Cosopt-Merck Sharp & Dohme Corp) is commercially available for twice-daily dosing. 	<ul style="list-style-type: none"> • Provide combined effect of both the drugs from their respective classes. 	
	<ul style="list-style-type: none"> • Brimonidine 0.2% and timolol 0.5% (Combigan-Allergan Inc. 		

		<ul style="list-style-type: none"> • Brimatoprost and 0.03% and timolol 0.5% (Ganfort- Allergan Inc.) 	
		<ul style="list-style-type: none"> • Travoprost 0.004% and timolol 0.5% (Duotrav-Alcon Canada) 	
Surgical and laser interventions (Second line therapy)	Type of procedure	Surgical procedure	Properties
	Trabeculectomy	<ul style="list-style-type: none"> • Excision of a small portion of TM or creating perforations in the TM is carried out in this procedure 	<ul style="list-style-type: none"> • Improved perforations/ incisions help in improvement of aqueous humor outflow thereby reducing the IOP (104).
	Laser trabeculoplasty	<ul style="list-style-type: none"> • In this method TM is treated with laser light that can cause perforation in the TM. 	<ul style="list-style-type: none"> • Laser treatment reduces the resistance to aqueous humor. • Patients lose the effect gradually due to closure of the openings in TM gradually (104).
	Micro-invasive glaucoma surgery (MIGS)	<ul style="list-style-type: none"> • A micro bypass stent is placed in the TM by surgery combined with phacoemulsification. 	<ul style="list-style-type: none"> • Micro-bypass stent placed in the TM helps in increased aqueous humor outflow by bypassing the TM perforations. • Good reduction in IOP<21 mmHg without medications and had a good safety profile (105, 106).

	Laser Iridotomy	<ul style="list-style-type: none"> • Laser Iridotomy is a process of making small perforations in the iris using laser beam in patients with closed angle glaucoma, while peripheral iridotomy is a surgical removal of a piece of iris 	<ul style="list-style-type: none"> • Surgical removal/ laser perforation in the iris helps in increased outflow of aqueous humor freely without resistance.
--	------------------------	--	--

B) Prospective small molecule IOP lowering drugs and macromolecular neuroprotective treatments

Prospective treatments in glaucoma			
	Class of drug/NTF	Properties	Mechanism of action
Drug treatments	Rho-kinase (ROCK) inhibitors	<ul style="list-style-type: none"> • These drugs are currently in phase II and III of clinical trials, they act by relaxing the smooth muscle of TM by inhibition of Rho associated protein kinase 1 and 2. • ROCK inhibitor AR-12286 has completed phase II studies to assess hypotensive effects in patients with exfoliative syndrome and ocular hypertensive patients, results demonstrated lower IOP compared to untreated subjects (NCT01936389). • Rho-kinase inhibitors such as Y-39983 have shown improved blood flow to optic nerve, while Y-27632 demonstrated neuroprotection and regeneration during pre-clinical studies in axon crush model (96, 107) (100, 108-110). 	<ul style="list-style-type: none"> • Inhibition of Rho-GTPase help in increased aqueous humor drainage by TM (111). • Rho-kinase inhibitors help reduce the IOP by increasing the aqueous humor outflow and decrease episcleral venous pressure, these effects take place when the rho-kinase pathway is inhibited which controls functions such as cell morphology, motility, adhesion and cytoskeletal dynamics, the actin disruption in the TM leads to increased AH outflow (112). • Neurite outgrowth by ROCK2 inhibitors along with CNTF treatment is promoted by blocking the axon growth inhibitory pathway by inhibiting the growth cone collapse, which can be achieved by elevated cAMP in conjunction with CNTF treatment (99).

Neuroprotective/gene therapies	Small molecules/ NTFs (BDNF, GDNF and CNTF)	<ul style="list-style-type: none"> • Brimonidine has also shown neuroprotective effect when administered systemically (113). • NTF delivery to RGCs help in their protection and survival. Efficient deoxyribonucleic acid (DNA) vectors are used to deliver the therapeutic DNA to target site and secrete NTFs (114). BDNF injected into SC protects the RGCs from cell death, glial-derived neurotrophic factor (GDNF) promotes the survival of the RGCs that are axotomized. • Non-viral/non-invasive gene therapy vehicles such as gemini-DOPE NPs are tried to deliver reporter gene by topical and intra-vitreous administration to explore the potential of these vehicles for gene therapy (30). 	<ul style="list-style-type: none"> • Brimonidine is an alpha2-adrenergic receptor agonist that help in lowering the IOP in glaucoma. It also promotes optic nerve regeneration by inducing extra cellular signal related kinases (Erk1/2) phosphorylation in an optic nerve injury model. Also, neurotrophin receptor gene p75 was upregulated and TrkB was decreased after brimonidine treatment, It has also been recently identified that it upregulates the excitatory amino acid carrier 1 (EAAC1) which expressed in neural cells that helps in neuroprotection (92, 93) • BDNF upon binding with TrkB receptor stimulates signalling pathways such as Erk1/2, that helps in survival of the RGCs (53).
	Over expression of Bcl-2 protein	<ul style="list-style-type: none"> • Over expression of Bcl-2 is another potential pathway that is being explored, RGC death is reduced in mice overexpressing bcl-2 (115, 116). • TAT-mediated delivery of Bcl-2 protein reduces the death of RGCs in an optic nerve lesion model, TAT peptide helps in carrying therapeutic DNA across cell membranes (117). 	<ul style="list-style-type: none"> • Bcl-2 is an anti-apoptotic gene that helps in increasing intracellular calcium signalling and activation of cAMP response element binding protein (CREB) and Erk phosphorylation and helps in promoting neuritogenesis (118).

1.3 Gene therapy: potential applications in the treatment of retinal neurodegenerative conditions

Gene therapy involves introduction or replacement of a gene into the host cell or organism by viral or non-viral methods to treat, maintain or prevent a disease or genetic predisposition and restore normal cell functions. Gene therapy generally uses a therapeutic DNA that is able to produce the required

therapeutic protein or correct a defective gene (119, 120). Retina is one of the primary targets for all the neurodegenerative diseases in eye. Current gene therapies in clinical trials for treating type 2 Leber's congenital amaurosis, Choroideremia, X-linked retinitis pigmentosa, achromatopsia, AMD were all based on viral vectors (Clinicaltrials.gov). The investigated retinal gene therapy treatments are all based on adeno-associated virus (AAV) mediated gene transfer and are administered through intravitreal injection. Luxturna® (voretigene neparvovec-rzyl) is another AAV based gene therapy which is the only gene therapy product approved to treat patients with inherited retinal disease having mutations in RPE65 gene that can lead to vision loss (121, 122), has sparked more interest in research on treatment of retinal neurodegenerative diseases and inherited retinal diseases. Pharmaceutical companies are investing in finding potential gene therapy treatments for many other neurodegenerative diseases. Apart from retinal gene therapy there are currently 110 gene therapy clinical trials underway for various other indications and diseases (123). With the significant advantages over the other diseases, gene therapy for the eye is at the forefront due to the small size, easily accessible nature reduced systemic access, lower immunogenic potential and ability to monitor treatment with cues such as visual function analysis and retinal anatomy imaging (124). A list of retinal gene therapies currently approved and the ones in clinical trials are listed in Table 1-3.

Table 1-3 List of retinal gene therapies currently approved and in clinical trials

Description of the gene therapy	Vector system	Indicated treatment	Status/Company/References*
Luxturna®- voretigene neparvovec- rzyl	AAV2	Early onset of vision loss due to mutations in RPE65 gene	Approved by Food and Drug Administration (FDA) on December 2017-Spark Therapeutics, NCT00999609 (122, 125, 126)
AAV8-RPGR	AAV8	X-Linked Retinitis Pigmentosa	Phase 2/3 clinical trials- NCT03116113, NightstaRx Ltd

rAAV2.REP1	AAV2	Choroideremia	Phase1/2 -Completed, NCT02077361, University of Alberta
AAV2/8- hCARp.hCNGB3	AAV2	Achromatopsia with defects in CNGB3	Phase 1/2 – Active, NCT03001310, MeiraGTx UK II Ltd
RGX-314 (Anti-VEGF gene)	AAV8	Anti-VEGF treatment for neovascular AMD	Phase 1/2, Active- NCT 03066258, Regenxbio Inc.
AAV8-scRS/IRBPhRS	AAV8	X- linked juvenile retinoschisis.	Phase 1/2 safety and tolerability assessment- Active recruiting- NCT02317887, National Eye Institute, MD, USA

* clinical trial identifiers are from clinicalTrials.gov

Until recently, gene therapies approved to treat other conditions were also based on viral vectors, but in 2018 FDA approved Onpattro[®] (patisiran), a lipid nanoparticle based small interfering ribonucleic acid (siRNA) based drug, for the treatment of polyneuropathies induced by hereditary transthyretin amyloidosis (127). Another non-viral siRNA therapy, which is not related to retinal gene therapy but significant as a non-viral gene therapy, Givlaari (givosiran) for the treatment of acute hepatic porphyria, was approved by FDA in November 2019 (128). The formulation is made by conjugation of N-acetylgalactosamine to the siRNA allowing an efficient delivery of siRNA to the liver. This marks the approval of two successful non-viral gene therapy treatments. The approval of non-viral vector-based gene therapies provided a boost to the research on viral vector alternatives, such as lipid, surfactant, polymer and peptide-based vectors. Synthetic gene delivery vectors with multi-functional properties are being explored to develop efficient non-viral systems.

1.4 Non-viral gene therapy: materials, properties and NP systems

Non-viral gene therapy utilizes synthetic materials to deliver the therapeutic DNA instead of viral vectors. Viral vectors despite high TE (129) possess disadvantages that may be life threatening, such as a strong immune response and possible recombination of viral vectors with host DNA (130, 131). Other complications involving viral vectors are the high cost of manufacture and low cargo carrying capacity (<4.7 KDa) (132). Despite these drawbacks viral vectors are currently the leading vectors for gene transfer because of their efficiency (123, 131, 133). Non-viral vectors have the potential to overcome the limitations of viral vectors, but they lack specificity and targeting ability. Non-viral gene delivery vectors are made up of synthetic materials such as lipids (134), surfactants (135, 136), polymers (137, 138). NPs made from these materials are complexed with the nucleic acid therapeutics by physical or electrostatic interactions. While non-viral vectors can also possess some disadvantages such as toxicity and storage stability issues, the development of a non-viral gene delivery system is less expensive and they have a better safety profile, customizable targetability and flexible administration modes. In a recent paper, we reviewed the non-viral systems made from lipids and polymers in clinical trials for various conditions (40). Current research in this field is still in the preclinical stages and the quest for novel materials and delivery systems to achieve retinal gene delivery has intensified. Synthetic materials such as lipid- and polymer- based materials are often used for making non-viral systems to deliver therapeutic DNA to host cells. Non-viral systems such as niosomes complexed with pCMSEGFP at 15/1 ratio to form NPs have shown improved internalization and transfection in HEK-293 and ARPE-19 cells. Intravitreal and subretinal injections in adult male Sprague-Dawley rats showed green fluorescent protein (GFP) expression in the GCL, IPL and INL layers with an intravitreal injection, while the subretinal delivery showed expression in the GCL, INL, partial colocalization of EGFP is observed in the bipolar cells (139). Lycopene containing cationic niosome formulations made with DOTMA and polysorbate 60 were successful in compacting the pCMS_EGFP DNA and *in vitro*

transfection studies performed on ARPE-19 cells showed 35% positive transfection of the cells with good viability. The *in vivo* studies in rats receiving niosomes intravitreally and subretinally showed the transfection of outer segments of the retina demonstrating the potential of surfactant-based formulations in delivering DNA to retinal cells in the eye (140). Topically administered liposomes made with hydrogenated soy L- α -phosphatidylcholine (HSPC), 1,2-dioleoyl-3-trimethylammonium-propane (DOTAP), cholesterol and 1,2-dimyristoyl-3-trimethylammonium-propane (DMTAP)/1,2-dimyristoyl-sn-glycero-3-phosphocholine (DMPC) and modified with Trf as a targeting ligand, appeared to move through the ciliary arteries, conjunctiva and produced a strong fluorescence signal at the RPE after 5 minutes. The results demonstrate the potential for small liposomes from non-viral materials to improve ciliary artery transport via their passage through the choroidal capillaries. Also, functionalization with synthetic peptides such as Trf improved liposome localization to the RPE which have an abundance of Trf receptors (141). Polymers have been highly exploited for non-viral ophthalmic gene delivery. Generally, polymers bind with the DNA through electrostatic or hydrophobic interactions and protect the nucleic acid from degradation. Some commonly used polymers for ocular gene delivery are chitosan (142), polyethylenimine (PEI)(143), polyamidoamine (PAMAM), polyethylene glycol (PEG), polyarginine and poly(D,L-lactide-co-glycolide) (PLGA) (144, 145). Polymeric gene delivery vectors depend mostly on endocytosis processes for delivering the gene cargo into the cells, they have shown to form stable complexes compared to liposomes and provide more efficient complexation. Dendrimers are a class of polymeric gene carriers. One notable factor that limit the use of high charge density polymers are their toxic effects on the cells. Liu et al, (2016) in their studies identified that low molecular weight dendrimers functionalized with penetratin made from G3 PAMAM were able to transfect retina after topical ocular application of the polymeric NPs into the conjunctival sac. The penetration route for these NPs was found to be through fundus (146). Above presented studies are few such examples of synthetic based non-viral gene therapy vectors for ophthalmic and retinal

delivery, the next few sections present a more in-depth discussion on the use of lipid and surfactant based non-viral vectors for retinal delivery.

More than 119 clinical trials have been carried out to date to deliver gene cargo using lipid vectors such as lipoplexes (LPXs) (LPXs are NPs made from synthetic materials such as surfactant or polymer along with lipid. Naked DNA delivery using electroporation (16.5% in 2017) currently tops the clinical trial list followed by lipofection with 4.5% of the total gene delivery clinical trials performed (123). Hence, interest on using non-viral vectors such as lipids, surfactants and polymers as gene delivery agents has considerably spiked in recent years due to concerns surrounding immunogenic issues related to viral vectors.

1.5 Lipid based nanomaterials in gene delivery

With the growing repertoire of nanomaterials, including polymers, lipids and surfactants, it may be possible to develop safe and effective non-viral delivery approaches. Developing highly efficient non-viral gene delivery vectors is slowly gaining momentum due to the versatility of these systems that allows functional modifications, ranging from their chemical structures to formulation characteristics allowing them to incorporate larger gene cargo, ability to circumvent the barriers and to efficiently target the cells. Few such systems from lipid, surfactant and polymer systems (Figure 1-4) that showed efficient gene delivery are listed in the following sections.

Lipids are one of the first materials used to formulate gene-based therapeutics and the term lipofection describes the transfection of cells with a lipid-based transfection agent. Cationic lipids such as N-[1-(2,3-dioleoyloxy)propyl]-*N,N,N*-trimethylammoniumchloride (DOTMA), [1,2 bis-(oleoyloxy)-3-(trimethylammonio)-propane] (DOTAP), 1,2-dipalmitoyl-*sn*-glycero-3-phosphocholine (DPPC) and a neutral lipid such as 1,2-dioleoyl-*sn*-glycero-3-phosphotidylethanolamine (DOPE) and dioleoylphosphatidylcholine (DOPC) are some of the first highly studied lipids to deliver the gene

cargo into the cells (147). DOPE is a widely used phospholipid to improve the colloidal stability as well as the transfection efficiency (TE) both *in vitro* and *in vivo*. Due to its neutral charge DOPE is used in conjunction with a cationic agent to complex the DNA. Lipid vesicles deliver the gene cargo into cells mostly by endocytosis and fusion. Cationic lipid such as DOTMA was formulated along with rhodamine conjugated DOPE and DNA and LPXs were shown to interact by fusion with the cell membranes (148). Cationic lipid DOTMA co-formulated with DOPE liposomes are mostly endocytosed by clathrin and caveolae mediated endocytosis (149). At low pH the DOPE vesicles undergo a phase transition and form inverted micelles to form a hexagonal phase which will help in endosomal escape function (150, 151). Cationic liposomes made with , DOTMA/DOPE at 1:1 molar ratio and DOTMA/cholesterol (Chol) at 1:1 molar ratio were prepared and conjugated with a luciferase DNA were intravitreally injected into the eye and after three days the expression of luciferase peaked for DOTMA/Cholesterol 1:1 liposomes compared to the DOTMA:DOPE liposomes and their expression was highly concentrated in the anterior chamber of the eye (152). These studies demonstrate the potential of lipid-based systems as non-viral gene delivery vector systems.

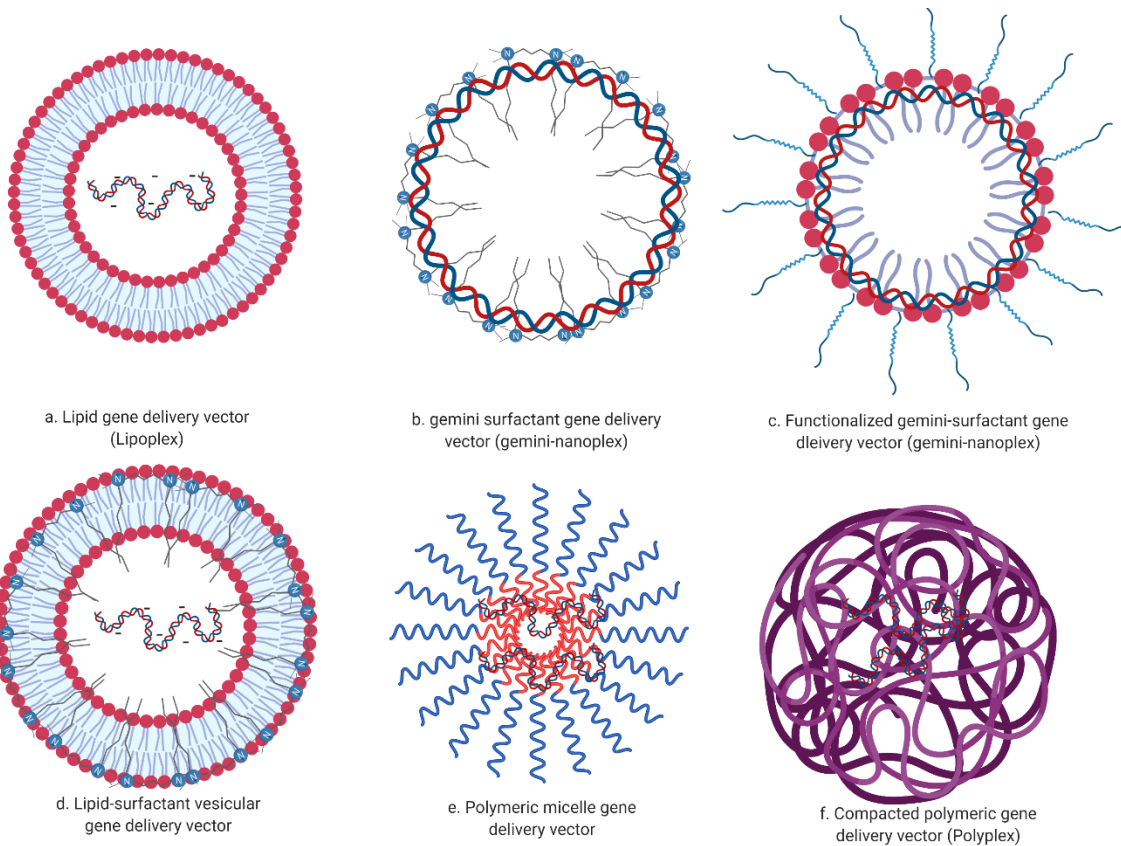


Figure 1-4 Schematic examples of non-viral gene delivery systems made of lipid, surfactant and polymeric systems, (a) lipid vectors engulf the therapeutic DNA (b) cationic gemini surfactants interact with the DNA and compact them due to charge interactions, (c) functionalized gemini-surfactant gene vectors contain a cell surface recognition peptide for improved interaction and delivery of therapeutic DNA, (d) Lipid-surfactant vectors help in compaction of DNA through electrostatic interaction between charged surfactant and DNA and the lipid vesicles provide the fusogenic property to the vectors, (e) polymeric micelle vectors interact with the therapeutic DNA through charge interactions and (f) highly compacted polyplex is formed with the charge interaction between the DNA and cationic polymer (40, 153, 154). Figure generated by Lokesh Narsineni using BioRender.com

1.6 Surfactant based gene delivery

Recent research publications in the field of nanomedicine show interest in using surfactants as nanoparticulate carriers for drug and gene delivery. Some of the potential surfactant-based gene

delivery vectors that have significantly contributed to the field of non-viral gene delivery are summarized below.

1.6.1 Gemini Surfactants

Gemini surfactants (GS) are a class of di-cationic amphiphiles with two long hydrophobic tail with ionic head groups separated by a rigid or flexible spacer. Over time, various generations of gemini surfactants with symmetric and non-symmetric alkyl tails, various ionic head groups, varying spacer length, pyrene ring, modified spacer and short dipeptide conjugations have evolved with structural and functional advancements making them suitable for many different applications (155-159). Gemini surfactants self-aggregating materials at very low concentration due to their low critical micelle concentration (CMC) which is an important factor that reduces the toxicity levels of surfactants used in the formulation. They form highly compacted NPs when cationic gemini surfactants are used to complex DNA. (160, 161). Over the past decade there has been a significant progress in improving physicochemical properties and transfection properties of the gemini surfactants.

1.6.2 Evolution of gemini surfactants

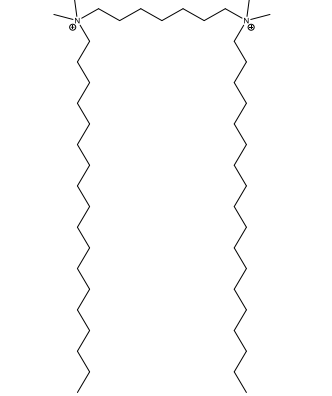
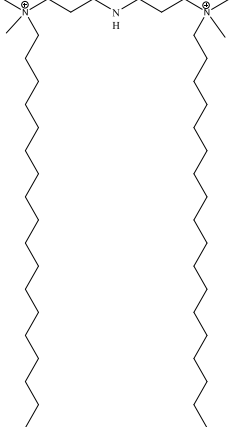
Gemini surfactants have proven to be versatile class of molecules since their synthesis and induction by Menger in 1991 (156, 162). The amphiphilic ‘bis-surfactants’ have unique structural and chemical properties that have rendered them useful in many applications such as skin care, cosmeceuticals, solubilization applications, oil spill cleaning, anti-bacterial and most notably an increased surge in the gene therapy application is predominant in recent years (160, 163-165). Gemini surfactants also help in forming gene vectors similar to LPXs. The presence of positively charged quaternary nitrogen head groups separated by a spacer are responsible for compacting the plasmid DNA and form surfactant nanoplexes (NPXs) (NPXs are NPs made from synthetic materials such as surfactant or polymer without lipid). The schematics of the general and gemini surfactants-DNA complexes are shown in

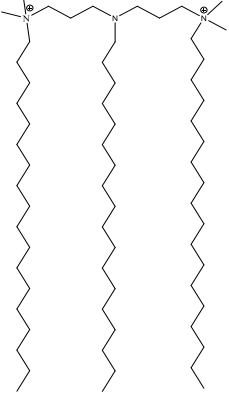
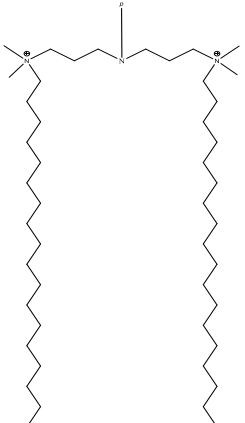
(Figure 1-5 a). These are currently being investigated by our and other groups for targeted gene delivery for various clinical indications (166, 167). Due to their unique properties versatile chemical modifications can be carried out to improve their gene delivery efficiency.

1.6.3 Classification and properties of amphiphilic gemini surfactants

Gemini surfactants are a classic example of dimeric surfactants and they are also known as “bi-quaternalary” ammonium surfactants or ‘bis-surfactants’ containing two hydrophilic head groups separated by a spacer group with or without amino substitution and the hydrophilic head groups are covalently bonded with hydrophobic alkyl tails either in symmetry or non-symmetry. These surfactants are simply referred as m-s-m surfactants which are the 1st generation gemini surfactant molecules where ‘m’ is the alkyl tail length and ‘s’ is the spacer group between the head groups. The presence of the two alkyl tails and two hydrophilic head groups makes them unique, their self-assembly in hydrophilic solvents differ from the conventional surfactants due to the presence of two polar head groups and a rigid spacer, It is was proposed that gemini surfactants rather self-coil initially than forming micellar structures and later on at the air-water interface they uncoil and reassemble to form submicellar structures (156, 162). In our laboratory gemini surfactants are classified into various categories based on the step-wise chemical and functional improvements and represented in this thesis as 1st, 2nd, 3rd generation gemini surfactants as shown in Table 1-4 and Figure 1-5.

Table 1-4 Foldvari Lab classification of gemini surfactants and various gemini surfactants used in gene delivery

Surfactant generic code	Gemini surfactant	Properties/groups	Model structure
m-s-m	12-3-12 12-7-12 16-3-16 16-7-16 18-3-18 18-7-18	1 st generation gemini surfactants, m=alkyl tail, s=spacer, m=7-18, s=3-7	 <p data-bbox="1027 955 1357 997">N⁺,N⁺,N⁺,N⁺-tetramethyl-N⁺,N⁺-dioctadecylheptane-1,7-diaminium m-s-m gemini surfactant 18-7-18</p>
m-sNH-m	12-7NH-12 16-7NH-16 18-7NH-18	2 nd generation gemini surfactants, m=7-18, s=7, amino substitution in the spacer group	 <p data-bbox="1060 1459 1396 1501">N,N'-(azanediybis(propane-3,1-diyl))bis(N,N-dimethyloctadecan-1-aminium) m-7NH-m gemini surfactant 18-7NH-18</p>

m-sN(p)-m,	12-7N(p)-12	3 rd generation gemini	 <p data-bbox="995 663 1295 709"><i>N,N'</i>-(octadecylazanediyl)bis(propane-3,1-diyl)bis(<i>N,N'</i>-dimethyloctadecan-1-aminium) m-s(m)-m gemini surfactant 18-7N(18)-18</p>
m-s(m)-m	16-7N(p)-16	surfactant, p= peptide	
	18-7N(p)-18	sequence, m=12, 16 and	
	12-7N(12)-12	18, s=7	
	16-7N(16)-16		
	18-7N(18)-18		
			 <p data-bbox="995 1167 1295 1192">(e) m-7N(p)-m gemini surfactant 18-7N(p)-18</p>

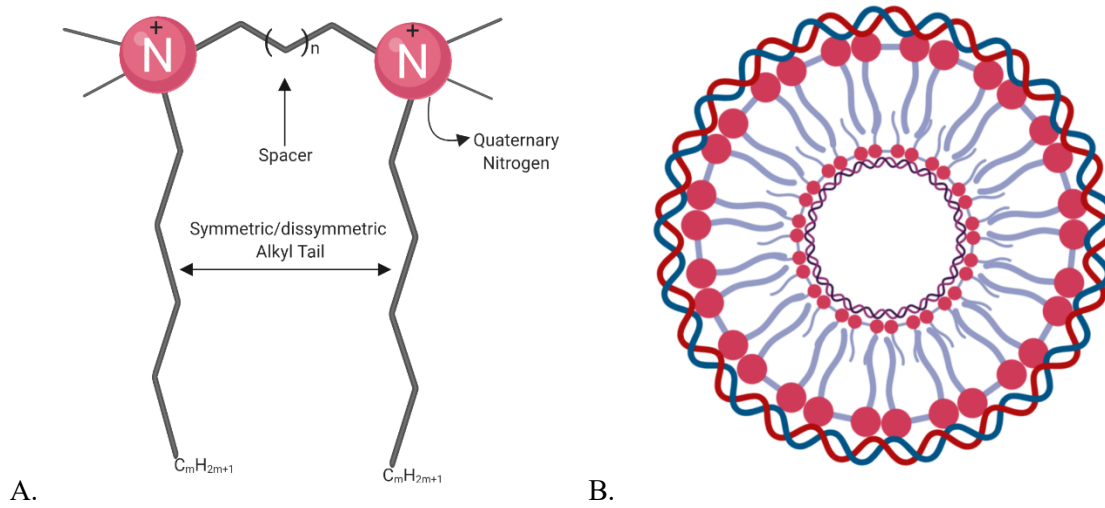


Figure 1-5 General schematic structures of gemini surfactants (A) and plasmid-DNA compacted by gemini surfactants, termed as NPXs (B). Figure generated by Lokesh Narsineni using BioRender.com

1.6.4 CMC and surface-active properties

The most striking difference between gemini surfactants and other conventional surfactants is their low CMC values, allowing their use at lower concentration since self-assembly occurs at low concentrations which is advantageous for therapeutic applications. The presence of two hydrophobic tails and a spacer contributes to the higher hydrophobicity leading to increased self-assembly and a stable interaction between the gemini surfactants and DNA (168, 169). The surfactants have shown to be three orders of magnitude more efficient in decreasing surface tension and two orders of magnitude more efficient in forming micelles by modifying the interactions with water (156).

1.6.5 Effect of spacer, amino substitution and alkyl tail length on transfection properties of gemini surfactants

The separation of two hydrophilic head groups in the gemini surfactant using a spacer has profound effect on the characteristics and the efficiency of the gemini surfactants in their performance as gene

delivery agents. The spacer plays an important role in the efficient interaction of the cationic head groups of gemini surfactants with the negatively charged DNA phosphate groups. An increase in the chain length of the spacer leads to increase in the CMC this results in use of higher concentration of surfactant to reach CMC (165, 170). Having a short spacer (<4) is preferred since it has been reported that 4.9Å between the spacer groups is efficient for interaction of the surfactant head groups with phosphate groups in DNA (171). The amino substitution in the spacer group preserves the short spacer length and also adds a pH responsive group to enhance the endosomal release of the gene cargo. Aza and amine groups incorporated into the gemini structure to induce a pH active function and improve the TE. The acidic pH caused by net influx of counter ions into the endosome results in phase inversion of the lipid structure, endosomal disruption and release of DNA (159). Alkyl tail length also plays a major role in self-assembly, DNA compaction and imparting hydrophobicity to the surfactant. As the length of the alkyl tail is increased, which results in the increase in Krafft temperature and decrease of CMC, and leads to an increase in TE (171) The longer alkyl tails help in enhanced encapsulation of DNA at lower concentration and this helps in reducing cellular toxicity (172). Since their induction by Menger et al. (1991), m-s-m gemini surfactants(169) were further improved by introducing NH groups into the spacer thereby increasing the TE by changing the membrane fusion properties, DNA release (173) and endosomal escape properties (159). 16-3-16 gemini NPs (100-200 nm) were effective in delivering interferon-gamma gene topically and gene expression without skin toxicity (174). Amino acid substituted gemini surfactants as gene carriers have shown higher TE than the un-substituted compounds partly because the DNA is highly protected by the glycine substitution. This opened doors for a chance to conjugate many more peptides and therapeutic molecules to be used as gene carriers (175).

The m-7NH-m gemini surfactant-based NPs were first developed to transfect retinal layers to treat glaucoma by intravitreal injection and topical delivery in our group. After intravitreal administration in

mice, the gemini-plasmid (tdTomato)-lipid (GPL) NPs dispersed evenly and localized at the retinal layer. The topically administered NPs followed a distinct movement pathway and were detected at various tissues such as iris, limbus and conjunctival layers. These results suggest the potential of gemini surfactant NPs as gene delivery systems especially by the intravitreal route (30). Although the topical application has not shown gene expression after three days of treatment, further testing will provide more information to optimize the topical approach. Only a few surfactant gene delivery systems have been developed which is related to the potential toxicity associated with surfactant systems. Gemini surfactants are surfactant systems but due to their dicationic head groups and the dimeric alkyl tails they behave similarly to lipids with respect to their molecular association and structures and also their lower CMC values provide lower toxicities.

1.6.6 Self-assembly of gemini surfactants

The length of spacer plays a crucial part in the defining the solution properties and the confirmation of the dimeric molecule (176). Menger et al, 1993 have mentioned that these gemini surfactants specially with alkyl tails 16 and above will behave in a very peculiar manner compared to lower length alkyl tails. They tend to first form submicellar aggregates initially when they are exposed to hydrocarbon or water to reduce water contact. Then upon application of increased temperatures they tend to uncoil and rearrange into their final assembly structures that are higher order aggregates (156). Molecular dynamics simulation of gemini dicarboxylate disodium surfactants have exhibited a concentration dependent self-assembly into lyotropic phases such as hexagonal, gyroid and lamellar morphologies at 30, 65 and 80 wt% of the surfactant (Figure 1-6). Along with the structural conformation they also affect the morphology and solution properties, organization into one of the above phases is dependent on the polar head groups and the counter ions present in the surfactant. Stronger electrostatic interaction favors lamellar phase while weaker interactions diminish the lamellar phase (177).

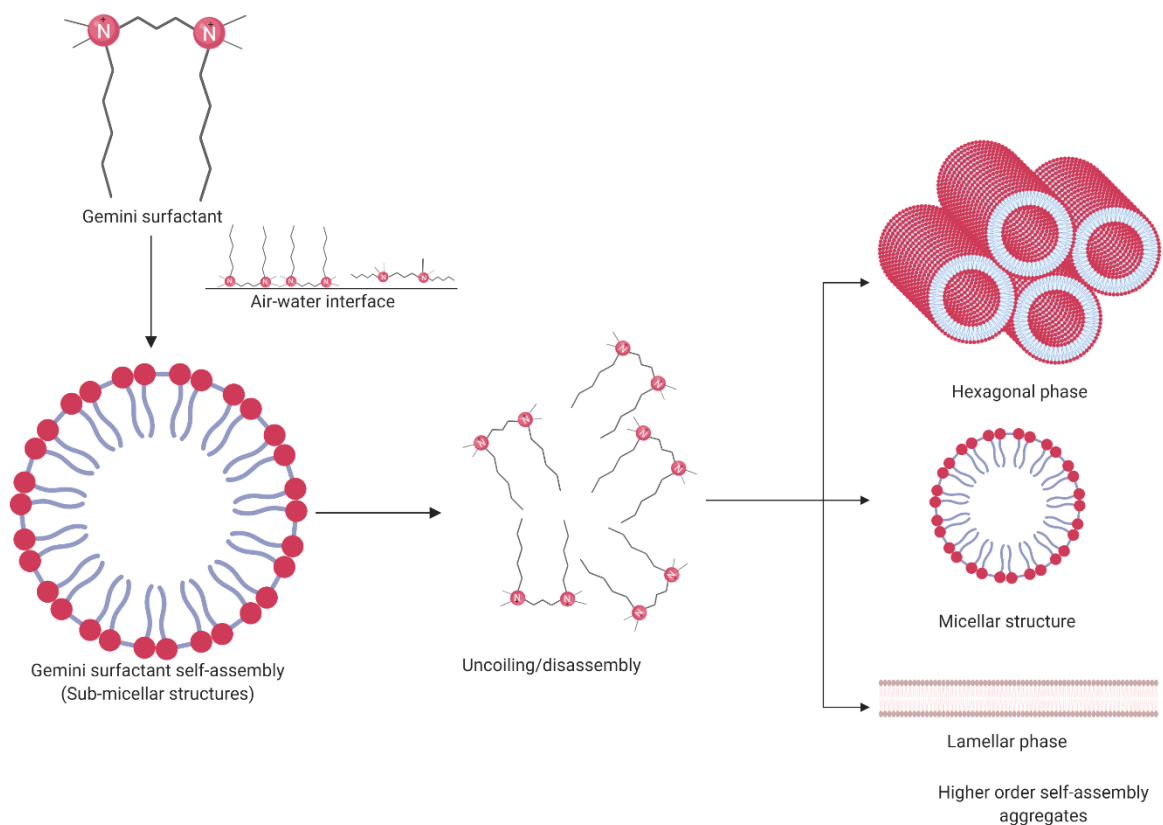


Figure 1-6 Schematic of self-assembly in gemini surfactants into higher order aggregates, gemini surfactants can re-assemble to form into various morphologies such as hexagonal, micellar and lamellar phases (177) Figure generated by Lokesh Narsineni using BioRender.com

1.7 Multi-functionalization: An approach to build intelligent non-viral gene delivery systems

With the advent of many novel lipid and surfactants the quest for an ideal formulation that can deliver therapeutic molecules safely and precisely has become an utmost priority. In particular, delivering therapeutics to the posterior segment of eye with all the hurdles presented in previous sections is a challenge in the field. ‘Bottom-up’ biomimetic principles are often used to target the cells to deliver therapeutic molecules. For example, anti-VEGF was delivered to the RPE by intravenous

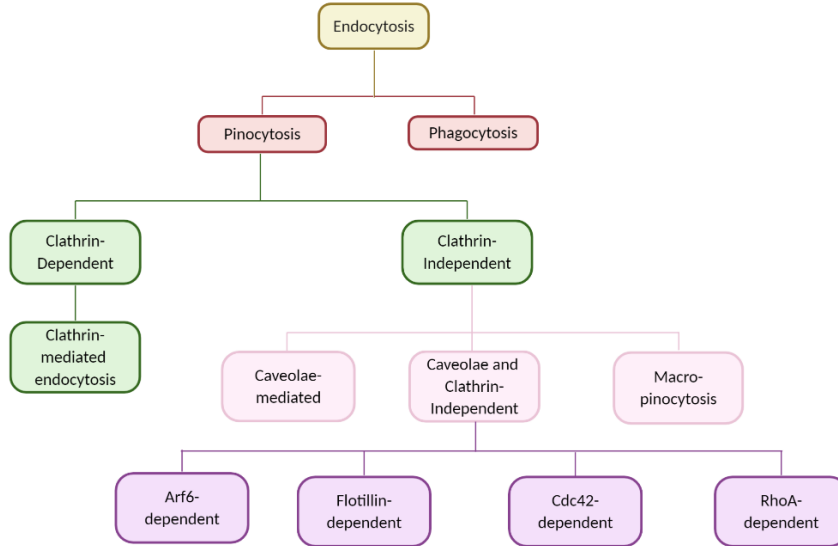
administration using a delivery system that was functionalized with Trf and RGD peptides (28). PEG coating helped cationic liposomes to cross the vitreous which is a barrier for cationic nanoparticle-mediated delivery due to the presence of various charged proteins such as albumin and glycosaminoglycans (GAGs) (178-180). Many other strategies such as charge masked liposomes (36), endosomal escape functionality by incorporating a pH induced escape method (159, 181) and long circulation by coating with PEG on liposomes are some of the strategies used to improve the delivery and efficiency of non-viral gene delivery systems.

By combining some of these strategies, multi-functional delivery vectors can be developed, e.g. targeting moieties, endosomal escape promoters, cell-surface receptor interacting peptides, cell-cell interaction promoters, neuroprotective and regenerative molecules can be combined within one nanoparticle system, which is most importantly, a carrier that can effectively compact the DNA and protect the gene cargo from degradation.

1.8 Mechanism of cellular interaction, uptake and processing of non-viral gene delivery systems

The cellular uptake mechanism of non-viral gene carriers occurs mainly by energy-dependent endocytic processes. The endocytic pathway includes phagocytosis and pinocytosis (Figure 1-7 A and B). The latter can be subdivided into macropinocytosis, clathrin-dependent and clathrin-independent endocytosis. Clathrin-independent endocytosis maybe classified further into caveolae-mediated, and clathrin and caveolae-independent pathways (including RhoA-, ARF6-, CDC2-, and Flotillin-1-mediated endocytosis) (see reviews (182-185)). Among the less frequent mechanisms, energy-independent processes such as passive diffusion, facilitated diffusion, membrane fusion, and membrane crossing (needle-effect or nanoporation) can be mentioned.

A)



B)

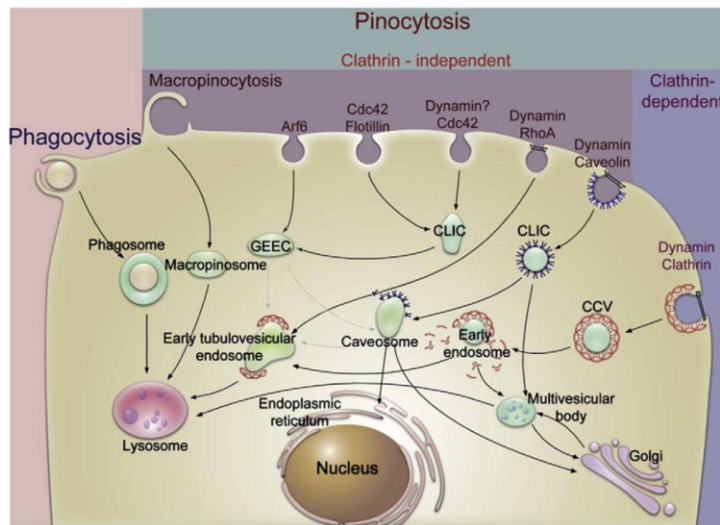


Figure 1-7 Classification and mechanisms of cellular uptake process, A) Classification B) Uptake methods and their mechanisms (Figure 1-7; B) is reprinted, Figure 1-7 (A) is modified using BioRender.com, with permission from Sahay et al. (Journal of Controlled Release (145), 182-195, 2010)

Phagocytosis involves large particles with sizes greater than 1-10 μm by specialized cell populations such as macrophages. The type of pinocytic process that may occur with nanomedicines will be dependent on the characteristics of the particles, more specifically their size, charge, shape, rigidity, surface morphology and coating. Macropinocytosis is also known as cell drinking where a non-specific uptake of extracellular material takes place and endocytosis happens by formation of vesicles of irregular size. Macropinocytosis is stimulated by the transient activation of receptor tyrosine kinases by cell growth factors such as colony stimulating factor and epidermal growth factor. It is still not sure if the macropinosome and lysosome fuse together for degradation of these macropinosomes. Macropinocytosis has also recently been identified as one of the routes for endocytosis for the gene delivery (186), where it can take up large amounts of macromolecule complexes and also can avoid lysosomal degradation. Blocking of macropinocytosis impaired gene expression mediated by the octa-arginine peptide which demonstrates the potential for this route in macromolecular expression (187, 188). The macropinocytosis also includes transport of molecules through Arf6, Cdc42 flotillin, dynamin, dynamin RhoA and dynamin.

Clathrin mediated endocytosis (CME) is a route of internalization for viruses (189), it helps in uptake of nutrients such as cholesterol by low density lipoprotein through its receptor, iron by Trf receptor, functional ligands and nanoparticle gene delivery systems. CME also helps in maintaining the homeostasis of the cells by internalizing and degrading membrane receptors. Actin is another protein that is involved in the spatial distribution and movement of the endocytic vesicle into the cell. The particle interaction with the lipid membrane forms clathrin coated pits which invaginate and detach from the lipid membrane and the particles are engulfed into the clathrin coated pits to form endosomes. Few examples of NPs that have been shown trafficking through CME were PEG-co-D, L-poly(lactide) (PLA) NPs and cationic particles made from polymers. It has been shown that the mechanism of

internalization of these particles depends on the cell types treated. Cationic particles mostly get internalized by CME and micropinocytosis in HeLa cancer cells, while anionic NPs have been shown to get internalized by CME and caveolae mediated endocytosis in MDCK epithelial cells (183, 190). PLGA NPs in vascular smooth muscles, silica-based NPs in cancer cells and chitosan NPs in respiratory epithelium and intestinal epithelium are few other NP systems that have been shown to be internalized by CME.

Caveolae-mediated endocytosis mostly happens with the help of a functional ligand molecule on the complexes endocytosed. Ligands that are conjugated on to the complexes determine the fate of the complexes especially the route of internalization. Ligands such as folic acid, albumin and cholesterol promote caveolae mediated endocytosis (191). The complexes during interaction with the cell membrane will lead to form vesicle and lead to formation of caveosome with the help of caveolae. The caveolae present in the cell membrane are the starting point of this endocytosis mechanism and they are known to endocytose complexes with particle size between 10-100 nm. Dynamin protein helps in the formation of vesicles and detachment from the cell membrane when the vesicles are internalized. It was also identified that caveolae-mediated systems do not degrade the complexes using pH drop function and this type of process does not involve fusion with lysosomes. But the internalization of the complexes into the cytoplasm and escape of complexes and DNA from the vesicles is needed to get access to the nuclear region (192). Lycopene containing niosome formulations made from DOTMA and polysorbate 60 were shown to internalize into the ARPE-19 cells by caveolae mediated endocytosis and macropinocytosis determined by uptake and distribution studies (140). Retinal cell uptake studies demonstrated the potential of caveolae and macropinocytosis mechanism in internalizing the NPs that are in the size range between 50-100 nm. into retinal cells. Apart from retinal cell targeted NPs, systems targeted to other tissue were also studied intensively to determine the uptake mechanisms of NPs.

DOXIL[®] liposomes are negatively charged PEGylated liposomes used to treat metastatic ovarian cancer. It has been demonstrated that DOXIL[®] liposomes use caveolae mediated endocytosis mechanism to internalize the liposomes into the epithelial cancer cells. The NPs normally adhere to the epithelial surface then they are internalized through the caveolae mechanism and enter the lysosomes finally where the drug is released. Another nanomaterial that enter the cell through caveolae mediated endocytosis are poly(ethylene oxide)-*b*-poly(methacrylic acid) cross-linked anionic NPs. RGD functionalized copolymer c(RGDfk)-PEG-*b*-poly(lysine) has shown to internalize the plasmid DNA (pDNA) into the HeLa cells by caveolae mediated endocytosis (193).

Apart from the endocytic pathways there are few non-endocytic pathways that contribute to the internalization of the non-viral gene therapy complexes. Important non-endocytic pathways to address the uptake and internalization issue are penetration mediated delivery and fusion mediated delivery. In the penetration mediated delivery functionalization of complexes with cell penetrating peptides and pore forming materials can help in directly internalizing the therapeutic DNA into the cytoplasm directly without undergoing through the lysosomal degradation. Another non-endocytic pathway which leads to direct release of DNA into the cytoplasm before leading to endocytic pathways is fusion of the LPXs. This pathway minimally contributes to the uptake of LPXs. Lipids such as cholesterol and DOPE help promote the fusogenic properties of the complexes. One such example is the hemagglutinating virus of Japan liposomes, that rapidly accumulate oligonucleotides in the nucleus. The nanoparticle systems made of lipid, surfactant and polymeric materials that act as non-viral gene delivery vectors adapt to one or multiple methods of internalization into the cell. The route of internalization can be identified by carrying out an inhibitor study that involved clathrin mediated endocytosis inhibitor such as chlorpromazine, nystatin to inhibit the caveolae/lipid mediated endocytosis and bafilomycin can be used an inhibitor for lysosomal degradation.

Hence, it is necessary to design NP systems in such a way they promote internalization through one of the mechanisms listed above by using specific materials and with controlled sizes. For promoting escape of NPs from the endosome to avoid degradation the use of peptides or pH sensitive groups can promote pH sensitive function or the fusion with membranes to escape from the endosome (194). Some materials such as PEI can induce a pH sensitive function by proton sponge effect leading to an osmotic pressure shift inside endosome and lysis will release the complexes (195). Similarly, cationic liposomes can help in fusion with the endosomal membrane and release the DNA through phase inversion (149). Another example where DOPE acts as a fusogenic lipid and interacts with endosomal membrane that lead to release of the therapeutic DNA, lipoplexes when prepared with DOPE/cationic lipid have shown structural transition and attain an inverted hexagonal phase (H_{II}) when the pH was changed from 7 to 4, the inverted hexagonal shape helps in interaction with the endosomal membrane leading to its destabilization and release of the DNA there by promoting the TE (196).

1.9 Peptide mediated ocular therapeutic cargo delivery

A large variety of peptide sequences were identified as potential enhancers of physical and biological functions for delivery systems. Cell-penetrating peptides (CPPs) are a diverse group of peptides that usually include a variety of peptides with many different functionalities. CPPs may include peptides from the following different functional categories, but peptides in these categories are not all necessarily a CPP: i) structural support and physicochemical stability enhancers; ii) Peptides for cell binding/ targeting and membrane translocation mechanism; iii) peptides for endosomal escape mechanism; iv) peptides for intracellular routing and organelle targeting; v) peptides for nuclear targeting.

The peptides can be attached to the gene cargo either by non-covalent addition or covalent conjugation techniques to the DNA itself or to the liposomal or polymeric carriers for transport. The non-covalent

bonding happens mostly due to the electrostatic and hydrophobic interactions and the excess peptides can form a coat around the DNA by hydrophobic and electrostatic interaction (197, 198). While covalent addition happens by forming a bond with the electron deficient group between peptide and lipids, polymers or oligonucleotides.

i) Structural support and physicochemical stability enhancers

Cationic peptides condense the DNA into small and compact particles and also facilitate delivery of the DNA to the target cells. The peptide sequence protects the DNA from degradation in serum and also serves to target cell surface proteins. Lysine and arginine-rich cationic peptides are frequently used in gene delivery. For example, cationic peptides with 13 or more lysine residues were shown to tightly bind and compact DNA to form particles of 50-200 nm. Other cationic peptide sequences such as YKAK₈WK, CWK₁₈ and CWK₁₇C improved the stability of the pDNA NPs and showed targeting ability (199). Chondroitin sulphate-coated and non-coated amphipathic and cationic rich peptide (CRHC and MGPE-9)-conjugated pEGFP-C2 polyplexes produced high transgene expression in ARPE-19 cells for retinal gene delivery (200).

Poly-lysine decorated PEG (CK30-PEG) NPs were able to deliver compacted plasmid DNA to retinal cells in eye of Balb/c mice. These NPs have high efficiency of compaction, carry gene cargo up to 20.2 kb and showed high GFP expression in RPE and photoreceptor cell after subretinal injection and in the RGC layer after intravitreal injection (138). The ellipsoidal shaped NPs made with trifluoroacetic acid (TFA) as counter ion have shown to had better TE compared to acetate counter ion. This increase in TE could be due to changes in the shape that enhanced the efficiency of movement and transfer of the NPs. Similarly, high level of gene expression was observed in RPE cells transfected with CK30-PEG NPs carrying RPE65 gene in an RPE 65 knockout mouse (RPE65^{-/-}) model of LCA disease (201, 202).

ii) Peptides for cell binding/ targeting and membrane translocation mechanism

Non-specific targeting is related to the physicochemical properties of the NP systems or the charge modifying peptides conjugated on to these systems. Non-specific binding maybe a charge interaction between the NP surface that possess cationic charge due to the components of the formulation or peptides with the negative charged cell membrane or based on a peptide sequence-specific binding mimicking a natural cell adhesion binding process. A good example for the latter is the arginine-glycine-aspartic acid (RGD) tripeptide sequence found in many ECM proteins that bind integrin molecules on cell surfaces. RGD is used for drug targeting in several therapeutic areas (see Section 1.10.1 for further discussion) (84, 203, 204).

In active targeting the interactions may be based on receptor-ligand interactions. The targeting or cell specific peptide sequences are ligands that mimic the binding sequences of a therapeutic protein or peptide. Antigen-binding fragments (Fab) derived from the antibodies are used for modifying immunogenicity and affinity towards antibodies of similar sequences (third generation antibody fragments or peptides) (205). These antibody fragments can help in actively targeting surface expressed antigen specifically such as in cancer. Antigen-binding short immunoglobulin sequences were also tried to target various disease conditions. Currently there are few approved Fab fragments for treating blood clots in angioplasty (abciximab), wet age-related macular degeneration (ranibizumab) and Crohn's disease (certolizumab), most of the immunoglobulin sequences currently in clinical trials are mostly anti-cancer agents. One such example from the single-chain variable fragment VB4-845 a humanized scFV conjugated to Pseudomonas exotoxin that targets epithelial cell adhesion molecule was used as cancer treatment (206).

CPPs that are classified under non-specific targeting peptides with membrane translocating properties lack specific targeting ability but can help deliver nucleic acids into the cell by direct cellular entry

through membrane translocation. The CPPs mediate the delivery of the cargo by helping to penetrate or translocate the gene cargo into the cells by either direct translocation or through endocytosis (207). Whereas cell targeting peptides (CTPs) recognize specific cell types in the tissue and target the gene cargo to those specific cell types and facilitate endocytosis (208, 209). Few examples of non-specific binding include surface modification with charged polymers and peptides include cationic amino acids $(Rn)_2KGGC$ or $(Kn)_2KGGC$, and peptides derived from cationic proteins such as TAT, KALA, GALA, penetratin (199). Peptides such as penetratin, TAT, poly-arginine and transportan were peptides that are known to translocate through the plasma membrane by an energy-independent pathway (210). It has also been identified that some peptides promote an endocytosis mechanism to get internalized into the cells (211). The use of such peptide-based delivery systems improves the transport of therapeutic agents to target sites and protect cargo from factors that would affect its stability (197). Penetratin conjugated to PAMAM and complexed with pRFP has shown improved delivery of the NPs to retinal layers. Penetratin is known to cause temporary disruption of the cell membrane by pore formation (212).

iii) Peptides for endosomal escape mechanism

CPPs are classified into two categories such as endosomolytic peptides and membrane-disrupting peptides, the endosomolytic peptides are known to buffer the endosome against the proton pump and lead to endosomal burst e.g. H5WYG and $CH_6K_3H_6C$, histidine groups are known to promote the endosomal disruption (213). KALA and TAT are known to disrupt the cell membrane by pore formation leading to translocation of the nucleic acids. The conjugation of these peptides can be carried out by either covalent or non-covalent conjugation (214). Many peptides and biomimetics were used to promote endosomal escape and improve the release of therapeutic complexes from the endosomes. Peptides such as haemagglutinin (HA2), HA2/PLL, TAT, KALA, GALA, penetratin and chemicals

such as polyethylenimine, poly(amidoamine) are few examples that have been successfully used as endosomal escape promoting agents by mechanisms such as fusion, pore formation, and proton sponge effect (215-217).

iv) Peptides for intracellular routing and organelle targeting

The peptides for cytosolic transport are known to promote the movement of the nucleic acids in the cytoplasm of the cells once they escape from the endosome. The nucleic acids released into the cytoplasm depending on their size and type will need to reach and cross the nuclear membrane. The conjugation of peptides sequences from dynein to nucleic acids is known to promote the movement of the nucleic acid inside the cytoplasm with the help of dynein proteins. Peptide sequences such as KSTQT, GIQVD and SKSCR improved trafficking in the cytoplasm utilizing dynein and microtubules (218).

v) Peptides for nuclear targeting

The NLS sequences are known to promote the entry or translocation of the nucleic acid into the nucleus of the cell through nuclear pores. The NLS peptide sequences can help in translocation of the gene cargo into the nucleus of the cell after internalization this helps in faster entry of the gene cargo into the nucleus and thereby promote quick expression of the therapeutic gene (219, 220). NLS peptides are mostly basic and charged peptides. Few examples of NLS sequences are Simian virus 40 (SV40) sequence PKKKRKV and KRPAATKKAGQAKKKK. As mentioned in the earlier sections the entry through the nuclear pore is promoted by the NLS sequences by improving the mobility by employing dynein, microtubules and importin- β that helps in faster movement of nucleic acid towards the nuclear membrane and can improve the TE (221). The protein importin- β is known to help in preparation of the nucleic acids for nuclear pore entry (222, 223).

1.10 Cell adhesion molecules

CAMs are a group of cell surface proteins expressed on membranes for cell-cell recognition and are involved in the activation of various cellular pathways during growth and development. CAMs are expressed in various tissues and are highly involved in the initial stages of the embryonic growth phase, proper development of neural tissues, cell growth and differentiation (224). CAMs are classified into 1. integrins, 2. IgSF CAMs, 3. cadherins and 4. selectins (225). IgSF CAM and cadherins mediate homophilic (between same molecules) or heterophilic cell-cell interactions, while integrins interact with components of the extra cellular matrix (ECM) (225-227). Selectins are a group of glycoprotein-based molecules, known as carbohydrate-binding proteins (228).

1.10.1 Integrins and integrin binding moieties in retinal gene delivery

Integrins are a class of heterodimeric transmembrane proteins, a family of 24 receptors with one α and one β subunit, that mediate adhesion to ECM proteins such as collagen, elastin, fibronectin and laminin (Frantz et al 2010). The RGD sequence is a major integrin-binding motif of ECM proteins and utilized in drug delivery system design for active targeting purposes. Generally, integrins play a role in ocular development, cell migration and inflammatory processes and tissue remodeling in the eye. Binding of RGD to integrin receptors lead to the activation of ERK pathway that modulates axonal growth and cell migration (229).

Integrin receptors, specifically $\alpha v \beta 3$ integrins, play a significant role in glaucoma as they are highly expressed in the TM, RGC layer and glial cells of the optic nerve head (230-232).

Recently, RGD oligopeptide was used as therapeutic agent for the treatment of ophthalmic diseases such as dry AMD in patients with vitreomacular adhesion and vitreomacular traction marketed as Luminate[®] RGD oligopeptide (ALG 1001) (233). Luminate[®] has also been tested to identify the safety and efficacy in inducing the posterior vitreous detachment to treat non-proliferative diabetic

retinopathy. A Phase 2 study (NCT02435862) carried out by Allegro Ophthalmics, LLC evaluated the RGD oligopeptide to treat posterior vitreous detachment induction in non-proliferative diabetic retinopathy. It was also shown that Luminate[®] treatment arrested or delayed progression to diabetic retinopathy by inhibiting the five types of integrin proteins known to promote angiogenesis (234).

In another study RGD peptide was used to target choroidal neovascularization (CNV) by Trf and RGD dual functionalized poly-(lactide-co-glycolide) NPs carrying the anti-VEGF gene to the CNV lesions. This was achieved by functionalizing the NPs with RGD and Trf to target delivery of anti-VEGF in the retinal layers and expression of the gene in the retinal vascular endothelial cells, photoreceptor and retinal pigment epithelial cells (235). Similarly conjugating iRGD (internalizing-RGD) and TAT peptide with poly(ethylene glycol)-poly(lactic-co-glycolic acid) NPs, the iRGD sequence was shown to specifically bind to $\alpha v\beta 3$, while TAT facilitated penetration through the ocular barriers after topical administration the NPs (84).

1.10.2 IgSF CAMs and their role in the eye

Proteins of the IgSF are involved in binding and recognition processes in many immunological and adhesion functions and contain at least one Ig domain that structurally resembles the variable or constant regions of antibodies. Neural IgSF CAMs are classified into several groups such as 1. IgSF CAMs with Ig domain(s) only, eg. P0, Thy-1, LAMP and MAG; 2. IgSF CAMs containing both Ig domain(s) and FNIII, eg. NCAM, L1 CAM, CHL1; 3. IgSF CAMs containing Ig domain(s), FNIII and tyrosine kinase domains in the cytoplasmic region, which are mostly involved in signal transduction and secretion of NTFs, eg. FGFR, TrK A, B and C; 4. IgSF CAMs containing small molecules that contain Ig as the extracellular domain, eg. Sema, epidermal growth factor (EGF) and leucine-rich repeat (Figure 1-8), The members of the IgSF CAMs play very distinctive roles in cell-cell interactions and aid in the development of neuronal structures (236).

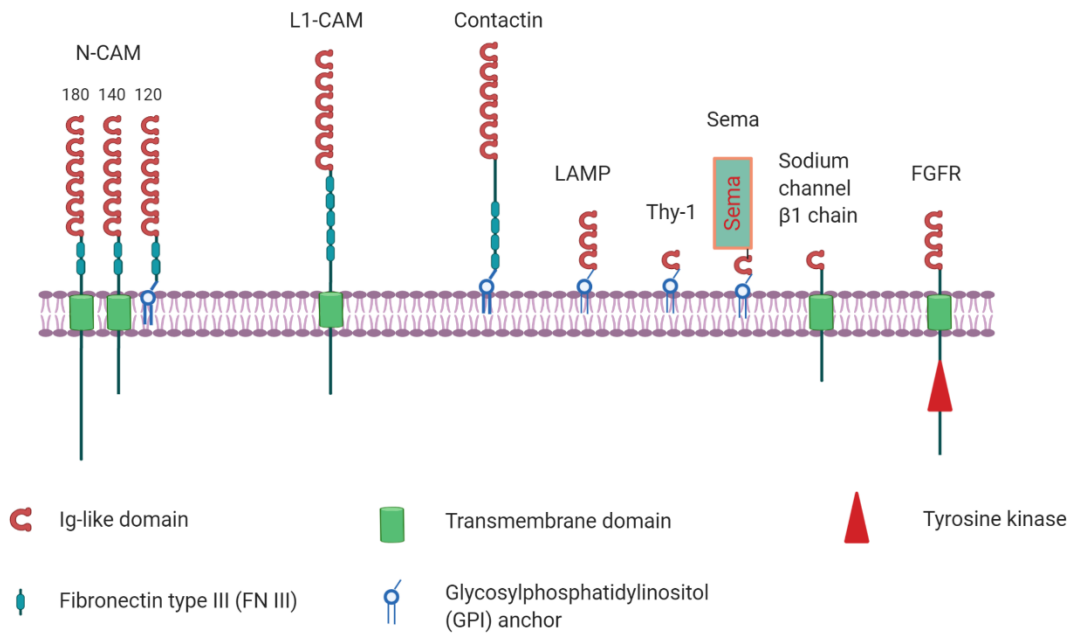


Figure 1-8 Structure of some immunoglobulin superfamily CAMs. Members of the IgSF have at least one Ig like domain, one or more fibronectin III domain, a transmembrane domain and a glycosylphosphatidylinositol and tyrosine kinase domain. Receptors from various sub-families such as Neural CAM (NCAM), limbic system associated membrane protein (LAMP) and fibroblast growth factor receptor (FGFR), Thy-1 were show (225, 237). Figure generated by Lokesh Narsineni using BioRender.com.

Chapter 2 Research Emphasis

2.1 Rationale

Current interventions for glaucoma focus mainly on managing the disease state and slowing progression by reducing the IOP by small molecules and surgical interventions. It is clear from recent research in this field that elevated IOP is just a contributing factor for glaucoma progression but the underlying causes such as, for example, the impairment of the bidirectional transport of NTFs, the activation of secondary mediators for apoptosis and many inflammatory processes including glial cell activation are also major pathways that contribute to disease progression. Intrinsic or extrinsic supply of NTFs was shown to be a viable strategy in protecting the health of RGCs and restoring vision. Moving towards alternative approaches in treating glaucoma is a long-awaited strategy. Hence, our focus in this thesis has been to deliver NTF support either through an extrinsic mechanism by delivering the gene capable of making the protein using the host's own cells. Current delivery systems have limited capability to deliver such macromolecules and gene cargo into the host cells. Many viral vectors have been used to deliver such gene cargo, but due to the more significant limitations such as immunogenicity and insertional mutagenesis, we focused on non-viral vectors. Despite holding an excellent potential for compacting a large size gene cargo, non-viral vectors lack specificity and targeting ability to deliver genes to targeted organs. Many lipid, surfactant and polymer based non-viral vectors were tried to deliver gene cargo into the retinal layers of the eye but crossing all the physicochemical barriers and achieving therapeutic levels at the target site has been one of the biggest challenges for these kinds of systems. Hence, to address these challenges, our focus and scope of this thesis was to develop targeted non-viral gene delivery systems that are capable of delivering plasmid DNA to retinal cells in the eye by conjugating a peptide functional moiety identified from the IgSF with second-generation m-7NH-m gemini surfactants and formulating NPXs. Such conjugation will

lead to addition of targeting functionality and cell surface recognition to bind and deliver the gene cargo into the targeted cells in the eye.

2.2 Hypothesis

2.2.1 Main hypothesis

The main hypothesis is that peptide-modified gemini nanoparticles will improve delivery of plasmid DNA encoding reporter gene/BDNF to the retina after intravitreal administration *in vivo* in a normal rat model and result in measurable BDNF gene expression.

2.2.2 Sub hypothesis

Sub hypothesis 1: Modified synthesis of dimeric m-7NH-m gemini surfactants by one-pot DMAP free method can produce higher yield of m-7NH-m gemini surfactant free from DMAP and m-7N(m)-m trimeric gemini impurity and can be used as a building block for conjugation of peptide to synthesize peptide functionalized gemini surfactants.

Sub hypothesis 2: Integrin-binding or IgSF-cell adhesion peptide (CAP) modified m-7N(p)-m gemini surfactants and plasmid DNA form nanoplexes (NPXs) and target the retinal cells in the eye, by efficiently transferring the reporter gene or NTF gene to the retina after intravitreal administration in a normal rat model.

Sub hypothesis 3: CAP-functionalized gemini NPXs (pGP-NPXs) can be evaluated in a ‘mini retina’ like 3D retinal neurospheres to assess the potential of the gene delivery system to deliver the gene cargo in a 3D like environment simulating retina helping to establish *in vitro-in vivo* correlations.

Sub hypothesis 4: *In silico* assessment of unmodified and peptide modified gemini surfactants as potential amyloid- β aggregation inhibitors by molecular docking studies, can serve as a tool for validating and establishing the *in silico-in vitro* correlation.

Sub hypothesis 5: m-7NH-m, m-7N(m)-m and m-7N(p)-m gemini surfactants can also reduce amyloid-beta aggregation which is known to contribute to glaucoma and prevent aggregation of A β fibrils to form higher order insoluble oligomers.

Chapter 3 Improved synthesis and formulation design of dimeric and trimeric gemini surfactants and their evaluation as gene delivery vectors

3.1 Background

The structure activity relationship between the gemini surfactants and the mechanism of internalization and release from endosome and various other properties of the NP shape and their phase inversion behavior to form multiple structures at various pH were discussed (135). Gemini surfactant NPs were evaluated for topical delivery of pGTmCMV.IFN γ -GFP plasmid into skin and it was demonstrated that the gemini NPs have improved IFN γ expression by 3-5 fold compared to naked DNA treatments and 4-6 fold compared to Dc-chol-DNA complexes. It had been observed that with decreasing CMC the transfection efficiency increased and also the DNA compaction was affected when excess gemini surfactant was present in the formulation. A balance between the charges on the DNA and gemini surfactants was vital to obtain an optimal formulation with high TE (136).

The evolution of gemini surfactant structures and classification was discussed in detail in Chapter 1, Section 1.6.

Gemini surfactant chemistry is quite versatile, and many new derivatives can be created. Several groups, including ours, created compound libraries with varying alkyl tail and functional spacer groups (157, 159, 163, 181) as well as amino acid and short peptide conjugation (166, 167, 175, 238) to enhance gene delivery.

The structural modifications produce new surfactant molecules that behave very differently from their parent molecule. For example, modification of the simple polymethylene spacer of m-s-m first generation gemini surfactants with an amino group, produced m-7NH-m second generation gemini

surfactants with pH-sensitive functionality (157, 159, 181). Additionally, this amino substituted gemini compound library with varying carbon chain length serves as the parent compounds for the third-generation peptide-conjugated gemini surfactants.

The most recent research is aimed at providing further functionalities to NPs made from gemini surfactants, such as targeting ability (167), optimization of the DNA release kinetics intracellularly (239), various other types of gemini surfactants were also synthesized and tested for their efficiency in delivering plasmid DNA to various targets (175, 238, 240).

3.1.1 Traditional methods of gemini synthesis and advantages of the one-pot reaction method

Early synthesis of gemini molecules was carried out with ionic head groups and a rigid spacer by reacting α,α' -di-bromo-*p*-xylene with a dianionic long-chain alkyl phosphate and another series by phosphorylating with POCl₃. The resulting compounds were purified by recrystallization as sodium salts (156, 162). Pertaining to the scope of this project most of the data represented in this project focus on m-s-m, m-7NH-m, m-7(m)-m gemini surfactants. Comprehensive approaches of gemini synthesis using two methods were described by Zana and coworkers (169). Various gemini surfactants with m=12 and varying spacers s= 2 to 12, and m=16 with spacers from s= 2 to 8 were synthesized. This was one of the first papers published outlining the synthesis of m-s-m gemini surfactants (169). Gemini surfactants with varying tails (m) and spacers (s) were synthesized using method A, which involved reaction of the α , ω -dibromoalkanes with *N,N,N*-octyl-, -dodecyl, or -hexadecyldimethylamine). Method A worked better for $s \geq 3$, however, this method was later not pursued due to the formation of CH₃ groups from unreacted CH₂Br groups, especially in the reactions with s= 1 or 2. In method B, reactions were carried out between α , ω -bis(dimethyl-amine) with 1-bromo-*n*-dodecane or *n*-hexadecane in dry ethanol and refluxed for 48 hours at 80°C to induce biquaternization, and surfactants

were recrystallized by using various solvent mixtures such as ethanol-ethyl acetate and acetone-ethyl acetate for $m=12$ compounds and chloroform-ethyl acetate for $m=16$ compounds (169).

The synthesis of m - s - m surfactants, that is now routinely followed, is a one-step process (Zana et al. 1991). Although with the introduction of second-generation amino substituted gemini surfactants more complicated protection, deprotection and multiple recrystallization steps are required to achieve the incorporation of the amino group into the spacer. Wettig et al. (2007) used the Boc protection method to protect the amino group in the 3,3'-iminobis(*N,N*-dimethylpropyl-amine), protection of amino group before proceeding with the quaternization, which is important to prevent the nucleophilic attack by the secondary amine with 1-bromododecane. In the reaction 1,1,4,7,10,10-hexamethyl-triethylenetetramine or 4-(dimethylamino) pyridine were used as base during the Boc protection (157, 241). These methods involve multiple steps and use large amounts of chemicals and solvents to synthesize the final products. In addition, during the purification steps, the recrystallizations result in yields that are often lower than 40% and many impurities and by-products may remain after the final recrystallization.

The one-pot synthesis is generally considered as the most efficient and most economical process for synthesizing an organic molecule, due to important benefits of this type of synthesis such as the use of lower volumes of organic solvents, smaller amounts of catalysts and starting products.

Recognizing the shortcomings of the existing synthesis method, an improved synthesis method was developed for the synthesis of m -7NH- m gemini surfactants. A one-pot reaction scheme was introduced where protection and nucleophilic bond formation steps are incorporated into a single reaction without multiple recrystallization. This approach saves time, chemicals, and more importantly, provide higher yields of the final product (242). Also, a solvent-free technique was adapted for Boc protection of the amine group in the spacer (243).

3.1.2 DMAP-free, solvent-free technique for Boc-protection of NH group in m-7NH-m gemini surfactant synthesis

Boc protection of amines can be carried out using many available Boc protecting agents such as di-*(tert*butyl) decarbonate (Boc_2O), *tert*-butyloxycarbonyloxyamine (BocONH_2) and *N-tert*-butyloxycarbonyl azide (BocN_3). Of these, Boc_2O is one of the most commonly used. *N,N*-dimethylpyridin-4-amine (DMAP), a catalyst, is generally combined with the Boc to speed up the protection reaction. While other catalysts are also used, DMAP is an efficient and suitable catalyst generally preferred (244). For example, DMAP has been used in Boc protection of 3,3'-iminobis(*N,N*-dimethylpropyl-amine) during m-7NH-m gemini surfactant synthesis (157). But DMAP can be difficult to remove when used in a Boc protection reaction, which is important, since residues could lead to potential cellular toxicity due to their high reactive nature with amines. It is also emphasized that using acetonitrile as a solvent and DMAP together in a Boc protection reaction cannot be carried out due to the production of mixtures of products that are hard to isolate from the reaction mixture (243). Hence, a solvent-free and catalyst-free method can provide a DMAP-free final product and a solvent-free technique that can contribute to improved synthetic and recrystallization methods by avoiding the use of non-recyclable reagents in the reaction.

3.1.3 Effect of DOPE on nanoparticle formulations and non-viral gene delivery systems

Lipids and lipidoids are major building blocks for LPXs (liposomes, complexes, NPs or nano-carriers) used for gene delivery. Many different cationic (245) and neutral lipids (246) have been employed in gene delivery. Pseudo-glycerol lipids, multi-valent lipids, bio-reducible and dimerizable lipids and various modified gemini surfactant lipids were used as gene delivery agents(247). Ionizable lipids such as heptatriaconta-6,9,28,31-tetraen-19-yl 4-(dimethylamino)butanoate (DLin-MC3-DMA or MC3) and 2,2-dilinoleyl-4-(2-dimethylaminoethyl)-[1,3]-dioxolane (DLin-KC2-DMA or KC2) have been used for gene silencing in hepatocytes(248) . Some of the earliest used cationic lipids were DOTAP and

DOTMA (148, 249, 250). Most cationic lipids were used in combination with other neutral lipids such as DOPE to facilitate transfection by providing a better surface charge balance and modify the structural characteristics of the LPXs. The combination of DOTMA and DOPE complexes had higher transfection and delivery of plasmid DNA by facilitating fusion of LPXs with the cell membrane (148.) It has been shown that at low pH in endosomes the presence of DOPE causes phase transition from a dominant condensed lamellar phase to various other polymorphic phases such as inverted hexagonal phase, inverted cylindrical micelles or cubic phase (251, 252).

3.2 Rationale and objective

Current protocols for m-7NH-m (m=12,16,18) synthesis use Boc₂O protection and DMAP as a catalyst, however, despite performing multiple recrystallizations and purification steps DMAP appears as a contaminant in the final product. The current synthetic schemes also produce both dimeric (m-7NH-m) and trimeric (m-7N(m)-m) surfactants after completing the synthesis as per published protocols. Multiple recrystallizations and purification, using various methods have failed to separate both species from the final product, as confirmed through ¹H-Nuclear Magnetic Resonance spectroscopy (¹H NMR) and mass spectrometry. The presence of DMAP and the existence of two species of gemini surfactants, one with three alkyl tails, may lead to increased toxicity and inconclusive results. Another relevant issue is related to using DOPE, a neutral lipid, in making the gemini LPXs. To address these issues, a solvent-free, DMAP-free synthesis of m-7NH-m gemini surfactant was assessed and by adapting a one-pot rapid synthesis technique, a pure product was synthesized, and the recrystallization protocols were modified to yield pure m-7NH-m gemini surfactant. DOPE was previously reported to be beneficial to increase TE but DOPE can also be toxic to cells (196). The effect of DOPE on the TE and toxicity in A7 astrocytes was assessed by a confocal microscopy and flow cytometry approach. This assessment provided vital information on the need for retaining DOPE in the gemini nanoparticle

formulation. Also, it was assessed if gemini surfactant based NPXs without helper lipids can act as a potential gene delivery vehicle without any additives and lipids included in the formulation.

3.3 Materials and Methods

The general and improved schemes for synthesis of m-7NH-m (m=12, 16 and 18) gemini surfactants is illustrated in Scheme 1 A, B and C and m-7N(m)-m gemini surfactant in

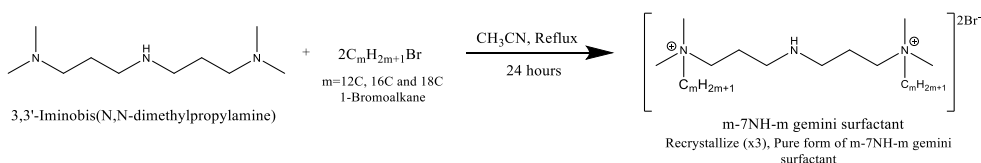
Scheme 2. All reactions were carried out under nitrogen using Radley's Carousel 6 Plus reaction station™ (Saffron Walden, Essex, UK). 3,3'-iminobis(*N,N*-dimethylpropylamine), (MW: 187.33g/mol, 97%), di-*tert*-butyl dicarbonate (Boc₂O) (MW: 218.25g/mol, >99%), acetonitrile anhydrous (MeCN) (99.8%), 1-bromododecane (MW:249.24g/mol, 97%), 1-bromohexadecane (MW:305.33g/mol, 97%), 1-bromooctadecane (MW:333.38g/mol, 97%), TFA (MW:114.02 g/mol, 99%), triisopropylsilane (TIS) (MW:158.36 g/mol, 98%) were purchased from Sigma-Aldrich (Oakville, ON, Canada). For formulations and assays molecular grade water (Fisher Scientific, CA, USA) or Milli-Q water (Millipore EMD, Canada) was used. DOPE was obtained from Avanti Polar Lipids, (Alabaster, AL, USA), gWiz™ GFP plasmid, pUMVC1 mock plasmid with no reporter gene was from Aldevron (Fargo, ND, USA).

3.3.1 Synthesis of m-7NH-m dimeric gemini surfactants by one-pot, DMAP-free technique

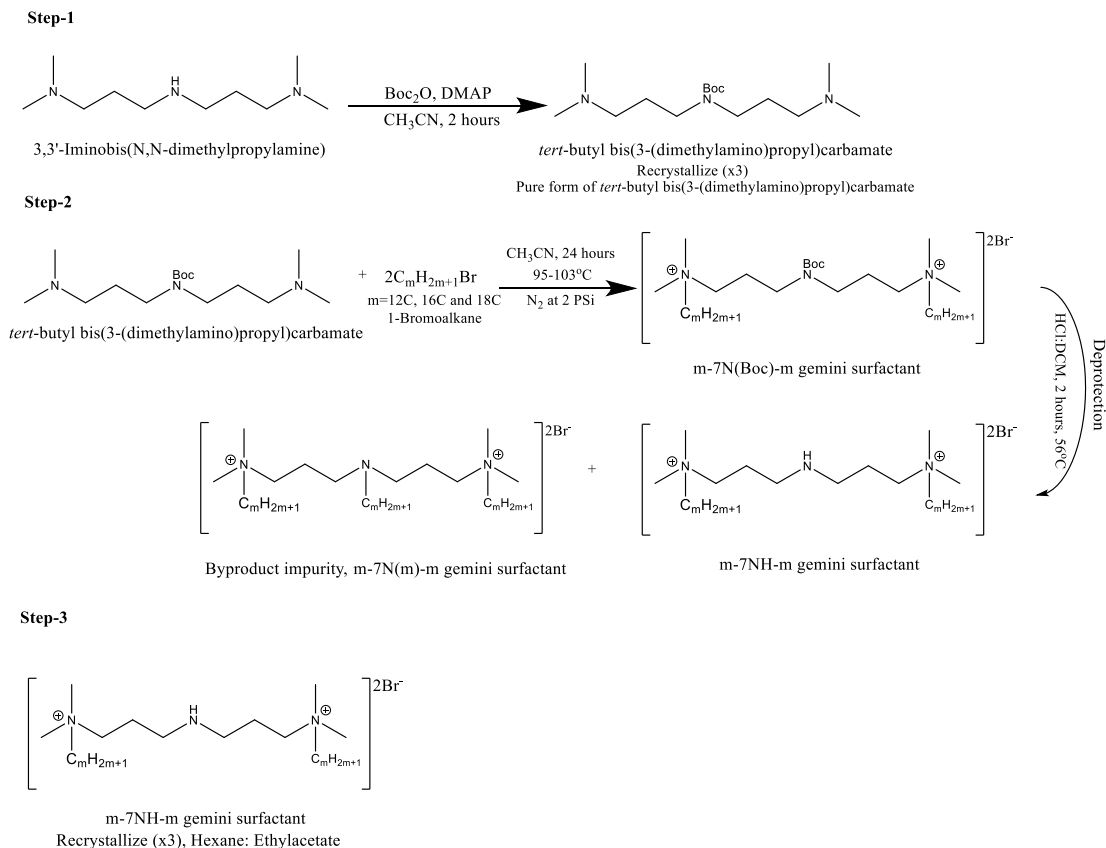
Synthesis of m-7NH-m (m=12, 16 and 18) gemini surfactants was previously reported (156, 157, 162, 169, 171) with 7C spacer group between the two polar head groups. Batches of 12-7NH-12, 16-7NH-16 and 18-7NH-18 have been synthesized previously in our lab using the above protocols and were used as reference compounds to compare the properties of NP formation, TE and toxicity with the m-7NH-m gemini surfactants synthesized using the improved protocol in this work. The gemini surfactant synthesis (Scheme 1 C) with amino substitution spacers was carried out in a Radleys reaction flask by Boc protection of 1 equivalent (0.01 M) of 3,3'-iminobis(*N,N*-dimethylpropylamine) using a 1.2

equivalent (0.012 M) of Boc_2O reagent directly without use of any other solvent. The reaction mixture was stirred at room temperature for 4 hours. Once the protection reaction was complete, 50 mL/3g of acetonitrile was added to the reaction vessel, followed by 2.1 equivalents of either 1-bromododecane (12-7NH-12) or 1-bromohexadecane (16-7NH-16) or 1-bromooctadecane (18-7NH-18), respectively and the reaction was run under nitrogen atmosphere at 2 Psi and 95°C for 24 hours.

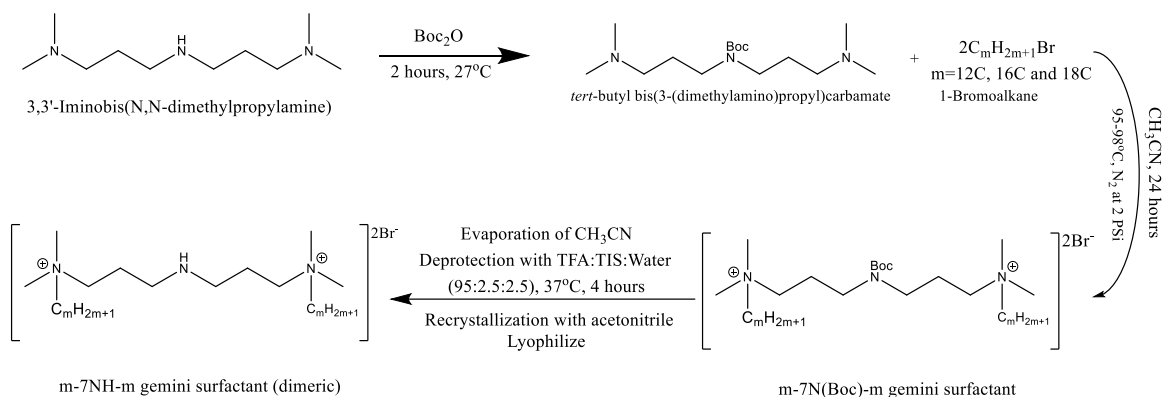
A)



B)



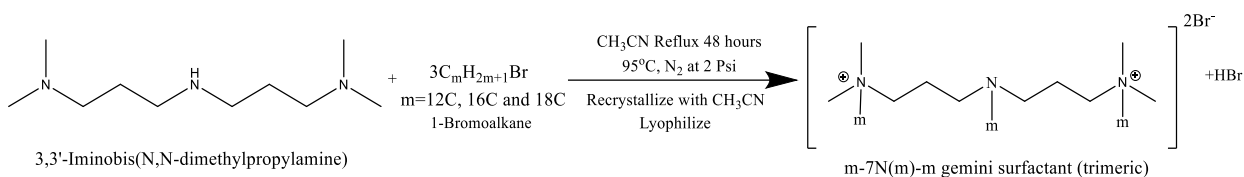
C)



Scheme 1 General and improved schemes for synthesis of m-7NH-m dimeric gemini surfactant A) General scheme for synthesis of m-7NH-m gemini surfactant from published protocols B) Synthesis method 1 with improvement from published schemes by using Boc protection and C) Synthesis method 2 current improvement using solvent-free, DMAP-free Boc protection, one-pot scheme. (m=alkyl tail chain length C₁₂, C₁₆ and C₁₈), DMAP- Dimethylaminopyridine, DCM-Dichloromethane, TFA-Trifluoroacetic acid, Boc₂O- *Di-tert*-butyl decarbonate and HCl- Hydrochloric acid.

Completion of the reaction was monitored using thin layer chromatography (TLC) on silica gel plates (TLC silica gel 60 F₂₅₄, Merck, MA, USA) and visual spots were developed using iodine vapors. After 24 hours, the reaction flask was cooled down to room temperature (RT) and the precipitate was filtered using a filtration apparatus with a Whatman filter 1 (Whatman™, Buckinghamshire, UK). Filtered precipitate was recrystallized successively using acetonitrile three times. The deprotection was carried out using TFA cleavage cocktail TFA/TIS/Water (95:2.5:2.5) and the excess TFA was evaporated by rotary evaporator (Heidolph, Schwabach, Germany). Precipitate was extracted by adding water into the flask to dissolve the pure surfactant and lyophilized using a Labconco Freezone 1 freeze dryer (Labconco, MO, USA) to obtain pure m-7NH-m gemini surfactant. Purity and identification of the surfactants was by mass spectrometry, ¹H NMR spectroscopy (Avance 500 MHz, Bruker, MA, USA)

using CDCl_3 as a solvent, and surface tension measurement was carried out using a Lauda TE3 automated tensiometer (Lauda, Germany) based on du Nuoy ring tensiometry technique.



Scheme 2 General scheme for synthesis of $m\text{-7N}(m)\text{-m}$ trimeric gemini surfactant using one-pot scheme. Quaternization using 1-bromo- m -alkane ($m=12\text{C}, 16\text{C}$ and 18C).

3.3.2 Synthesis of $m\text{-7N}(m)\text{-m}$ trimeric gemini surfactants using one-pot method

The trimeric bis-quaternary gemini surfactant synthesis was carried out with alkyl tail ligation at both the quaternary nitrogens and on the amino substitution in the spacer in a Radley's reaction flask. One equivalent (0.01M) of 3,3'-iminobis (N,N -dimethyl propylamine) reagent was added and 50mL/3g of acetonitrile was added to the reaction vessel. Then 3.1 equivalents (0.031M) of either 1-bromododecane (12-7N(12)-12) or 1-bromohexadecane (16-7N(16)-16) or 1-bromooctadecane (18-7N(18)-18) was added for the respective gemini surfactant synthesis and the reaction was run under nitrogen atmosphere at 2 Psi, at 95°C for 48 hours. Completion of the reaction was monitored by TLC. After 48 hours, the reaction flask was cooled to RT and the precipitate was filtered using a filtration apparatus with Whatman filter paper 1. Filtered precipitate was recrystallized successively using acetonitrile three times. Precipitate was extracted by adding water into the flask to dissolve the pure surfactant and lyophilized to obtain pure $m\text{-7N}(m)\text{-m}$ gemini surfactant. Purity of the surfactants was assessed using mass spectrometry and ^1H NMR spectroscopy using CDCl_3 as a solvent.

3.3.3 Formulation of $m\text{-7NH-}m$ and $m\text{-7N}(m)\text{-m}$ gemini NPXs and LPXs

Formulation of $m\text{-7NH-}m$ and $m\text{-7N}(m)\text{-m}$ ($m=12, 16$ and 18 C, alkyl tail) gemini surfactants was carried out using two different compositions. Here after, for the scope of this thesis the NPXs are

composed of gemini surfactant (m-7NH-m or m-7N(m)-m) and plasmid (GP) and LPXs are composed of gemini surfactant, plasmid and DOPE neutral lipid (GPL) and are referred to as LPXs (Figure 3-2). The NPs were prepared at various ratios such as 2.5:1, 5:1, 7.5:1 and 10:1 (G:P) and DOPE vesicles were added at 1:0.5 and 1:1 (G:L) weight ratio to assess the effect of charge ratio and lipid ratio on TE and viability.

Various optimizations and performance improvement assessments were carried out to improve the TE and to lower the toxicity of gemini surfactants using a modified protocol. To select the most optimum composition and component ratios for subsequent experiments, m-7NH-m and m-7N(m)-m NPXs and LPXs were screened in A7 astrocyte cells *in vitro*.

Optimizations performed: 1. Comparison of TE and toxicity of gemini surfactants old stock (OS) and new stock (NS) at varying ratios (2.5:1, 5:1, 7.5:1 and 10:1), 2. Effect of duration of NPXs and LPXs treatment (5 hours of incubation or longer) and gene expression kinetic study for 24, 48 and 72 hours by flow cytometry, 3. Effect of DOPE lipid inclusion and ratio in the formulation on TE and toxicity by flow cytometry and confocal microscopy.

3.3.3.1 Formulation of NPXs

The assembly process was carried out by mixing the required amount of plasmid solution with a calculated amount of gemini surfactant solution to get required charge ratio $\rho \pm$ 2.5:1, 5:1, 7.5:1 and 10:1. The mixture was left at room temperature for 15 minutes for the plasmid to form complexes with gemini surfactants by charge interactions and obtain highly compacted NPXs (Figure 3-2). TE studies were performed in A7 astrocyte cell culture in 96-well plates at a plasmid dose of 0.5 μ g/well.

3.3.3.2 Formulation of LPXs

In this formulation modality the plasmid was first mixed with gemini surfactant to obtain the required charge ratio $\rho \pm$ 2.5:1, 5:1, 7.5:1 or 10:1 and incubated for 15 minutes to form G:P complexes (NPXs).

DOPE helper lipid vesicles (5mM; preparation protocol section 3.3.3.3) were added to the G:P complexes at G:L- 1:0.5 or 1:1 weight ratio to form LPXs. TE studies were performed in A7 astrocyte cell culture in 96-well plates at plasmid dose of 0.5 $\mu\text{g}/\text{well}$.

3.3.3.3 Preparation of DOPE vesicles using LV1 microfluidizer

DOPE helper lipid vesicles were prepared using a high-pressure LV1 Microfluidizer (Microfluidics Corporation, Newton, MA, USA) (Figure 3-1). Five mM DOPE dispersion was prepared in 9.25% (w/v) sucrose solution at pH 9, followed by bath sonication (Branson Ultrasonics, CT, USA) for 15 minutes to disaggregate any larger particles. The DOPE dispersion was processed through the LV1 Microfluidizer (module Z8; 87 μm pore size) after priming it with 2mL of sucrose solution. The particle size reduction at high pressure allows the lipid to form self-assembled vesicles and translucent solution of DOPE vesicles was obtained. The fine DOPE vesicles were filtered using a 0.45 μm poly-ether sulfone (PES) or cellulose acetate filter.

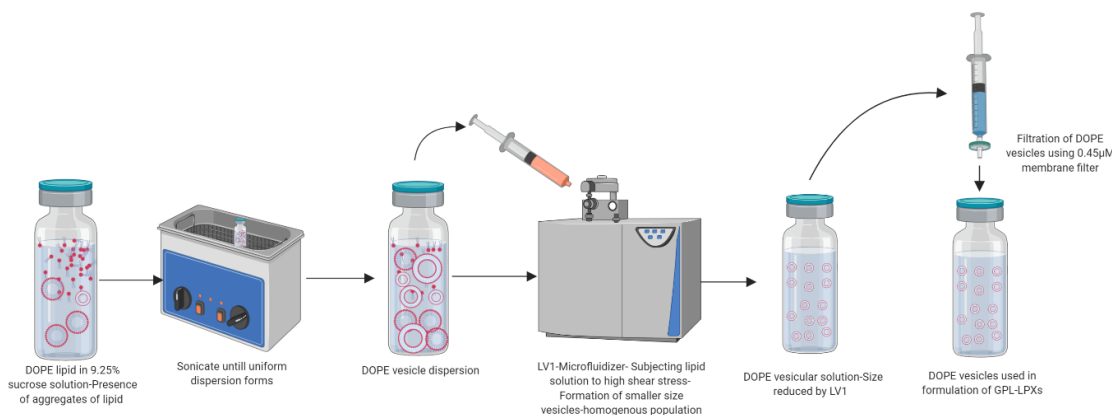


Figure 3-1 DOPE vesicles processing and nanoparticle assembly. DOPE vesicles were prepared using LV1 Microfluidizer: DOPE lipid in 9.25% sucrose solution, pH=9, sonicated to form uniform dispersion; DOPE dispersion is homogenized in an LV1-microfluidizer until uniform liposomes obtained; liposomes are filtered through 0.45 μm filter. Figure generated by Lokesh Narsineni using BioRender.com

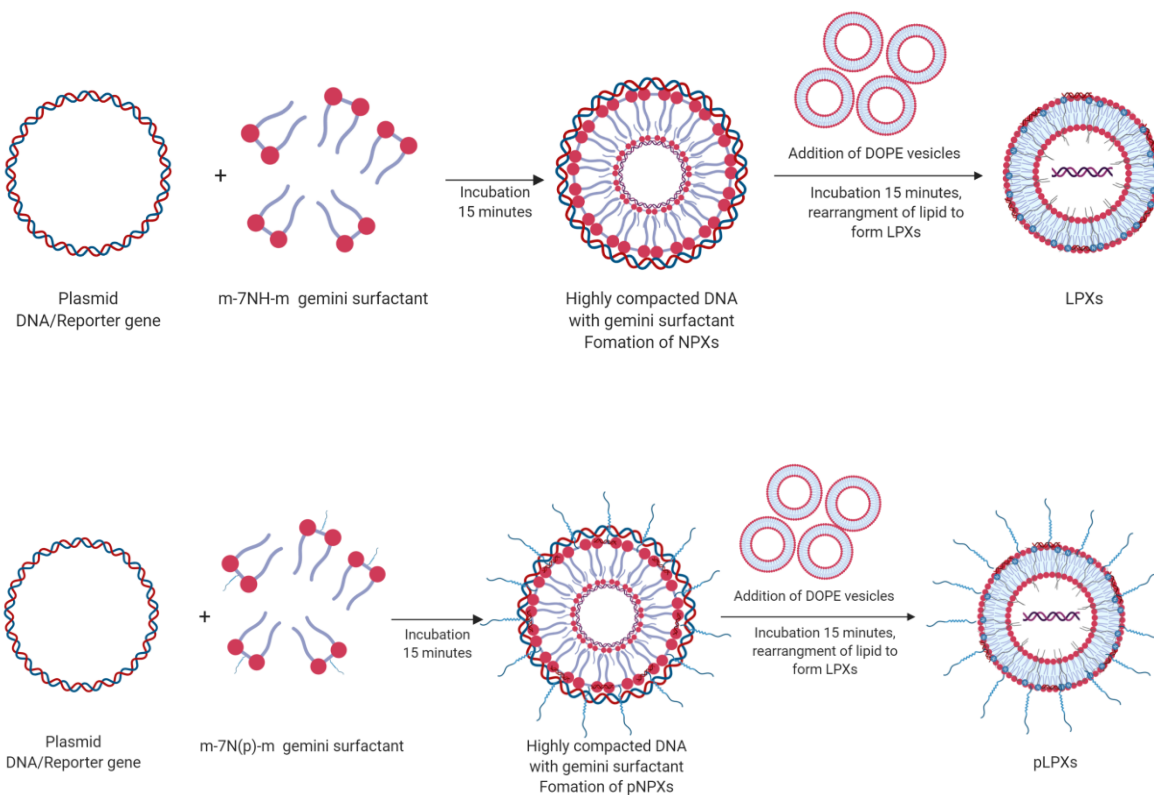


Figure 3-2 General formulation steps and schematic models of compacted NPXs/pNPXs and LPXs/pLPXs. Figure generated by Lokesh Narsineni using BioRender.com.

3.3.4 Characterization of gemini surfactants and nanoparticle systems

Gemini surfactants synthesized using Scheme 1 C and Scheme 2 were characterized using Electrospray ionization-mass spectrometry (ESI-MS), ^1H NMR spectroscopy and their CMC was determined by du Noüy ring tensiometry. NP characterization was carried out to determine size and zeta potential by dynamic light scattering (DLS) technique.

3.3.4.1 ESI-MS and ¹H NMR spectroscopy

ESI-MS and ¹H NMR spectroscopy were used to determine the purity and identity of the obtained gemini surfactants. The gemini surfactants were dissolved in 50:50 mixture of methanol: formic acid (99.9:0.1%) and water: formic acid (99.9:0.1%). The aliquot was injected into the Thermo Q-Exactive hybrid orbitrap system using low- or high-resolution analysis coupled with ESI ion source (positive mode). ¹H NMR analysis of the gemini surfactants was carried out using Bruker Avance 300 MHz and 500 MHz instruments with fully automated probe tuning. Samples were dissolved in deuterated chloroform (CDCl₃) and ¹H NMR analysis was carried out to determine the chemical shifts of the gemini surfactants. Evaluations were carried out at Department of Chemistry, University of Waterloo.

3.3.4.2 CMC determination

Surface tension measurements for 18-7NH-18 was carried out using the du Noüy ring tensiometry method on Lauda TE3 model automated tensiometer. Surface tension was measured after calibrating the tensiometer using standard weights. The vessel was filled with 40mL of ultrapure water and the concentrated surfactant solution (130µmol/L) was titrated into the ultrapure water and the surface tension was measured after every addition. The water-bath was kept at 45°C ± 0.1°C during the surface tension measurements. Surface tension values were subjected to Harkin and Jordan's correction and used to determine the CMC from a surface tension vs logarithmic concentration plot.

3.3.4.3 Particle size and zeta potential analysis

Particle size analysis of NPXs and LPXs was carried out by DLS technique using Zetasizer Nano ZS (Malvern Instruments, Worcestershire, UK). Particle size distribution is determined by using 60µL samples with 10 repeat readings setup on each sample were performed by the instrument and averages were reported. particle size reported for each sample was as an average of three independent samples

nm \pm SD (n=3). Zeta potential provides valuable information about the colloidal stability of the particles by determining the surface charge of the electrical double layer on the particles. The measurements were carried out using phase analysis light scattering and a mixed mode technique using Zetasizer Nano ZS (Malvern Instruments). The analysis was carried out in a specialized folded capillary cell (DTS1070) with gold plated electrodes. NPX and LPX samples were diluted with ultrapure water at 1:25 (v/v) ratio and measured by taking an average of at least three readings. The zeta potential values are reported as mV \pm SD (n=3).

3.3.5 Transfection efficiency and viability studies by flow cytometry

A7 astrocytes from rat (received from Dr Jeremy Sivak, University of Toronto) were cultured in Dubecco's modified eagle's medium (DMEM)/high glucose media (Hyclone, GE Healthcare Life Sciences, Logan, Utah, USA) supplemented with 10% fetal bovine serum (FBS) (Hyclone, GE Healthcare Life Sciences, Logan, Utah, USA) and 1% Penicillin/streptomycin (Hyclone, GE Healthcare Life Sciences, Logan, Utah, USA) at 37 °C in a 95% air/5% carbon dioxide atmosphere. Cells were seeded in 96-well flat bottom tissue culture plates (Grenier Bio-one, Monroe, NC, USA) at 15,000 cells/well. After 24 hours, at 80-90% confluency complete media was removed from the plates and replaced with fresh basic media (without serum). Formulations were freshly prepared and used immediately. Cells were treated with formulations containing 0.5 μ g of pDNA/dose per well and incubated for 5h at 37 °C in an incubator (VWR scientific, PA, USA). After 5 hours the basic media was replaced with complete media and incubation continued for 24 or 48 hours. After the incubation period cells were detached from the plate using Accutase™ (Innovative Cell Technologies, San Diego, CA, USA) and stained with MitoTracker Deep Red FM (500 nM) (Thermo Fisher Scientific), in Accumax™ (cell dissociation solution) (Innovative Cell Technologies, San Diego, CA, USA) and incubated for 30 minutes. After incubation, TE (%) and viability (total live population %) were

analyzed by Attune[®] acoustic focusing cytometer with auto-sampler (Life Technologies, Carlsbad, CA, USA). The expression of GFP was detected using the BL1 channel excited by a 488 nm laser and captured with a band pass filter of 530nm \pm 30nm for GFP detection and the red fluorescence of Mitotracker[™] Deep Red was excited using the 638 nm laser and was detected using a RL1 channel and captured with a band pass filter of 650nm \pm 20nm. Photo multiplier tube (PMT) voltages for forward scatter and side scatter of A7 astrocytes were set at 1300 and 2400 mV respectively. Whereas, the voltages for BL1 and RL1 channels were set at 1500 mV and 1400 mV respectively.

3.3.6 Kinetics of gene expression in A7 astrocytes treated with NPXs

To establish the peak gene expression kinetics for gemini surfactant NPXs, A7 astrocyte cells were plated in three 96 well plates (as per protocol mentioned in 3.3.5), at 80% confluency they were treated with gemini NPXs at various ratios 2.5, 5:1 and 7.5:1 (gemini: gWIZ-GFP plasmid). Each plate was processed for analysis at 24-, 48- and 72-hours incubation using flow cytometer. Cells were assessed for TE and viability using Mitotracker[™] Deep Red as viability stain to identify the time point for peak gene expression analysis. Additionally, the effect of gemini NPXs incubation time on TE and viability was assessed at 24, 48- and 72-hour time points, after the removal of NPXs at the 5-hour time point or after continuous exposure for the total incubation.

3.3.7 Assessment of helper lipid DOPE as a formulation component by flow cytometric and confocal microscopy

The role of DOPE helper lipid in the formulation of a gemini surfactant NP system in improving TE and its effector cell toxicity was evaluated in A7 astrocytes. LPXs with varying concentration of DOPE helper lipid (1: 0.5, 1:1, 1:1.5 and 1:2.0 ratio of gemini:DOPE) and NPXs without DOPE were formulated and tested for TE and viability in A7 astrocytes as described in Section 3.3.3, gWIZ-GFP was used as a reporter gene. The ratio of G:P used for this study was 5:1. For the confocal microscopic

study 30,000 cells per well were plated in 24-well glass-bottom multiwell plates (MatTek Corporation, Ashland, MA, USA) (as per protocol in Section 3.3.5). After 24 hours, cells were treated with NPXs (2.5:1, 5:1 and 7.5:1 G:P ratio) and LPXs (with 1:0.5 ratio of gemini:DOPE with the above-mentioned ratios of NPXs) in serum free DMEM media. After 5 hours, the serum free media were replaced with complete media (DMEM high glucose with FBS) and incubation continued for 24, 48 and 72 hours. Confocal microscopic imaging of the treated and control wells was carried out on a Zeiss LSM 710 confocal laser scanning microscope (CLSM) (Carl Zeiss AG, Oberkochen, Baden-Wü, Germany) using 20x objective. Cells were stained with 5 μ M DRAQ 5 (Thermo Fisher Scientific, Waltham, MA, USA) as a nuclear stain. At least three areas of each well were captured to determine the TE and viability.

3.3.8 In vitro corneal penetration studies using the 3D EpiCorneal™ model

Corneal tissue interaction studies for dimeric and trimeric gemini surfactants, specifically 18-7NH-18 and 16-7N(16)-16, were carried out using EpiCorneal™ COR-100 (MatTek Corporation, Ashland, MA) (Figure 3-3) to determine the degree of adherence and penetration ability of the NPXs. Cy5 labelled gWIZ-GFP was used to track the movement and gene expression of NPXs in the corneal tissue after treatment. Each well received 50 μ L of formulation with 2.5 μ g of Cy5 labelled gWIZ-GFP at 5:1 (G:P) ratio. Experimental steps are shown in (Figure 3-4). Briefly, on the day of the experiment after the equilibration of the tissues, media was aspirated from each well and replaced with 1 mL fresh, prewarmed media and incubated again for 1 hour. Tissues in each well were dosed with NPXs. After dosing the tissues were returned to the CO₂ incubator for 0.5 and 1 hour for the tissue penetration study. At each time point tissues were isolated from the plate, washed with phosphate buffer saline (PBS) three times to simulate removal of surface-bound NPXs by tear, and stained and processed for imaging

using CLSM. Calcein AM (Invitrogen, Thermo Fisher Scientific) was used as a live cell stain and Image IT[®] (Invitrogen, Thermo Fisher Scientific, Waltham, MA, USA) was used as a dead cell stain.

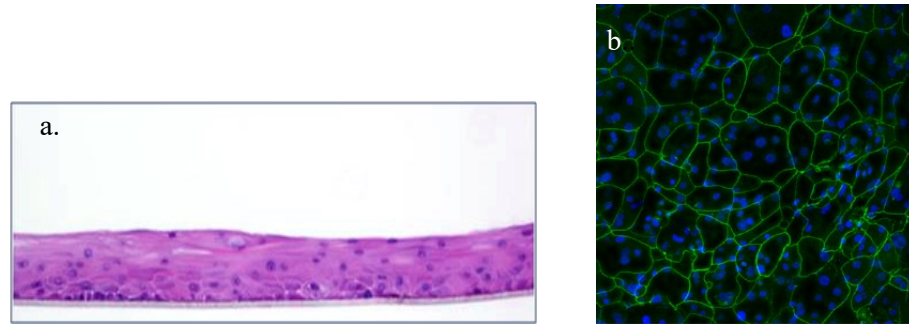


Figure 3-3 MatTek Human EpiCorneal tissue model (COR-100). a. Stained cross-section showing human corneal epithelial cells cultured to form a stratified, squamous epithelium that resembles human cornea; b. corneal tissue stained for Tight Junction Protein ZO-1 (green) (Figures reprinted with permission from MatTek)

3.3.9 Cy5 labelling of pDNA for 3D EpiCorneal™ penetration studies

gWIZ-GFP was tagged with Label IT nucleic acid labelling agent Cy5 (Mirus Bio LLC., Madison, WI) to allow for tracking NPXs in the corneal tissue. Labelling procedure was performed as per manufacturer's protocol. The labelling reagent was incubated at 0.5:1 ratio of plasmid DNA for 1 hour at 37°C. The plasmid was precipitated by adding 5M sodium chloride and 100% ice cold ethanol to the mixture and allowed to incubate for 30 minutes. The labelled plasmid was separated by centrifugation and then washed using 70% ethanol. Plasmid concentration was verified using Nanodrop 2000c (Thermo Fisher Scientific, Waltham, MA)

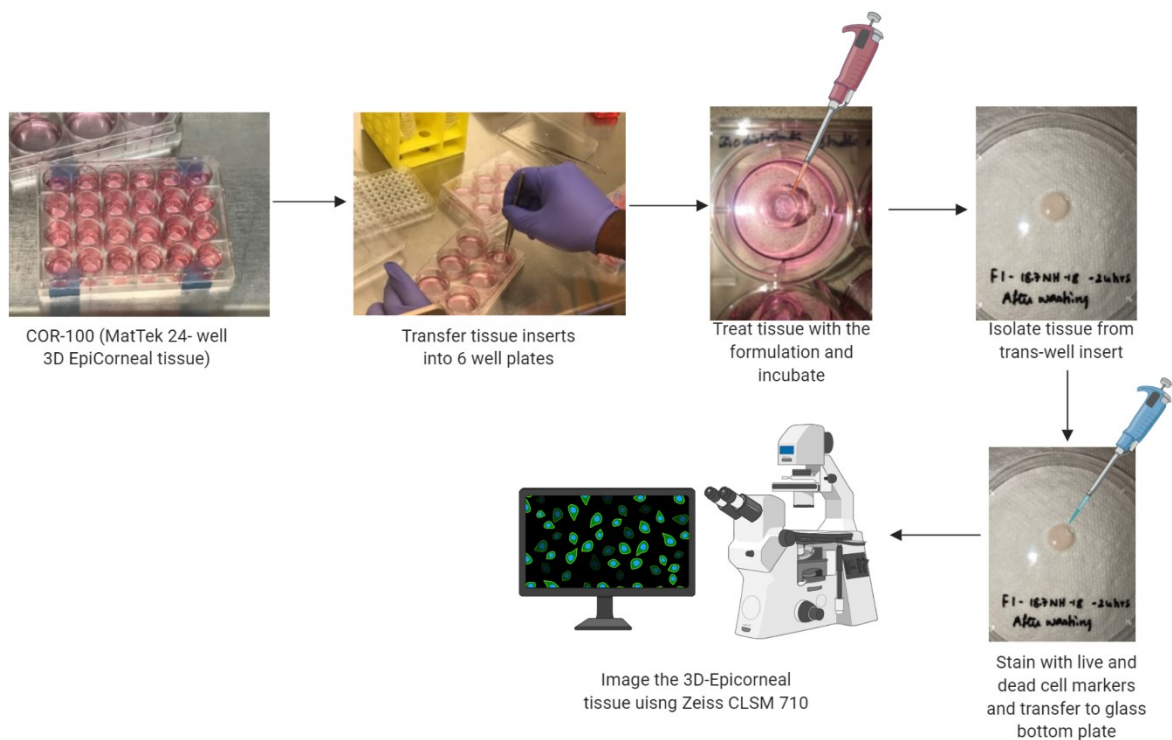


Figure 3-4 Illustration of nanoparticle penetration studies in the 3D-EpiCorneal™ tissue model. Figure generated by Lokesh Narsineni using BioRender.com.

3.3.10 Statistical analysis

The statistical analysis was performed using the GraphPad Prism software (GraphPad Software, La Jolla, CA, USA). One-way analysis of variance (ANOVA) and two-way ANOVA in conjunction with Tukey's multiple comparison tests were used to analyze TE and viability of the treated samples compared with controls. A P-value of less than 0.05 was considered as statistically significant.

3.4 Results

3.4.1 Synthesis of dimeric and trimeric gemini surfactants

Synthesis, purification and characterization of 18-7NH-18, 16-7N(16)-16 and 18-7N(18)-18 gemini surfactants was carried out successfully. Analysis of structure, molecular weight, CMC of the above mentioned gemini surfactants, using techniques such as ESI-MS, ¹H NMR spectroscopy and tensiometry confirms the formation of desired products. The purity levels were found to be between 95-98% for the synthesized surfactants and the yields were around 70-73%, calculated from the theoretical yield compared with the obtained yield of the products. The modified one-pot synthetic scheme and the use of solvent-free NH group protection made it simple to synthesize m-7NH-m gemini surfactants with high purity and eliminate impurities such as the trimeric gemini surfactant. Also, the pure compounds synthesized will serve as the parent compounds for further conjugation of peptides onto the amino group in the spacer, presented in the following chapter.

3.4.1.1 Mass Spectrometry analysis:

18-7NH-18

ESI-MS: Chemical formula- $C_{46}H_{99}N_3^{2+}$, molecular weight: 694.3179 (without Br⁻ counter ions), 854.1270 (with 2 Br⁻), charge ratio: +2, expected peaks m/z: 346.8914, found peaks m/z: 346.8914 (m/z spectra captured using Thermo Q-Exactive orbitrap system with ESI, yield- 70-73%)

16-7N(16)-16

ESI-MS: Chemical formula- $C_{58}H_{123}N_3^{2+}$, molecular weight- 862.6419 (without Br⁻ counter ions), 1022.4510 (with 2 Br⁻), charge ratio: +2, expected peaks m/z: 430.9853, found peaks m/z: 430.9853 (m/z spectra captured using Thermo Q-Exactive orbitrap system with ESI, yield- 72%)

18-7N(18)-18

ESI-MS: Chemical formula- $C_{64}H_{135}N_3^{2+}$, molecular weight- 946.8039 (without Br^- counter ions), 1106.6130 (with 2 Br^-), charge ratio: +2, expected peaks m/z: 473.0323, found peaks m/z: 473.0323 (m/z spectra captured using Thermo Q-Exactive orbitrap system with ESI, yield- 78%).

3.4.1.2 1H NMR Spectroscopy analysis

1H NMR Spectroscopy analysis was carried out on Bruker Avance 500 MHz instrument by dissolving the sample in the $CDCl_3$ solvent and the chemical shifts obtained were confirmed for 18-7NH-18 new stock (NS) (Figure 3-5) (Table 3-1).

Table 3-1 1H NMR analysis of 18-7NH-18 (NS) gemini surfactant

Group	δ (ppm)	Total number of protons
N^+-CH_3	3.28	12
$N^+-CH_2-CH_2-CH_2-NH-$	3.14	4
$N^+-CH_2-CH_2-(CH_2)_{15}-CH_3$	3.14	4
$N^+-CH_2-CH_2-(CH_2)_{15}-CH_3$	0.85	6
$N^+-CH_2-CH_2-(CH_2)_{15}-CH_3 \times 2$	1.23	60
NH	1.55	1
$N^+-CH_2-CH_2-(CH_2)_{15}-CH_3$	1.65	4
$N^+-CH_2-CH_2-CH_2-NH-$	1.95	4
$N^+-CH_2-CH_2-CH_2-NH-$	2.44	4

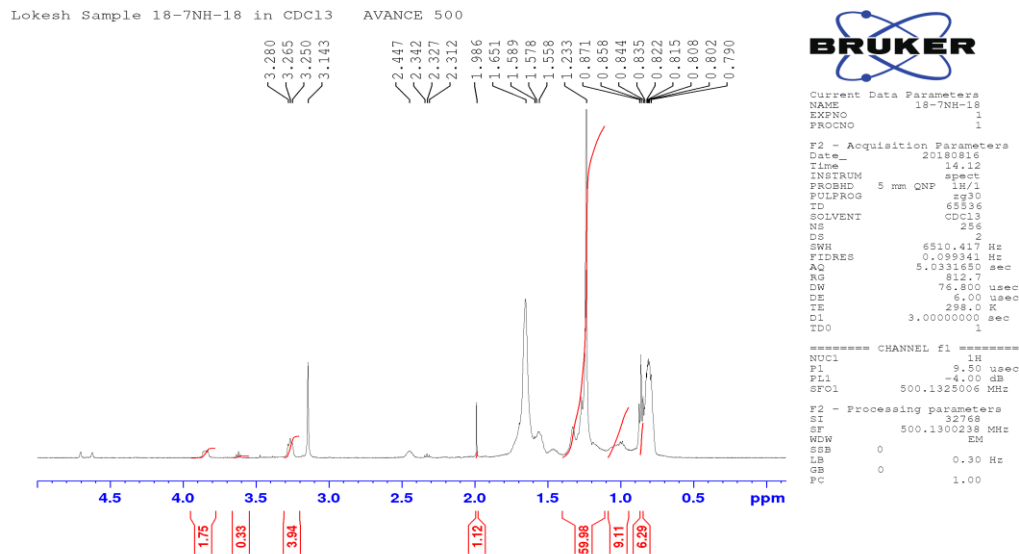


Figure 3-5 ¹H NMR spectrum of 18-7NH-18 gemini surfactant synthesized using DMAP free-one pot reaction method, impurities were also observed in the proton NMR spectra.

3.4.1.3 Surface tension and CMC determination

In order to confirm the purity of the newly synthesized 18-7NH-18 (the parent gemini for all peptide modification) CMC determination was carried out. The surface tension vs log concentration for 18-7NH-18 gemini surfactant were analyzed and plotted (Appendix 1 Table 1) and CMC value was determined by carrying out the regression analysis. The CMC value of the 18-7NH-18 pure surfactant was determined to be 51.69 μ M (Figure 3-6). It was noted that the CMC value obtained in this work for 18-7NH-18 differed from the previously reported CMC value 13 μ M (159), which was expected due to improved purity obtained in this work (Figure 3-6).

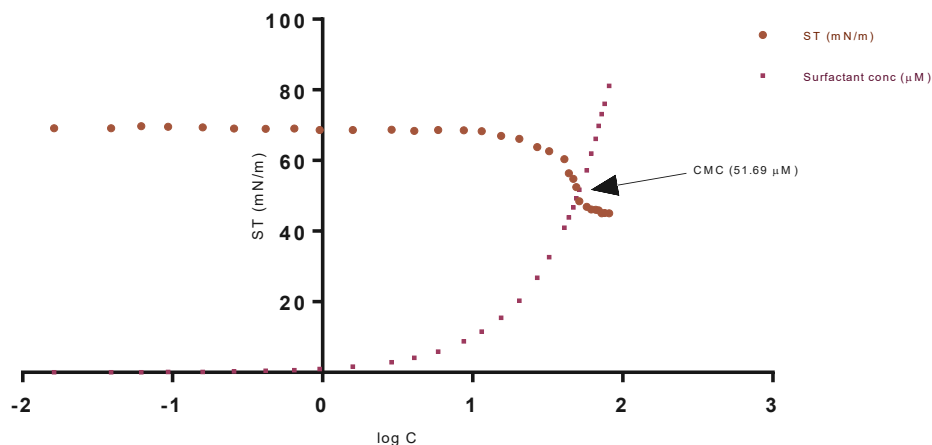


Figure 3-6 Surface tension vs log concentration plot for 18-7NH-18 gemini surfactant. CMC value was obtained from the graph as the point where surface tension dissects the concentration plot. All surface tension measurements were obtained by applying Harkin-Jordan's correction.

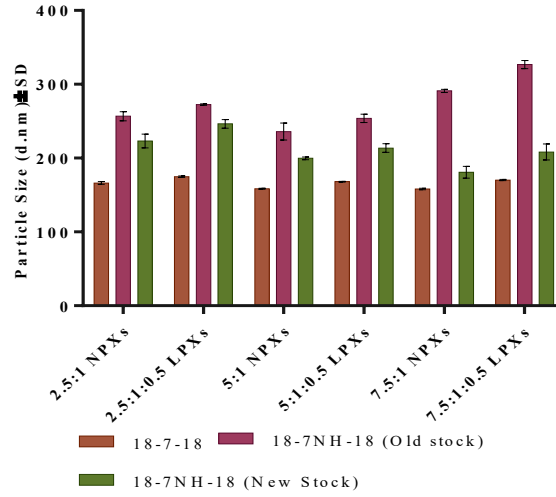
3.4.2 Physicochemical characterization of dimeric and trimeric gemini surfactant NPXs (*m*-7NH-*m* and *m*-7N(*m*)-*m*)

3.4.2.1 Particle size distribution and zeta potential

Particle size and zeta potential of the formulated NPXs and LPXs were analyzed in an attempt to establish a correlation between the functional properties (stability, toxicity and TE) and the structural parameters (particle size, polydispersity index and charge distribution on the particles). Charge plays the most imperative role in compacting DNA with a cationic delivery vehicle and the compacted DNA remains in this state until it enters the cell. The compacted DNA is protected from the surrounding environment during its transit into the cell and prevents its degradation. Similarly, charge plays a vital role in interaction of the gene delivery system with the cell.

Particle size of the first generation (m-s-m) and second generation (m-7NH-m) gemini surfactant NPXs and LPXs varied between 150-350 nm based on the charge ratio and the presence of DOPE lipid in the formulation (Figure 3-7 A).

A.



B.

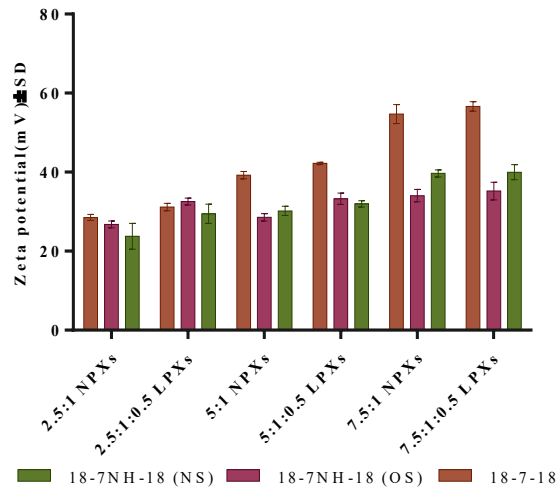


Figure 3-7 Physicochemical characterization of dimeric gemini surfactant NPXs and LPXs, Effect of charge ratio on (A) particle size and (B) zeta potential of the gemini NPXs and LPXs

There was no significant difference in particle size between different charge ratios of the 18-7-18 gemini surfactant NPXs, all were between 150-200 nm. But the second generation gemini surfactant NPs made with 18-7NH-18 by both old and new methods of synthesis (labelled as old and new stocks, OS and NS) have shown a significant difference in particle size in par with the charge ratio. In case of the OS gemini NPXs the particle size was reduced up to 5:1 compared to 2.5:1 but then there was an increase in particle size with 7.5:1 charge ratio. The particle size of NPXs made from NS on the other hand, was lower as the charge ratio increased.

The results of the particle size distribution of the 18-7NH-18 gemini surfactant NPXs were in agreement with previous evaluations (253, 254), which showed that an increase in the charge ratio resulted in particle size reduction due to higher compaction of surfactant with plasmid DNA, (Figure 3-7 B). Similarly, the zeta potential data also demonstrated that the zeta potential increased as the G:P charge ratio increased.

There is a corresponding increase in zeta potential of the 18-7NH-18 gemini NPXs as the charge ratio was increased (Figure 3-7 B) Adding DOPE into the formulation had no significant change in the zeta potential as DOPE is a neutral lipid, but adding DOPE correlated with an increase in particle size of 18-7NH-18 LPXs. Despite the higher charge of some NPX systems, (zeta potential around +54 mV and particle size as low as 158 nm), TE was higher, and toxicity was lower with formulation that had an optimum value of both particle size and zeta potential. The optimal TE is achieved with 18-7NH-18 gemini surfactant NPXs at charge ratio of 5:1, particle size of $199.8 \pm 1.83 \text{ nm} \pm \text{S.D.}$ and zeta potential of $+30.18 \pm 1.17 \text{ mV} \pm \text{S.D.}$

3.4.2.2 Optimization of transfection efficiency and viability of NPXs in A7 astrocytes

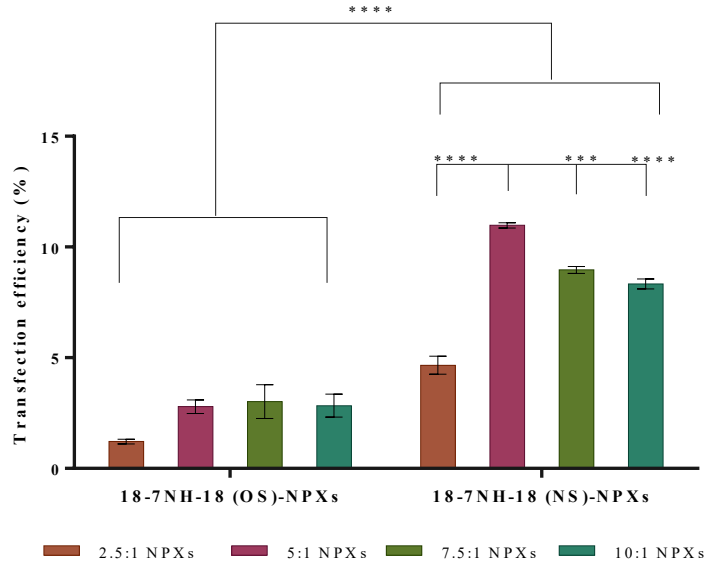
3.4.2.2.1 Effect of charge ratio on the transfection efficiency and viability

NPXs were made using OS and NS 18-7NH-18 gemini surfactant at 2.5:1, 5:1, 7.5:1 and 10:1 charge ratio. TE of 18-7NH-18 OS-NPXs was found to be significantly lower (**** $p < 0.0001$) compared to the 18-7NH-18 (NS)-NPXs treatment at all ratios (Figure 3-8). The TE obtained were $1.21 \pm 0.1\%$, $2.79 \pm 0.3\%$, $3.020 \pm 0.76\%$ and $2.833 \pm 0.51\%$ for 18-7NH-18 OS-NPXs and $4.66 \pm 0.4\%$, $10.97 \pm 0.11\%$, $8.96 \pm 0.16\%$ and $8.33 \pm 0.22\%$ for 18-7NH-18 NS-NPXs at 2.5:1, 5:1, 7.5:1 and 10:1 ratios, respectively. The TE of the 18-7NH-18 NS-NPXs increased up to 5:1 ratio then decreased with increasing charge ratio (Figure 3-8).

Statistical analysis confirmed that 18-7NH-18 NS-NPXs treated cells consistently showed higher TE compared to 18-7NH-18 OS-NPXs treatment at 48 hours (**** $p < 0.0001$) (Figure 3-8 A).

The viability of the 18-7NH-18 NS-NPXs treated A7 astrocytes was higher compared to the 18-7NH-18 OS-NPXs treated cells at all charge ratios (Figure 3-8 B).

A)



B)

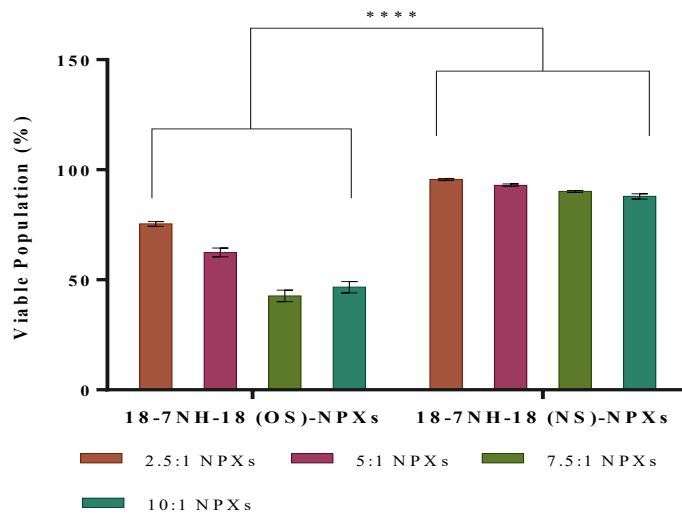


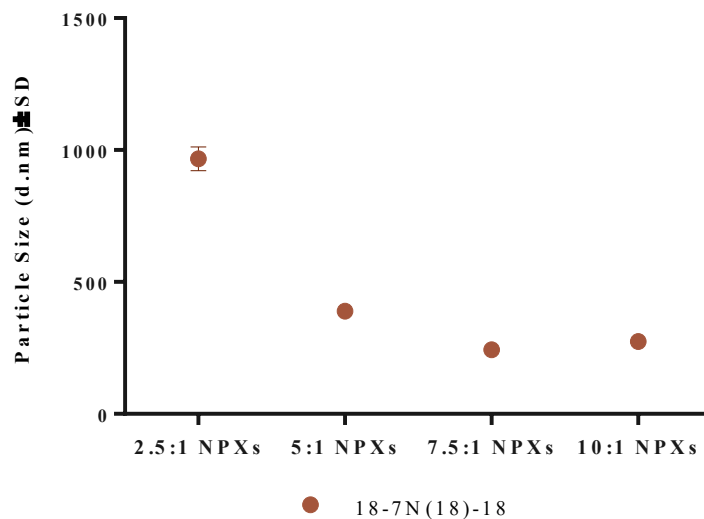
Figure 3-8 Assessment of TE and viability on A7 astrocytes treated with 18-7NH-18 (OS) and 18-7NH-18 (NS). A) TE was measured by tracking the GFP expression, B) viability studies profile of 18-7NH-18 (OS) and 18-7NH-18 (NS). Viability was assessed using MitoTracker® Deep Red by flow cytometry. All values expressed as mean \pm S.D., n=3, ***p<0.001, ****p<0.0001

It is evident from the data that the percent viable population decreased with increasing NPX charge ratio. The viability was found to be $75.37 \pm 1.03\%$, 62.47 ± 2.02 , 42.71 ± 2.606 and 46.63 ± 2.53 for 18-7NH-18 (OS)-NPXs and $95.55 \pm 0.50\%$, $92.97 \pm 0.57\%$, $90.18 \pm 0.43\%$ and $87.91 \pm 1.17\%$ for 18-7NH-18 (NS)-NPXs at 2.5:1, 5:1, 7.5:1 and 10:1 ratios, respectively. Data confirmed that 18-7NH-18 NS-NPXs treated cells significantly ($****p < 0.0001$) had higher viabilities compared to 18-7NH-18 OS-NPXs treated cells (Figure 3-8 B).

The particle size of NPXs were formulated using 18-7N(18)-18 gemini surfactants decreased with increasing charge ratio 966 ± 46 , 389 ± 4.68 , 243.23 ± 3.49 and 274 ± 3.29 nm \pm S.D., while the zeta potential increased $+5.29 \pm 1.57$ mV, $+36.90 \pm 1.25$ mV, $+40.36 \pm 1.71$ mV and $+41.43 \pm 0.80$ mV for 2.5:1, 5:1, 7.5:1 and 10:1 ratios respectively (Figure 3-9 A and B). The TE for trimeric gemini surfactant NPXs were found to be $3.42 \pm 0.814\%$, $3.16 \pm 0.29\%$ and $1.51 \pm 0.33\%$ for 18-7N(18)-18 NPXs and $3.267 \pm 0.156\%$, $4.174 \pm 0.23\%$ and $4.67 \pm 0.718\%$ for 16-7N(16)-18 NPXs at 2.5:1, 5:1 and 7.5:1 ratios respectively. Statistical analysis confirmed that the trimeric gemini surfactants have shown significantly lower TE compared to 18-7NH-18 and Lipofectamine[®] 3000 (Figure 3-10 A).

The results confirm that an increase in the charge ratio reduces the TE in case of 18-7N(18)-18 gemini surfactant NPXs, while 16-7N(16)-16 has shown increased efficiencies when charge ratio was increased up to 7.5:1 (Figure 3-10 A). The percent viable population was found to be between 90-97% for 18-7NH-18 gemini NPXs, 88-90% for 18-7N(18)-18 and 87-95% for 16-7N(16)-16 gemini NPXs. The 18-7NH-18 NPXs treated cells had significantly higher viabilities compared to 18-7N(18)-18 ($****p < 0.0001$) and 16-7N(16)-16 NPX ($**p < 0.01$) treated cells and also their viabilities were affected by the charge ratio. Increase in charge ratio has reduced the viability in treated A7 astrocyte cells (Figure 3-10 B).

A)



B)

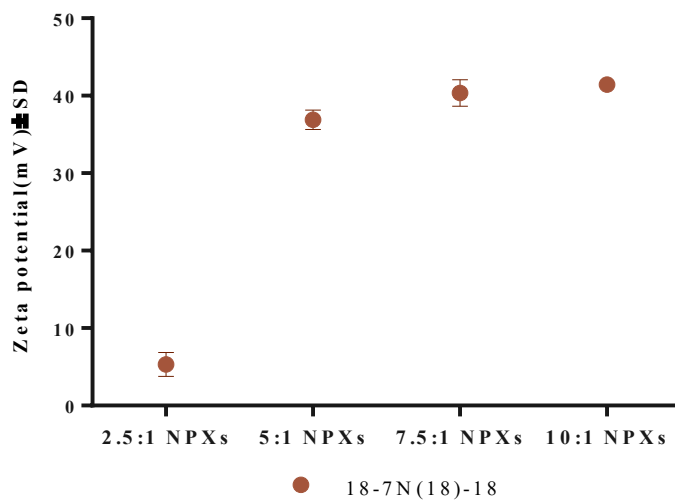
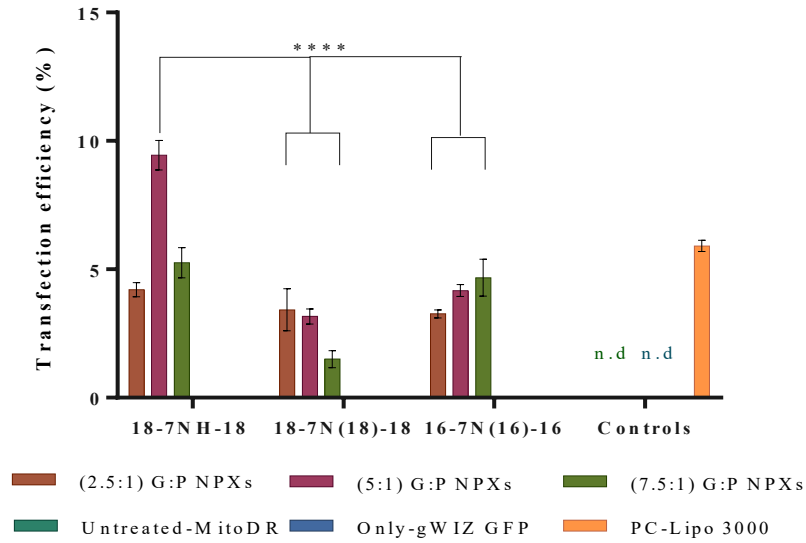


Figure 3-9 Particle size distribution (A) and zeta potential data (B) of 18-7N(18)-18 gemini NPXs
Additional information on the effect of charge ratio of 18-7NH-18 (NS) gemini surfactant with and without DOPE on the viability of the A7 astrocytes is presented in Appendix 1-Figure 3 .

A)



B)

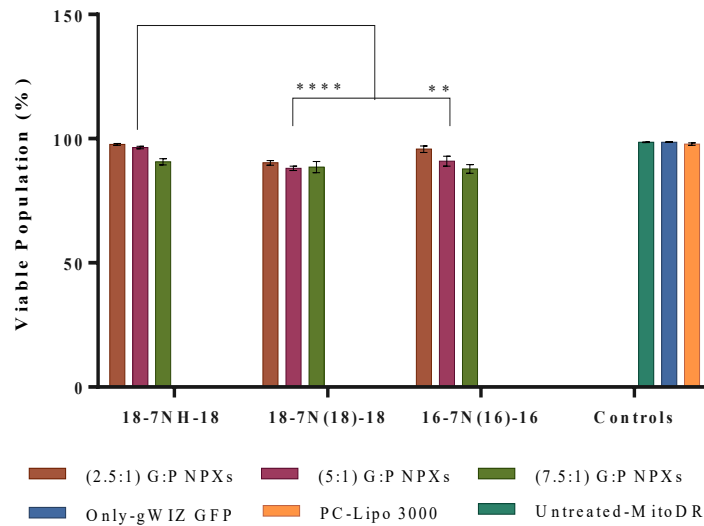
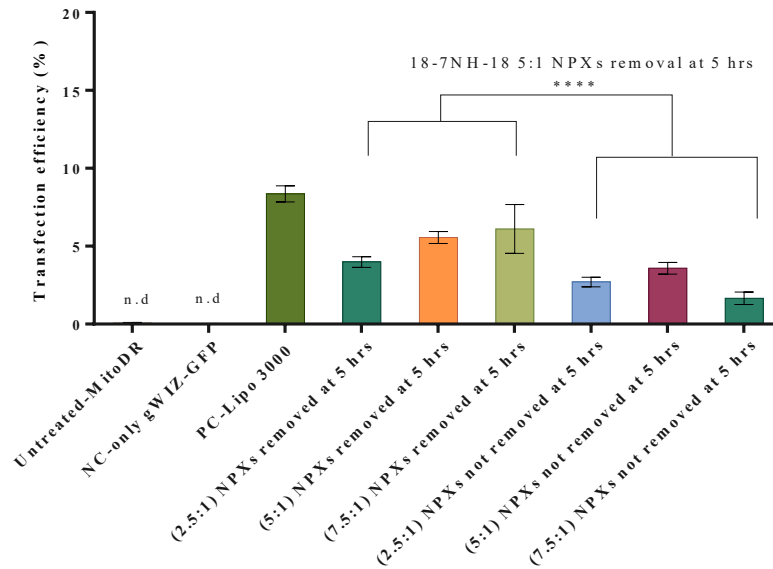


Figure 3-10 Assessment of TE of 18-7N(18)-18 and 16-7N(16)-16 NPXs in A7 astrocytes. TE was measured by tracking GFP expression and viability was assessed using MitoTracker® Deep Red by flow cytometry. All values expressed as mean \pm S.D., n=3, **p<0.01, ****p<0.0001; n.d.=not detected)-untreated-MitoDR and only-gWIZ GFP treatments.

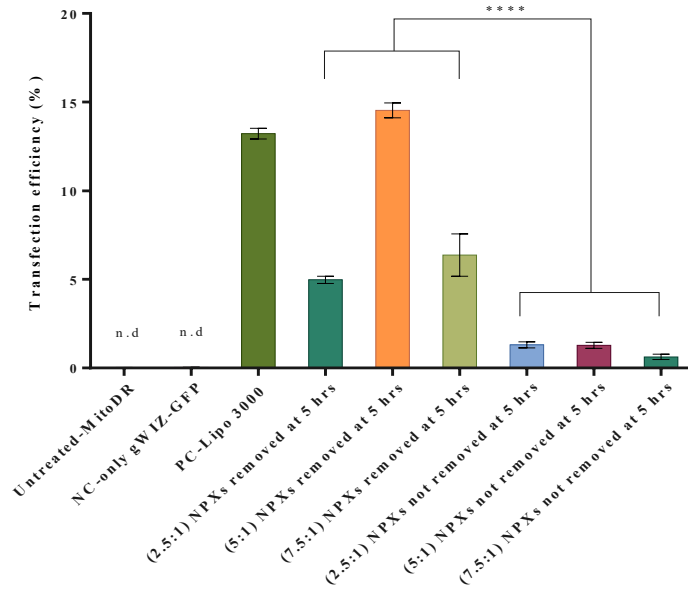
3.4.2.2.2 Kinetics of gene expression in A7 astrocytes treated with *m*-7NH-*m* gemini NPXs by flow cytometry and confocal microscopy

An incubation study to determine if the NPXs need to be removed at 5 hours after treatment or left throughout the period of incubation was assessed. 18-7NH-18 NPXs were formulated at 2.5:1, 5:1 and 7.5:1 ratio with gWIZ-GFP plasmid and treated on A7 astrocytes in a 96 well plates. Three plates each for 24-, 48- and 72-hour time points were treated, and media is replaced at 5 hours after treatment. Similar ratios of treatments with NPXs not removed after 5-hour time points were assessed to determine the effect of non-removal of NPXs after 5 hours on transfection and viability along with the kinetics of gene expression time-point assessment, to identify the ideal time-point for assessment of gene expression of gemini surfactant NPXs treated cells.

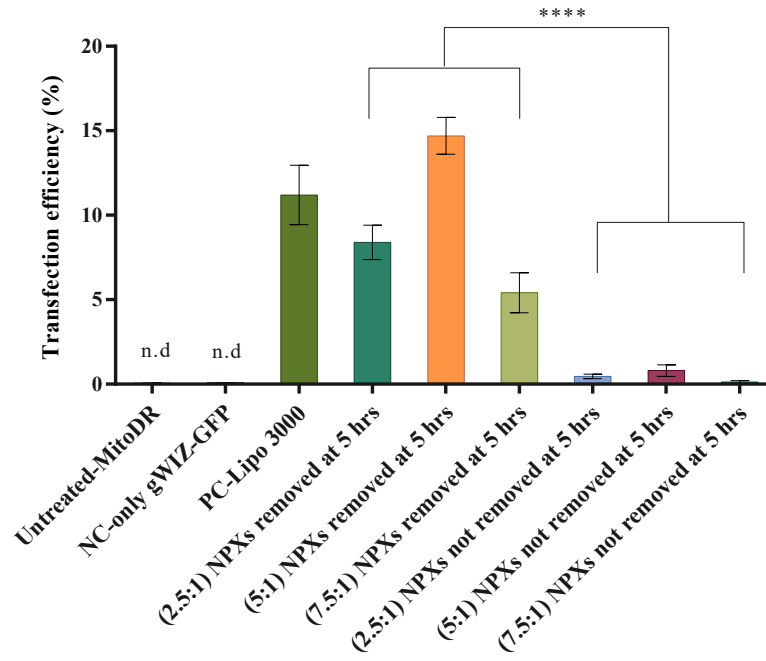
A)



B)



C)



D)

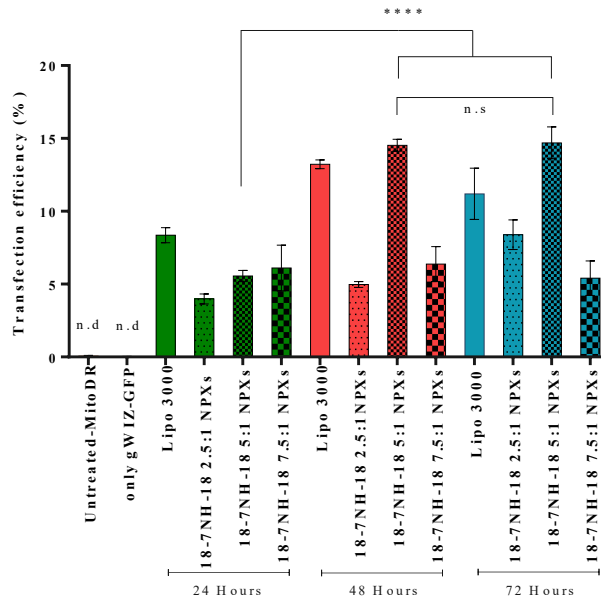


Figure 3-11 Kinetics of gene expression and optimization of TE A) TE of 18-7NH-18 NPXs in A7 astrocytes treated for 5hours and TE measured at 24 hours; B) TE of 18-7NH-18 NPXs in A7 astrocytes treated for 5hours and TE measured at 48 hours; C) TE of 18-7NH-18 NPXs in A7 astrocytes treated for 5hours and TE measured at 72 hours; and D) Comparative graph of gene transfection assessment at 24, 48 and 72 hours. TE was measured by tracking the GFP expression. All values expressed as mean \pm S.D., n=3, *p<0.05, **p<0.01, ***p<0.001, ****p<0.0001, n.d-not detected and n.s-non-significant.

It was shown that TE was higher when cells were exposed to NPXs for 5 hours and not continuously during the entire incubation period (Figure 3-11 A, B, C and D; ****p<0.0001) The lower TE was mainly due to the toxicity induced by the NPXs when incubated for prolonged time with the cells (viability results are shown in Appendix 1 Figure 4).

Assessment of the kinetics of gene expression demonstrated that the 48-hour time point showed maximum gene expression (t_{max}) (Figure 3-11 B). At the 48-hour time point 18-7NH-18 5:1 NPXs had a significant three-fold increase (****p<0.0001) in TE to $14.53 \pm 0.41\%$ compared to $5.55 \pm 0.38\%$ at 24 hours, but no further increase was observed and TE remained at similarly high level ($14.69 \pm$

1.094%) at the 72-hour time point (Figure 3-11 C). In subsequent studies the 48-hour incubation was chosen for all TE assessments.

3.4.2.2.3 Assessment of DOPE in gemini LPXs for gemini NPXs by flow cytometry and confocal microscopic imaging

To assess the effect of DOPE on the TE and viability of cells, we formulated two sets of LPX formulations with the same charge ratios, that is 2.5:1, 5:1 and 7.5:1 (G:P), one set with 1:0.5, 1:1:1.5 and 1:2 G:L ratios and one set of NPXs without DOPE. The flow cytometry results demonstrated that increasing DOPE in the formulation resulted in a decrease of TE. The 1:0.5 G:L ratio showed significantly (****p<0.0001) higher TE compared to 1, 1.5 and 2.0 ratios of DOPE, while the 1:1 and 1:2 ratio of gemini: DOPE LPXs treatment did not have any significant difference in their TE values Figure 3-12. From the above ratios tested, best performing lipid ratio (1:0.5, G:L) was used to make LPXS, treated on A7 astrocytes and imaged using confocal microscopy.

Results from the confocal imaging studies (Figure 3-13) were in agreement with the flow cytometry results and confirmed that TE was highest with 18-7NH-18 5:1 NPXs compared to other charge ratios tested. Whereas containing LPXs with 5:1 (G:P) charge ratio and 1:0.5 G:L ratio had lower TE and higher cell toxicities compared to 18-7NH-18 5:1 NPXs (without DOPE) at 48 hours. (Figure 3-12).

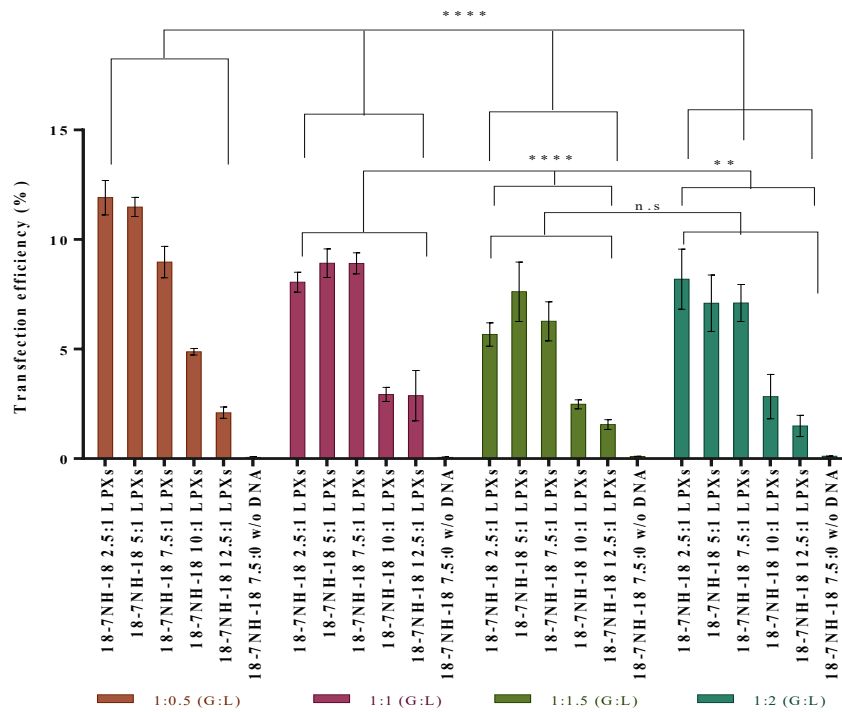
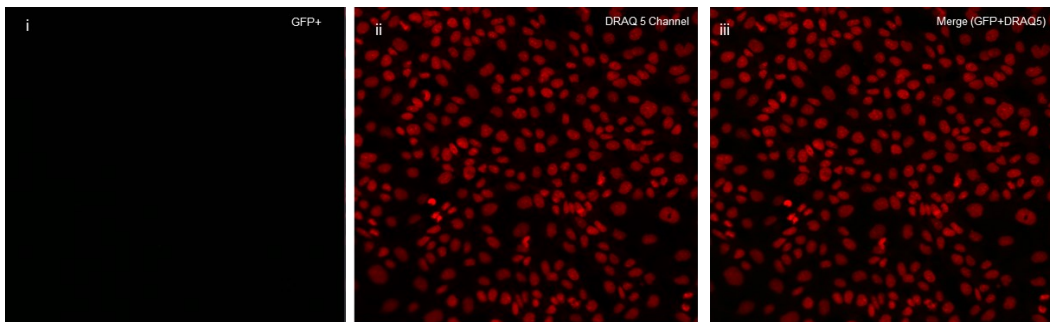


Figure 3-12 Assessment of DOPE concentration in LPXs on TE. All values expressed as mean \pm S.D., n=3, *p<0.05, **p<0.01, ***p<0.001, ****p<0.0001, n.d=not detected and n.s=non-significant.

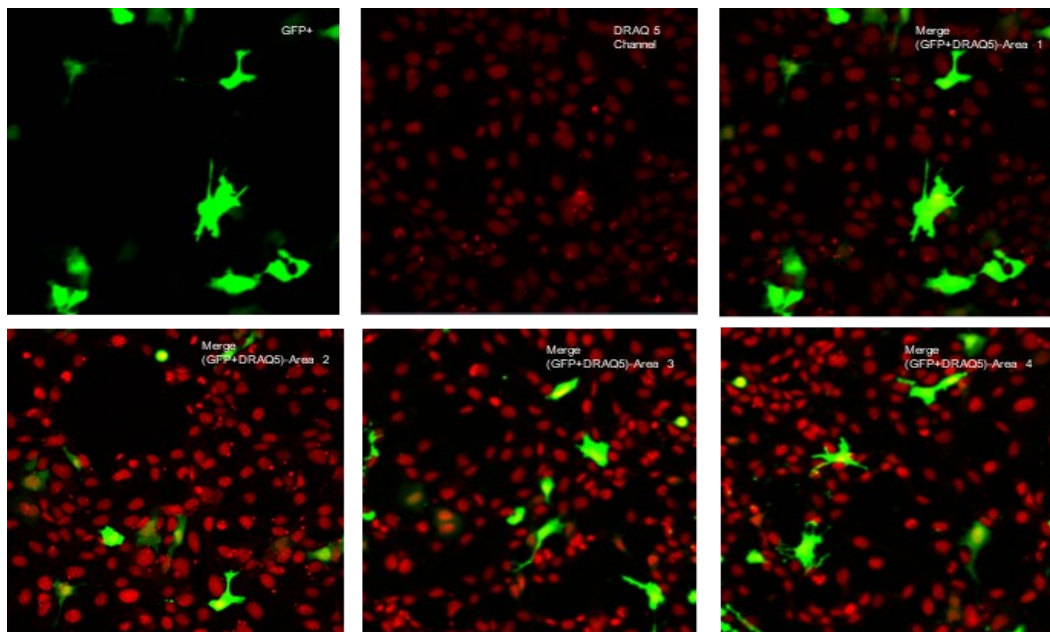
A. Untreated-Unstained



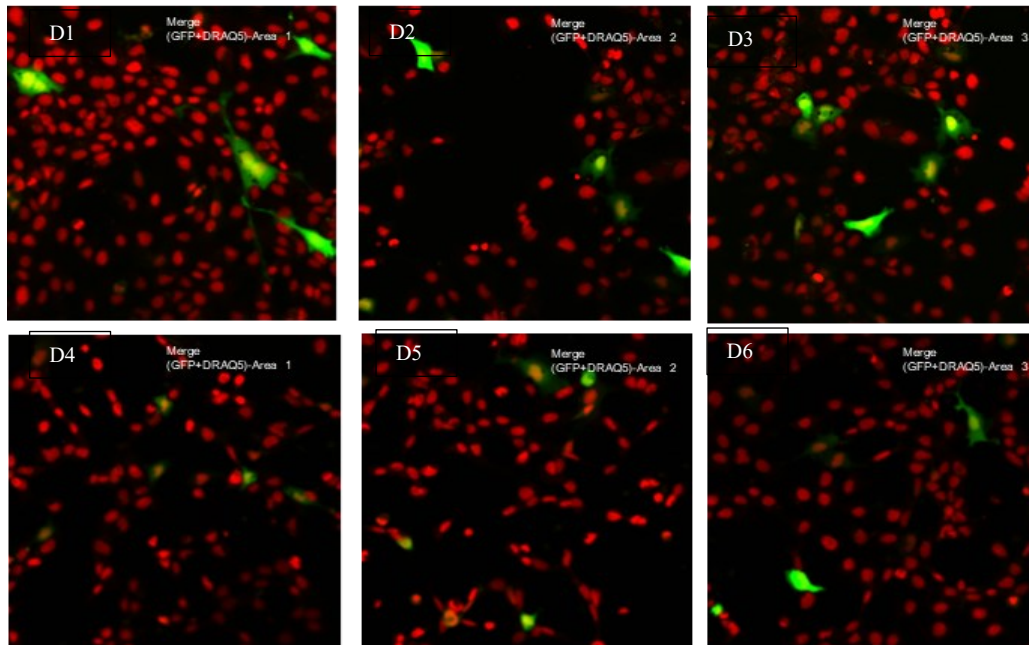
B. Untreated-DRAQ5 stained



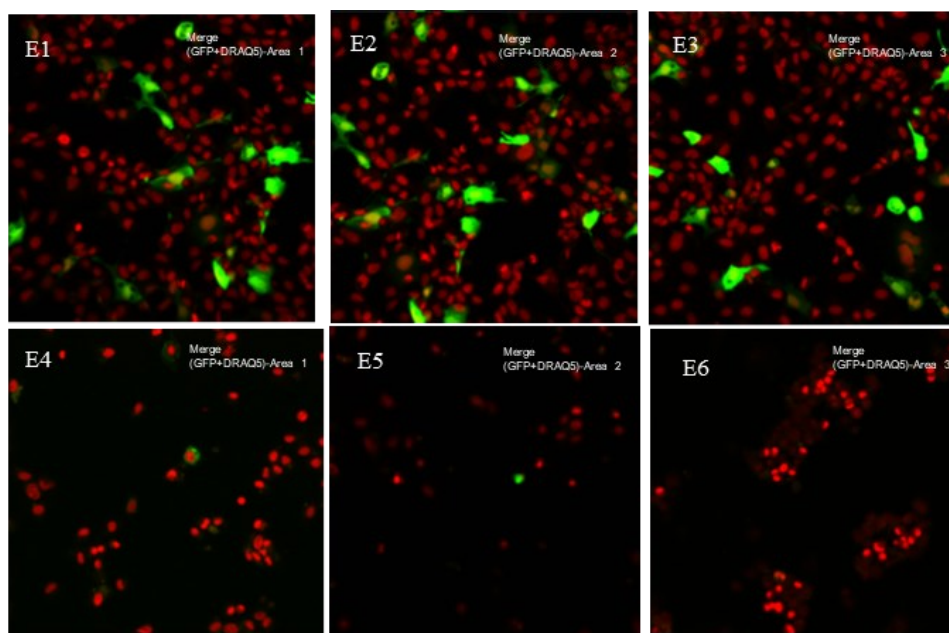
C. Lipofectamine 3000 treated-24 hours



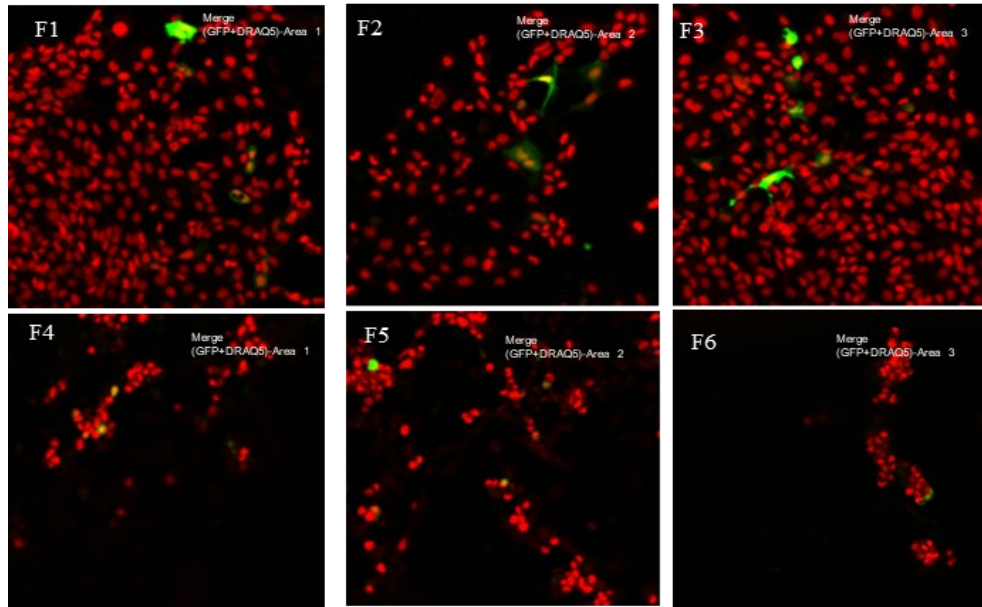
D. 18-7NH-18 2.5:1 NPXs treated (D1, D2 and D3), 18-7NH-18 2.5:1 (G:P)-1:0.5 (G:L) LPXs treated (D4, D5 and D6)-24 hours



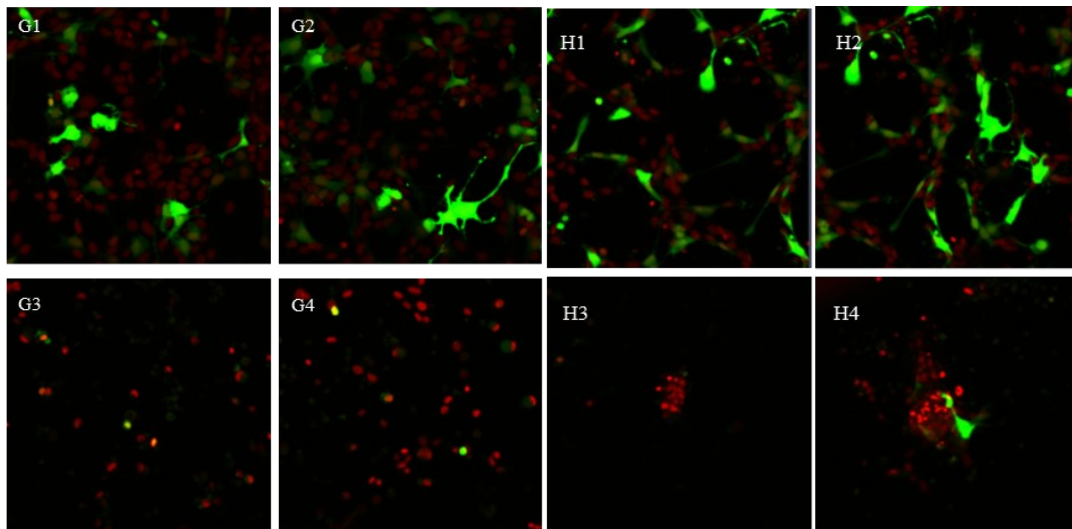
E. 18-7NH-18 5:1 NPXs treated (E1, E2 and E3), 5:1 18-7NH-18 5:1 (G:P)-1:0.5 (G:L) LPXs treated (E4, E5 and E6)-24 hours



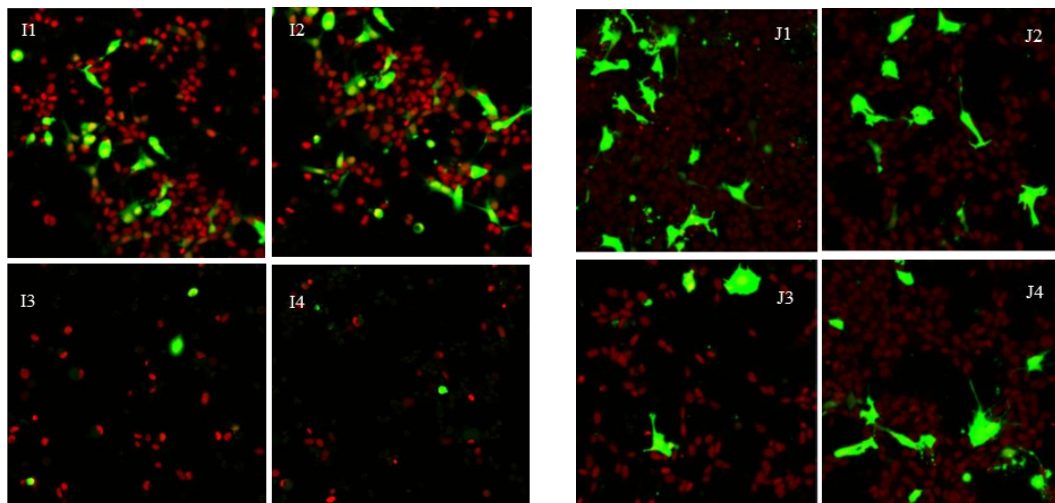
F. 18-7NH-18 7.5:1 NPXs treated (F1, F2 and F3), 18-7NH-18 7.5:1 (G:P)-1:0.5 (G:L) LPXs treated (F4, F5 and F6)-24 hours



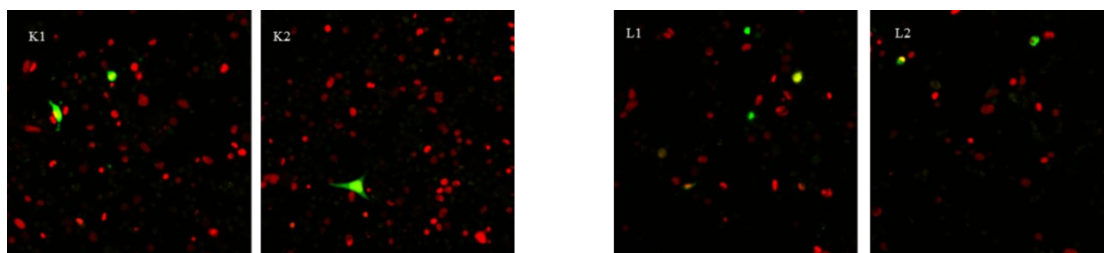
G. 18-7NH-18 2.5:1 NPXs treated (G1 and G2), 18-7NH-18 2.5:1 (G:P)-1:0.5 (G:L) LPXs treated (G3 and G4), H. 18-7NH-18 5:1 NPXs treated (H1 and H2), 18-7NH-18 5:1 (G:P)-1:0.5 (G:L) LPXs treated (H3 and H4)-48 hours



I. 18-7NH-18 7.5:1 NPXs treated (I1 and I2), 18-7NH-18 7.5:1 (G:P)-1:0.5 (G:L) LPXs treated (I3 and I4), **J.** Lipo-3000 treated (J1, J2, J3 and J4)-48 hours



K. 18-7NH-18 2.5:1 NPXs treated (K1 and K2), **L.** 18-7NH-18 5:1 NPXs treated (L1 and L2), 5:1 18-7NH-18- 72 hours



M. 18-7NH-18 7.5:1 NPXs treated (M1 and M2), **N.** Lipo 3000 treated (M1 and M2)-72 hours.

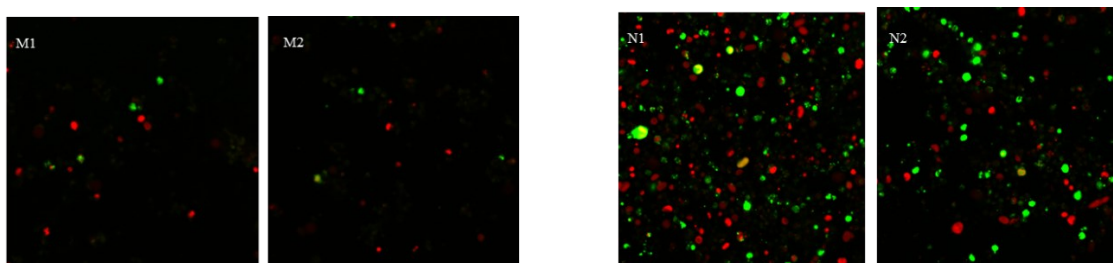


Figure 3-13 Confocal microscopic study of maximum gene expression time point assessment and DOPE inclusion effects on TE and viability at 24 (A-F), 48 (G-J) and 72 hours (K-N).

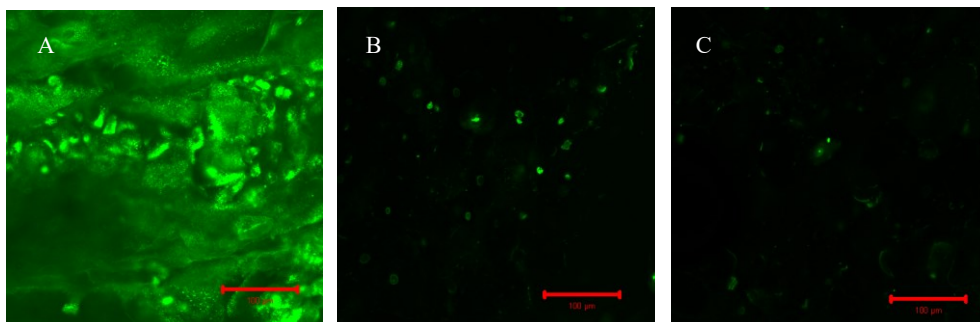
The results demonstrate that the inclusion of DOPE into the formulations even at low concentrations was toxic to cells and longer incubations lead to irreversible damage to cell membranes and cell death. At 72 hours low amounts of green GFP or red nucleic acid stain fluorescence was detectable which could have been due to reduction in the number of viable cells owing to the prolonged incubation time (72 hours) after treatment with NPXs and LPXs.

3.4.3 In vitro studies of interaction of 18-7NH-18 and 16-7N(16)-16 NPXs with EpiCorneal tissue

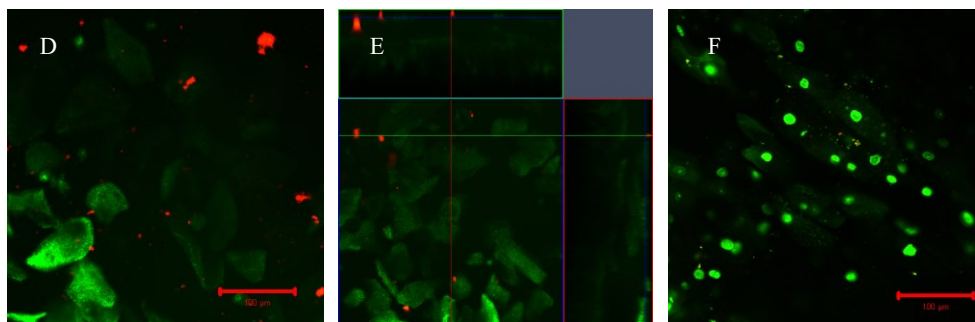
We used the 3D EpiCorneal tissue model that mimics the cell layers of cornea to evaluate the interaction of 18-7NH-18 5:1 NPXs and 16-7N(16)-16 5:1 NPXs carrying Cy5 labelled gWIZ-GFP plasmid. Confocal microscopic imaging after treatment for 0.5 hour with 18-7NH-18 and 16-7N(16)-16 NPXs showed that 18-7NH-18 NPXs rapidly penetrated into the cornea and NPXs were visible across the entire 100-120 μ m thickness of the tissue (Figure 3-14 G and H. This shows that the NPXs were strongly interacting with the cell surface and penetrated into the tissue reaching deeper layers. 18-7NH-18 NPXs also started clearing up from the surface due to their penetration to deeper layers, this also demonstrates the adherence of the particles to the surface despite repeated washes with PBS as seen on the Z-stack image the Cy5 labelled particles are still visible on the surface of the retina (Figure 3-14 panel ii A and B and C).

In case of the 16-7N(16)-16 NPXs, most NPXs remained on the corneal surface and only minimum penetration into the cornea was observed during the first half an hour (Figure 3-15 A-D). The NPXs were well adhered to the surface despite three repetitive steps of washing before imaging. At 1 hour incubation the NPXs showed limited penetration of approximately 30-40 μ m into the cornea (Figure 3-15 E-H).

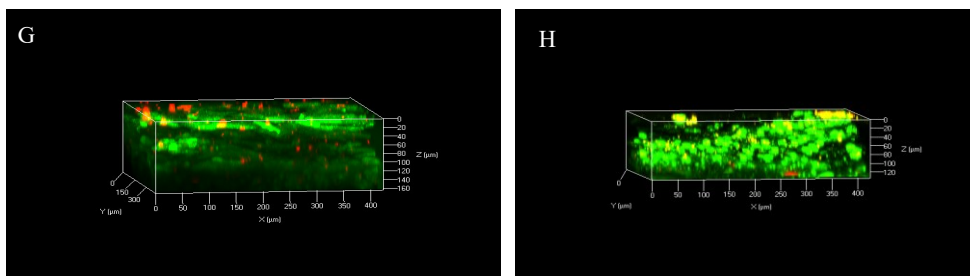
i)



Controls- (A) Untreated with calcein, (B, C) Untreated tissue treated with Image IT

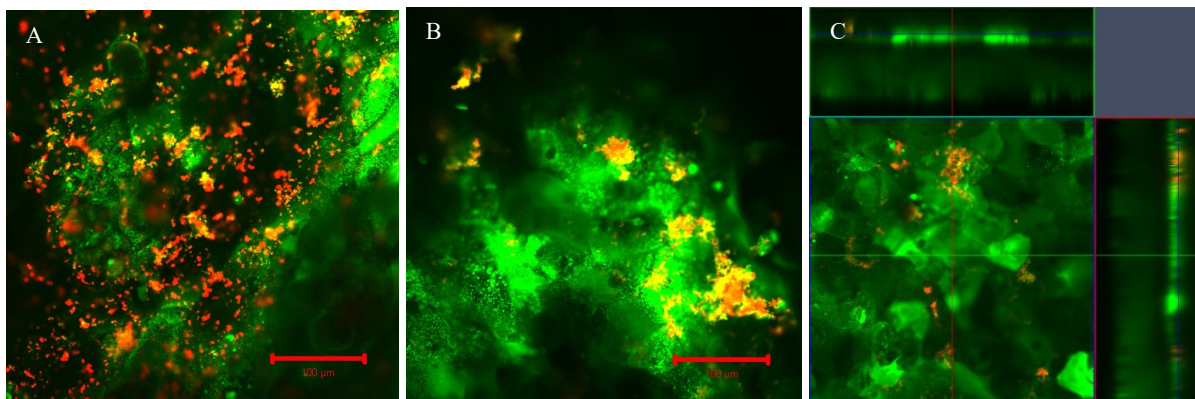


Treatments -(D, E) 18-7NH-18 5:1 NPXs-0.5 hrs treated with Calcein and (F) 18-7NH-18 5:1 NPXs with Image-IT-0.5 hour, images obtained at the surface of the tissue.

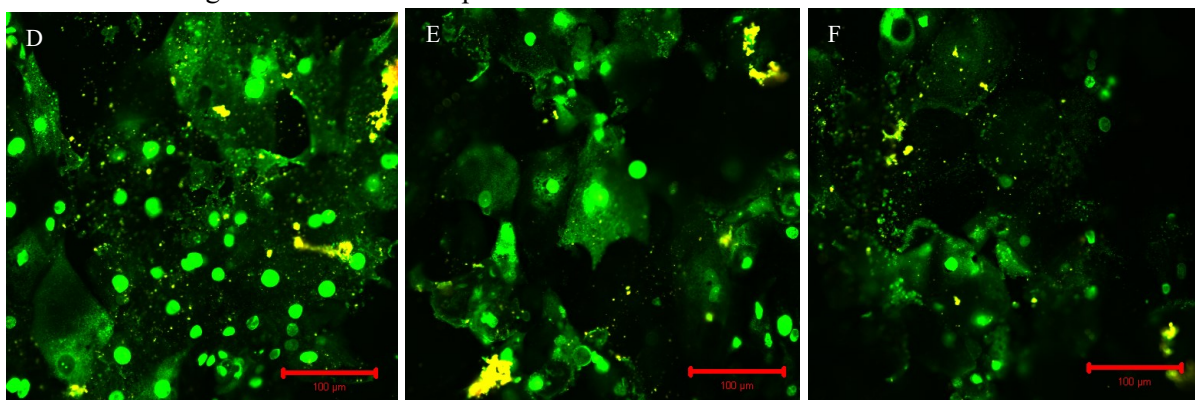


(G) 3D z-stack image of cornea treated with 18-7NH-18 5:1 NPXs carrying Cy5 labelled plasmid (red) at 0.5 hour stained with Calcein AM live cell stain (green); (H) 3D z-stack image of cornea treated with 18-7NH-18 5:1 NPXs carrying Cy5 labelled plasmid (red) at 0.5 hour stained with Image IT dead cell stain (green).

ii)

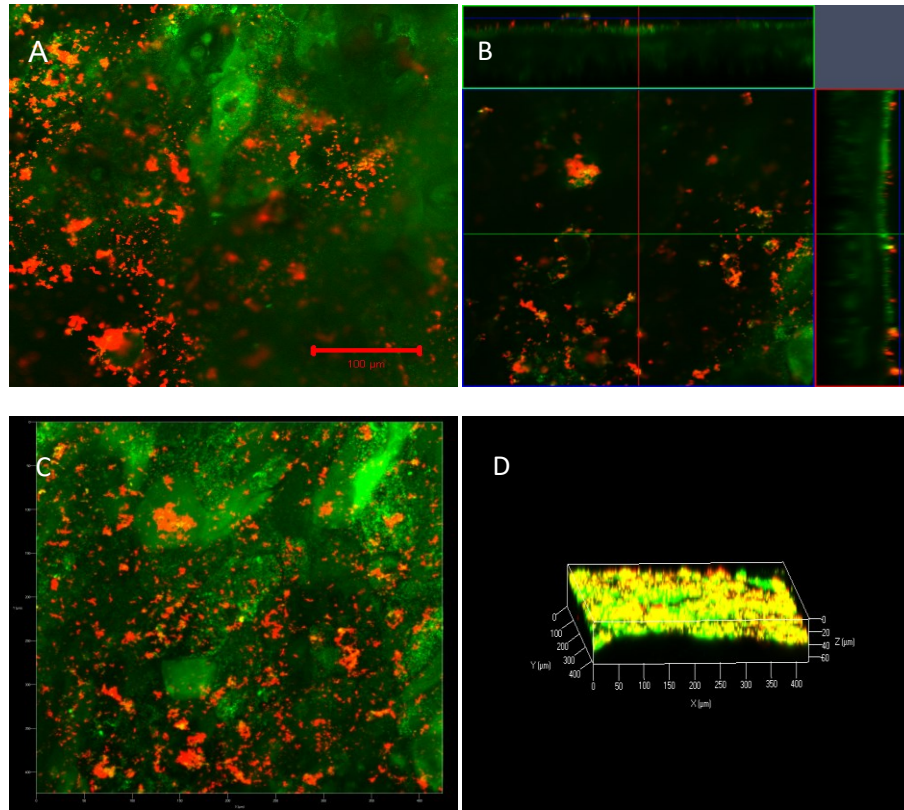


Treatments- A, B and C- 18-7NH-18 5:1 NPXs carrying Cy5 labelled plasmid (red) at 1 hour treated with calcein images taken at the surface of the tissue. Image A obtained at surface, image B from depth of tissue and image C z-stack at full depth.

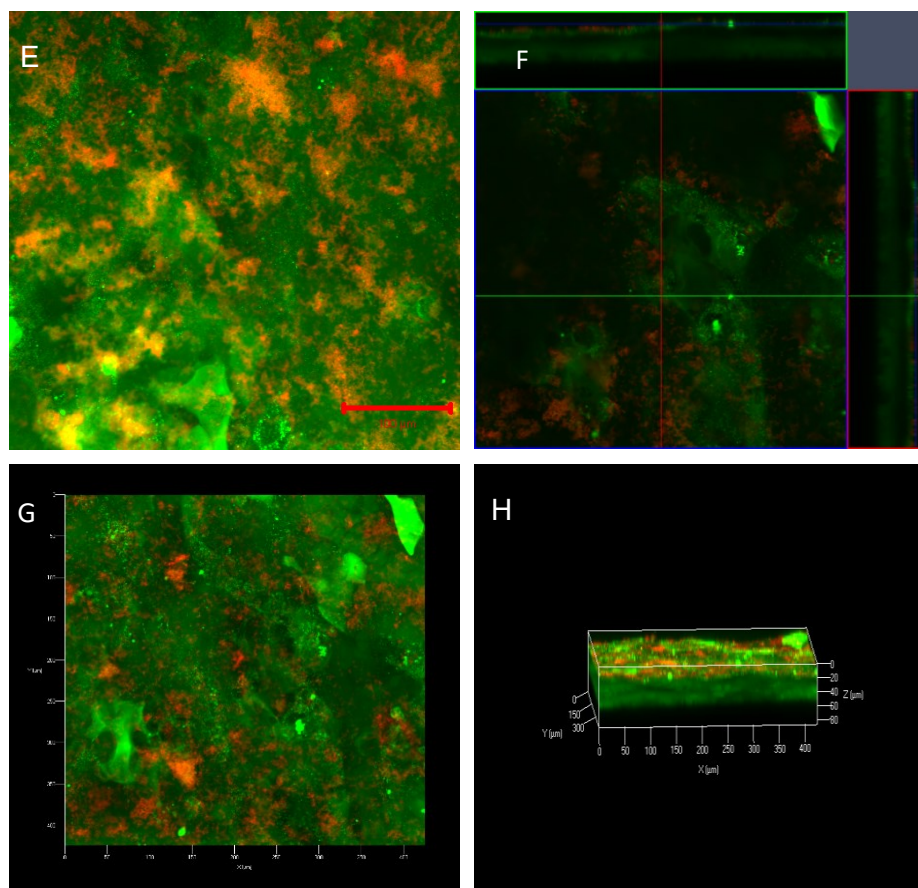


Treatments- D, E and F- 18-7NH-18 5:1 NPXs treated with Image IT at surface (D), mid (E) and deeper (F) z-axis-1 hour

Figure 3-14 *In Vitro* 3D-EpiCorneal model penetration studies for i) 18-7NH-18 5:1 NPXs treatment at 0.5 hours and ii) 18-7NH-18 5:1 NPXs at 1 hour



(i) EpiCorneal section treated with 16-7N(16)-16 5:1 NPXs-0.5 hours and stained with Calcein AM (A), 3D and full depth z-stacks (C, D) z-Stack images of the tissue section treated with 16-7N(16)-16 5:1 NPXs-0.5 hour (B). Images obtained at the surface and z-stacks at full length of tissue.



(ii) EpiCorneal sections treated with 16-7N(16)-16 5:1 NPXs stained with Calcein AM-1 hour (E, F, G and H), imaged on the surface (F) z-stack, 3D and full depth Z-stack images (G and H) showing penetration.

Figure 3-15 *In Vitro* 3D-EpiCorneal model penetration studies for 16-7N(16)-16 NPXs- 0.5 and 1 hour

3.5 Discussion

To develop a topical gene delivery system for ocular administration with the goal to reach the retina requires crossing tough barriers within the eye and demands the design of a delivery system that has a suitable combination of properties, such as sufficient residence time within the precorneal chamber, permeability to the posterior segment of the eye, suitable TE, biocompatibility and pharmaceutical properties. We have formulated a novel nanoparticle system based on the 18-7NH-18 second-

generation gemini surfactant and evaluated their transfection properties and interaction with the corneal surface. Compared to previously studied gemini derivatives 12-7NH-12 and 16-7NH-16, the longer alkyl tail may provide advantages for topical application, including higher TE.

Synthesis of m-7NH-m gemini surfactant (m=18) was carried out using a new method that incorporates a DMAP-free, one-pot, solvent-free technique (243). Previously published protocols and in-house protocols used to synthesize m-7NH-m gemini surfactant yielded very low amounts of final product due to the number of steps involved.

In addition to the approximately two-fold better yield and 'green' solvent-free one-pot approach, the improved synthesis method presented here provides two additional crucial advantages. The use of DMAP provides a significant challenge with purification and can remain at various levels as an impurity in the final product even after multiple recrystallizations. This could be due to the strong interaction of the DMAP with the quaternary nitrogens. During the reaction another derivative (previously unidentified), a trimeric m-7N(m)-m can also form at different levels depending on the conditions used and its removal during purification may not be easily achieved. Using a solvent-free and DMAP-free approach, Boc₂O protection before quaternization, and TFA deprotection at the end of synthesis after recrystallization allows for the production of a pure species of m-7NH-m. Furthermore, the one-pot reaction scheme allows for increased yield with low product loss that happens with multiple recrystallizations in a multi-step synthetic scheme.

Synthesis of m-7N(m)-m (m=12, 16 and 18) trimeric gemini surfactants with a two 3C spacers were previously reported for the first time in 1996 (158, 255). Trimeric gemini surfactants synthesized by this protocol have an alkyl tail attached to the amine substitution in the spacer having similar alkyl chain length equivalent to other two alkyl tails at the two-quaternary nitrogens making them bis-quaternary-trimeric gemini surfactants (Scheme 2). Unlike the tris-gemini surfactants (158) these

surfactants only possess bis-quaternary nitrogens. Because, the amine group in the spacer is not quaternarized it remains a tertiary nitrogen. Schematic structures of bis-quaternary and tris-quaternary trimeric gemini surfactants are shown under.

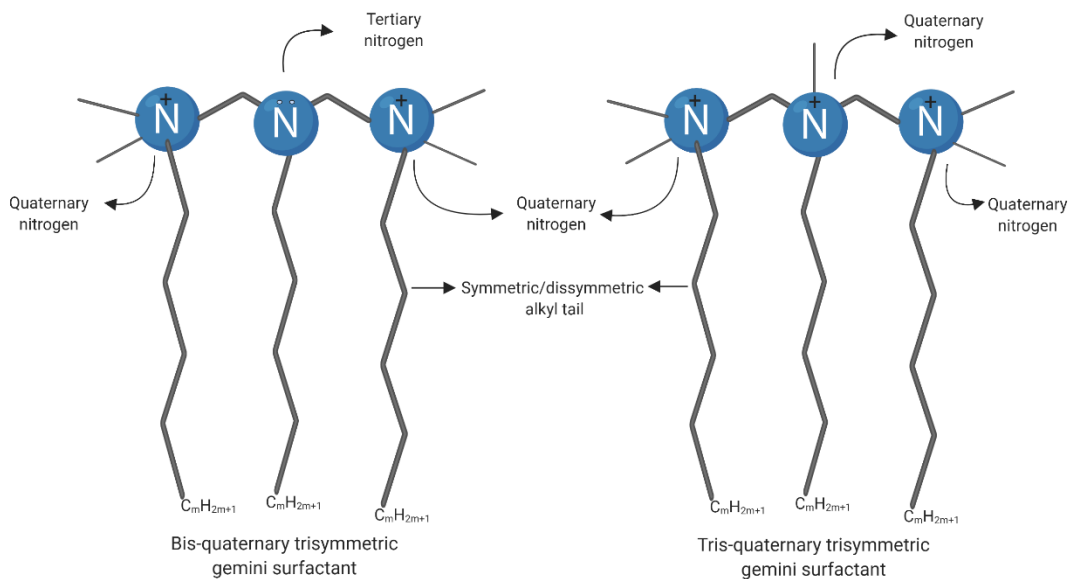


Figure 3-16 General schematic structures of bis- and tris-quaternary trimeric gemini surfactants. Figure generated by Lokesh Narsineni using BioRender.com.

Dimeric gemini surfactant NPXs made from 18-7NH-18 (OS), due to presence of mixed species of m-7NH-m and m-7N(m)-m gemini surfactants and DMAP as bound impurity in the final product (observed from the mass spectrometry and NMR spectroscopy as shown in Figure 1 (H) and Figure 2 N(B)), could have induced toxicity leading to low cell numbers and reduced TE. The trimeric gemini surfactant impurities could lead to increased hydrophobicity of the NPXs. This can lead to increased interaction of the DNA with the surfactant and can delay the DNA release inside the cell and increase the interaction of the surfactant with lipid bilayers.

The cationic charge on the NPs favor their interaction with cellular membranes facilitating internalization and leading to higher transfection efficiencies. Hence, charge ratio is a vital factor in NP design for therapeutic DNA delivery into cells. However, higher charge ratio can also lead to increased toxicity of the NP systems due to prolonged interaction and damage to the cell membrane leading to irreversible lipid cell membrane damage and eventually cell death.

The length of the alkyl tail, spacer group and the head groups are the important factors influencing the CMC values of the surfactants. Dimeric surfactants have significantly lower CMC values compared to monomeric surfactants (169). Owing to the above discussed reasons that are responsible for determining the CMC values, it is understood that the long chain alkyl tails play a significant role in lowering the CMC values in gemini surfactants. This could be one factor for lower CMC values for 18-7NH-18 gemini surfactants synthesized using published protocols (Scheme 1 A and B). However, synthesis of the 18-7NH-18 gemini surfactant using the new method (Scheme 1 C) produces more pure form of dimeric 18-7NH-18 gemini surfactant and less percent of trimeric 18-7N(18)-18 gemini surfactant which could have led to increase in the CMC values (51.69 μM) compared to 18-7NH-18 reported values (13 μM).

As the amount of surfactant is increased per unit ratio of plasmid DNA, the overall charge of the system increased from +5.29 to +41.43mV, which is in agreement with previously published data (159). The 16-7N(16)-16 NPXs treated cells showed better transfection efficiencies compared to 18-7N(18)-18 GP-NPXs. This can be attributed to the shorter alkyl tail length which could have reduced the overall hydrophobicity of the molecules contributing to lower DNA binding and allowing for easier disassociation inside the cells (256).

Gene expression kinetic studies for 18-7NH-18 NPXs to assess their peak gene expression kinetic profile over 3 time points 24, 48- and 72-hours (Figure 3-11) using flow cytometry and confocal

microscopy demonstrated that at 48 hours, 18-7NH-18 NPXs treated cells produce higher gene expression (Figure 3-11 and Figure 3-13).

The incubation study to determine NPX exposure showed that a treatment for 5 hours followed by replacement of cell supernatant with fresh complete media was optimal and longer nanoparticle exposure was not useful increasing uptake and/or gene expression. Assessment of kinetics of gene expression over time demonstrated that TE was highest at 48h after treatment application with the m-7NH-m NPXs (Figure 3C). At the 48-hour time point the 18-7NH-18 5:1 ratio gemini NPXs had the highest TE of $14.53 \pm 0.41\%$ compared to $5.55 \pm 0.38\%$ at 24 hours ($****p < 0.0001$) with no further increase at 72 hours ($14.69 \pm 1.094\%$).

To assess the effect of DOPE on TE and viability of cells, we formulated two sets of formulations, i.e. LPXs with the same charge ratios, such as 2.5:1, 5:1 and 7.5:1 (G:P) and with (1:0.5, 1:1, 1:1.5 and 1:2 G:L ratios) and NPXs without DOPE, but the same (G:P) charge ratios. The flow cytometry results demonstrated that increasing DOPE in the formulation resulted in a decrease of TE. The 1:0.5 G:L ratio had significantly higher TE compared to higher ratios ($****p < 0.0001$) (Figure 3-12). In all subsequent studies the 1: 0.5 G:L ratio was used for LPX formulations.

Results from the confocal microscopic imaging studies, were in agreement with the flow cytometry results and confirmed that TE was highest with 18-7NH-18 5:1 NPXs compared to other charge ratios tested. Whereas DOPE (1:0.5 G:L ratio) containing LPXs (5:1 G:P charge ratio) had lower TE and higher cell toxicities compared to 18-7NH-18 5:1 NPXs without DOPE at 48 hours (Figure 3-13). Flow cytometry results confirmed the number of cells expressing GFP at 48 hours was higher compared to 24 hours (Figure 3-11). At 72 hours the number of cells expressing GFP protein diminished and cells showed signs of toxicity, which was evident from reduced Mitotracker red staining. The results demonstrate that DOPE inclusion into the formulations, even at lower concentrations, caused

cytotoxicity. At 72 hours there was minimal GFP and Mitotracker red fluorescence observed in the wells treated with DOPE containing LPXs, this could be due to reduced cell number due to cell death which could have been caused due to prolonged incubation up to 72 hours and toxicity induced by the LPX system.

DOPE, a neutral helper lipid, is frequently used in NPs to facilitate gene delivery due to its ability to form inverted hexagonal (H_{II}) polymorphic structures with membrane fusogenic functions. DOPE may facilitate cellular uptake or endosomal escape by membrane fusion (147, 257).

Recent reports indicate that DOPE can also contribute to cell toxicity, and it is known to perform better *in vitro* but often fails *in vivo* (258, 259). For example, it was shown that at a charge ratio of $\rho = 5$ DOTAP/DOPE showed toxicity and nonspecific knockdown of the gene in an siRNA based system (260).

In this study we showed that DOPE at low levels (1:0.5 G:L ratio) was useful to enhance TE without lowering cell viability, however, 18-7NH-18 NPX formulations without DOPE comparatively performed better than 18-7NH-18 LPXs. 18-7NH-18 2.5:1:0.5 LPXs (G:P:L ratio) produced similar TE as 18-7NH-18 5:1 NPXs (G:P ratio) without DOPE. This effect could be due to the display of similar level of fusogenic or temporary disruption effects with the 18-7NH-18 2.5:1 LPXs with 1:0.5 of G:L ratio as that of 18-7NH-18 5:1 NPXs. Theoretical modeling studies combined with experimental data the DOPE concentration and charge ratio have specific importance. It was shown that the NPs at DOPE: gemini ratio 2-3 and gemini surfactant cationic charge ratio of 2.7, at pH 5 form a stable fusogenic lamellar/ H_{II} structure, characterized by a low free energy value, playing a role in endosomal escape leading to higher TE (261).

Also, while the increase in the lipid concentration disturbs the charge ratio required for the efficient transfection, at safe levels DOPE can help in reducing the charge on the particle and allow for increased

TE (262). On contrary, increase in gemini surfactant in the formulation leads to increased toxicity due to their increased charge density and cell toxicity as seen in the current study and correlates with the previous published studies (263). Hence, identifying an optimal concentration of gemini surfactant itself or in combination with lipid is vital for achieving higher gene cargo delivery into cells with lower toxicities.

The presence of the longer alkyl tails such as C₁₈ are known to modulate interaction with the lipid bilayer membranes to cause higher lipid order that can form more stable phase transitions (264). Hence, total concentration of lipid/surfactant in the formulation plays a role in how the NPXs/LPXs interact with the lipid bilayers of cells and cause temporary perturbation. LPXs deliver the plasmid DNA by various active transport mechanisms and get endocytosed (147, 257). Later, due to pH changes in the endosome the LPX attains an inverted hexagonal shape leading to interaction with endosomal membrane, rupture and releasing the therapeutic DNA (196). Some lipid based systems such as the ones made with DOPE and DOTMA are known to deliver DNA by fusion of the liposomes with the plasma membrane and leads to intracellular delivery of DNA (147).

The development of nanoparticles as a non-invasive topical eye drop dosage form require information about penetration or crossing the corneal tissue. Assessment of 18-7NH-18 and 16-7N(16)-16 NPXs using an *in vitro* 3D human EpiCorneal™ tissue model (MatTek®) demonstrated the importance of having an optimal particle size and charge density for the NPXs. The penetration was found to be higher for 18-7NH-18 5:1 NPXs, compared to 16-7N(16)-16 5:1 NPXs. Further increase in the alkyl tail number and size produced larger particles which could affect the route of cellular entry and intracellular fate (265). While 18-7NH-18 5:1 NPXs were found to have particle sizes below 250 nm, the 16-7N(16)-16 5:1 NPXs were found to be around 350-400 nm, which could have impeded their free movement in the tissue and their endocytosis (192). It was also shown that 18-7NH-18 5:1 NPXs

carrying Cy5 labelled gWIZ-GFP plasmid penetrated 80-100 μ m deep into the cornea within the first 0.5-1 hour (Figure 3-14). The NPXs were well adhered to the surface even after three repetitive steps of washing before imaging. The 18-7NH-18 5:1 NPXs penetrated into the tissue and reached deeper layers of the corneal tissue. The 18-7NH-18 5:1 NPXs were observed to be taken up into the cells within the first hour in large numbers as shown in Figure 3-14 (i and ii). The 16-7N(16)-16 5:1 NPXs showed a different interaction pattern with the cornea. There was significant superficial binding and penetration up to about 30-40 μ m depth during the first 0.5-1 hour (Figure 3-15 i and ii), but despite of the presence of a lot of NPXs on the surface no significant amount of NPX penetration was observed into deeper layers. A possible reason could be related to the larger particle size of 16-7N(16)-16 5:1 NPXs compared 18-7NH-18 5:1 NPXs, which could have impeded their movement and cell interaction in the tissue (192). Another factor might be related to the comparatively higher hydrophobicity of the trimeric gemini surfactants, which could decrease partitioning into the hydrophilic corneal tissues and also possibly providing increased DNA binding which could inhibit effective dissociation of the plasmid.

We have shown before that gemini nanoparticles have the ability to interact with membranes and induce temporary increase of permeability by ‘nanoporation’ (266). This phenomenon is associated with the permeation of typically membrane-impermeable stains used for imaging studies (eg. dead-cell stains) but at the same time the cells also stain positive with metabolic cell viability dyes (eg. Mitotracker Deep Red or calcein). In the confocal microscopic study, we used Image[®] IT dead cell stain, which stained the corneas treated with NPXs. Interestingly, the staining pattern corresponded to the pattern of NPX diffusion indicating that temporary cell membrane disruption was caused by the NPXs. However, the tissue appeared normalized several hours later and as the nanoparticles diffused out of the cornea, the membrane integrity recovered and the cells treated with Mitotracker Green have produced the

metabolic dye in the mitochondria of the cells as seen from the EpiCorneal treatment images at 24 hours (results not shown).

3.6 Conclusion

We have formulated a novel gene delivery nanoparticle system based on the 18-7NH-18 second-generation gemini surfactant for retinal gene therapy by ocular topical application. The m-7NH-m series of gemini surfactant building blocks were synthesized by an improved one-pot, DMAP free reaction scheme with 2-fold increase in yield and high purity without contamination of a previously unidentified trimeric gemini surfactant by-product (m-7N(m)-m) and DMAP.

NPXs made from 18-7NH-18 gemini surfactant made with the new synthetic scheme showed high TE and reduced toxicities in A7 astrocytes at the optimum 5:1 ratio of gemini: plasmid. The presence of DOPE was shown to be detrimental for both transfection and cell viability, that is 18-7NH-18-NPXs consistently showed higher TE and cell viability compared to LPXs. *In vitro* corneal interaction assessment of the 18-7NH-18 NPXs showed penetration and crossing of the cornea within 0.5-1h after treatment. NPXs made from m-7N(m)-m trimeric gemini surfactant showed very low TE, increased cell toxicity and corneal surface binding without penetration into the cornea.

Overall, the NPXs made from 18-7NH-18 gemini surfactant are potential gene delivery systems for ocular topical administration and for further *in vivo* studies.

Chapter 4 Development of multifunctional gemini nanoplexes for non-viral neurotrophic factor gene delivery to the retina

4.1 Introduction

Our group has shown previously that dicationic amphiphilic gemini surfactants (second generation gemini surfactants; m-7NH-m) form complexes and/or NPs and deliver therapeutic DNA to various cells (136, 159, 173). Compared to first generation gemini surfactants (m-s-m), the presence of a pH sensitive spacer amino group in the second generation gemini surfactants facilitates endosomal escape and increases TE (159). Additional chemical modifications at the amino group, such as addition of peptide moieties can provide further functionalities, eg. cell binding and increased recognition. Peptide modification is a potential method to increase functionalities of NPs. Several groups of peptide ligands have been used for NP conjugation such as cell penetrating peptides (CPPs), cytosolic transport peptides and nuclear localization peptides.

4.1.1 Functionalization of gemini surfactants with integrin-binding and IgSF cell adhesion peptides (CAPs)

The utilization of CAPs is a new direction in cell targeting. CAPs are peptide sequences from one of the four major classes of CAMs. In this study we selected one CAP from the integrin-binding family, namely Arg-Gly-Asp (RGD) sequence, and three peptides from CAMs of the IgSF (Table 4-1).

Integrins are highly expressed in the retina (230). They are characterized by α and β subunits arranged together in various configurations, with $\alpha_5\beta_3$ the most widely distributed configuration in the retina. They possess extracellular, intracellular and transmembrane domains that can recognize the integrin ligands, promote cell-cell adhesion, ocular development and other wound healing functions. It has been well established that the integrin receptors are distributed in the cornea, TM, retina, choroid and an increased expression of the integrins was shown after a glaucomatous damage or induced insults in the

optic nerve to initiate a repair process (232, 267). RGD peptide is a well-established ligand with high affinity for integrin receptors. The sequence of Arg-Leu-Glu (RLE) was chosen as a reference peptide since it was used before as a non-binding control for Thy-1 targeting studies (204, 268).

Members of the IgSF possess the so-called Ig domain or fold that plays a role in cell recognition, binding and adhesion. Three peptide sequences derived from neural cell adhesion molecules (NCAMs) were selected for this study (Table 4-1). One of these is a peptide derived from L1CAM with the sequence of Phe-Ala-Ser-Asn-Lys-Leu (FASNKL). The second peptide is from the extracellular domain of P₀ protein, with the sequence of Tyr-Thr-Asp-Asn-Gly-Thr-Phe (YTDNGTF), which our group has shown previously to exhibit heterophilic binding properties with other membrane CAMs, for example ICAM-1 (269-271), and the third is a short dipeptide Leu-Ile (LI) that could provide non-specific binding through hydrophobic interactions and could be beneficial as an inducer of BDNF and GDNF and enhance RGC survival (272-274).

Table 4-1 Integrin-binding and neural IgSF-derived peptides used for gemini NP design

Peptide	Sequence	Origin	Molecular weight (Da)	Function	Reference
I. Integrin-binding					
p ₁	Arg-Gly-Asp (RGD)	Fibronectin	346.35	Integrin-binding ligand	(275)
p ₂	Arg-Leu-Glu (RLE)	Thy-1 RLD (non-binding mutant)	416.48	Non-binding control of RGD/RLD	(204)
II. Neural IgSF					
p ₃	Phe-Ala-Ser-Asn-Lys-Leu (FASNKL)	in L1CAM Ig1	678.78	in L1CAM Ig1 promotes binding to neuropilin-1 (NP-1) a component of semaphorin 3A (sema 3A)	(276, 277)

				receptor complex	
p ₅	Tyr-Thr-Asp-Asn-Gly-Thr-Phe (YTDNGTF)	P0 protein extracellular domain	816.82	Homophilic and heterophilic binding with other IgCAMs in nervous and immune system	(226, 269, 270)
III. BDNF inducer peptide					
p ₄	Leu-Ile (LI)	Hydrophobic dipeptide	244.34	Induces production of BDNF and GDNF	(272, 278)

4.2 Rationale and Objective

4.2.1 Rationale

The 18-7NH-18 gemini surfactant produced with high purity using the improved synthetic method (as shown in Chapter 3) was used to generate the third-generation peptide conjugated gemini surfactants. By selecting peptide sequences from cell adhesion molecules found in the nervous system, improved functionality can be built into the NPXs. Cell adhesion peptides (CAPs) conjugated to the spacer NH group of second-generation surfactants provide the building blocks for pNPXs with adhesive properties that enhance cell binding, uptake, and potentially enhanced affinity to the retina.

4.2.2 Objective

The overall objective of the work in the current chapter was to synthesize integrin-binding and IgSF peptide functionalized gemini surfactants for use in the formulation of peptide-functionalized pNPXs and evaluate their gene delivery properties both *in vitro* and *in vivo*. Specific objectives included

- i. Design and synthesis of five peptide-modified m-7N(p₁₋₅)-m gemini surfactants; the peptides are identified from integrin-binding and IgSF sequences.

- ii. Formulation design, development and physicochemical characterization of m-7N(p₁₋₅)-m pNPXs carrying reporter and/or BDNF gene.
- iii. Evaluate the *in vitro* TE of m-7N(p₁₋₅)-m pNPXs carrying reporter and/or BDNF gene in A7 astrocytes, neurospheres and the EpiCorneal tissue model.
- iv. Evaluate the delivery and TE of m-7N(p₁₋₅)-m pNPXs carrying reporter and/or BDNF gene to the retina *in vivo* in CD1 mice by confocal microscopic imaging and quantitative enzyme-linked immunosorbent assay (ELISA) of BDNF levels after IVT injections.

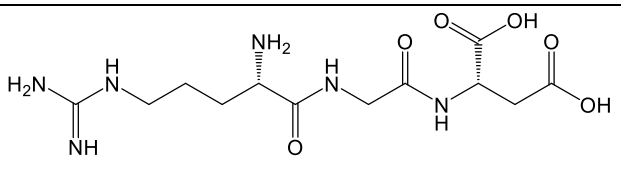
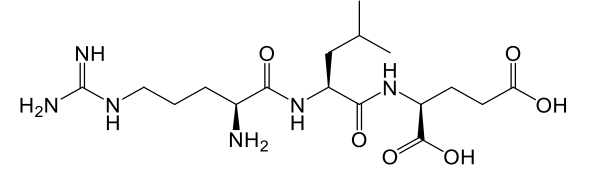
4.3 Materials and Methods

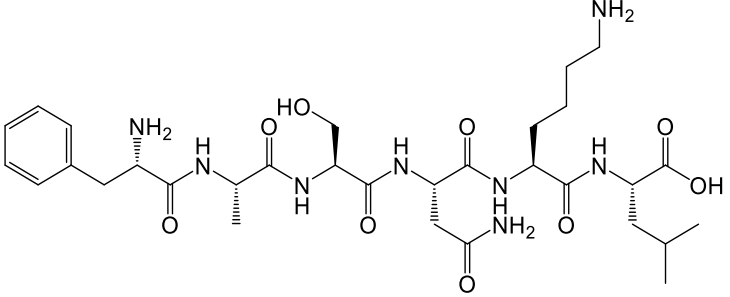
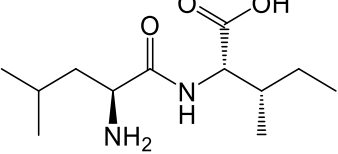
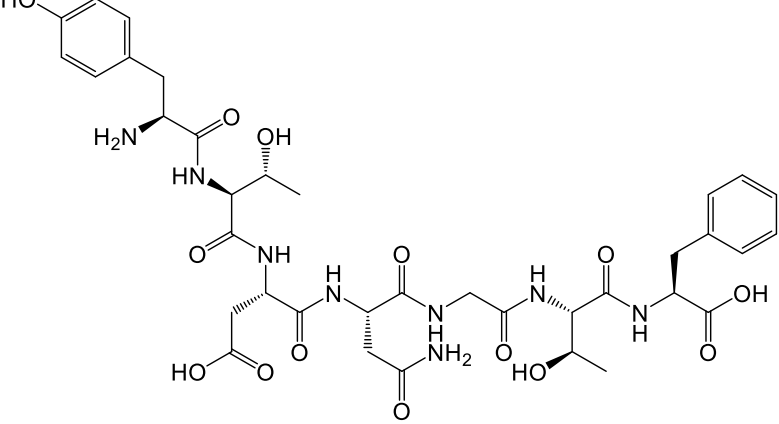
The general scheme for synthesis of m-7N(p)-m (m=C₁₂ and C₁₈, p= integrin-binding or IgSF peptides p₁, p₂, p₃, p₄ and p₅) gemini surfactants (G) is illustrated in Scheme 3. All reactions were carried out using Radley's Carousel 6 plus reaction station™ (Radley's). The 12-7NH-12 gemini surfactant (*N,N'*-(azanediylbis(propane-3,1-diyl))bis(*N,N*-dimethyldodecan-1-aminiium) (Batch: FL12GLN-061216-R10-001, 92%), and the 18-7NH-18 gemini surfactant (*N,N'*-(azanediylbis(propane-3,1-diyl))bis(*N,N*-dimethyldodecan-1-aminiium) (Batch: FL18GLN-053117-RX9-001, 94%) were synthesized in-house based on Scheme 1 C (see Chapter 3). Peptides (p₁₋₅) (Table 4-2) and peptide-functionalized gemini surfactants (18-7N(p₁₋₅)-18) were synthesized at Celtek Biosciences LLC, TN, USA (technology transfer for synthesis of peptide ligated compounds was carried out between Drug Delivery and Pharmaceutical Nanotechnology Laboratory (Foldvari Lab) and Celtek Biosciences LLC) as follows: (percentages indicate the purity as determined by Celtek using HPLC).

p₁: RGD (Arg-Gly-Asp, >95%, MW:346.35), p₁G_m: m=C₁₂ or C₁₈, 18-7N(RGD)-18 (>95%, MW:1022.65), p₂: RLE (Arg-Leu-Glu, 99.26%, MW: 416.48), p₂G_m: 18-7N(RLE)-18 (>95%, MW:1092.78), p₃: FASNKL (Phe-Ala-Ser-Asn-Lys-Leu, 98.90%, MW:679.60), p₃G_m: 18-

7N(FASNKL)-18 (99.78%, MW: 1355.09), p₄: LI (Leu-Ile, 97.17%, MW:244.34), p₄G_m: 18-7N(LI)-18 (>95%, MW: 920.64), p₅: YTDNGTF (Tyr-Thr-Asp-Asn-Gly-Thr-Phe, >95%, MW:816.82), p₅G_m: 12-7N(YTDNGTF)-12, (>95%, MW:1324.80) 18-7N(YTDNGTF)-18 (>95%, MW:1493.12). 1-[Bis(dimethylamino)methylene]-1*H*-1,2,3-triazolo[4,5-*b*]pyridinium 3-oxid hexafluorophosphate (HATU) (MW:380.23%, 97%), DIPEA (MW:129.24, 99%), *N,N*-dimethylformamide (DMF) (MW:73.09, 99.8%), TFA (MW:114.02 g/mol, 99%), TIS (MW:158.36 g/mol, 98%), methanol HPLC grade (MW: 32.04, 99.9%), acetonitrile HPLC grade (MeCN, MW:41.05, 99.9%) were purchased from Sigma-Aldrich (Oakville, ON, Canada).

Table 4-2 Peptides used in the peptide-modified dicationic gemini surfactant synthesis and their properties

Peptide	Structure	Properties- Chemical formula and mol. wt.
p ₁ (RGD)		C ₁₂ H ₂₂ N ₆ O ₆ 346.34
p ₂ (RLE)		C ₁₇ H ₃₂ N ₆ O ₆ 416.48

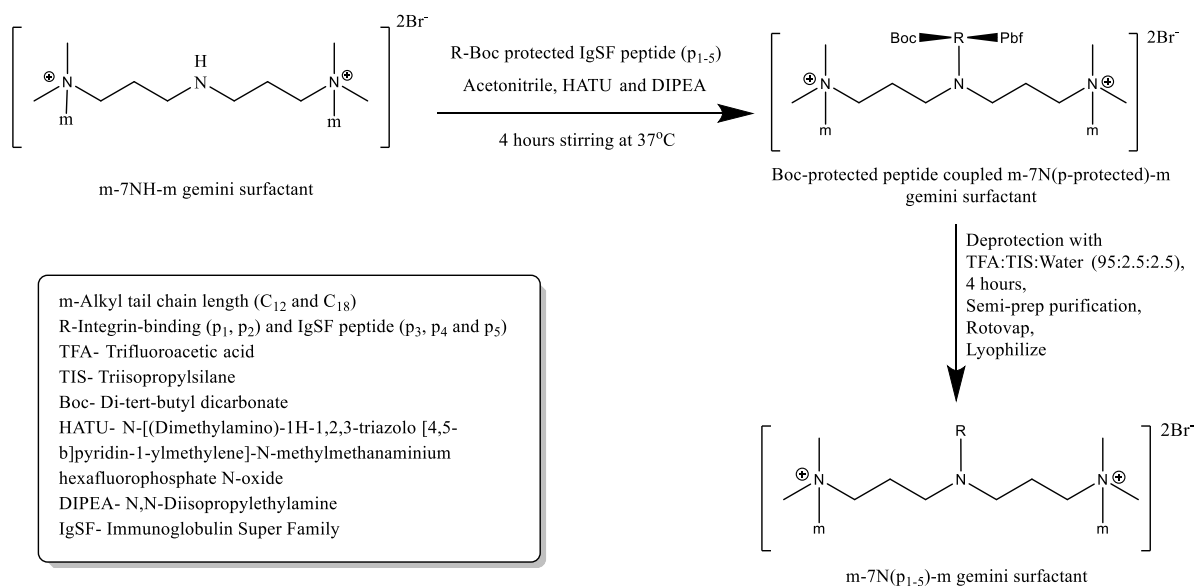
p ₃ (FASNKL)		$C_{31}H_{50}N_8O_9$ 678.79
p ₄ (LI)		$C_{12}H_{24}N_2O_3$ 244.34
p ₅ (YTDNGTF)		$C_{36}H_{48}N_8O_{14}$ 816.82

4.3.1 Synthesis, purification and characterization of peptide-modified m-7N(p)-m gemini surfactants

Synthesis of m-7N(p₁₋₅)-m gemini surfactants were carried out using second generation m-7NH-m gemini surfactants as shown in Scheme 3. The covalent ligation reactions, to form an amide bond, were carried out in the liquid phase using anhydrous acetonitrile as a solvent. The batch size was 30 μmol in 20 mL of acetonitrile. HATU was used as a coupling agent and DIPEA as a base. The appropriate protected peptide (p₁₋₅) and HATU were added into the required volume of acetonitrile, dissolved and

the temperature of the reaction vessel (Radleys) was maintained at 37°C. The required volume of DIPEA was added to the reaction mixture, followed by the addition of m-7NH-m (m=12 and 18 C) gemini surfactant. The reaction was monitored by UPLC (Waters H-class Bio system with PDA and FLR detectors) (Waters, Milford, USA) on a C₁₈ column at 210 nm with solvent A as 0.1% TFA in water v/v and solvent B as 0.1%TFA in acetonitrile v/v. Gradient elution method was developed for 25 mins with 70-100% acetonitrile as solvent A and UPLC grade water as solvent B in 15 minutes (Appendix 2, Figure 5 and Figure 6). 3D scans were also tracked initially to identify the product formation and its λ_{max} absorbance which was determined to be 210 nm from the scans. After 4 hours the reaction was complete, the crude products were collected and purified using a semi-preparative method using a HPLC (Waters e2695 separations module with a UV/VIS detector 2489) (Waters, Milford, USA) with UV detection on a C₁₈ semi-preparative column where solvent A was 0.1% TFA in HPLC grade water v/v and solvent B was 0.1%TFA in Acetonitrile v/v. Gradient elution method was developed with 70-100% solvent B in 18 minutes. The excess solvent was evaporated from the collected fractions containing the protected peptide conjugated gemini surfactant m-7N(p(protected))-m (Figure 7). Deprotection was carried out using TFA cleavage cocktail (TFA:TIS:Water 95:2.5:2.5) for 4 hours. Deprotection monitoring was carried out by UPLC with solvent A (0.1% TFA in HPLC grade water v/v) and solvent B (0.1%TFA in acetonitrile v/v) with a gradient elution method, 70-100% Solvent B in 15 minutes. After deprotection the crude products were collected and purified using a semi-preparative HPLC method developed on a C₁₈ semi-preparative column with UV detection (Figure 8), with solvent A (0.1% TFA in HPLC grade water v/v) and solvent B (0.1%TFA in acetonitrile v/v). Gradient elution method was developed with 70-100% solvent B in 18 minutes. All products were purified using the same method and the collected samples were concentrated by evaporating the excess solvent. The pure product was lyophilized and stored at -20°C. The analysis of purity and confirmation of compound identities were carried out using UPLC and ESI-MS. A general protocol for synthesis of

m-7N(p₁₋₅)-m gemini surfactants was developed in our lab for both m=C₁₂ and C₁₈ alkyl tail gemini surfactants and p₅ peptide was used for synthesis and characterization of the peptide conjugated compounds. The technology of peptide modified gemini surfactant synthesis was transferred to Celtek Biosciences for 200 mg scale synthesis of m-7N(p₁-p₅)-m (m=18) gemini surfactants. The m-7NH-m (m=18) gemini surfactant was synthesized in our lab (as per Scheme 1 C) and supplied to Celtek Biosciences LLC. The 18-7N(p₁-p₅)-18 with a purity >95% were provided by Celtek and characterized using HPLC and ESI-MS methods in our lab.



Scheme 3 General scheme for synthesis of integrin-binding and IgSF peptide functionalized m-7N(p₁₋₅)-m gemini surfactant

4.3.2 Formulation and characterization of m-7N(p₁₋₅)-m (m=12 and 18) gemini surfactant pNPXs and pLPXs

Formulation of peptide-functionalized m-7N(p₁₋₅)-m (m=C₁₂ and C₁₈ C alkyl tail) gemini surfactant pNPXs and pLPXs was carried out using two methods. pNPXs are composed of peptide modified-gemini surfactant (pG, p=peptide₁₋₅) and plasmid (P) and pLPXs are composed of peptide modified-

gemini surfactant (pG, p=peptide₁₋₅), plasmid (P) and DOPE neutral lipid (L) (Figure 3-2). The pNPXs were prepared at charge ratios 2.5:1, 5:1, 7.5:1 and 10:1 (pG:P) and varying DOPE weight ratios such as 1:0.5 and 1:1 (pG:L). DOPE vesicles were prepared as described earlier (see Section 3.3.3.3 and Figure 3-1).

4.3.2.1 Formulation of pNPXs and pLPXs

pNPX and pLPX assembly was carried out by mixing the required amount of plasmid solution with a calculated amount of pG solution to obtain the required charge ratio (ρ_{\pm}) of 2.5:1, 5:1, 7.5:1 and 10:1. The mixture was left at room temperature for 15 minutes to obtain highly compacted pNPXs (Figure 3-2). To prepare pLPXs after the 15 minutes incubation, 5mM DOPE vesicles (see Section 3.3.3.3), were added at 1:0.5 and 1:1 pG:L weight ratio.

4.3.2.2 Physical mixture formulations

For comparative studies bi-component and tri-component physical mixtures of the peptides (p₁₋₅) and plasmid (p+P) were mixed together at 2.5:1, 5:1 and 7.5:1 ratios (p:P) and incubated for 15 minutes to evaluate the effect of unconjugated peptide on transfection. In the tri-component physical mixture, 18-7NH-18 gemini surfactant was combined with the appropriate peptide p₁-p₅ (p_n+G) followed by the addition of plasmid (p_nG+P). The G:P ratio was kept at 5:1 for all formulations while the ratios of peptides tested were varied between 1:2.5, 1:5 and 1:7.5 (final ratios 2.5:5:1, 5:5:1 and 7.5:5:1 (p:G:P) by weight).

4.3.3 Characterization of pNPXs and pLPXs

4.3.3.1 Particle sizing and zeta potential analysis

Particle size analysis of pNPXs and pLPXs was carried out by DLS using Zetasizer Nano ZS (Malvern Instruments, Worcestershire, UK). Particle size distribution was determined by using 60 μ L samples

and the average of three separate readings were taken and each reading was performed with n=3 analyses set per sample and 10 repetitions per each reading by the instrument. Z-average size of each sample was reported as an average of three separate readings (n=3) nm. \pm SD. Zeta potential measurements were carried out using phase analysis light scattering and a mixed mode technique with Zetasizer Nano ZS. The analysis was carried out in a specialized folded capillary cell with gold plated electrodes. pNPXs and pLPXS were diluted with ultrapure water (Milli-Q) at 1:25 (v/v) ratio and measured by taking an average of at least three readings. The zeta potential values are reported as mV \pm SD (n=3).

4.3.4 In vitro transfection efficiency and toxicity studies of pNPXs and pLPXs in A7 astrocytes

The TE assay of pNPXs and pLPXs and bi-component and tri-component physical mixtures was carried out in A7 astrocytes. Rat A7 astrocytes (received from Dr Jeremy Sivak, University of Toronto) were cultured in DMEM/high glucose media (Hyclone, GE Healthcare Life Sciences, Logan, Utah, USA) supplemented with 10% FBS (Hyclone, GE Healthcare Life Sciences, Logan, Utah, USA) and 1% Pen/Strep (Hyclone, GE Healthcare Life Sciences, Logan, UT, USA) at 37 °C in a 95% air/5% carbon dioxide atmosphere. Cells were seeded into 96-well flat bottom tissue culture plates (Grenier Bio-one, Monroe, NC, USA) at 15,000 cells/well. After 24 hours, at 80-90% confluency, the complete media was removed from the wells and replaced with fresh basic media (without serum). Formulations were freshly prepared and dosed immediately to their respective well as per the plate plan. Cells were treated with formulations containing 0.5 μ g of pDNA/dose per well and incubated for 5h at 37 °C in a CO₂ incubator (VWR Scientific, PA, USA). After 5 hours the basic media was replaced with complete media and incubation continued for 24 or 48 hours. After the incubation period cells were detached from the plate using Accutase™ (Innovative Cell Technologies) and stained with MitoTracker Deep Red FM (500nM) (Thermo Fisher Scientific), prepared as a 1000nM stock in Accumax™ (Cell dissociation

solution) (Innovative Cell Technologies) and incubated for 30 minutes. TE (%) and viability (total live population %) both were analyzed by flow cytometry (Attune, Life Technologies). The expression of GFP was detected using the BL1 channel excited by a 488 nm laser and captured with a band pass filter of 530nm \pm 30nm for GFP detection and the red fluorescence of Mitotracker™ Deep Red was excited using the 638 nm laser and was detected using a RL1 channel and captured with a band pass filter of 650nm \pm 20nm. Photo multiplier tube (PMT) voltages for forward scatter and side scatter of A7 astrocytes were set at 1300 and 2400 mV respectively. While the voltages for BL1 and RL1 channels were set at 1500 mV and 1400 mV respectively.

All statistical analyses were carried out on GraphPad Prism (GraphPad software, La Jolla, CA, USA), and data are presented as mean \pm S.D, (n=3). Two-way ANOVA with Tukey multiple comparison tests were carried out to analyze the obtained data sets. A P-value less than 0.05 is considered as significant and the level of significance is indicated on the graphs with (*).

4.3.5 In vitro corneal penetration and toxicity studies using a 3D EpiCorneal tissue model

In vitro tissue penetrations studies were carried out using the EpiCorneal™ COR-100 3D tissue model (MatTek Corporation, Ashland, MA) to determine the degree of permeation ability of the pNPXs and pLPXs prepared with Cy5 labelled gWIZ-GFP (see Section 3.3.9). Each tissue was dosed with 50 μ L of formulation containing 2.5 μ g of Cy5 labelled gWIZ-GFP. Experimental steps followed the same steps shown in Figure 3-4. Briefly, on the day of the experiment after the equilibration of the tissues, media was aspirated from each well and replaced with 1 mL fresh, prewarmed media and incubated again for 1 hour. Tissues in each well were dosed with 18-7N(p₁)-18 pLPXs, 18-7N(p₃)-18 pLPXs, 18-7NH-18 pNPXs). After dosing, the tissues were returned to the CO₂ incubator for 0.5 and 1 hour for the tissue penetration study. The corneas treated with 18-7N(p₁)-18 pLPXs was further incubated for 24 hours for evaluation of gene expression. At each time point, tissues were isolated from

the plate, stained and processed for imaging using CLSM. Calcein AM and Mitotracker Deep Red (at 24h) was used as a live cell stain and Image IT[®] (Invitrogen, Thermo Fisher Scientific) was used as a dead cell stain.

4.3.6 In vitro transfection studies in retinal stem cell-derived neurospheres

The evaluation of pNPXs and pLPXs as potential transfection agents was carried in a 3D retinal neurosphere model developed previously from CD 1-4 multipotent retinal stem cells (MRSC) in our lab (279). The “MiEye 8” protocol was followed for 3D MRSC neurosphere formation, testing of the formulations and analysis using CLSM as shown in Figure 4-1.

Briefly, on Day 1, a 12-well plate was coated with 200-300 μ L 0.2% gelatin and incubated for 1 hour. After one hour the excess gelatin was removed and three of the wells were seeded by mixing 1 million cells with 3 mL of retinal stem cell media-3 (RSCM-3) and were distributed into three wells equally. The RSCM-3 media was previously prepared with Advanced DMEM/F12 (RSCM-1) with 0.1% w/v glucose, 0.1% w/v lactose, 0.1% w/v bovine serum albumin (BSA), 0.045% w/v proline, 0.02422% w/v nicotinamide and 1%v/v L-glutamate, filtered through 0.45 μ M filter and 1% penstrep added to make RSCM-2. Supplements such as 10 μ L of insulin-transferrin-supplement-A, 50 μ L of knockout serum replacement, 20ng of EGF and 20 ng of basic-fibroblast growth factor (bFGF) were added per 1 mL of RSCM-2 media to make RSCM-3. On Day 2, at 80% confluency the cells were split, after detaching with 1x Accutase solution, into remaining 0.2% gelatin-coated wells (at 1:20 split ratio) to culture enough cells for seeding 15000 cells/well.

On Day 3 (Day 1 differentiation protocol) the cells were detached, pelleted and suspended in RSCM-3. Cells were withdrawn and resuspended in RSCDM-1 (Advanced DMEM containing 2mM of L-glutamine, 1:50 (1x) B-27 supplement and 10ng/mL bFGF) at 10,000 cells per 250 μ L per well for the 96-well PrimeSurface[®] 3D Culture Spheroid Ultra-Low Attachment (ULA) Plate (S-bio, Hudson, NH,

USA). Sphere formation was monitored and imaged by light microscopy daily until Day 10. The 3D spheroids were differentiated using RSCDM-1 from Day 3 to 4 (Day 1 and 2 differentiation protocol). On Day 5 (Day 3 differentiation protocol) media was changed to RSCDM-2 (Advanced DMEM containing 2mM of L-glutamine, 1:50 (1x) B-27 supplement, 1:100 N2-supplement and 10ng/mL bFGF) and continued growing until Day 8.

On Day 8 (Day 6 of differentiation protocol) 15 μ L formulations containing 0.5 μ g reporter gene (gWiz-GFP) of 18-7NH-18 NPXs, 18-7N(p₁)-18 pNPXs, 18-7N(p₃)-18 pNPXs and Lipofectamine[®] 3000 was added to the spheroids and incubated for 48 hours (Day 8-10). After treatment, the spheroids were transferred into a 24-well glass bottom plate (MatTek[™]), stained with DRAQ-5 nuclear stain for 15-30 minutes and were imaged using CLSM to determine the TE. For 18-7N(p₃)-18 pNPXs treated neurospheres were immuno-stained with RNA-binding protein with multiple splicing (RBPMS) antibodies (Santa Cruz Biotechnology, TX, USA) and counter stained with Goat anti-Human IgG (H+L) Cross-Adsorbed Secondary Antibody, Alexa Fluor 647 (Thermo Fisher Scientific) to determine the presence and location of differentiated RGCs. This was carried out by fixing the cells using 4% PFA (Alfa-Aesar, MA, USA) for 0.5 hours followed by permeabilization with 0.1% triton X-100 (Sigma Aldrich) in phosphate buffer saline (PBS), for 15 minutes, wash and remove permeabilization solution with PBS and add blocking solution (15% BSA with 0.5% Triton X-100 in PBS) and incubated for 0.5 hours. The blocking solution was removed and the spheres were washed with PBS three times and incubated with RBPMS antibody (Santa Cruz Biotechnology) for 1hour at 37°C or overnight at 4°C. The primary antibody was removed by washing three times with PBS, followed by incubation with a secondary antibody (goat anti-human IgG (H+L) cross-adsorbed secondary antibody-Alexa Fluor 647 conjugate) for 1 hour at 37°C or overnight at 4°C, then washed with PBS and imaged using

CLSM (Carl-Zeiss AG). Viability of the untreated 3D retinal neurospheres were tracked with Mitotracker[®] Deep Red (Invitrogen) live cell stain and Image IT[®] (Invitrogen) dead cell stain.

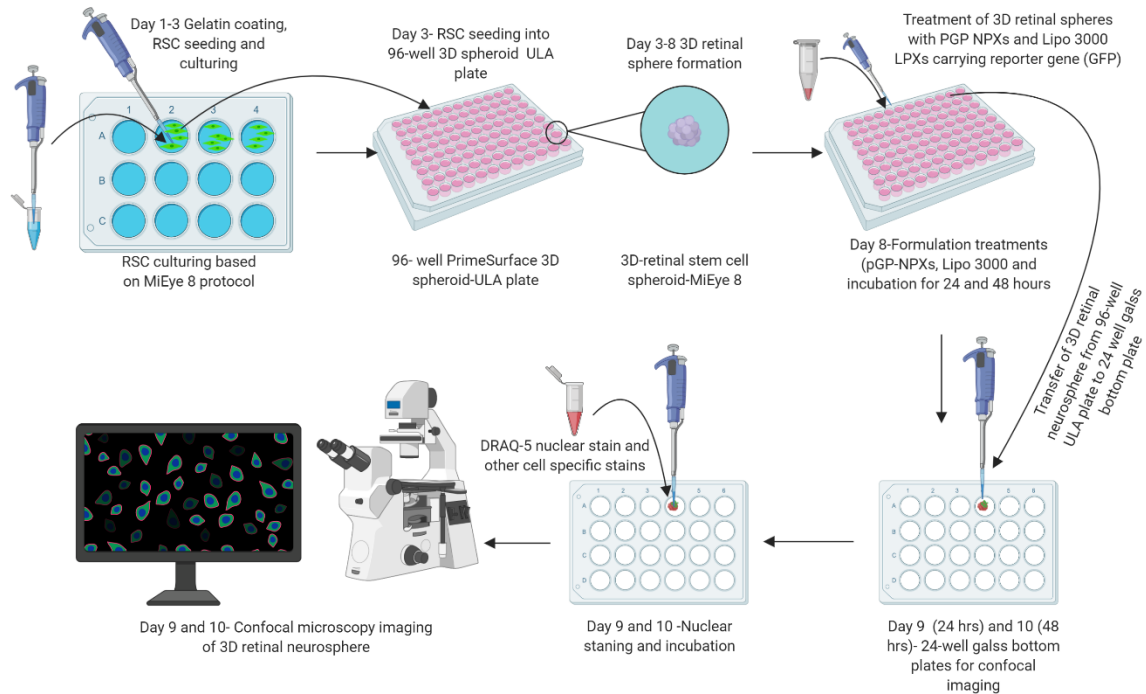


Figure 4-1 Schematic for evaluation of the TE and toxicity of pNPXs and pLPXs in 3D retinal stem cell derived neurospheres, i) Day 1: RSC seeding into a 12-well plate; ii) Day 3-8: neurosphere formation using culturing and differentiation media as per MiEye8 protocol (279); iii) Day 8: neurosphere treatment with formulations and incubation for 24 and 48 hours; iv) Day 9-10: neurosphere staining with DRAQ5 nuclear stain and cell specific antibody stains (Alexa Fluor 647 RBPMS) and imaged using CLSM. Figure generated by Lokesh Narsineni using BioRender.com.

4.3.7 *In vivo* retinal gene transfer studies in a CD1 mice

All animal experiments performed in this section were approved by the Office of the Research Ethics (ORE), University of Waterloo and all the protocols designed were in agreement with the Canadian

Council on Animal Care (CCAC). Based on results from the *in vitro* studies, selected formulations were advanced for *in vivo* evaluation in a CD1 mouse model. CD1[®]IGS Mice 4-6 weeks old (Charles River Laboratories, USA) were anaesthetized using freshly prepared ketamine (Vetoquinol, QC, Canada)/xylazine (Modern Veterinary Therapeutics LLC, FL, USA) (10mg/mL/1mg/mL) solution by intraperitoneal (IP) injection. 18-7N(p₁)-18 pNPXs, 18-7N(p₃)-18 pNPXs (both 5:1 ratio) and Lipofectamine 3000 prepared with tdTomato plasmid (Clontech, WI, USA) were administered bilaterally by IVT injection under a trinocular stereo microscope (Omax, ON, Canada). Prior to IVT injections, one drop of Mydrin (Phenylephrine HCl) 2.5% (pupil dilator) (Alcon, ON, Canada) and Alcaine (proparacaine HCl) 0.5% (local anaesthesia) (Alcon) was applied into each eye. A small incision using a 30-gauge needle (BD, NJ, USA) was made between the cornea and conjunctiva and around 205µL of the vitreous humor is flown out to make room for the formulation. A 2µL dose of test formulations containing 0.5µg of tdTomato plasmid or plasmid encoding BDNF were injected into the eye using a blunt end needle using a Hamilton syringe with needle (blunt end) with -10µL capacity (Hamilton Company, NV, USA).

Three days post administration, the eyes were surgically removed and fixed in 4% paraformaldehyde (Alfa-Aesar) for 2 hours using a rotary shaker at 4°C followed by 15% sucrose solution in PBS overnight. The left eyes from each animal were dissected under stereo microscope to isolate the retinas which were flat mounted on super frost micro-slides (VWR International, PA, USA), stained with Syto 13 (Invitrogen[®]) nucleic acid stain and covered with mounting media and cover slip. The right eyes from each animal were frozen in OCT medium (VWR) and placed in moulds for cryosectioning as whole eyes using cryostat (Thermo Scientific, USA). The retinas and eye cross sections were imaged by CLSM (Carl-Zeiss AG). At least four images from each retinal whole mount were selected

randomly and analyzed for cumulative mean fluorescence intensity (cMFI) of the RFP channel to identify the mean fluorescence of RFP expression in control and treated groups.

Similarly, whole eyes from groups treated with pNPXs carrying BDNF encoding plasmid were isolated (n=3; total of 6 eyes per group) and stored at -80°C for further evaluation of by ELISA.

4.3.8 BDNF expression in eyes treated with pNPXs in CD1 mice

Eye samples were retrieved from -80°C and 300µL/5mg tissue of extraction buffer was added and the samples were homogenized using a gentleMACS™ Dissociator (Miltenyi Biotec, Auburn, CA, USA) in gentleMACS™ M tubes. After homogenization the blades of the homogenizer tubes were rinsed with 150µL of extraction buffer and low agitation was continued for 2 h in an orbital shaker at 4°C. The samples were centrifuged for 20 minutes at 13000 RPM at 4°C. Supernatants were aliquoted into another vial and the aliquots were concentrated with Amicon centrifugal filters (3kDa cut-off). A 200 µL of the obtained aliquots were transferred into the Amicon centrifugal filters and were centrifuged at 14000 RPM for 5 minutes, 110 µL of the concentrate is recovered and stored at -80°C and used for evaluation of BDNF concentration using BDNF-ELISA kit (BioTechne, ON, Canada).

ELISA assay was carried out according to the manufacturer's protocol, with BDNF standards between 15.6-1000 pg/mL, and the Calibrator Diluent was used as a zero standard (0 pg/mL). Standards, control and sample aliquots were added to the wells at 50 µL per well and incubated for 2 hours at room temperature on an orbital shaker set at 500 ± 50 rpm. The contents of the wells were aspirated and washed with 400 µL of wash buffer four times. Total BDNF conjugate was added into each well and incubated for 1 hour. After incubation wells were washed using wash buffer four times and 200µL of substrate solution was added into each well and incubated for 30 minutes at room temperature, protected from light. After incubation, 50 µL of stop solution was added into each well which changed the color from blue to yellow, the plate was gently tapped to allow for proper mixing. The optical density (OD)

of the samples was determined within 30 minutes of adding the stop solution using a SpectraMax M5 microplate reader (Molecular Devices, Sunnyvale, CA, USA) and the optical density readings were read at 450 nm. Duplicate readings were averaged and adjusted after correcting with the O.D readings at 540 n.m. BDNF concentration in the homogenate samples was determined based on the BDNF standard plot (see Appendix 2-Figure 12). The average weight per eye was 17.45 ± 0.65 mg (n=6 eyes) and this value was used to calculate the average amount of BDNF produced per mg tissue. The standard plot values and the sample concentration values were reported and statistical analysis such as curve fitting, standard plot construction and one-way ANOVA on the total BDNF produced between various groups were carried out using GraphPad Prism[®] software (La Jolla, CA, USA).

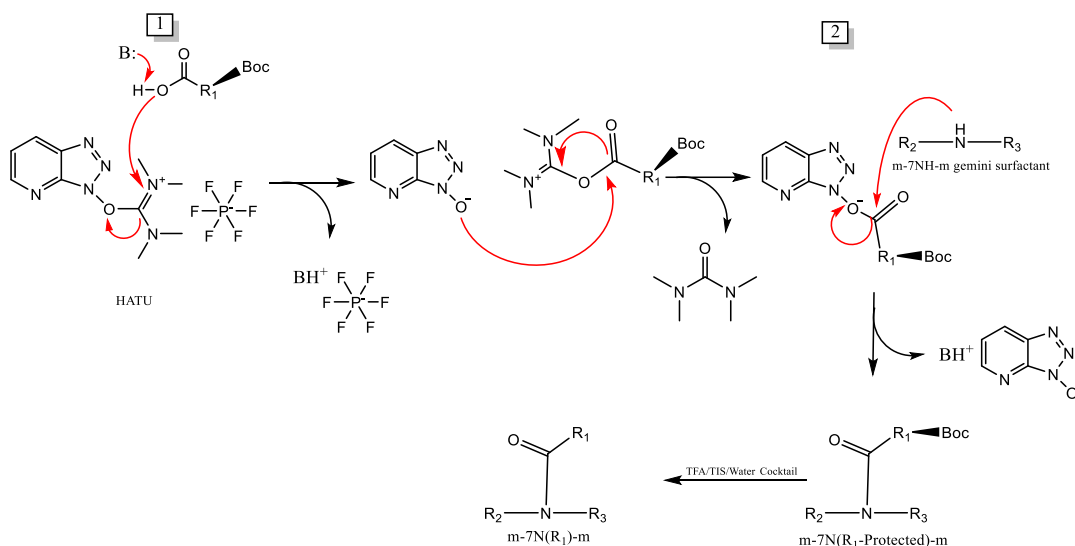
4.4 Results

4.4.1 Synthesis, purification and characterization of peptide-modified di-cationic m-7N(Pn)-m gemini surfactants

Peptide-modified gemini surfactants (m-7N(p_n)-m, m=12 and 18 p_n=p₁, p₂, p₃, p₄ and p₅) were synthesized using an amide bond coupling technique with HATU/DIPEA as coupling agent (Scheme 3). This technique allows for the direct conjugation of the peptide to the parent gemini compound, m-7NH-m, making it a simpler and more scalable method, compared to previous methods which utilized a more complicated multistep approach of conjugating the peptide to an intermediate component of the gemini compound (238, 263, 280).

The amide bond formation reaction was carried out using coupling agents such HATU/ *N,N*-diisopropylethylamine (DIPEA), EDC/HOBt, DCC/DMAP and acid chloride/AgCN reagents (281, 282). This reaction is based on the mechanism of HATU/DIPEA in forming an amide bond between the secondary amine in the spacer group and the carboxylic group of the Boc-protected peptide (Scheme 4). The base added to the reaction deprotonates the carboxylic acid. This species attacks the electron

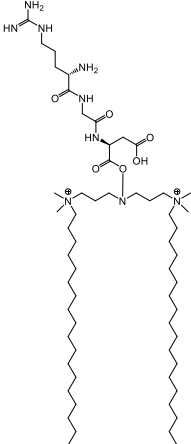
deficient HATU and forms HOAt anion and that in turn reacts with another carboxylic acid intermediate to form OAt activated ester, this step is identified by formation of a pale-yellow color in the reaction vessel. Finally, when the secondary amine (*m*-7NH-*m* gemini surfactant) was added into the reaction, the base deprotonates the amine resulting in reactive species that reacted with the OAt activated ester to form the amide bond (283). After the reaction was complete, the peptide was deprotected using the TFA/TIS/Water (95:2.5:2.5) cocktail (284). TFA cleavage cocktail was very effective in removing the protecting groups used in the peptide. The reaction times depended on the protecting group, presence of multiple heavy groups such as tert-butyl (tBu), 2,2,4,6,7-pentamethyldihydrobenzofuran-5-sulfonyl chloride (Pbf) groups require 6-12 hours while Boc groups can be deprotected within 4 hours. Hence, deprotection monitoring helped in identifying the ideal time for deprotection.

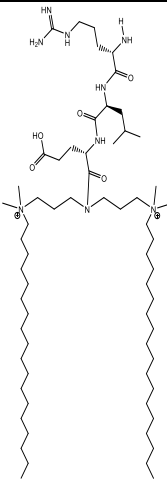
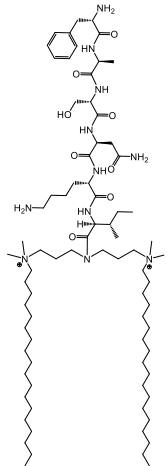
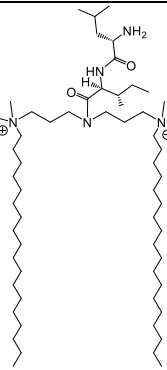


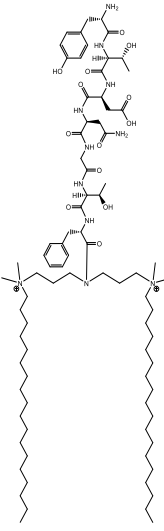
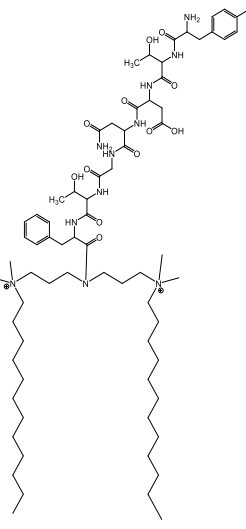
Scheme 4 Schematic of HATU/DIPEA mechanism to form amide bond between peptide and *m*-7NH-*m* gemini surfactant, B-Base (DIPEA), HATU- 1-[Bis(dimethylamino)methylene]-1*H*-1,2,3-triazolo[4,5-*b*]pyridinium 3-oxid hexafluorophosphate, Boc-Di-tert-butyl decarbonate, TFA- Trifluoroacetic acid and TIS- Triisopropylsilane. The coupling is a two-step process Step 1: the carboxylic acid of the Boc-protected peptide reacts with HATU to form the OAt-active ester, step-2: addition of a nucleophile (amino substituted gemini) to the active ester leads to formation of an acylated product (*m*-7N(*R*-protected)-*m*) and Boc protection is removed by treating the products with TFA cleavage cocktail.

The initial coupling technology was developed using the p₅ peptide to produce 12-7N(p₅)-12 and 18-7N(p₅)-18. The addition of DIPEA generated a deprotonated carboxylic acid species of the peptide and after a series of rearrangement reactions a reactive species of peptide with HATU was generated. Reaction monitoring was carried out using UPLC on a C₁₈ column using PDA detector at 210 nm (Appendix 2, Figure 5 , Figure 6). The 12-7N(p₅)-12 and 18-7N(p₅)-18 peptide-conjugated gemini surfactants were purified using HPLC system with a C₁₈ semi-prep column (Figure 7). The purified products were then deprotected using TFA cleavage cocktail (TFA:TIS:Water) (95:2.5:2.5). The deprotection reaction was monitored and the final products were purified, lyophilized and the identity of the products were confirmed by ESI-MS. The purity of the obtained products was analyzed using UPLC and the purity was found to be between 96-100%. The mass spectra of all peptide-modified gemini surfactants synthesized were shown in Appendix 2, Figure 10.

Table 4-3 Peptide-modified gemini conjugates produced using the HATU/DIPEA reaction scheme

Conjugate	Structure	Properties Chemical formula and mol. weight (Da)
<p>18-7N(p₁)-18</p> <p>p₁=RGD</p>		<p>C₅₈H₁₁₉N₉O₅²⁺</p> <p>1022.65</p>

<p>18-7N(p₂)-18</p> <p>p₂=RLE</p>	 <p>The structure shows a central nitrogen atom bonded to two long, zigzag hydrocarbon chains. The nitrogen is also bonded to a complex organic group containing several amide and amine functional groups.</p>	<p>C₆₃H₁₂₉N₉O₅²⁺</p> <p>1092.782</p>
<p>18-7N(p₃)-18</p> <p>p₃=FASNKL</p>	 <p>The structure shows a central nitrogen atom bonded to two long, zigzag hydrocarbon chains. The nitrogen is also bonded to a complex organic group containing several amide, amine, and hydroxyl functional groups.</p>	<p>C₇₇H₁₄₇N₁₁O₈²⁺</p> <p>1355.09</p>
<p>18-7N(p₄)-18</p> <p>p₄=LI</p>	 <p>The structure shows a central nitrogen atom bonded to two long, zigzag hydrocarbon chains. The nitrogen is also bonded to a complex organic group containing several amide and amine functional groups.</p>	<p>C₅₈H₁₂₁N₅O₂²⁺</p> <p>920.638</p>

<p>18-7N(p₅)-18</p> <p>p₅=YTDNGTF</p>		<p>$C_{82}H_{145}N_{11}O_{13}^{2+}$</p> <p>1493.12</p>
<p>12-7N(p₅)-12</p> <p>p₅=YTDNGTF</p>		<p>$C_{70}H_{121}N_{11}O_{13}^{2+}$</p> <p>1324.80</p>

4.4.2 Formulation and characterization of *m*-7N(p₁₋₅)-*m* (*m*=12 and 18) gemini surfactant *p*NPXs and *p*LPXs

Formulation of peptide-conjugated gemini pNPXs and pLPXs was successfully carried out at three different, 2.5:1, 5:1 and 7.5:1, charge ratios (ρ_{\pm}). pNPXs were formulated without DOPE helper lipid,

whereas pLPXs were formulated with DOPE (see section 3.3.3.2 and 3.3.3.3). DOPE vesicles were prepared as described in Section 3.3.3.3.

4.4.2.1 Particle size and zeta potential

The particle size (mean hydrodynamic diameter, z-average diameter), PDI and zeta-potential values are presented in Table 4-4 for charge ratio 5:1 pNPXs and 5:1:0.5 pLPXs as this ratio was found to have the most optimum TE and viability.

The particle size range for all gemini pNPXs was approximately between 180-320 nm regardless of the charge ratio (Figure 4-2 A). Within this range there were differences in particle diameters for the different pNPXs prepared from the different peptide-conjugated gemini surfactant building blocks. All pNPXs were larger than the NPXs made from the parent 18-7NH-18 gemini surfactant.

The PDI values were between 0.2 and 0.5 (Table 4-4). Values closer to 0.2 are indicative of more uniform size distribution. 18-7N(p₃)-18 pNPXs have a PDI closer to 0.2 ± 0.01 while unconjugated 18-7NH-18 NPXs had a PDI of 0.27 ± 0.01 , and 18-7N(p₁)-18 pNPXs and 18-7N(p₄)-18 pNPXs had a PDI of 0.36 ± 0.01 . When lipid was included in the formulation the PDI of the formulations increased with the exception of 18-7N(p₁)-18 pLPXs where despite increase in particle size the PDI remained 0.36 ± 0.06 . Higher PDI was noted for 18-7N(p₃)-18 pLPXs (0.41 ± 0.01) and 18-7NH-18 LPXs (0.42 ± 0.06) and the highest was for 18-7N(p₅)-18 pLPXs (0.52 ± 0.009) and 18-7N(p₂)-18 pLPXs (0.47 ± 0.04). The results overall revealed that higher charge ratio and the inclusion of DOPE resulted in increased particle size, and the heterodispersity of the pNPXs or pLPXs was always higher compared to the parent m-7NH-m at all the charge ratios tested.

Also, the results revealed that higher charge ratio and the inclusion of DOPE resulted in increased particle size, the particle size distribution of the peptide-modified pNPXs or pLPXs was always higher compared to its unmodified m-7NH-m counter parts at all the charge ratios tested.

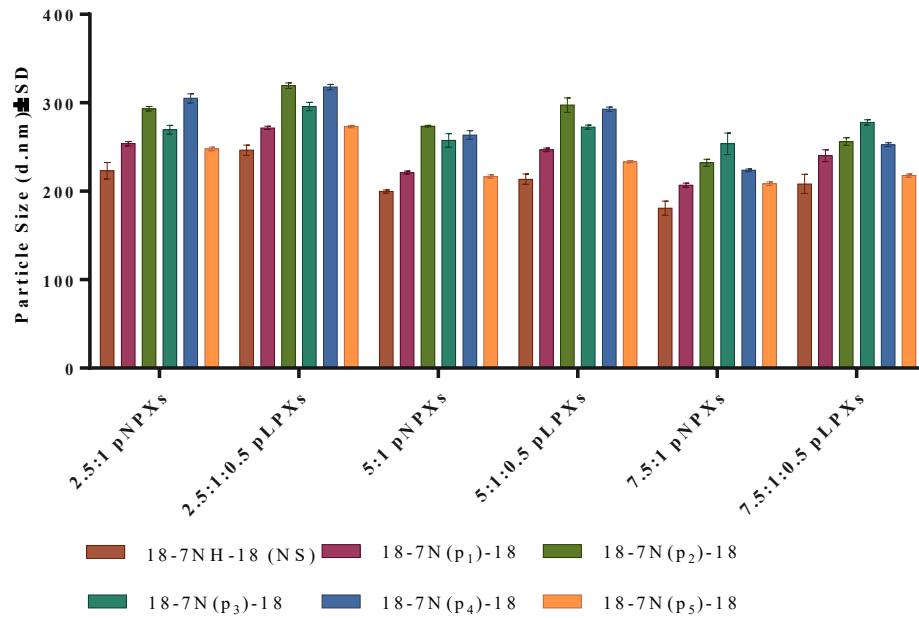
Table 4-4 Particle size (Z-average diameter), PDI and zeta (ζ) potential data for pNPXs (5:1 P:G ratio) and pLPXs (5:1:0.5 P:G:L ratio)

Formulation	Particle size (d.nm)±	PDI ± S.D.	ζ -Potential (mV) ±
	S.D. (n=3)	(n=3)	S.D. (n=3)
18-7NH-18 5:1 NPXs	199.80 ± 1.83	0.27 ± 0.01	30.18 ± 0.36
18-7NH-18 5:1:0.5 LPXs	213.63 ± 5.87	0.42 ± 0.06	32.24 ± 0.82
18-7N(p ₁)-18 5:1 pNPXs	220.96 ± 1.87	0.36 ± 0.007	30.76 ± 0.153
18-7N(p ₁)-18 5:1:0.5 pLPXs	246.86 ± 2.10	0.36 ± 0.01	33.91 ± 1.001
18-7N(p ₂)-18 5:1 pNPXs	273.60 ± 0.75	0.45 ± 0.02	36.26 ± 0.80
18-7N(p ₂)-18 5:1:0.5 pLPXs	297.40 ± 8.12	0.47 ± 0.04	41.65 ± 0.98
18-7N(p ₃)-18 5:1 pNPXs	257.40 ± 7.70	0.2 ± 0.01	37.13 ± 0.850
18-7N(p ₃)-18 5:1:0.5 pLPXs	272.50 ± 2.45	0.41 ± 0.01	40.17 ± 1.14
18-7N(p ₄)-18 5:1 pNPXs	263.66 ± 4.76	0.36 ± 0.01	34.80 ± 0.26
18-7N(p ₄)-18 5:1:0.5 pLPXs	292.73 ± 2.46	0.39 ± 0.006	39.67 ± 0.693
18-7N(p ₅)-18 5:1 pNPXs	216.63 ± 1.71	0.46 ± 0.002	37.73 ± 2.65
18-7N(p ₅)-18 5:1:0.5pLPXs	233.30 ± 1.03	0.52 ± 0.009	42.60 ± 3.1
12-7N(p ₅)-12 5:1:0.5pLPXs	272.41 ± 4.23	0.28 ± 0.02	36.98 ± 1.22

Note: Z-average size and respective size distribution by intensity graphs obtained for the various compositions of m-7-m, m-7NH-m and m-7N(p_n)-m (p_n=p₁₋₅) are shown in Appendix 2 (Figure 11).

The zeta potential of 18-7NH-18 NPXs and 18-7N(p_n)-18 pLPXs increased when the charge ratio was increased (Figure 4-2 B). Adding DOPE lipid did not increase the zeta potential of the formulations significantly. Except for 18-7NH-18 NPXs and 18-7N(p₂)-18 pNPXs at 2.5:1 G:P ratio all pNPXs and pLPXs had zeta potential above + 25mV. The highest and lowest zeta potential was measured for 18-7N(p₅)-18 7.5:1:0.5 pLPXs and 18-7N(p₂)-18 2.5:1 pNPXs, $+53.667 \pm 1.15$ and 13.13 ± 0.451 mV \pm S.D., respectively.

A.



B.

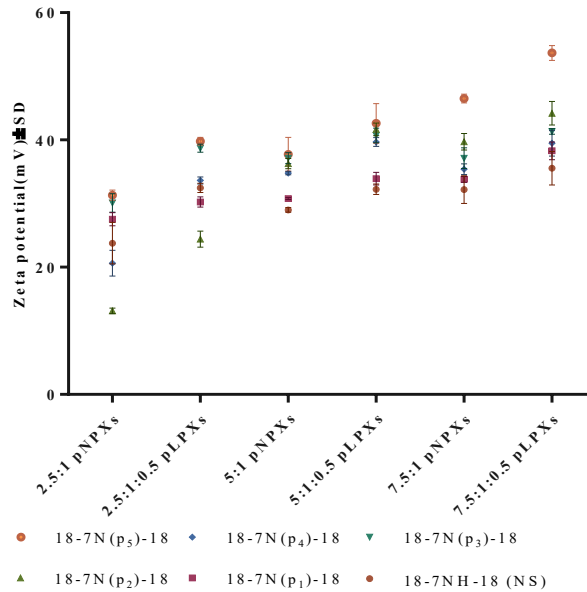


Figure 4-2 Physicochemical properties of 18-7NH-18 NPXs and LPXs and 18-7N(p₁₋₅)-18 pNPXs and pLPXs. A) Z-average particle size of the five 18-7N(p₁₋₅)-18 pNPXs and pLPXs, and the parent 18-7NH-18 NPXs and LPXs at 2.5:1, 5:1 and 7.5:1 G:P ratio and 2.5:1:0.5, 5:1:0.5 and 7.5:1:0.5 G:P:L ratios; B) Zeta potential for 18-7NH-18 NPXs and LPXs and 18-7N(p₁₋₅)-18 pNPXs and pLPXs. All values expressed as mean ± S.D., n=3.

4.4.3 *In vitro* assessment of transfection efficiency and toxicity of pNPXs in A7 astrocytes using flow cytometry

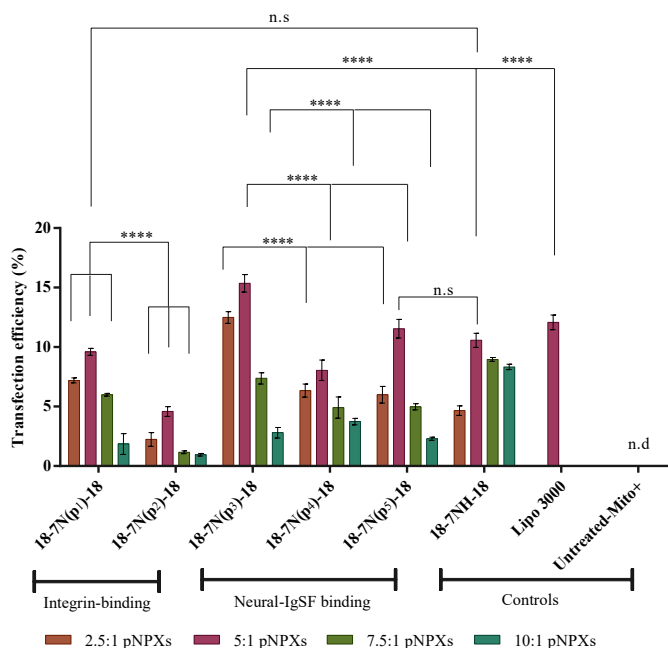
4.4.3.1 Assessment of pNPXs as potential gene delivery vectors

Transfection properties of 18-7N(p_n)-18 pNPXs at 2.5:1, 5:1, 7.5:1 and 10:1 G:P ratio (n=1,2 (integrin-binding) and n=3,4,5 (neural IgSF CAM) peptide modified) were assessed in A7 astrocytes based on the gWIZ-GFP reporter plasmid using flow cytometry. Reference formulations were 18-7NH-18 NPXs and Lipofectamine™ 3000. Figure 4-3A shows the percent of A7 cells expressing GFP (TE%) for each NPX formulation. TE increased up to 5:1 ratio followed by a decrease for all NP formulations. The 18-

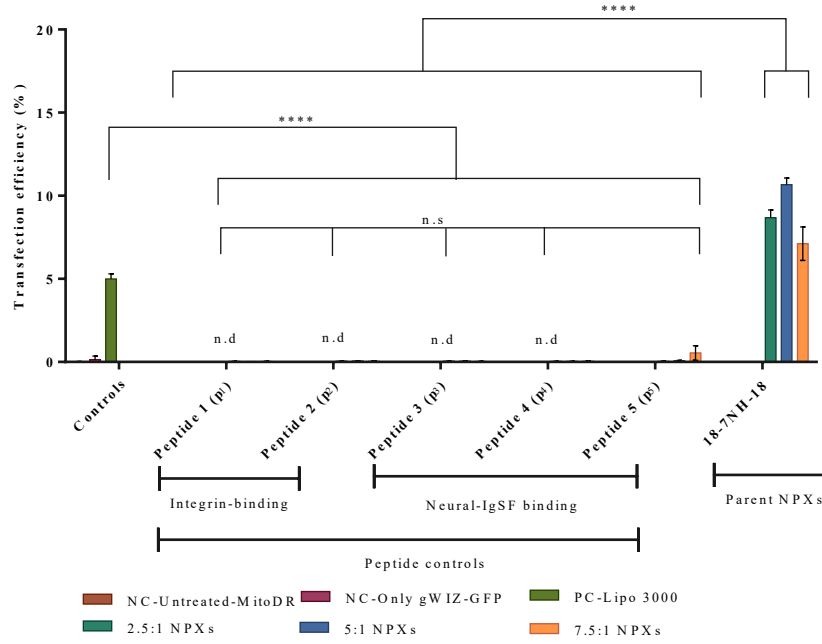
7N(p₁)-18 5:1 pNPXs (p₁-RGD, integrin binding) has shown significantly higher TE (****p<0.0001), compared to its non-binding mutant RLE conjugated 18-7N(p₂)-18 5:1 pNPXs, 9.6 ± 0.28% and 4.58 ± 0.4%, respectively. All three ratios (2.5:1, 5:1 and 7.5:1) of 18-7N(p₁)-18 pNPXs tested have shown significantly higher TE compared to 18-7N(p₂)-18. No significant difference in the TE was observed between the 18-7N(p₁)-18 5:1 pNPXs and 18-7NH-18 5:1 NPXs

From the IgSF CAM family, TE of 18-7N(p₃)-18 pNPXs at 2.5:1 and 5:1 ratio was 12.48 ± 0.49% and 15.36 ± 0.73%, respectively, and 18-7N(p₅)-18 5:1 pNPXs treated cells have shown a TE of 11.53 ± 0.78%. The of 18-7N(p₃)-18 pNPXs at 2.5:1, 5:1 and 7.5:1 ratio have shown significantly higher TE (****p<0.0001) compared to 18-7N(p₄)-18 and 18-7N(p₅)-18 pNPXs at similar ratios. No significant difference was observed in TE between 18-7N(p₅)-18 pNPXs and 18-7NH-18 NPXs. Parent 18-7NH-18 5:1 NPXs and Lipofectamine™ 3000 treated cells have shown TE of 10.67 ± 0.46% and 12.15 ± 0.43%, respectively.

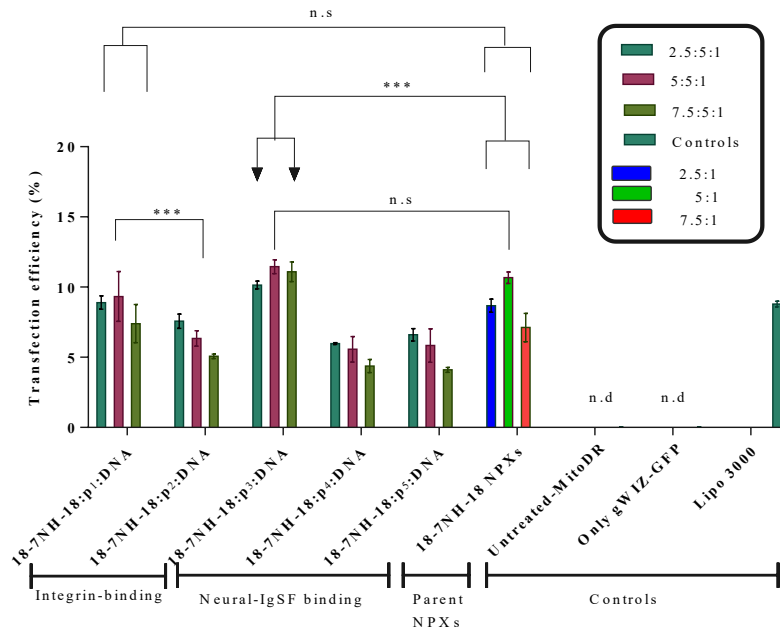
A.



B.



C.



D.

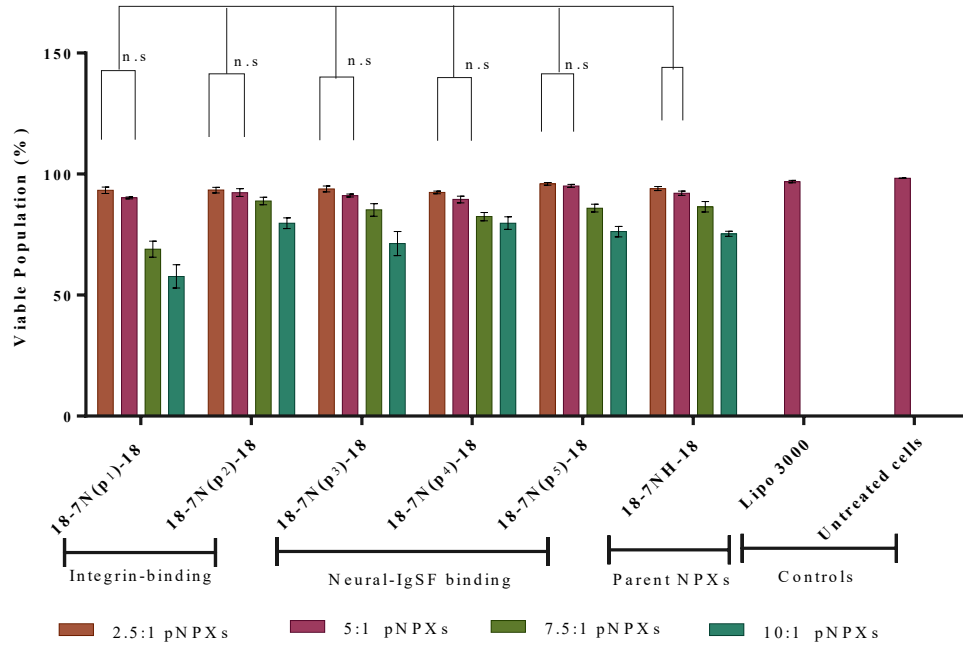


Figure 4-3 TE and toxicity of pNPXs and their physical mixtures in A7 astrocytes by flow cytometry. A) TE of pNPXs at 2.5:1, 5:1, 7.5:1 and 10:1 G:P ratios; B) TE of bi-component mixtures of p₁-p₅ peptides mixed with plasmid at 2.5:1, 5:1 and 7.5:1 ratios; C) TE of tri-component mixtures of p:G:P at 2.5:5:1, 5:5:1 and 7.5:5:1 ratios; D. cell viability assessment after treatment with various pNPXs. TE was measured at 48 hours after dosing by counting the GFP positive cells. Viability was evaluated by Mitotracker Deep Red staining. All values expressed as mean \pm S.D., n=3. ****p<0.0001, ***p<0.001, not detected (n.d) and non-significant (n.s)

From the Integrin-binding CAP modified class 18-7N(p₁)-18 2.5:1 pNPXs have shown improved TE compared to 18-7NH-18 2.5:1 NPXs, while 18-7N(p₁)-18 5:1 pNPXs have shown no significant improvement in TE compared to 18-7NH-18 5:1 NPXs. Similarly, from the IgSF CAM modified class two sequences p₃-FASNKL and p₅-YTDNGTF modified pNPXs have shown to perform better or in par with the 18-7NH-18 NPXs. 18-7N(p₃)-18 NPXs at 2.5:1 and 5:1 ratio has shown to perform significantly better (****p<0.0001) compared to 18-7NH-18 NPXs at similar ratios. However, 18-

7N(p₅)-18 5:1 pNPXs have shown no significant difference in the TE compared to 18-7NH-18 NPXs. While, 18-7N(p₄)-18 5:1 pNPXs have under performed compared to 18-7NH-18 5:1 NPXs. Hence, based on these results one nanoparticle system from each group of the CAP modified class such as 18-7N(p₁)-18 pNPXs from the integrin-binding class and 18-7N(p₃)-18 pNPXs from the IgSF CAM class were selected for further *in vitro* and *in vivo* testing.

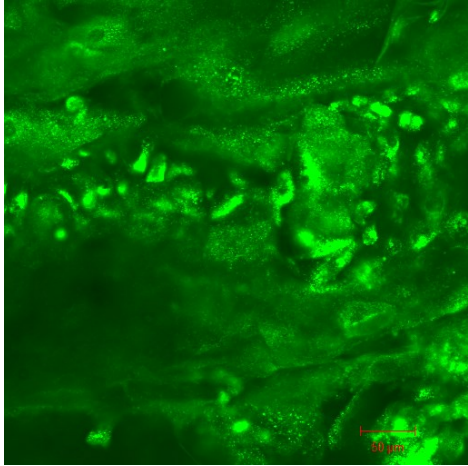
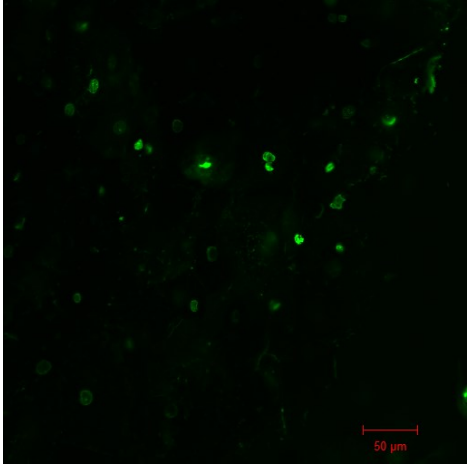
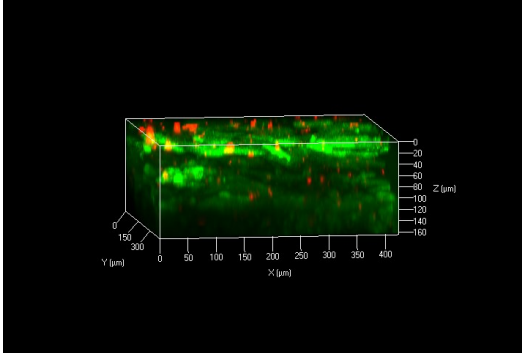
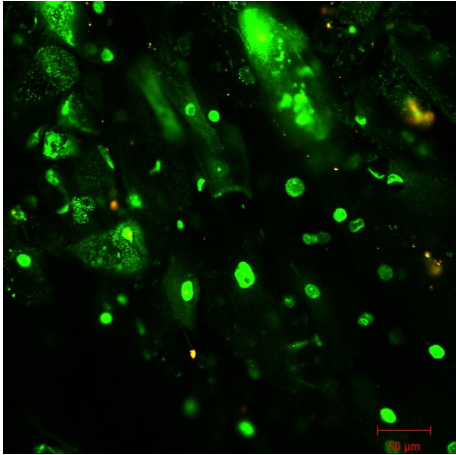
Comparative studies between peptides (bi-component) and peptide modified gemini surfactant pNPXs showed that the peptides themselves (unconjugated) complexed with plasmid DNA did not facilitate gene delivery (Figure 4-3b). The cells treated with 18-7NH-18 5:1 NPXs and Lipofectamine[®] 3000 showed $10.66 \pm 0.4\%$ and $4.99 \pm 0.316\%$ TE, respectively, which were significantly higher (****p<0.0001) compared to peptide-DNA complexes. From the result it is evident that the all the peptides from both the integrin-binding and IgSF CAM class have shown either negligible amount of TE or were not detected.

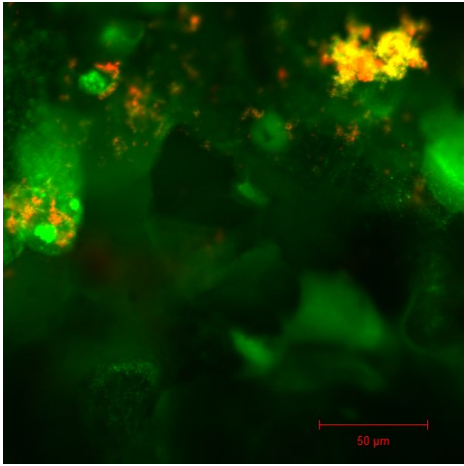
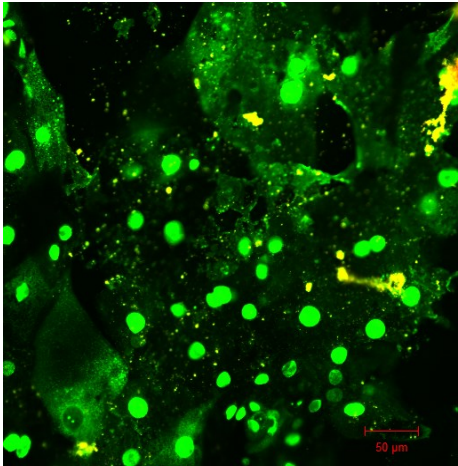
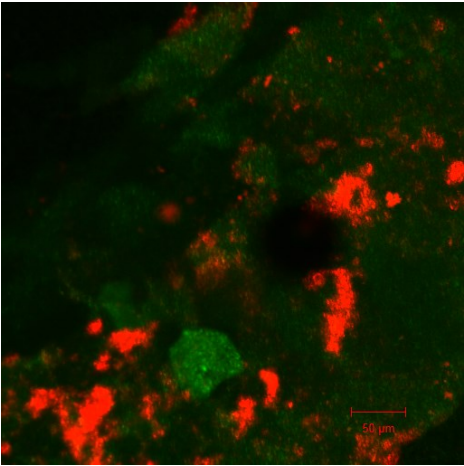
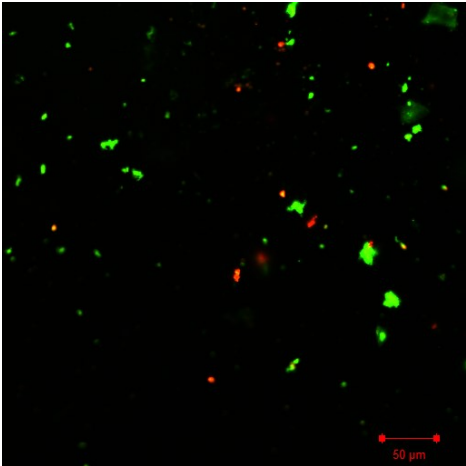
The addition of peptides to 18-7NH-18 5:1 NPXs at 1:2.5, 1:5, 1:7.5 (GP:p) ratios (tri-component physical mixtures) (Figure 4-3 C) improved gene delivery and GFP expression. From the integrin-binding class the non-covalently added p₁ peptide:18-7NH-18 NPX mixtures (5:5:1 ratio, p:G:P) showed significantly higher TE, $9.32 \pm 1.77\%$, compared to its non-binding mutant p₂ peptide added 18-7NH-18 NPX system, $6.33 \pm 0.54\%$ (***p<0.001). Similarly, from the IgSF CAM class the non-covalently added p₃ peptide to 18-7NH-18 5:1 NPXs at 2.5:5:1 and 7.5:5:1 p:G:P ratios showed significantly higher TE, $10.14 \pm 0.27\%$ and $11.09 \pm 0.70\%$ compared to 18-7NH-18 NPXs, $8.67 \pm 0.46\%$ and $7.119 \pm 1.00\%$, at 2.5:1 and 5:1 ratios (***p<0.001). No significant difference in the TE was observed between non-covalently added p₃ peptide:18-7NH-18 5:5:1 mixture and 18-7NH-18 5:1 NPXs. The p₁ peptide:18-7NH-18 physical mixtures did not show any significant difference (n.s) in TE compared to 18-7NH-18 NPXs (Figure 4-3 C).

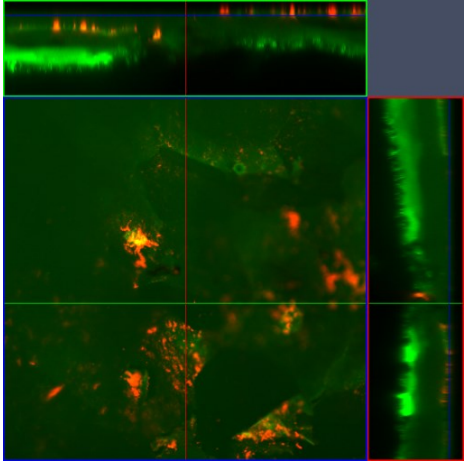
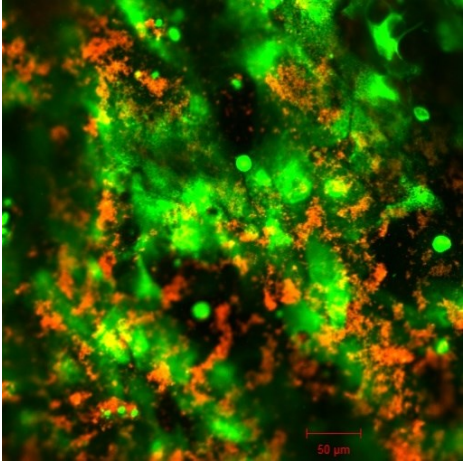
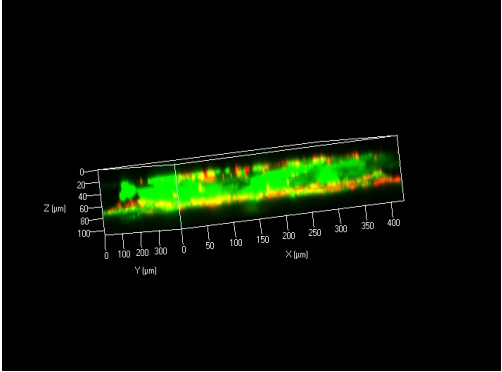
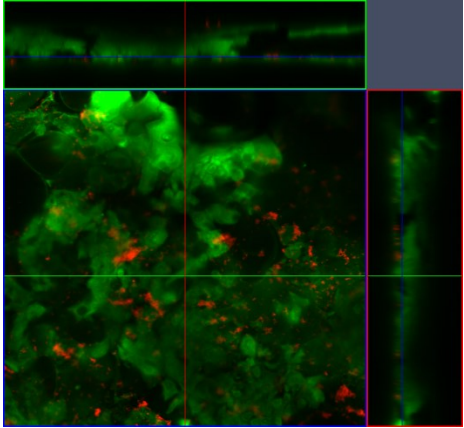
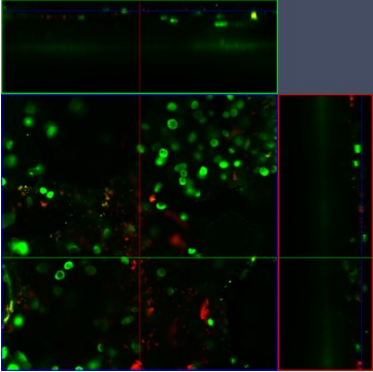
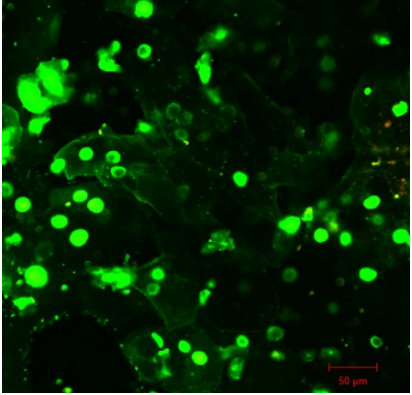
The A7 cell treatments indicated high level of viability (94.007 ± 0.828 and 92.05 ± 0.886 % mean \pm S.D. for 2.5:1, and 5:1 ratios) for all 18-7NH-18 NPXs and 92-93.5%, 91-94%, 89-93% and 95-956%, for p₁₋₅NPXs at 2.5:1 and 5:1 pG:P ratios. However, increased pG:P ratios of 7.5:1 and 10:1 resulted in decreased cell viability (57-85%) with lowest viability observed for 18-7N(p₁)-18 pNPXs (57.72-68.96%). This indicates that the peptide modification performed on amino group of the 2nd generation gemini surfactant did not contribute to any significant ($p > 0.05$) increase in toxicity on the A7 astrocyte cell line up to 5:1 ratio (Figure 4-3D).

4.4.4 In vitro EpiCorneal tissue penetration studies for NPXs and pNPXs

Figure 4-4 shows the results for corneal interactions of 18-7NH-18 NPXs, 18-7N(p₁)-18 pNPXs and 18-7N(p₃)-18 pNPXs (all 5:1 ratios). It was observed that 18-7NH-18 NPXs penetrated through the whole length of the corneal tissue within the first 0.5-1 hours. Similarly, 18-7N(p₁)-18 pNPXs and 18-7N(p₃)-18 pNPXs showed good adsorption to the cell surface at 0.5 and 1 hours. 18-7N(p₁)-18 pNPXs were incubated up to 24 hours to identify their penetration and Mitotracker™ Green FM was used as live cell stain, the viability was found to be good based on the staining pattern at 24 hours. Cell toxicity was assessed using Image IT® dead cell stain that specifically stains dead cell nuclei. Cells produced mitotracker dye when treated with Mitotracker™ Green FM at 24 hours showing the recovery of the cells from the NPXs induced cell membrane disruption that was noticed at 0.5 and 1 hour when treated with Image IT dead cell stain. The pNPXs well adhered to the surface even after three repetitive steps of washing before imaging. This demonstrates the strong interactions of pNPXs to the cell surface. pNPXs also penetrated well into the tissue reaching deeper layers of the corneal tissue. 18-7N(p₁)-18 and 18-7N(p₃)-18 pNPXs were shown to be internalizing (colocalization was assessed) with in the first hour and are seen interacting on the surface of the cell in large number (Figure 4-4 v and viii).

Treatment	Calcein/Mitotracker [®] Green FM stained	Image [®] IT stained
i) Untreated		
ii) 18-7NH-18 NPXs 0.5 hours		

<p>iii) 18-7NH-18 NPXs 1 hours</p>		
<p>iv) 18-7N(p₁)-18- pNPXs 0.5 hours</p>		

<p>v) 18-7N(p₁)-18 pNPXs 1 hours</p>		
<p>vi) 18-7N(p₁)-18 pNPXs-24 hours</p>	<p>Calcein stained</p>  <p>Mitotracker green stained</p> 	 

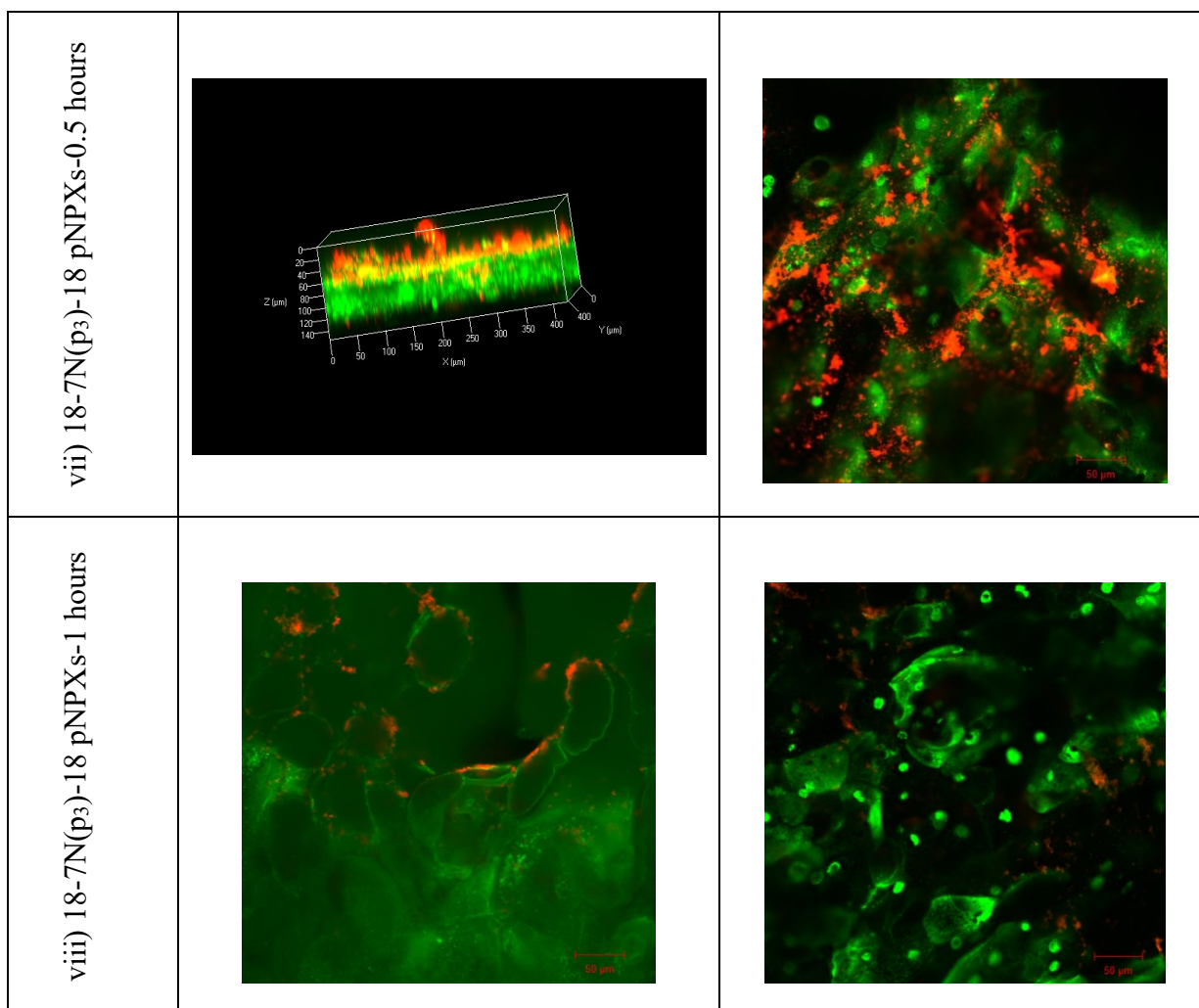


Figure 4-4 Confocal microscopic images of NPX interactions with 3D EpiCorneal tissue model. (i) untreated, stained with Calcein AM and Image IT; (ii) cornea treated with 18-7NH-18 NPXs for 0.5 hour, stained Calcein AM, z-stack and treatment with 18-7NH-18 NPXs for 0.5 hour, stained with Image IT; (iii) cornea treated with 18-7NH-18 NPXs for 1 hour, stained with Calcein AM treatment with 18-7NH-18 NPXs for 1 hour, stained with Image IT; (iv, v and vi) cornea treated with 18-7N(p₁)-18 5:1 pNPXs, stained with Calcein AM/Mitotracker green and Image IT at 0.5 and 1 and 24 hours respectively; (vii and viii) cornea treated with 18-7N(p₃)-18 5:1 pNPXs, stained with Calcein AM and Image IT at 0.5 and 1 hour, respectively.

4.4.5 Transfection studies in 3D retinal neurospheres

Selected pNPXs from integrin-binding (18-7N(p₁)-18 5:1 pNPXs) and IgSF CAM (18-7N(p₃)-18 5:1 pNPXs) along with 18-7NH-18 5:1 NPXs were evaluated for their efficiency to transfect in a 3D environment using retinal neurospheres. MiEye8 neurospheres were generated according to a protocol developed in our laboratory (279) and treated with 18-7N(p₁)-18 5:1 pNPXs and 18-7N(p₃)-18 5:1 pNPXs. Figure 4-5, column 1 shows the morphology and viability of neurospheres with about 200-250 μ m diameter. Mitotracker Deep Red (live cell stain) and Image IT (dead cell stain) indicated the viability with limited number of green dead cells on the surface prior to treatment (Figure 4-5 B and C). It was noted that the 30-minute staining was not sufficient to stain the center of the spheres, and overall, the NPX interactions and staining may not represent penetration into the entire sphere.

Neurospheres treated with 18-7N(p₁)-18 5:1 pNPXs for 48 hours showed no transfected cells, however 18-7N(p₃)-18 5:1 pNPXs treated spheres showed GFP expression in numerous cells on the surface (seen as medium intensity green cells) (Figure 4-5 column 2 treatment groups). Comparatively, both 18-7NH-18 NPX and Lipofectamine[®] 3000 treated spheres showed a 1-3 bright green cells and some medium intensity fluorescence on the surface.

To explore whether the cells transfected were RGCs, the 18-7N(p₃)-18 pNPXs treated neurospheres were immunostained with anti-RBPMS primary antibody and an Alexa 647-labelled anti-human IgG secondary antibody.

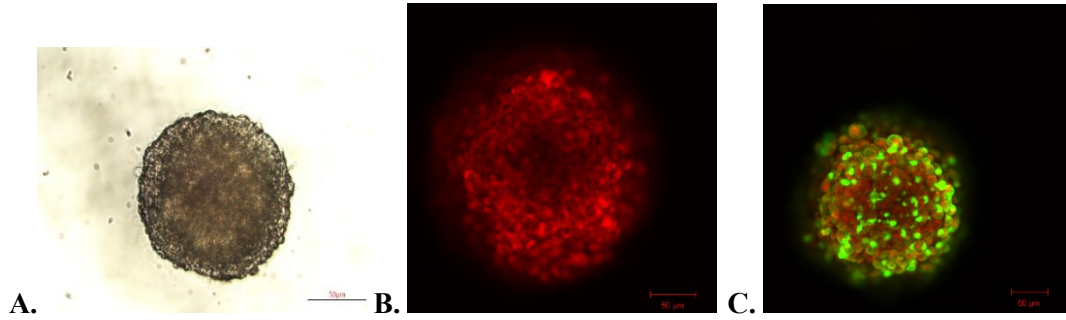
The co-localization assessment on neurospheres treated with 18-7N(p₃)-18 5:1 pNPXs indicated multiple areas of GFP (green) and anti-RBPMS (red) fluorescence indicating GFP expression in RGC cells of the neurospheres (Figure 4-5 Q, R, S and T). A selected path of interest in a neurosphere and corresponding fluorescence intensity v_s distance graph is shown in Figure 4-5 T.

Controls-Untreated

Brightfield images

MitoTracker DR

Image® IT

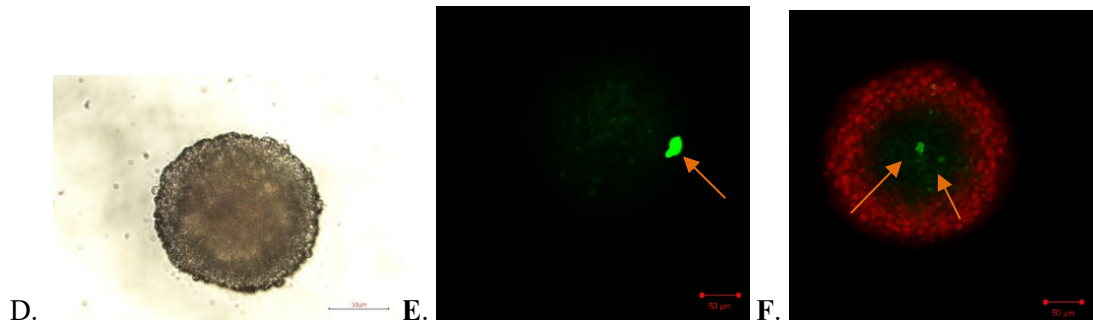


Treatment group- Lipofectamine 3000

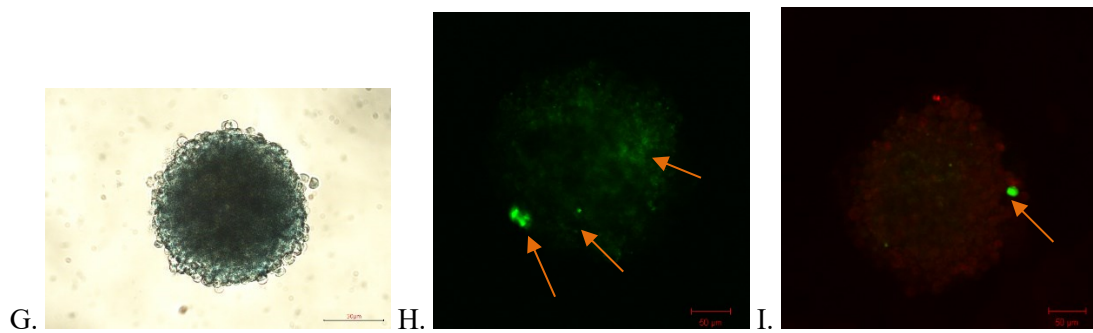
Brightfield images

GFP channel

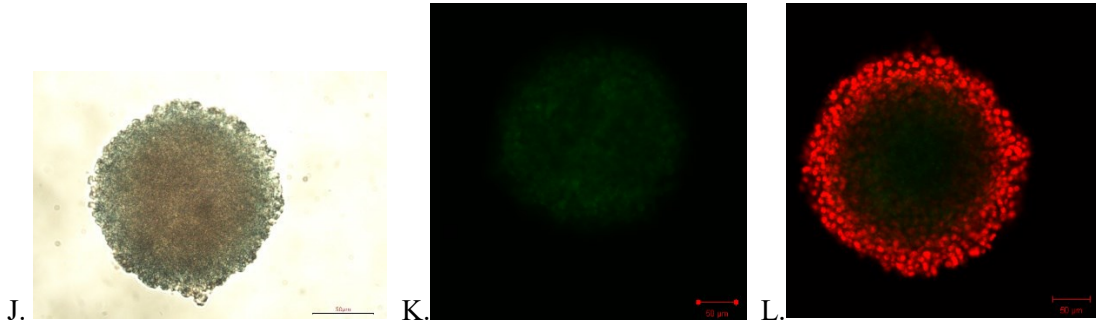
DRAQ5+GFP channel



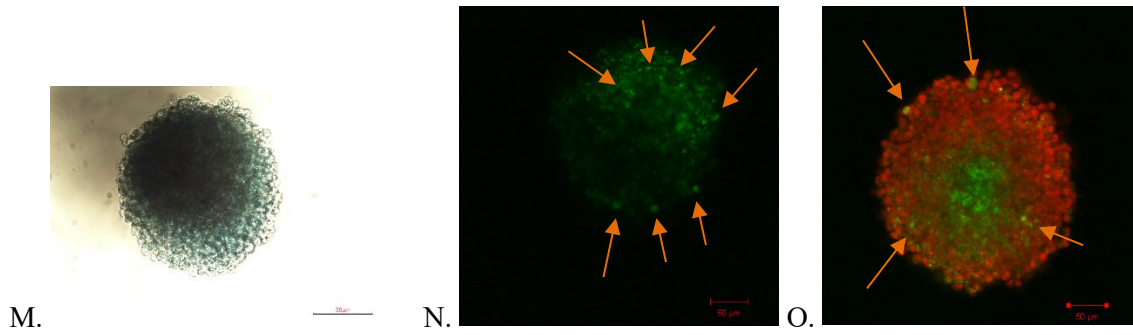
Treatment group- 18-7NH-18 NPXs



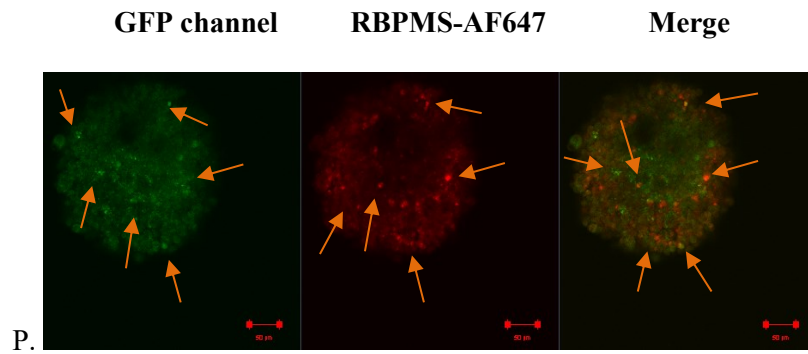
Treatment groups- 18-7N(p₁)-18 pNPXs: Integrin-binding peptide group



Treatment groups- 18-7N(p₃)-18 pNPXs: IgSF CAM peptide group



Treatment groups- 18-7N(p₃)-18 pNPXs stained with RBPMS antibody-counter stained with secondary antibody-AF647



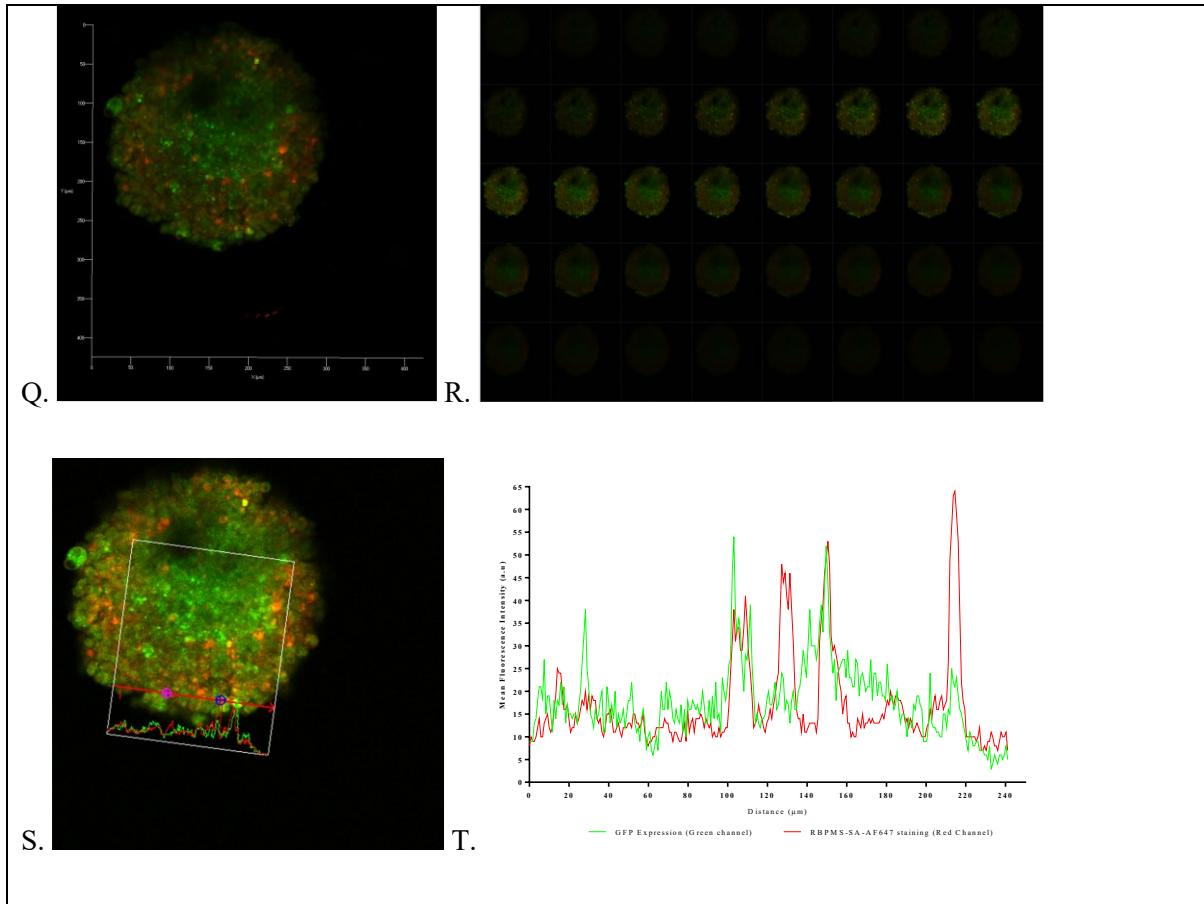


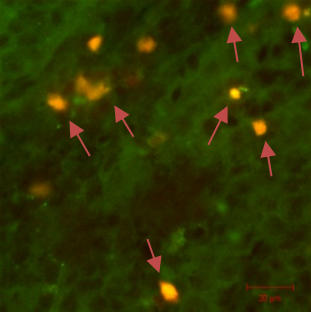
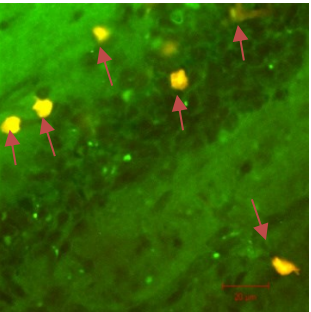
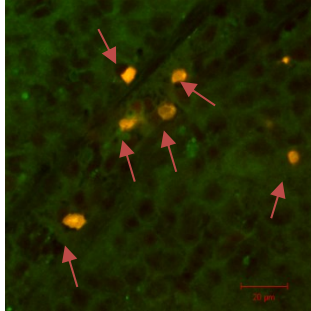
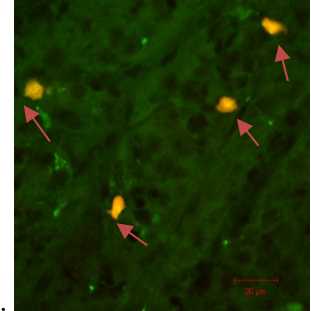
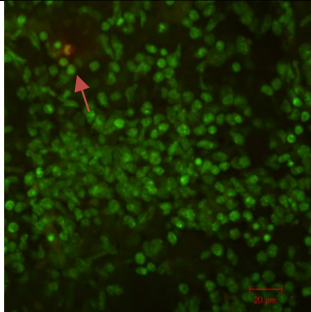
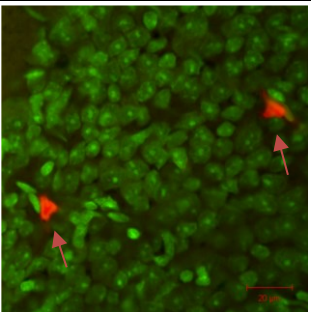
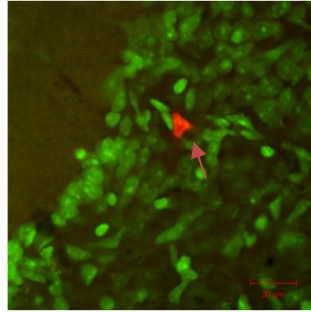
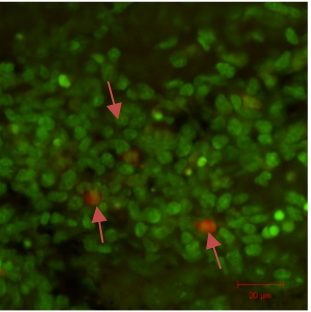
Figure 4-5 Transfection of MiEye8 3D retinal neurospheres with pNPXs. Confocal microscopic images captured 48 hours post treatment with 18-7NH-18 (parent gemini), 18-7N(p₁)-18 (Integrin-binding peptide) and 18-7N(p₃)-18 (IgSF-binding peptide modified) pNPXs. Above presented figure shows controls and treated groups. Untreated controls- A, B and C, Lipofectamine 3000 treated- D, E and F, 18-7NH-18 NPXs treated- G, H and I, 18-7N(p₁)-18 pNPXs treated- J, K and L, 18-7N(p₃)-18 pNPXs treated- (M, N and O) and (P) shows 18-7N(p₃)-18 pNPXs treated neurospheres counter stained with Rbpms antibody tagged with Alexa Fluor 647 (RGC marker, merge image shows both GFP expression (GFP channel) and Rbpms staining (RFP channel) (signifies presence of RGCs differentiated using MiEye8 protocol) and Q. 3D retinal neurosphere showing GFP expression and RBPMS staining, R- 40 optical slices showing the distribution of GFP expression and RBPMS staining, S. illustration of MFI analysis on GFP and anti-RBPMS (red) colocalization analysis, T. Representative colocalization profile of GFP and RBPMS staining (signifies mature RGC population). Blunt end of arrow starts at 0µm and arrowhead represents the 241 µm. All experiments were carried out at least n≥2 neurospheres and images were obtained from at least 2 different neurospheres. The mean fluorescence intensity of the colocalization was carried out on at least 3 different images obtained from two different spheres (n=2). Note: Neurospheres may have moved slightly after DRAQ5 staining therefore their orientation may be different in column 2 and 3 for the same treatment.

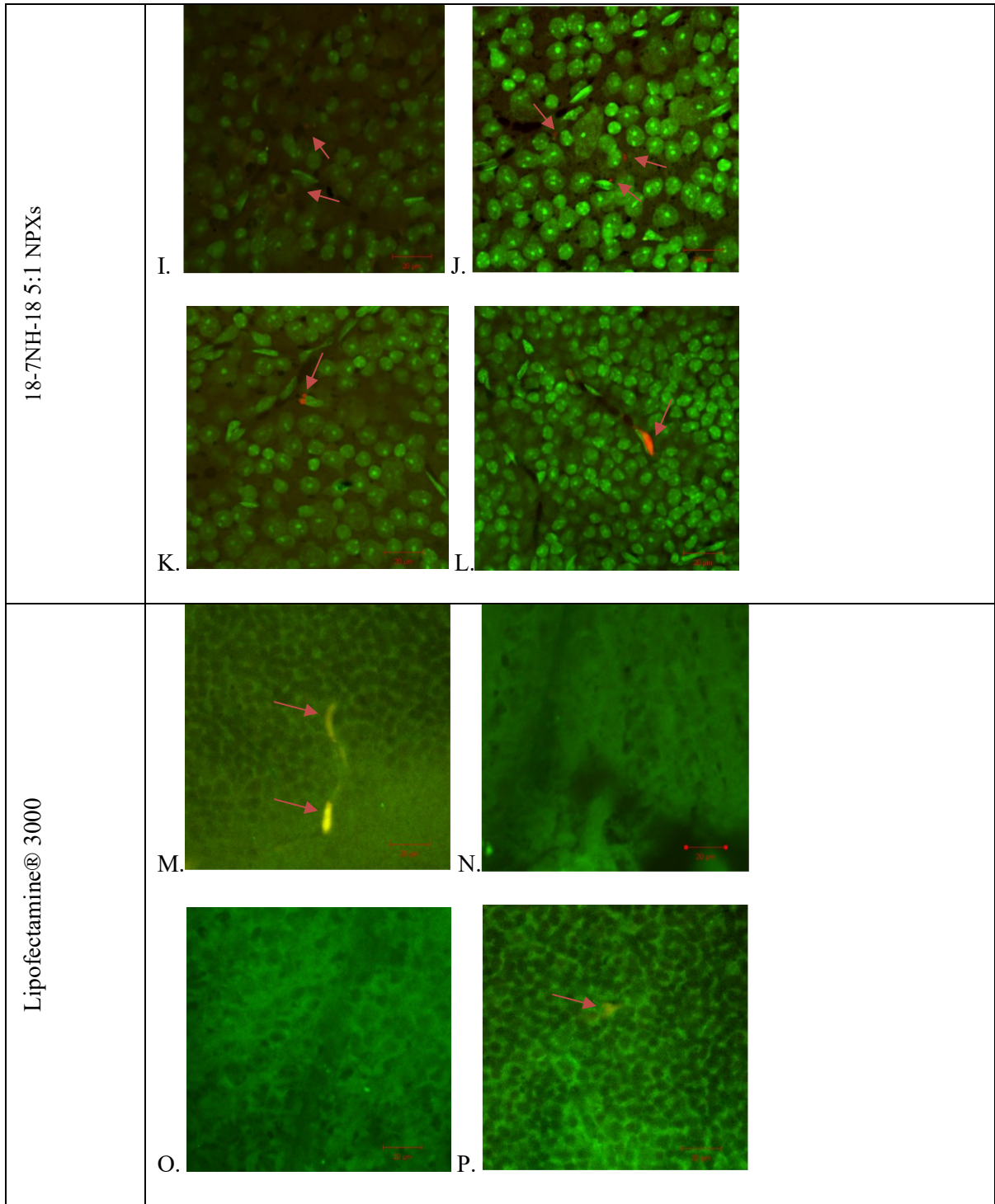
4.4.6 Gene delivery to the retina *in vivo* in a CD1 mouse model

Analysis of flat mount retinas and Z-stack images captured for the retinal whole mounts showed RFP expression in the 18-7NH-18 5:1 pNPXs, 18-7N(p₁)-18 5:1 and 18-7N(p₃)-18 5:1 pNPXs treated retinas.

Retinas treated with 18-7N(p₃)-18 5:1 pNPXs showed strong positive RFP expression (Figure 4-6, A-D) which was comparatively higher compared to all other treated groups and controls. It was observed that the RFP expression was localized in RGC layer (Figure 4-6 U). The RGD-conjugated 18-7N(p₁)-18 5:1 pNPXs treated retina (Figure 4-6 E-H) showed few areas of strong RFP expression, whereas the retinas treated with 18-7NH-18 5:1 NPXs (Figure 4-6 I-L) and Lipofectamine 3000 (Figure 4-6 M-P) showed weak positive gene expression in limited areas. The saline controls did not show any red fluorescence (Figure 4-6 Q-T) but accounted for some background fluorescence in the cMFI analysis.

The cMFI analysis compared the average MFI values for each image obtained from the retinal whole mounts based on at least four of different 70µm² total areas in the retina (Figure 4-7). Based on the calculated cMFI values 18-7N(p₃)-18 5:1 pNPXs produced approximately 2-fold higher (32.40 ± 0.80 a.u) gene expression compared to Lipofectamine[®] 3000 (18.07 ± 1.487 a.u, ****p<0.0001), 18-7N(p₁)-18 5:1 pNPXs (16.16 ± 0.80 a.u , ***p<0.001) and 18-7NH-18 5:1 NPXs (14.79 ± 4.24 a.u , ****p<0.0001). No significant difference in cMFI was observed between 18-7N(p₁)-18, Lipofectamine 3000 and 18-7NH-18 5:1 NPXs (Figure 4-7).

Treatment	Images showing tdTomato (red) and Syto 13 (green) fluorescence	
$^{18}\text{-}^7\text{N}(\text{p}_3)\text{-}18\text{ } 5:1\text{ pNPXs}$	<p>A. </p>	<p>B. </p>
	<p>C. </p>	<p>D. </p>
	<p>E. </p>	<p>F. </p>
	<p>G. </p>	<p>H. </p>



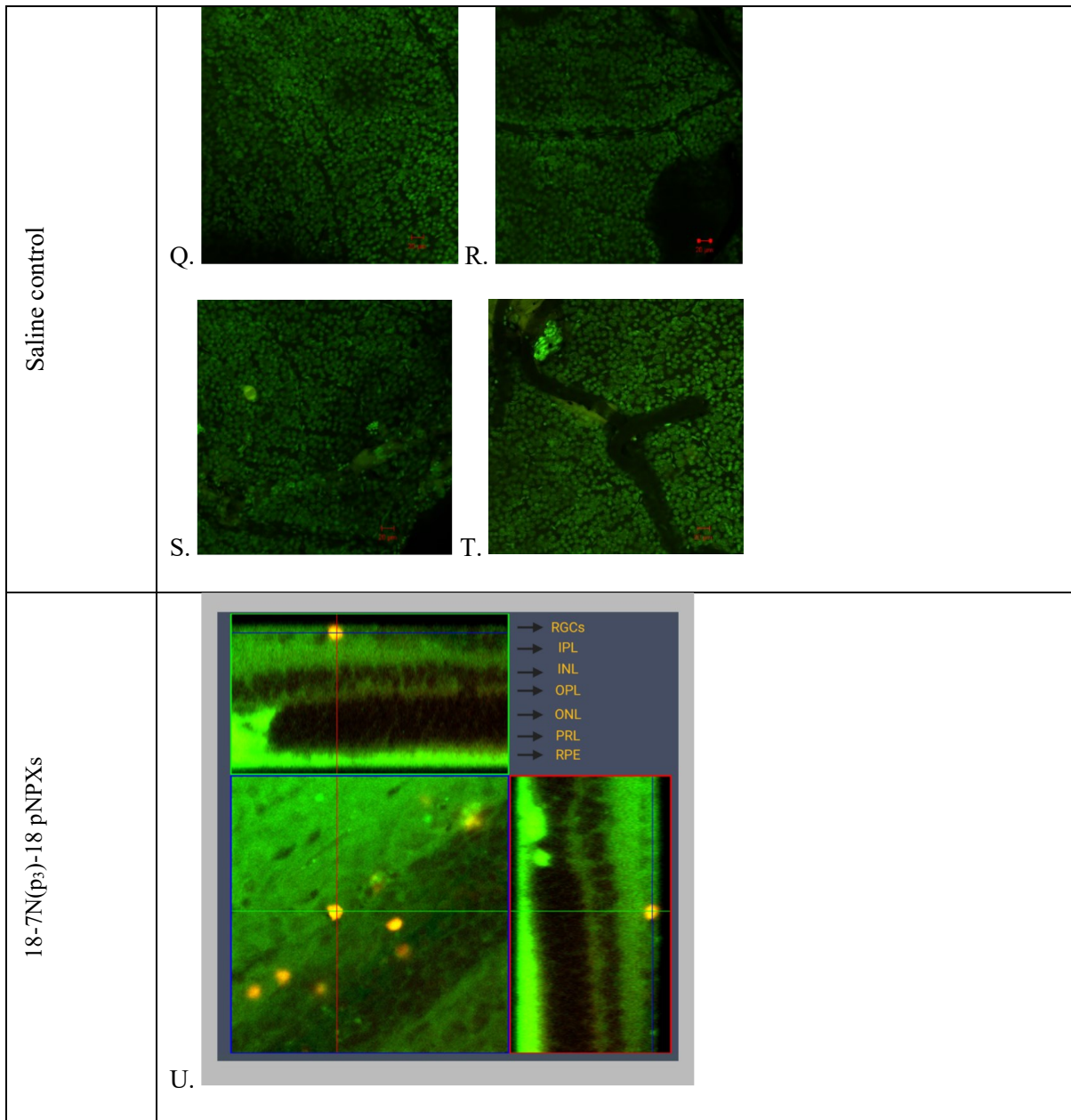


Figure 4-6 Confocal microscopic images of whole mount retinas from CD1 mice treated with 18-7N(p)-18 pNPXs. Whole mount images of retina treated with 18-7N(p₃)-18 5:1 pNPXs (A-D), 18-7N(p₁)-18 5:1 pNPXs (E-H), 18-7NH-18 5:1 NPXs (I-L), Lipofectamine[®] 3000 (M-P) and Saline controls (Q-T). Whole mount retinas were isolated post 72 hours of administration by intravitreal injection. Retinas were stained with Syto 13 and imaged using CLSM 710 using green (Syto 13) and red channel (tdTomato). Image (U) shows 3D Z-stack orthogonal section analysis of 18-7N(p₃)-18 pNPXs treated retinas showing gene expression in the RGC layer and INL.

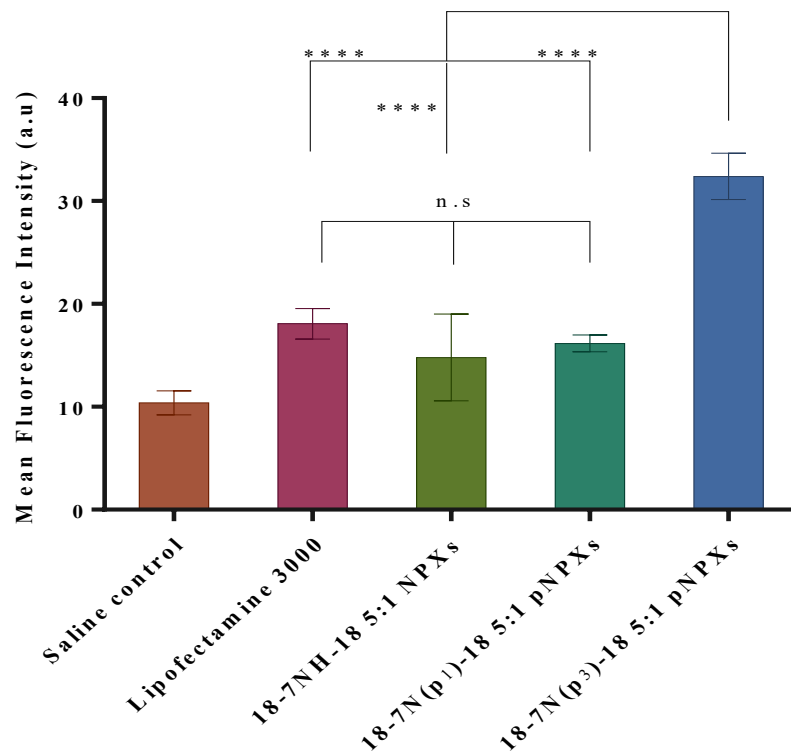


Figure 4-7 Quantitative assessment of gene expression by cMFI analysis of whole mount retinas from CD1 mice treated with pNPXs and NPXs along with controls. All treatment groups were significantly different from saline. All values expressed as mean \pm S.D., n=4. ****p<0.0001, ***p<0.001 and non-significant (n.s)

4.4.7 BDNF gene expression in the retina in vivo in mice treated with integrin and IgSF binding peptide modified gemini surfactant pNPXs

The ELISA assessment showed significant expression of BDNF in the eye homogenates of mice treated with all nanoparticles tested (Figure 4-8). The highest amount of BDNF was produced after treatment with 18-7N(p₃)-18 pNPXs (422.60 ± 42.60pg/eye (average weight of an eye-17.71 mg), n=6, ****p<0.0001), followed by 18-7NH-18, 18-7N(p₁)-18 and Lipofectamine® 3000 (245.90 ± 39.72, 230.62 ± 24.47, 199.99 ± 29.90 pg/eye, respectively). The latter three treatments produced significantly lower BDNF than the treatment with 18-7N(p₃)-18 pNPXs, but still significantly higher than the untreated background BDNF levels, 131.33 ± 20.30 pg/eye (****p<0.0001, **** p<0.0001 and *** p<0.001, respectively). It was noted that BDNF gene expression was not significantly different between treatments with 18-7NH-18 and 18-7N(p₁)-18 pNPXs and Lipofectamine® 3000 (Figure 4-8).

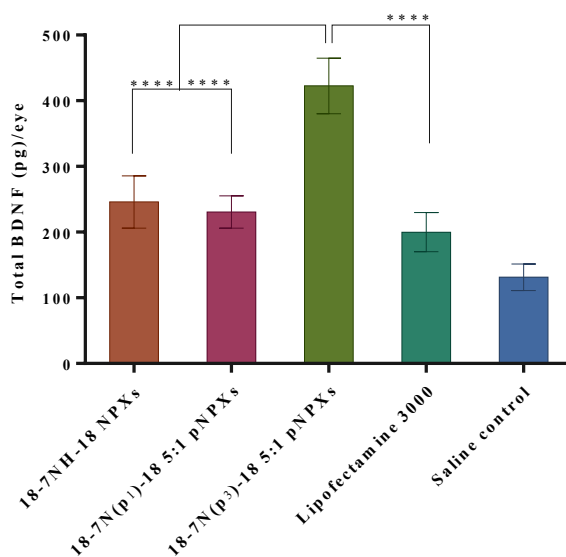


Figure 4-8 BDNF gene expression in the eye in vivo after treatment with peptide-conjugated pNPXs. Total BDNF produced in each eye was assessed after treating with 18-7NH-18, 18-7N(p₁)-18, 18-7N(p₃)-18 pNPXs, Lipofectamine 3000 and saline controls. No significant difference between 18-7NH-18 NPXs, 18-7N(p₁)-18 pNPXs and 18-7N(p₃)-18 pNPXs. All treatments were significantly higher than saline control. Values expressed as mean ± S.D., n=6; **p<0.01; ****p<0.0001, n.s.= not significant.

4.5 Discussion

Neural IgSF and integrin-binding peptides were used to improve delivery of reporter/BDNF plasmid by gemini pNPXs to the retinal layers in the eye. Based on *in vitro* and *in vivo* gene expression studies, we have shown that neural IgSF CAM peptide based pNPXs have potential as gene delivery systems to the retina. The IgSF peptide 18-7N(p₃)-18 5:1 pNPXs performed consistently better *in vitro* in A7 astrocytes and in CD1 mice *in vivo* than the parent unmodified NPXs and integrin-binding peptide modified 18-7N(p₁)-18 pNPXs. In the *in vitro* studies better TE was achieved with two formulations, 18-7N(p₁)-18 5:1 pNPXs with particle size of 220.96 ± 1.87 nm and zeta potential of $+30.76 \pm 0.153$ mV and 18-7N(p₃)-18 5:1 pNPXs with particle size of 257.40 ± 7.70 nm. and a zeta potential of $+37.13 \pm 0.850$ mV.

Previous work in our laboratory made significant contributions to improve TE by various modifications to gemini surfactants such as incorporation of an amino group into the gemini surfactant to facilitate pH induced endosomal escape (157, 159, 173). The 18-7NH-18 NPs with DOPE were recently used to improve the delivery of DNA to the retina in the eye in our group. After IVT injection the NPs localized near the retina in the vitreous within 4hours and dispersed evenly at the NFL, GCL and IPL layers within 48 hours (30). It was also shown that 4 hours after topical application NPs were present in various anterior eye tissues such as iris, limbus and conjunctival layers, i.e. the direction of the lacrimal drainage, but at the 48-hour time point there were no NPs either in the anterior or in the posterior segment of the eye.

The development of amino-acid modified gemini surfactants have shown improved transfection properties and better release kinetics of the plasmid DNA from the surfactant this is one of the first study on the idea of having to modify the amino group of gemini surfactants to improve transfection efficiencies (238). This conjugation of the amino-acid moieties to the gemini surfactant was made

possible with the development of amino substituted gemini surfactants (m-7NH-m) development (157) that allowed for more modifications on the gemini surfactants.

In this current chapter, we have designed and synthesized two integrin-binding CAP-conjugated gemini surfactants and three neural IgSF binding peptide-conjugated m-7N(p_n)-m (m=12 and 18, n=1-5) gemini surfactants (Table 4-3).

Size and zeta potential can have profound effect on the stability, uptake and release of the therapeutic DNA from the vectors inside the cell (285). It has been observed that the size of the pNPXs and pLPXs decreased as charge ratio increased in agreement with previous reports for gemini based NP systems (159). The peptide modification on the amino group could have led to higher particle sizes due to the structural complexity and increased molecular weight, but size only marginally increased and did not have any correlation with molecular weight (Table 4-4). The 18-7N(p₃)-18 and 18-7N(p₅)-18 pNPXs containing 6 and 7 amino acid sequences, respectively had a particle size of 257.40 ± 7.70 and 216.63 ± 1.71 , compared to 18-7N(p₂)-18 and 18-7N(p₄)-18 pNPXs modified with a 3 and 2 amino acid peptides, respectively, with a particle size of 272.60 ± 0.75 and 263.66 ± 4.76 . Also, the inclusion of DOPE into the formulation increased the particle size of the LPX by 10-50nm (Table 4-4), which is likely due to the neutral DOPE reducing the overall zeta potential of the pLPX system. Higher net positive charge of the pG with the DNA favours higher compaction resulting in a smaller particle size. At the same time, zeta potential of the pNPXs and pLPXs increased with an increase in the charge ratio, in agreement with previously published sources. The high cationic charge, however, can also lead to increased toxicity during a more prolonged interaction with cell membranes (168). This explains the reduction in TE and increase in toxicity observed in longer pNPXs and pLPXs treatments. Hence, an optimization of the charge ratio is important as part of the NP design (286).

In vitro transfection studies in A7 astrocytes with the 18-7N(p₁-p₂)-18 pNPXs from integrin-binding group, 18-7N(p₃-p₅)-18 pNPXs from neural IgSF CAM binding group, and 18-7NH-18 NPXs showed

that regardless of the peptide modification the TE increased for all the treatments with increase in the ratio up to 5:1, and any further increase in the charge ratio reduced TE (Figure 4-3). This could be due to the excess interaction of the plasmid DNA with the gemini surfactant leading to failure to the release DNA inside the cell and eventually being eliminated by the cell endosomal mechanisms (263).

TE studies with p₁ (RGD) peptide modified 18-7N(p₁)-18 pNPXs have shown significantly higher (****p<0.0001) TE at all three ratios (2.5:1, 5:1 and 7.5:1) compared to p₂ (RLE) peptide, a mutant non-binding form of the integrin peptide, modified 18-7N(p₂)-18 pNPXs. The results confirm the cell adhesion potential of the RGD peptide compared to its non-binding Thy-1 RLD mutant (RLE) (268). The conjugation of RLE (p₂) was predicted to have low TE, due to the inability to bind with cell surface Thy-1 or $\alpha_5\beta_3$ (204), which could have led to low NPX internalization, unlike RGD peptide that can elicit good cell adhesion properties. However, it was observed that the p₁ peptide conjugation was not significant in improving the TE compared to parent 18-7NH-18 NPXs in A7 cells (Figure 4-3 A). This could be due to many factors that allow for adhesion or binding of the peptide modified pNPXs to the cells such as the presence of relevant cell surface proteins such as integrins ($\alpha_5\beta_3$ on astrocytes) and the particle physicochemical characteristics such as net charge, pH, size and zeta potential that dictate the interaction of the pNPXs with the cell membrane and cell surface proteins.

TE of p₃ (FASNKL) peptide modified 18-7N(p₃)-18 pNPXs was found to be significantly higher (****p<0.0001) (15.36 ± 0.73%) compared to p₄ (LI) and p₅ (YTDNGTF) IgSF CAM binding peptide modified gemini surfactant pNPXs and controls (Figure 4-3 A). Hydrophobic dipeptide LI (p₄) peptide conjugation was not beneficial in improving the delivery of the reporter gene into the cells. The hydrophobic nature of the short dipeptide could have imparted excess hydrophobicity on the pNPXs leading to reduced disassembly of the plasmid DNA from pNPXs due to strong interaction and later would have been cleared by the cell's natural clearance mechanisms. Similar reduction in TE was

noticed when the hydrophobicity of the NPXs was increased with the trimeric gemini surfactants and gemini surfactants with longer alkyl tail in earlier studies (263).

FASNKL (p₃) peptide, identified from L1CAM, conjugated to gemini surfactant can induce affinity towards binding with IgSF CAMs such as neuropilin-1 and Sema3A structures that helps in axonal growth and regeneration. NCAMs such as L1CAM were shown to create interactions between neuron-glia (287), improve the signal transduction, axon guidance, neuronal migration (229) and repair of damaged axons in the retina (288, 289). The L1CAMs are highly expressed in the retinal layers and increase in number during an injury in the retinal layers.

The L1 soluble peptide FASNKL was selected based on its affinity towards neuropilin-1 (NP-1) a component of semaphorin 3A (sema 3A) receptor complex in the first immunoglobulin domain of L1CAM (276, 290). Therefore, the FASNKL binding ligand and the other optimized physicochemical properties of the 18-7N(p₃)-18 pNPXs combined (positive net charge, small particle size) improved the cell adhesion to IgCAMs expressed in the retinal cell layers and lead to improved TE.

Generally, non-covalently added peptides to gemini-DNA formulations (tri-component mixtures) showed TE similar to that of the parent 18-7NH-18 NPXs, except for p₄ peptide which showed even lower TE compared to 18-7NH-18 NPXs. Collectively, these results indicate that the conjugation of peptide to the gemini surfactant is necessary to enhance TE.

The cells across all treatments showed viability values ranging between 86-96% (Figure 4-3 D). The change in physicochemical characteristics imparted by the peptide modifications such as charge, or hydrophobicity did have negative effects on cell viability. Increased cationic charge lead to prolonged interaction of particles with cell membrane and eventually lead to cell toxicity.

A 3D retinal stem cell-derived MiEye neurosphere model (291) served as a suitable model to assess the TE of 18-7N(p₁)-18 5:1 pNPXs and 18-7N(p₃)-18 pNPXs in a 3D retina mimicked environment. MiEye8 neurospheres contain differentiated retinal cells, including RGCs, which stain

positive with anti-RBPMS antibody. Treatment of neurospheres with 18-7N(p₃)-18 pNPXs indicated that the transfected cells expressing GFP also co-localized with the RGCs (Figure 4-5 P Q and T). The 18-7N(p₁)-18 pNPXs treated neurospheres did not show any GFP expression. Overall, compared to monolayers, the TE in the 3D environment was generally lower. The thickness of the neurospheres was likely a hindrance for both NP penetration and imaging the deeper layers by confocal microscope.

In vivo analysis of the retinal flat mounts after treatment with 18-7N(p₁)-18 pNPXs and 18-7N(p₃)-18 pNPXs showed gene expression in various layers of the retina such as RGCs, IPL, INL, OPL and ONL (Figure 4-6 U). cMFI analysis (Figure 4-7) demonstrated higher amount of gene expression in 18-7N(p₃)-18 5:1 pNPXs treated retina compared to integrin-binding peptide modified 18-7N(p₁)-18 5:1 pNPXs. The cMFI analysis showed a 2.0-fold higher cMFI for 18-7N(p₃)-18 5:1 pNPXs treated eyes compared to 18-7N(p₁)-18 5:1 pNPXs, 2.2-fold increase compared to 18-7NH-18 5:1 NPXs and 1.8-fold compared to Lipofectamine[®] 3000. While, no significant difference in the cMFI was observed between the 18-7N(p₁)-18 5:1 pNPXs, 18-7NH-18 5:1 NPXs and Lipofectamine[®] 3000 treated retinas. The BDNF ELISA assay also confirmed the same trend (Figure 4-9). Overall, it was found that 18-7N(p₃)-18 5:1 pNPXs produced higher gene expression compared to any other NPXs and pNPXs tested. This is a significant finding since the levels of BDNF expressed (about 422 pg/eye for 18-7N(p₃)-18 5:1 pNPXs or 23.84 pg/mg eye tissue; (Average weight of eye-17.71 mg) are pharmacologically relevant and merit further functional evaluations. The effect of IVT doses between 50ng/mL to 1.5µg-10µg of BDNF have been evaluated before on RGC population after an injury (292-294). In an earlier study, BDNF production in genetically engineered astrocytes was found to be 83-166 pg/10⁵ cells/h which was sufficient to rescue degenerating neurons (295). In a recent study Domenici et al, reported about 400pg/mg protein and 200 pg/mg protein BDNF levels after 1µg/µL IVT and 12µg/µL topical administration of BDNF in saline in rats, respectively, (about 50pg/mg in mice after 2µg/µL IVT dose) (296). In our study the 422 pg/eye BDNF level was achieved after a 0.5µg/µL single IVT injection of

pNPXs, assessed after 72 hours. 72 hours was chosen as a time-point to analyze the transfection efficiency based on few published studies (152) and *in vitro* analysis carried out on A7 astrocytes also demonstrated the gene expression from 24 hours with peak levels at 48-72 hours. Optimization of the dosage, incubation time can be potential avenues to explore further increase. Also, testing these 18-7N(p₃)-18 pNPXs in glaucoma disease animal models can determine whether this level of BDNF produced will be able to protect the RGCs.

This improved gene expression is attributed to the presence of IgSF CAP on the NPs. FASNKL-conjugated pNPXs may interact with other neural IgSF CAM on retinal cells by either homophilic or heterophilic binding, thereby leading to enhanced internalization through various endocytosis mechanisms (183). Also, the presence of ionizable NH groups in the peptide could have also led to change in the pH of the endosome by creating an influx of protons leading to an endosomal escape of the pNPXs. The lower pH may induce polymorphic phase inversion and interaction of the pNPXs with the bilayer membrane, leading to rupture of the endosomal membrane, endosomal escape was shown previously for other gemini NPs (159, 297).

In case of p₅, a myelin P₀ protein-derived peptide, the heterophilic binding properties with other membrane CAMs were employed for NP design. The P₀ protein and a P₀ peptide sequence (p₅ in this study) was formulated into liposomes to target melanoma cells and keratinocytes with high level of ICAM-1 expression (269, 270, 298, 299). Interestingly, in the current study the 18-7N(p₅)-18 pNPXs did not show significant improvement in the TE compared to 18-7NH-18 parent NPXs. The reasons could be further explored in the future whether this is related to the physicochemical properties or the binding characteristics of NPs.

Overall, the results demonstrate the potential of integrin and IgSF CAM-binding peptide-modified pNPXs in delivering the therapeutic DNA to the retina and produce BDNF.

BDNF have shown to rescue the retinal cells from induced cell death and promotes neuronal survival by binding with TrKB receptor on RGCs (78) (86) (63). Local production of NTFs supports RGC survival during the optic nerve injury or due to increased IOP leading to blockade of axonal bidirectional transport of the BDNF and triggering RGC death (45). Earlier in our laboratory, we showed that transfected A7 astrocytes expressed bioactive BDNF and promoted neurite outgrowth in both unstressed and oxidatively stressed SH-SY5Y neuroblastoma cells in a 3D co-culture model (82). In this study, both transfection and BDNF production *in vivo* in a normal mouse model was achieved using the novel peptide targeted NPXs administered by IVT injection.

4.6 Conclusion

Overall, two sets of peptide-modified gemini pNPXs were formulated. Integrin-binding 18-7N (p₁₋₂)-18 and neural IgSF CAM binding-peptide-modified 18-7N(p₃₋₅)-18 were synthesized and pNPXs were formulated. Their efficiency in delivering reporter/therapeutic gene to the retina was evaluated *in vitro* and *in vivo*. The pNPXs with CAPs from the neural IgSF represents a novel approach to non-viral gene delivery to the retina. The IgSF peptides are known to elicit a cell adhesion and binding interaction between the neural IgCAMs and have potential to engage in homophilic and heterophilic interaction with other cell surface proteins. This property of IgSF CAPs was exploited to improve the adhesion and delivery of pNPXs to the retinal cells by conjugating them on to gemini surfactant gene vectors. The conjugation of peptide to the 18-7NH-18 gemini surfactant and the pNPXs prepared from the IgSF peptide-modified gemini surfactants have enhanced the TE with low toxicities.

Over the course of the development of peptide functionalized gemini surfactant pNPXs in this thesis, the following conclusions and key findings are drawn:

- Synthesis of one integrin binding, one non-binding peptide and three neural IgSF peptide modified gemini surfactants (18-7N(p₁₋₅)-18 and one p₅ peptide modified 12-7N(p₅)-12 gemini

surfactant were successfully carried out using HATU/DIPEA coupling technique and were characterized using mass spectrometry.

- Formulation optimization and physicochemical characterization of 18-7N(p₁₋₅)-18 pNPXs showed that the optimal ratio for highest TE was found to be 5:1 (G:P) for all pNPXs in *in vitro* transfection studies with A7 astrocytes. The IgSF-binding 18-7N(p₃)-18 pNPXs treated cells demonstrated a $15.36 \pm 0.73\%$ TE, a 1.4-fold increase compared to $10.57 \pm 0.58\%$ for parent 18-7NH-18 NPXs, $10.67 \pm 0.46\%$ for integrin-binding 18-7N(p₁)-18 pNPXs and $11.53 \pm 0.43\%$ for IgSF-binding 18-7N(p₅)-18 pNPXs with overall viability values between 86-95%.
- The 18-7N(p₃)-18 pNPXs transfected RGCs in a 3D environment, in MiEye8 neurospheres.
- In the *in vivo* CD1 mouse model 18-7N(p₃)-18 pNPXs administered by IVT injection delivered tdTomato/BDNF plasmid to retinal cells and produced higher gene expression than the 18-7N(p₁)-18 pNPXs, the parent 18-7NH-18 NPXs and Lipofectamine® 3000 as demonstrated by confocal microscopy of whole mount retinas.
- The BDNF gene expression, assessed by ELISA, showed significantly high levels of BDNF with 18-7N(p₃)-18 (422.60 ± 42.60 pg/eye), followed by 18-7N(p₁)-18 pNPXs (230.62 ± 24.47 pg/eye), 18-7NH-18 NPXs (245.90 ± 39.72 pg/eye), Lipofectamine® 3000 (199.99 ± 29.90 pg/eye) and untreated controls (131.33 ± 20.30 pg/eye). In sum, the 18-7N(p₃)-18 pNPXs induced 3.4-fold higher BDNF level compared to controls and 2-fold higher than 18-7N(p₁)-18 pNPXs.
- In conclusion, the novel multifunctional IgSF peptide and integrin-binding peptide conjugated gemini NPXs provide a promising non-viral *in vivo* gene delivery approach to retinal cells.

Chapter 5 Investigation of amphiphilic gemini surfactants and peptide-modified gemini surfactants as potential Amyloid- β_{1-40} self-aggregation inhibitors

5.1 Introduction

Glaucoma is the result of RGC neurodegeneration leading to first a loss in peripheral vision and eventually leading to complete vision loss (41). But when looking at the pathophysiology of the disease more closely, it shows similar ties to the neuroinflammation pathways in the Alzheimer's disease and Parkinson's disease. These neuroinflammatory processes are characterized by activation of the microglial cells to promote phagocytosis of the dying RGCs and axons (55). With the above manifestations, the deposition of amyloid- β ($A\beta$), synuclein and pTau were also detected in the retinas of glaucoma affected individuals and experimental animal glaucoma models (300).

5.2 Amyloid- β hypothesis- A pathophysiology of glaucoma and IOP associated with Alzheimer's disease

Until recently the relation between the $A\beta$ deposition in the retinal layers and the glaucoma remained a grey area and is not understood properly. Despite the uncertainty in pathophysiology of activation of $A\beta$ deposition in both Alzheimer's and in glaucoma, it has been identified that an increase in the IOP can lead to injury of RGCs and activation of $A\beta_{1-42}$ and p-Tau protein deposition leading to neurodegeneration and glaucomatous condition (301). It has also been recognized that Alzheimer's and glaucoma have some common pathophysiological elements and also the loss of RGCs and optic nerve in both Alzheimer's and glaucoma proceeds in a similar fashion (302). A study by Mckinnon et al. (2003) found a link between neurodegeneration and activation of caspases. Caspase-8 and caspase-3 activation can lead to triggering of apoptosis but studies have shown that the activation of caspases and the neurodegeneration were triggered by the secretion of amyloid precursor protein (APP) (303).

Glaucoma and Alzheimer's disease show common manifestations such as A β aggregation, few studies where antibody-based immunotherapy with aducanumab has shown targeted inhibition of the A β aggregation and was shown to reduce both soluble and insoluble A β during their phase 1 and phase 2 clinical trials for Alzheimer's disease (304), but later the phase 3 clinical trials have been terminated as the antibody did not meet its primary endpoints but had shown a dose-dependent reduction in A β plaques. Similarly, solanezumab another antibody-based treatment for A β aggregation has failed phase 3 trials and did not reach its primary outcomes (305). Another potential novel A β aggregation inhibition therapies (GAL-101 and GAL-201) entered phase 2 clinical trials. The treatments have shown positive results during phase 1 trial, and their novel targeting compared to previously tried antibody therapies, makes them first of its kind in targeting the misfolded A β and prevent their aggregation, the treatment can lead to neuroprotection in the RGCs (306).

5.2.1 Amyloid- β implications in glaucoma and RGC neurodegeneration

Recent studies on identifying the relation between Alzheimer's and glaucoma also provide evidence for the role of A β in both Alzheimer's and glaucoma and their similar pathophysiology leading to apoptosis and cell death. It was shown that A β colocalizes in the apoptotic RGCs in experimental glaucoma models and induces RGC apoptosis. Also, targeting the A β pathway has resulted in reduction of RGC apoptosis and helped in the protection of RGCs from degeneration (307). Both these neurodegenerative conditions were characterized with neuroinflammation as their primary pathway in which microglia plays a significant role in their activation and lead to the localized aggregation of proteins and pro-inflammatory mediators that can aid in the progress of neurodegeneration in glaucoma (Figure 5-1) (308). The activation of the glial cell pathway can trigger secondary events such as NTF deprivation, reactive oxygen species (ROS) production, mitochondrial dysfunction and glutamate toxicity (308). Hyperphosphorylated tau proteins also lead to accumulation of the A β deposits leading

to neurodegeneration in the retina and optic nerve. Specimens from human donors of ocular tissues with uncontrolled IOP and with glaucoma have shown the characteristic presence of abnormal tau (AT8) and phosphorylated tau (pTau), respectively (301, 309). The tau accumulation is known to cause the impairment of the anterograde axonal transport leading to neuronal dysfunction and neurodegeneration in the retina that is characterized with tau accumulation. Reduction in the tau accumulation helps in improving the axonal transport and reduce neuronal dysfunction (310, 311). Hence, it is evident from these studies that targeting the A β pathway along with other neuroprotective therapies in eye can help in effective neuroprotection along with IOP reduction-based strategies and treatments.

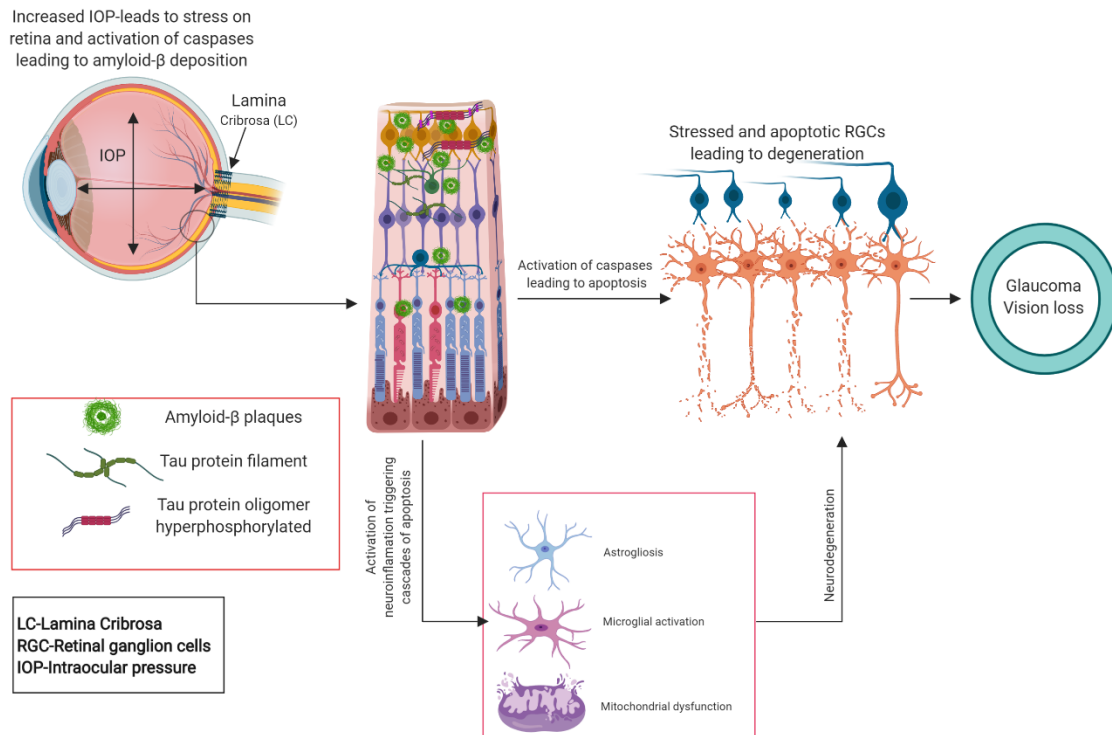


Figure 5-1 Schematic implications of amyloid-beta accumulation in retina on glaucoma and neurodegeneration (308, 309). Figure generated by Lokesh Narsineni using BioRender.com.

5.2.2 Amyloid- β peptide: Structural characteristics

The A β -peptide ranges from 34 to 43 amino acids released from the β and γ -secretase pathway, two species of A β peptides that are implicated in the A β fibril formation are A β_{40} which is abundantly produced amyloid peptide and A β_{42} is generally the most toxic form of amyloid that are produced from the amyloid precursor pathway due to genetic mutations (312). The abnormal tau protein AT8 accumulation in the retina of the uncontrolled IOP eyes is evident from the surgical glaucomatous specimens and were mostly identified in the outer border of the INL and this abnormal tau protein accumulation can be having a shared common pathway with other neurodegenerative diseases. The abnormal tau protein AT8 can lead to disturbances in the structural integrity of the microtubule associated protein (MAP) which is a vital factor for the structural integrity of the neurons. Disintegration in MAP caused by abnormal tau protein accumulation in a fibril form can lead to blockade of the neuronal transport thereby leading to neurodegeneration (Figure 5-2). Studies carried out in normal retina and glaucomatous retina demonstrate a deposition of abnormal tau protein AT8 which is absent in normal retinas. This deposition could be one of the main reason for the secondary neurodegeneration due to the insult caused by the tau protein deposition leading to microtubule disintegration (309).

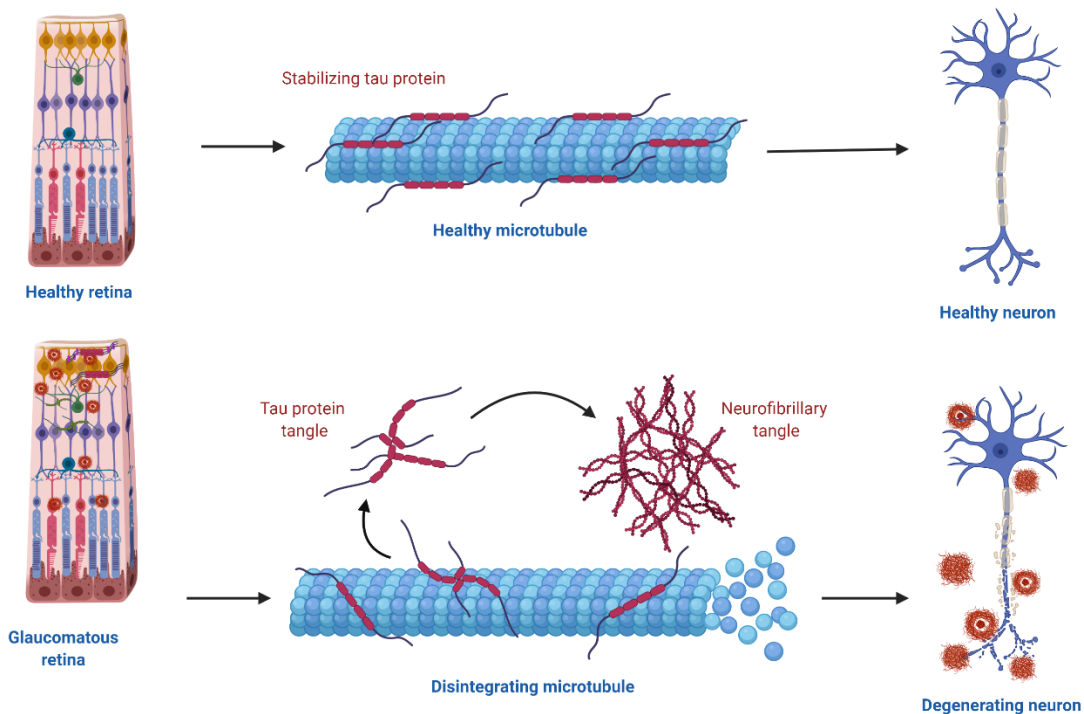


Figure 5-2 Hypothetical schematic of tau protein accumulation implications in retinal neurodegeneration. Glaucomatous retina with uncontrolled IOP shows marked increase in abnormal tau AT8 and leads to changes in the structural integrity of the microtubules leading to neuronal injury and neurodegeneration (309). Figure generated by Lokesh Narsineni using BioRender.com.

A β -peptide contains a number of hydrophobic residues that drive its aggregation property. The amino acid sequence KLVFFA is generally considered as the hydrophobic in the A β -peptide structure that helps in the binding and aggregation of the A β -peptides to bundle into higher order oligomers and finally into A β -fibrils which are the toxic (313). The core hydrophobic pocket of KLVFFA in the A β -peptide responsible for the self-induced aggregation of the A β -peptides into A β -fibrils is shown in Figure 5-3 (314).

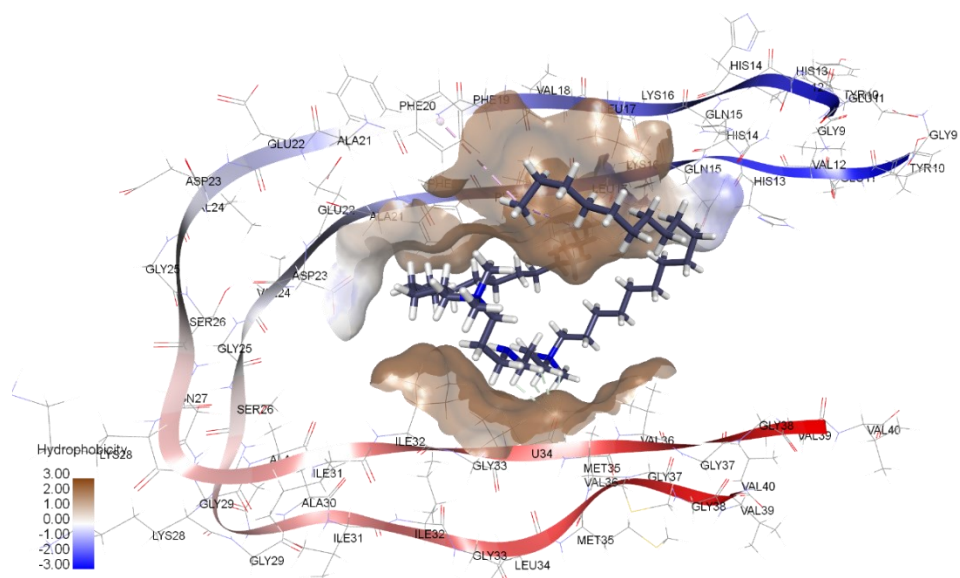


Figure 5-3 A β ₄₀-peptide showing the hydrophobic regions (brown mesh like structure) in the peptide that help in formation of A β -fibril (313, 314). Peptide structure obtained from RCSB protein data bank (PDB ID:2LMN).

5.2.3 Amphiphilic surfactants in amyloid- β aggregation inhibition

Amphiphilic surfactants could be useful as amyloid fibril aggregation inhibitors as shown first by wang et al. (2005). Two surfactants 1,2-dihexanoyl-sn-glycero-3-phosphocholine (di-C6-PC) and 1,2-diheptanoyl-sn-glycero-3-phosphocholine (di-C7-PC), at pH 7.2 were shown to inhibit the aggregation of amyloid fibrils in a concentration and time dependent manner using thioflavin T (ThT) fluorescence method. At 100 μ M complete inhibition of fibril formation was found (315). Preliminary work showed that the inhibition of the fibril formation takes place by preventing the α -helix structure from forming the highly ordered β -sheets which is an insoluble form of the amyloid fibril. This could be due to charge interactions between the amphiphilic surfactant and the A β (316). The addition of cationic gemini surfactant could lead to disruption of the ordered β -sheets on a concentration dependent manner, it was identified that addition of monomers slowly will first lead to charge interactions between the A β ₄₀

peptide leading to aggregation and β -sheets formation, later when the concentration is slowly increased above the CMC level the cationic gemini surfactants will start to show repulsive forces due to the head groups leading to disruption. It was also identified that compared to DTAB, gemini surfactants have higher charge interaction ability with $A\beta_{40}$ (317).

5.3 Rationale and Objective

Gemini surfactants are a class of dicationic amphiphilic surfactants and conjugation of peptide on to the gemini surfactant imparts further amphiphilic characteristics on the final molecule which can help in the inhibition of $A\beta_{1-40}$ fibril formation. The $A\beta_{40}$ aggregation inhibition can lead to dual action of the NPX systems prepared using gemini surfactants. Since, amyloid cascade is also part of glaucoma pathophysiology along with targeted gene delivery to the retinal cells in eye the administered NPXs can lead to $A\beta_{40}$ aggregation inhibition. Hence, to assess the potential of 18-7NH-18, 18-7N(18)-18 gemini surfactants, peptides p_{1-4} and peptide modified gemini surfactant (18-7N(p_{1-4})-18) for inhibiting the $A\beta_{1-40}$ fibril formation an $A\beta$ aggregation inhibition assay was carried out using ThT-binding fluorescence assay. Molecular docking studies with $A\beta_{1-40}$ peptide dimer were also carried out for all the above gemini surfactants to understand the interactions and to establish an *in vitro- in silico* correlation of the inhibition assay.

The objectives of this chapter is to present the $A\beta$ aggregation inhibition potential of amphiphilic-gemini surfactants (m-7NH-m), peptide-modified gemini surfactants (m-7N(p)-m) and peptides using a ThT fluorescence kinetic assay and to correlate the efficiency of their $A\beta$ aggregation inhibition of the ligand molecules with the $A\beta$ peptide through *in-silico* molecular docking studies.

5.4 Materials and methods

Chem Draw 18.0 (Perkin Elmer, Santa Clara, CA, USA), BIOVIA Discovery Studio (Dassault Systems, San Diego, CA, USA), Research Collaboratory for Structural Bioinformatics (RCSB)- Protein Data Bank (PDB), A β ₄₀ peptide (2LMN), Ligands- Chem Draw structures (.sdf files) were used for molecular docking studies. Pure compounds of 18-7NH-18 gemini surfactant (N, N'-(azanediylbis(propane-3,1-diyl))bis(N,N-dimethyldodecan-1-aminium) (Batch: FL18GLN-053117-RX9-001). 18-7N(18)-18 gemini surfactant (Batch: RX18-001-Jan 08 2018) were synthesized in-house, p₁ peptide (RGD), p₂ peptide (RLE), p₃ peptide (FASNKL), p₄ peptide (LI), 18-7N(p₁)-18, 18-7N(p₂)-18, 18-7N(p₃)-18 and 18-7N(p₄)-18 gemini surfactant were synthesized by Celtek peptides, TN, USA, Thioflavin T (ThT), Glycine, Na₂HPO₄·7H₂O, NaOH, Ultra-pure water (UPW) and DMSO (HPLC grade) were obtained from Sigma Aldrich (Oakville, ON, Canada), A β ₁₋₄₀ peptide in hexafluoro isopropanol (HFIP) (rPeptide, Bogart, USA).

5.4.1 A β -aggregation inhibition studies

The efficiency of gemini surfactants and peptide-modified gemini surfactants to inhibit the self-aggregation of A β was determined using a ThT fluorescence binding assay. The assay was carried out in a Costar 384 well clear bottom plates (Corning Inc, MA, USA) on a BioTek Synergy H1 microplate reader (BioTek®, VT, USA). The kinetic assay for A β ₄₀ was carried out by measuring the fluorescence intensity obtained from the ThT binding with the A β fibrils. The ThT fluorescence was excited at 440nm and emission was captured at 490nm and the reading were taken every 5 minutes with frequent shaking of the plate for 30 seconds for 24 hours. Before starting the kinetic assay, gemini surfactant stock solutions were prepared in DMSO and diluted with sodium phosphate buffer pH 7.4 composition to make sure the total concentration of DMSO was kept below 7.5%, to 1 μ M, 5 μ M, 10 μ M, 25 μ M and 50 μ M. A β ₄₀ in HFIP samples were dissolved in 1% ammonium hydroxide in milli-Q water, sonicated

at room temperature for 5 minutes and diluted up to 50 μM . Positive and negative controls such as methylene blue and Oregon-green were prepared at 1 μM , 5 μM , 10 μM , 25 μM and 50 μM and used along with test compounds and A β ₄₀ control. The assay was carried out by treating each well with 44 μL ThT, (35 μL buffer for control, 28 μL of buffer for compound backgrounds and 27 μL for A β ₄₀ control and 20 μL for test compounds treatment), 1 μL DMSO (only for background and A β ₄₀ controls), 8 μL of test compound (1-50 μM concentrations mentioned above). Final volume of the well is kept at 80 μL . Initially before adding the A β ₄₀ an interference test was carried out by covering the 384 plate with the cover strip and then analyzing for ThT background fluorescence with compounds for 5 minutes. After 5 minutes, the freshly prepared A β ₄₀ peptide was added into the A β ₄₀ control wells and kinetic assay was run for 24 hours. Kinetic assay was at $E_{\text{ex}}=440$ nm and $E_{\text{em}}=490$ nm for 24 h at 37°C. Readings were recorded every 5 min with shaking for every 30 seconds between each reading. Data were analyzed by constructing concentration over time of ThT concentration plots. Data presented is an average of triplicate values. Relative fluorescence units (RFU) values were corrected with ThT-interference before calculating the final RFU values plotted on the graph and inhibitory constant values were drawn from the corrected values (318-320).

5.4.2 Molecular docking studies -binding interactions assessment of amphiphilic gemini surfactants, integrin, IgSF-peptides and peptide-modified gemini surfactants with A β ₄₀ peptide

Based on the *in vitro* A β aggregation inhibition studies four peptides (p₁, p₂, p₃ and p₄), 18-7NH-18 gemini surfactant and peptide-modified gemini surfactants (18-7N(p₁)-18, 18-7N(p₂)-18, 18-7N(p₃)-18 and 18-7N(p₄)-18) were selected for this study to assess the binding affinity, bonding and non-bonding interaction of the ligand molecules with the A β ₄₀ peptide. The molecular docking studies outline the assessment of the binding interactions of amphiphilic-gemini surfactants, peptide-modified gemini surfactants along with gemini surfactants and peptides with A β ₄₀ peptide (PDB ID: 2LMN). The solid-

state NMR structure of A β ₄₀ peptide (2LMN) was obtained from RCSB-PDB(321). The peptide is prepared for docking (319). Ligand molecules were sketched using Chem Draw (PerkinElmer) and imported into Discovery Studio to prepare for docking. CHARMM forcefield was applied and energy minimization was carried out using steepest-descent protocol with 1000 iterations. After minimizing energy for ligand molecules, ligand-peptide interaction studies were carried out by defining the active site. Ligand active site of 20Å was selected and the best iterations were reported. Molecular docking was carried out using the ‘*receptor-ligand interactions*’ module (322). CDOCKER algorithm was used to find the most appropriate binding sites and interactions for p₁ peptide (RGD), p₂ peptide (RLE), p₃ peptide (FASNKL) and p₄ peptide (LI), 18-7NH-18, 18-7N(p₁)-18, 18-7N(p₂)-18, 18-7N(p₃)-18 and 18-7N(p₄)-18 gemini surfactants. The docked ligand poses were ranked based on the CDOCKER energy scores. Polar and non-polar interaction were also analyzed, and all the important interactions displayed by the ligand were visualized and analyzed (323).

5.5 Results

5.5.1 A β ₄₀-aggregation inhibition studies

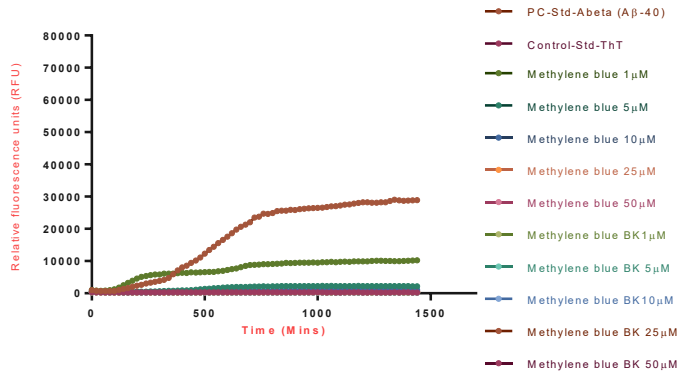
The ability of amphiphilic gemini surfactants with and without peptide modification and peptides themselves to inhibit the self-aggregation of the A β ₄₀ was assessed using the ThT-binding fluorescence assay. From the obtained results it is evident that the all the control and treatment backgrounds did not show any increase in the relative fluorescence units (RFU) which signifies that the background controls without A β ₄₀ peptide did not contribute to the background fluorescence in the treatments with A β ₄₀ peptide. Methylene blue positive control has shown inhibition of the A β ₄₀ aggregation form as low as 1 μ M and complete inhibition is identified from 5 μ M (Figure 5-4 A). Orange-green negative control treated wells containing A β ₄₀ peptide did not show any inhibition of the self-aggregation of the A β to

form higher order oligomers with increase in the concentration of Orange-G up to 50 μ M, compared to A β ₄₀ control without any treatment (Figure 5-4 B).

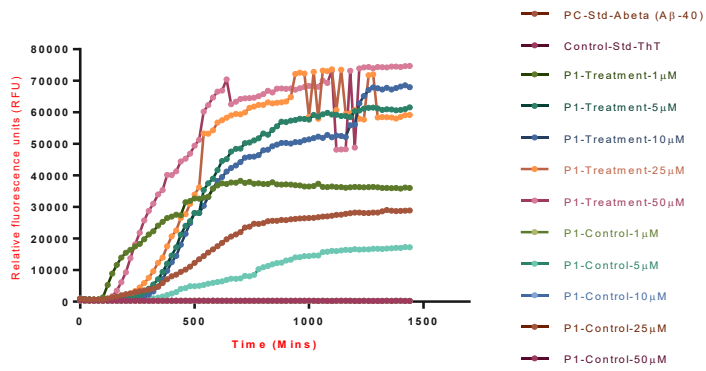
Peptides p₁, p₂, p₃ and p₄ did not show any strong inhibition of the A β ₄₀ aggregation. It was observed that increased concentration of peptide p₁, p₂, p₃ and p₄ increased aggregation of the A β ₄₀ peptide compared to A β ₄₀ peptide control confirms that the peptides themselves do not contribute to any decrease in the A β ₄₀ peptide aggregation (Figure 5-4 C-F). The 18-7NH-18 gemini surfactant on the other hand reduced the A β ₄₀ peptide aggregation by 50% value compared to the A β ₄₀ controls at 10 μ M, and up to 90% at 25 μ M. However below 10 μ M the A β ₄₀ peptide aggregation is higher compared to the control (Figure 5-5 A).

From the peptide-modified amphiphilic gemini surfactants (18-7N(p₁₋₄)-18) it has been identified that the 18-7N(p₁)-18, 18-7N(p₂)-18 and 18-7N(p₃)-18 gemini surfactants have shown inhibition of A β ₄₀ peptide aggregation from as low as 5 μ M (Figure 5-5 B-D). Whereas 18-7N(p₁)-18 and 18-7N(p₂)-18 inhibited about 90% of the aggregation at 25 μ M, 18-7N(p₃)-18 gemini inhibited the aggregation up to 90% compared to A β ₄₀ control at a concentration of 10 μ M (Figure 5-5 C) and 18-7N(p₄)-18 gemini surfactants on the other hand started inhibiting at 10 μ M and reached peak efficiency at 25 μ M. Hence, from the results it is evident that efficiency of the inhibition, in the decreasing order, is 18-7N(p₃)-18 > 18-7N(p₁)-18 > 18-7N(p₂)-18 > 18-7N(p₄)-18 gemini surfactants.

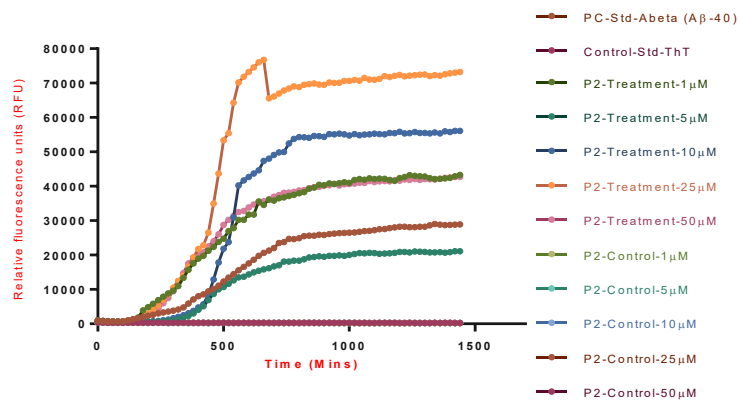
A.



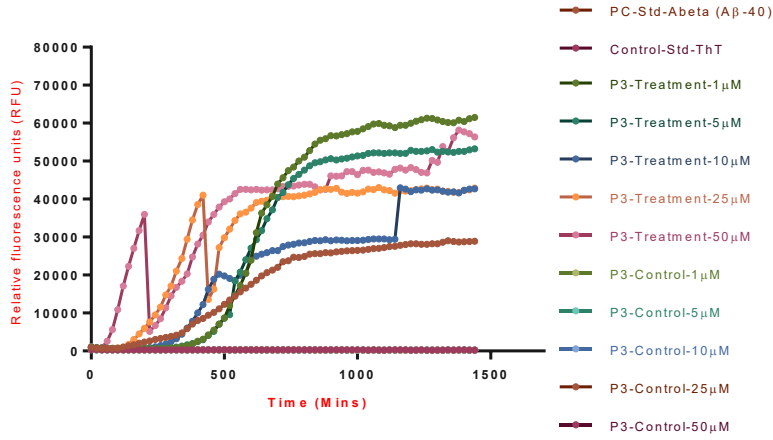
B.



C.



D.



E.

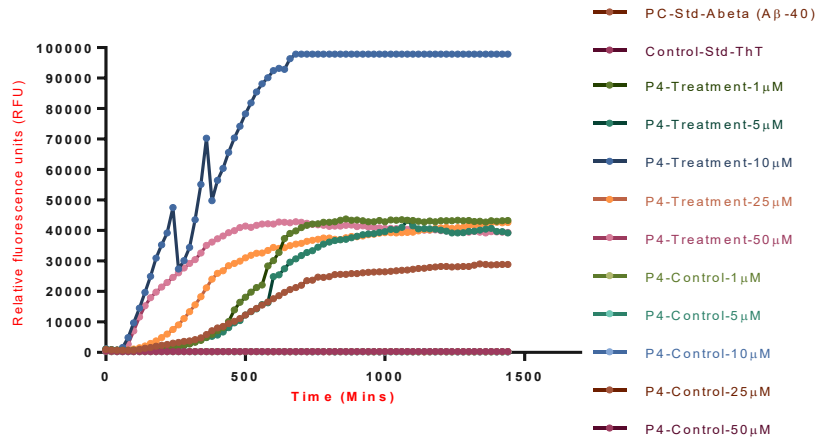
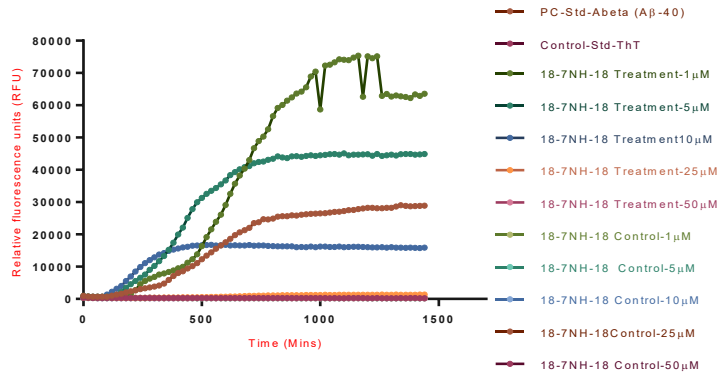
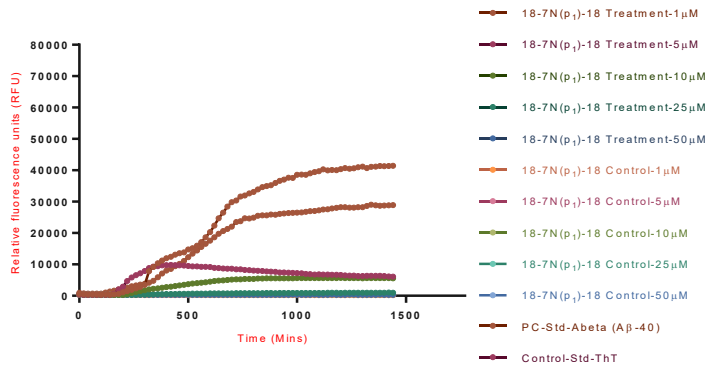


Figure 5-4 Aβ₄₀ aggregation inhibition studies of peptide controls (A) Methylene blue treatment-positive control, (B-E) peptide p₁, p₂, p₃ and p₄ treatments respectively. All treatments were tested from 1 μM to 50 μM concentrations. Peptide treatments did not show any inhibition of Aβ₄₀ aggregation (n=2, data points are average of 3 independent samples).

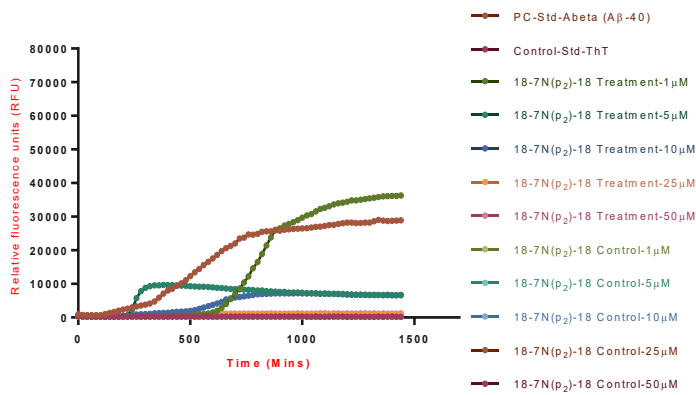
A.



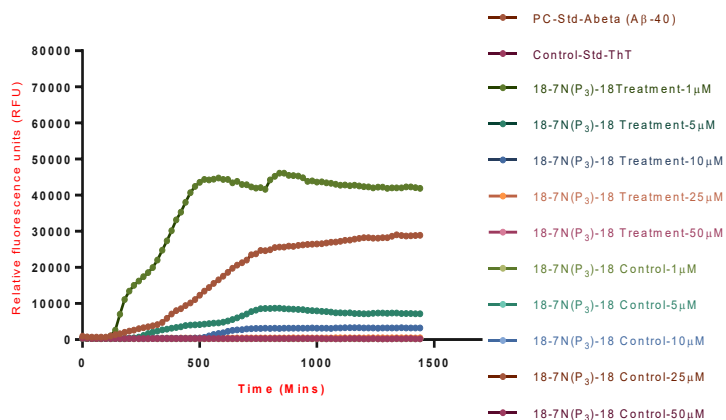
B.



C.



D.



E.

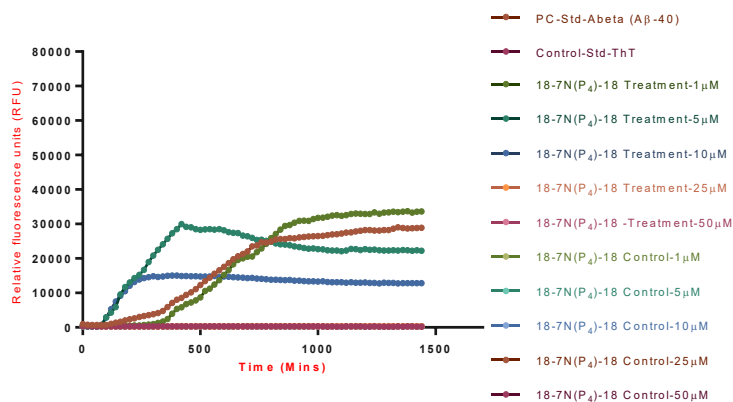


Figure 5-5 A β ₄₀ aggregation inhibition studies of treatment groups (A) 18-7NH-18 (B) 18-7N(p₁)-18 (C) 18-7N(p₂)-18, (D) 18-7N(p₃)-18 and (E) 18-7N(p₄)-18 amphiphilic gemini surfactant treatments and backgrounds. All treatments were tested from 1 μ M to 50 μ M concentrations, 18-7N(p₁)-18 and 18-7N(p₃)-18 gemini surfactants showed inhibition of A β ₄₀ aggregation from 5 μ M and peptide modified gemini surfactants performed better compared to peptides only treatments and 18-7NH-18 gemini surfactant (n=2, data points are average of 3 independent samples).

5.5.2 Molecular docking studies

Molecular docking studies of 18-7NH-18, 18-7N(p₁)-18, 18-7N(p₂)-18, 18-7N(p₃)-18 and 18-7N(p₄)-18 gemini surfactants and p₁ and p₃ peptide ligands with the A β ₄₀ peptide (2LMN) was successfully carried out. The results of the molecular interactions of each of the ligand molecule with the A β ₄₀ peptide are shown in Figure 5-6 to Figure 5-10 and Table 5-1 to Table 5-5. All the non-bonding interactions of the ligand molecule with the amino acids of the A β ₄₀ peptide were identified and the top 10 hits with the highest CDOCKER energy are reported. The top hit of 18-7NH-18 gemini surfactant docked on to the A β ₄₀ peptide has a CDOCKER energy score of -36.16 Kcal/mol and a CDOCKER interaction energy of -51.41 Kcal/mol (top 10 hits were shown in Appendix 4 Table 8). Some of the non-bonding interactions obtained were pi-alkyl hydrophobic interactions between PHE19:C31 (BL:4.71), the interactions were between the pi-orbitals and the alkyl tail of the 18-7NH-18 gemini surfactant (Figure 5-6), all the non-bonding interactions can be seen in Table 5-1(B).

Table 5-1 Top hits and non-bonding interactions from molecular docking studies of 18-7NH-18 gemini surfactant with 2LMN

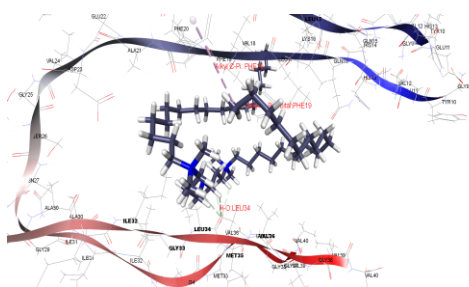
A) Top hit of 18-7NH-18 docked on to A β ₄₀ peptide

Top Hit	(-) CDOCKER energy kcal/mol	(-) CDOCKER interaction energy kcal/mol
1	36.16	51.41

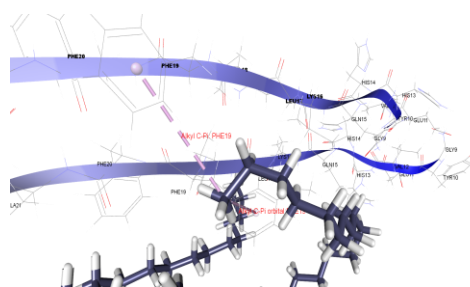
B) Non-bonding interactions

Non-bond interactions	Bond length (Å)	Bond Type	Interaction	Donor group	Function	Acceptor group	Function
A:PHE19 - m-7NH-m.sdf:C31	4.71	Hydrophobic	Pi-Alkyl	A: PHE19	Pi-Orbitals	m-7NH-m.sdf:C31	Alkyl
B:PHE19 - m-7NH-m.sdf:C31	5.35	Hydrophobic	Pi-Alkyl	B:PHE19	Pi-Orbitals	m-7NH-m.sdf:C31	Alkyl

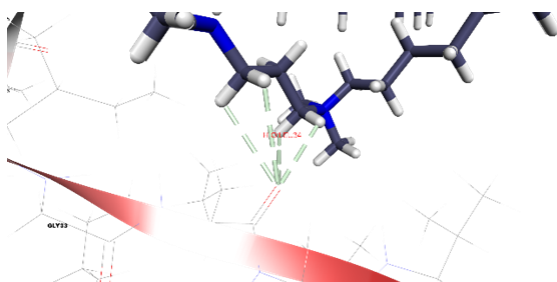
A.



B.



C.



D.

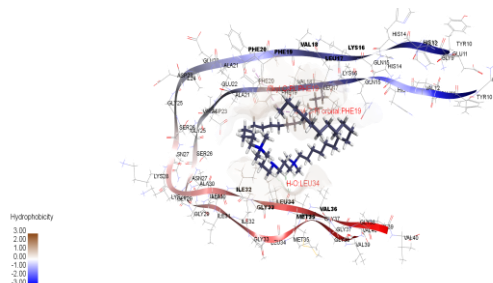


Figure 5-6 Molecular docking studies of 18-7NH-18 with 2LMN using CDOCKER algorithm, (A) 18-7NH-18 binding into the pocket of A β ₄₀ peptide (B) Pi-alkyl interactions of 18-7NH-18 alkyl tail with pi-orbitals of PHE12, (C) Hydrogen bonding of 18-7NH-18 with LEU34 (D) Binding of 18-7NH-18 into the hydrophobic area where A β ₄₀ monomers interact to form oligomers.

Peptide modified gemini surfactant 18-7N(p₁)-18 docked on to Aβ₄₀ peptide exhibited a CDOCKER energy of -60.57 kcal/mol and CDOCKER interaction energy of -70.69 kcal/mol (Table 5-2 A-B) (top 10 hits were shown in Appendix 4, Table 9 A). Non-bonding interactions such as hydrogen bonding was found to be the predominant interaction between the ligand molecule and the peptide and some of them with the lowest bond length were between VAL24:O70 (BL: 2.16Å), SER26:H190 (BL: 2.24 Å), ASP23:O70 (BL: 2.77 Å). Electrostatic interactions were also identified between the ASP23:N9 (BL: 5.32 Å) and hydrophobic interactions were observed between HIS14:C47 and HIS13:C29. The interactions were between the pi-orbitals of the amino acids in the peptide with the alkyl tail groups of the ligand molecule (Figure 5-7 C). Whereas p₁ peptide alone docked on to Aβ₄₀ peptide showed a CDOCKER energy of -45.23 kcal/mol and a CDOCKER interaction energy of -29.34 Kcal/mol for the top hit (Table 5-2 C) and only hydrogen bonding was observed as the non-bonding interactions between the ligand and the Aβ₄₀ peptide (Appendix 4 Table 9 B).

Table 5-2 Top hit and non-bonding interactions from molecular docking studies of 18-7N(p₁)-18 gemini surfactant with 2LMN

A) Top hit of 18-7N(p₁)-18 docked on to Aβ₄₀ peptide

Top Hit	(-) CDOCKER energy kcal/mol	(-) CDOCKER interaction energy kcal/mol
1	60.57	70.69

B) Non-bonding interactions

Non-bond interactions	Bond length (Å)	Bond Type	Interaction	Donor group	Function	Acceptor group	Function
m-7N(p ₁)- m_molecule.sdf:N9 - A:ASP23:OD2	5.32532	Electrostatic	Attractive Charge	m-7N(p ₁)- m_molecul e.sdf:N9	Positive	A:ASP23:OD2	Negative
A:VAL24:HN - m- 7N(p ₁)- m_molecule.sdf:O7 0	2.16178	Hydrogen Bond	Conventional Hydrogen Bond	A:VAL24: HN	H-Donor	m-7N(p ₁)- m_molecule.sd f:O70	H- Acceptor
m-7N(p ₁)- m_molecule.sdf:H1 90 - A:SER26:OG	2.24474	Hydrogen Bond	Conventional Hydrogen Bond	m-7N(p ₁)- m_molecul e.sdf:H190	H-Donor	A:SER26:OG	H- Acceptor
A:HIS14 - m- 7N(p ₁)- m_molecule.sdf:C47	4.38018	Hydrophobic	Pi-Alkyl	A:HIS14	Pi- Orbitals	m-7N(p ₁)- m_molecule.sd f:C47	Alkyl
B:HIS13 - m- 7N(p ₁)- m_molecule.sdf:C29	5.0307	Hydrophobic	Pi-Alkyl	B:HIS13	Pi- Orbitals	m-7N(p ₁)- m_molecule.sd f:C29	Alkyl
m-7N(p ₁)- m_molecule.sdf:N9 - A:ASP23:OD2	5.32532	Electrostatic	Attractive Charge	m-7N(p ₁)- m_molecul e.sdf:N9	Positive	A:ASP23:OD2	Negative

C) Top hit for p₁ peptide docked on to 2LMN

Top Hit	(-) CDOCKER energy kcal/mol	(-) CDOCKER interaction energy Kcal/mol
1	45.23	29.34

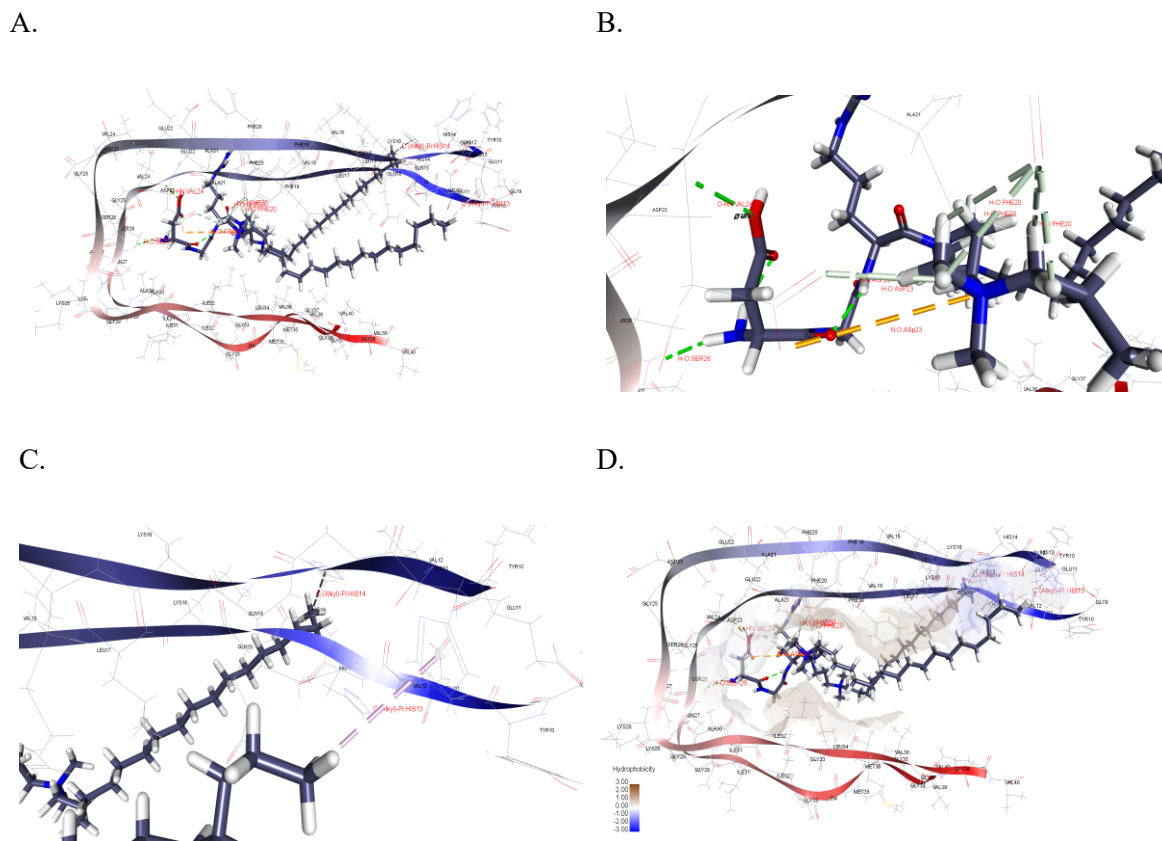


Figure 5-7 Molecular docking studies of 18-7N(p₁)-18 with 2LMN using CDOCKER algorithm, (A) 18-7N(p₁)-18 binding into the pocket of Aβ₄₀ peptide, (B) Hydrogen bonding interactions between ligand and VAL24:O70, SER26:H190, ASP23:O70 and electrostatic interaction between N-O:ASP23, (C) Pi-alkyl interactions of alkyl tail with HIS13 and HIS14 and (D) Binding of 18-7N(p₁)-18 ligand into the hydrophobic pocket of Aβ₄₀ peptide and its interaction with the amino acids responsible for binding for Aβ₄₀ peptide monomers to form oligomers thereby inhibiting the oligomer formation.

The 18-7N(p₂)-18 gemini surfactant docked on to Aβ₄₀ peptide demonstrated a CDOCKER energy of -63.36 kcal/mol and CDOCKER interaction energy of -59.86 kcal/mol (complete list of top hits were shown in Appendix 4- Table 10 A) and non-bonding interactions such as hydrogen bonding, electrostatic and hydrophobic interactions were obtained from the 18-7N(p₂)-18- Aβ₄₀ peptide docking studies. Hydrogen bonding interaction between the ligand molecule and the amino acids VAL18

(BL:2.02Å), LYS16 (BL: 2.69Å), PHE20 (BL: 2.53 Å) of Aβ₄₀ peptide were noticed (Table 5-3 A-B). Other interactions such as electrostatic interaction (Pi-Cation) between Nitrogen (N1): PHE20 (BL: 4.84 Å) and hydrophobic interaction between the alkyl tails of ligand molecule with alkyl tail of LYS16 (BL: 4.02Å) were identified (Figure 5-8).

Table 5-3 Top hits of 18-7N(p₂)-18, p₂ peptide and non-bonding interactions of 18-7N(p₂)-18 with 2LMN

A. Top hit for 18-7N(p₂)-18

Top Hit	(-) CDOCKER energy kcal/mol	(-) CDOCKER interaction energy kcal/mol
1	63.36	59.86

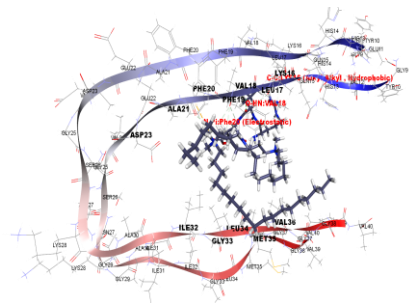
B. Non-bonding interactions of 18-7N(p₂)-18 with 2LMN

Non-bond interactions	Bond length (Å)	Bond Type	Interaction	Donor group	Function	Acceptor group	Function
A:VAL18:HN - m-7N(P2)-m.sdf:O65	2.02574	Hydrogen Bond	Conventional Hydrogen Bond	A:VAL18:HN	H-Donor	m-7N(P2)-m.sdf:O65	H-Acceptor
m-7N(P2)-m.sdf:N1 - A:PHE20	4.84854	Electrostatic	Pi-Cation	m-7N(P2)-m.sdf:N1	Positive	A:PHE20	Pi-Orbitals
m-7N(P2)-m.sdf:C66 - A:LYS16	4.02573	Hydrophobic	Alkyl	m-7N(P2)-m.sdf:C66	Alkyl	A:LYS16	Alkyl

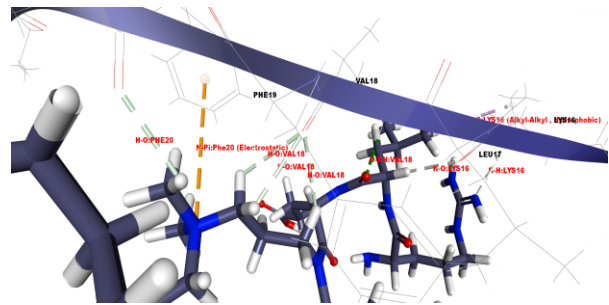
C) Top hit for p₂ peptide docked on to 2LMN

Top Hit	(-) CDOCKER energy kcal/mol	(-) CDOCKER interaction energy kcal/mol
1	38.62	23.15

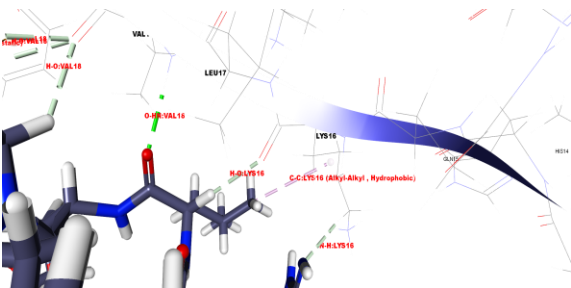
A.



B.



C.



D.

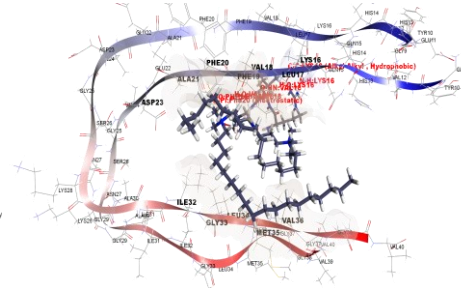


Figure 5-8 Molecular docking studies of 18-7N(p₂)-18 with 2LMN using CDOCKER algorithm, (A) 18-7N(p₂)-18 binding into the pocket of Aβ₄₀ peptide, (B) Pi-cation electrostatic interaction between N1 and pi-orbitals for PHE20, (C) Hydrogen bonding interactions of ligand with VAL18, LYS16 and hydrophobic interaction between alkyl tails of gemini surfactant and LYS16, (D) binding of 18-7N(p₂)-18 ligand into the hydrophobic pocket of Aβ₄₀ peptide.

Peptide p₂ docked on to Aβ₄₀ peptide showed a CDOCKER energy of -38.62 kcal/mol and a CDOCKER interaction energy of -23.15 kcal/mol for the top hit (Table 5-3 C) and hydrogen bonding interactions were identified between p₂ peptide: VAL18, ASP23 and LEU34 (Appendix 4, Table 10 B). The CDOCKER energy and the CDOCKER interaction energy have been higher for the 18-7N(p₂)-18 compared to the peptide itself.

When, 18-7N(p₃)-18 gemini surfactant was docked with Aβ₄₀ peptide the CDOCKER energy of the complex of 18-7N(p₃)-18 and Aβ₄₀ peptide was found to be -86.38 kcal/mol and a CDOCKER interaction energy of -72.09 kcal/mol (complete list of top hits were shown in Appendix 4-Table 11 A). Non-bonding interactions such as hydrogen bonding between H123:LEU34 (BL:2.28Å), H117:ASP23 (BL:2.69Å), H121:PHE20 (BL: 2.89Å) was pre-dominant while hydrophobic interactions such as between C31:ALA21 (BL: 3.92Å), C49:LEU17 (BL:5.25Å), C49:LEU17 (BL: 5.30Å) were also observed and electrostatic interaction was evident between N9:ASP23 (BL: 4.60Å) (Table 5-4 A-B) (Figure 5-9). Similarly, p₃ peptide alone is docked on to Aβ₄₀ peptide to identify if the p₃ peptide alone can induce similar strong interactions with the Aβ₄₀ peptide that can prevent Aβ₄₀ oligomer formation. The CDOCKER energy of the p₃ peptide docking with 2LMN peptide was found to be -69.61 kcal/mol and the CDOCKER interaction energy obtained was -40.87 kcal/mol (Table 5-4 C). Non-bonding interactions such as hydrogen bonding interactions and hydrophobic interactions were identified from the docking studies (Appendix-4, Table 11 B).

Table 5-4 Top hits of 18-7N(p₃)-18, p₃ peptide and non-bonding interactions of 18-7N(p₃)-18 with 2LMN

A. Top hit of 18-7N(p₃)-18 with 2LMN

Top Hit	(-) CDOCKER energy kcal/mol	(-) CDOCKER interaction energy kcal/mol
1	86.38	72.09

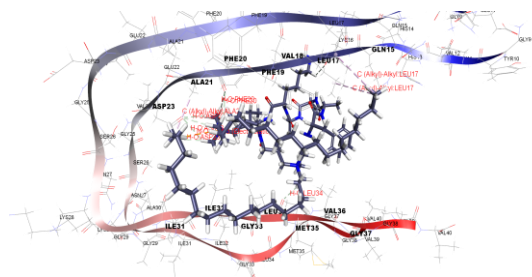
B. Non-bonding interactions of 18-7N(p₃)-18 with 2LMN

Non-bond interactions	Bond length (Å)	Bond Type	Interaction	Donor group	Function	Acceptor group	Function
18-7N(P3)- 18.sdf:N9 - A:ASP23:OD2	4.60755	Electrostatic	Attractive Charge	18-7N(P3)- 18.sdf:N9	Positive	A:ASP23:OD2	Negative
A:ALA21 - 18- 7N(P3)-18.sdf:C31	3.92653	Hydrophobic	Alkyl	A:ALA21	Alkyl	18-7N(P3)- 18.sdf:C31	Alkyl
18-7N(P3)- 18.sdf:C49 - A:LEU17	5.25479	Hydrophobic	Alkyl	18-7N(P3)- 18.sdf:C49	Alkyl	A:LEU17	Alkyl
18-7N(P3)- 18.sdf:C49 - B:LEU17	5.3029	Hydrophobic	Alkyl	18-7N(P3)- 18.sdf:C49	Alkyl	B:LEU17	Alkyl

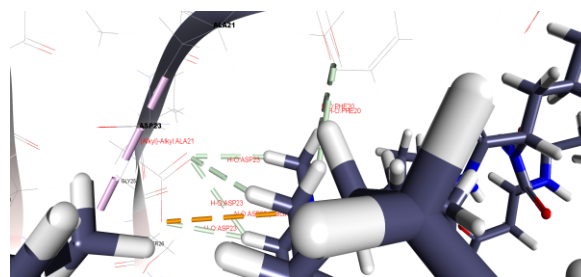
C. Top hit of p₃ peptide with 2LMN

Top Hit	(-) CDOCKER energy kcal/mol	(-) CDOCKER interaction energy kcal/mol
1	69.61	40.87

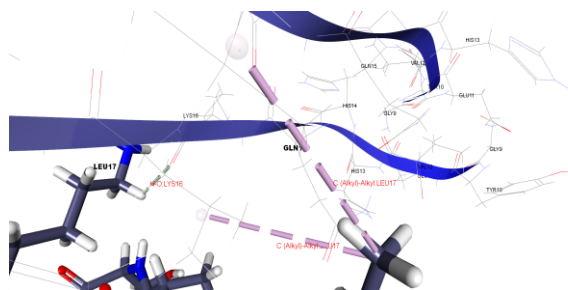
A.



B.



C.



D.

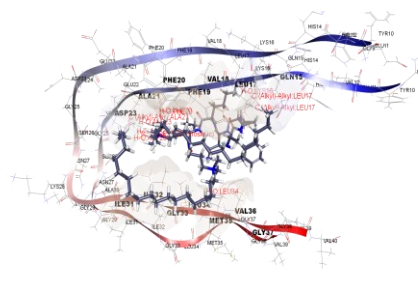


Figure 5-9 Molecular docking studies of 18-7N(p₃)-18 with 2LMN using CDOCKER algorithm, (A) Docked top hit of 18-7N(p₃)-18 with Aβ₄₀ peptide, (B) Electrostatic and hydrogen bonding interactions of ligand molecule with ASP23, PHE20, LEU34 and LYS16, (C) Hydrophobic interactions of ligand with ALA21 and LEU 17 of Aβ₄₀ peptide and (D) binding of 18-7N(p₃)-18 ligand into the hydrophobic pocket of Aβ₄₀ peptide

After docking with A β ₄₀ peptide for gemini surfactant 18-7N(p₄)-18 the CDOCKER energy of the complex of 18-7N(p₄)-18 and A β ₄₀ peptide was found to be -42.47 kcal/mol and a CDOCKER interaction energy of -58.35 kcal/mol (complete list of top hits were shown in Appendix 4, Table 12 A). Non-bonding interactions such as hydrogen bonding between ligand molecule and ASP23 (BL:2.72Å), PHE20 (BL:1.75Å), hydrophobic interactions such as between C31:LYS16 (BL: 4.94Å), LEU17 (BL:4.59Å), C57, C58:VAL24 (BL:4.37 and 3.98Å), C49:LEU17 (BL: 5.30Å) were also observed (Table 5-5 A-B) (Figure 5-10). When p₄ peptide was docked on to A β ₄₀ peptide the CDOCKER energy of the p₄ peptide docking with A β ₄₀ peptide was found to be -23.29 kcal/mol and the CDOCKER interaction energy obtained was -20.18 kcal/mol (Table 5-5 C). Non-bonding interactions such as hydrogen bonding interactions and hydrophobic interactions were identified from the docking studies (Appendix-4 Table 12 B). It was evident that all interactions of the ligand molecule were with LEU34 of the A β ₄₀ peptide.

Table 5-5 Top hits of 18-7N(p₄)-18, p₄ peptide and non-bonding interactions of 18-7N(p₄)-18 with 2LMN

A. Top hit of 18-7N(p₄)-18 with A β ₄₀ peptide

Top Hit	(-) CDOCKER energy kcal/mol	(-) CDOCKER interaction energy kcal/mol
1	42.47	58.35

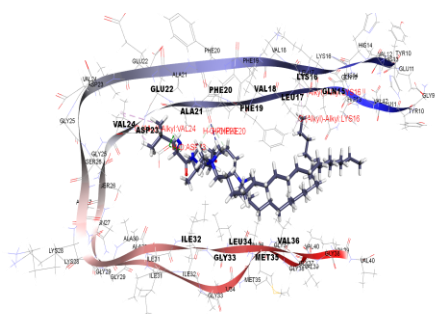
B. Non-bonding interactions of 18-7N(p₄)-18 with Aβ₄₀ peptide

Non-bond interactions	Bond length (Å)	Bond Type	Interaction	Donor group	Function	Acceptor group	Function
m-7N(P4)- m.sdf:C31 - A:LYS16	4.94039	Hydrophobic	Alkyl	m-7N(P4)- m.sdf:C31	Alkyl	A:LYS16	Alkyl
m-7N(P4)- m.sdf:C31 - A:LEU17	4.59534	Hydrophobic	Alkyl	m-7N(P4)- m.sdf:C31	Alkyl	A:LEU17	Alkyl
m-7N(P4)- m.sdf:C57 - A:VAL24	4.37433	Hydrophobic	Alkyl	m-7N(P4)- m.sdf:C57	Alkyl	A:VAL24	Alkyl
m-7N(P4)- m.sdf:C58 - A:VAL24	3.98023	Hydrophobic	Alkyl	m-7N(P4)- m.sdf:C58	Alkyl	A:VAL24	Alkyl

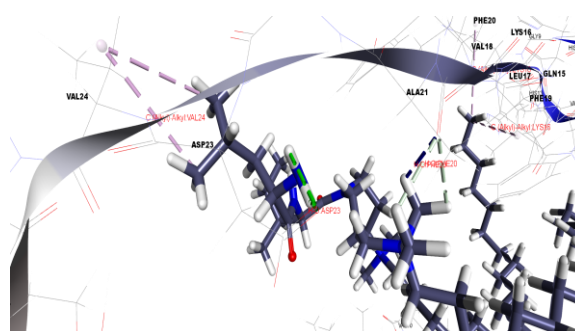
C. Top hit of p₄ peptide with Aβ₄₀ peptide

Top Hit	(-) CDOCKER energy kcal/mol	(-) CDOCKER interaction energy kcal/mol
1	23.29	20.18

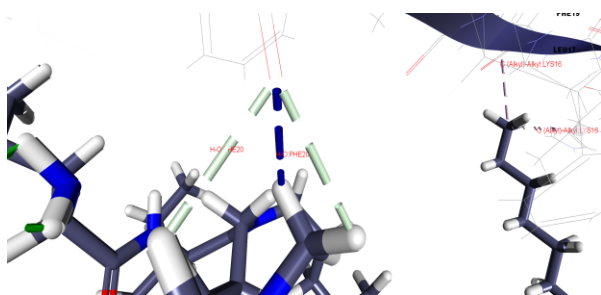
A.



B.



C.



D.

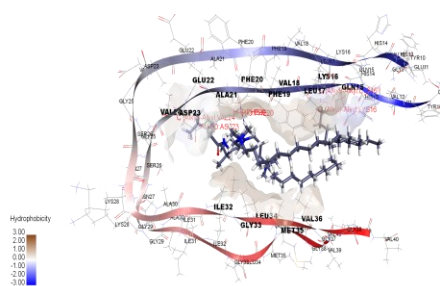
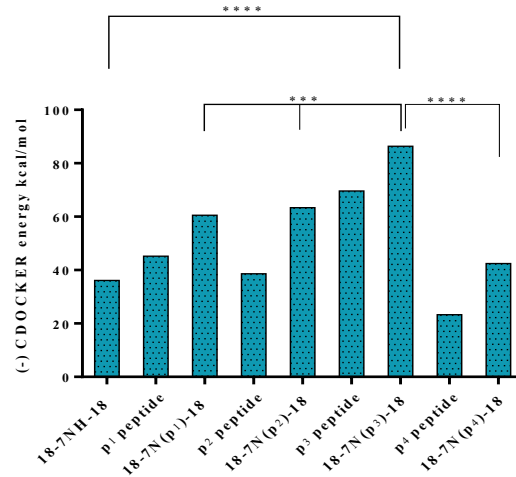


Figure 5-10 Molecular docking studies of 18-7N(p₄)-18 with 2LMN using CDOCKER algorithm, (A) Docked top hit of 18-7N(p₄)-18 with Aβ₄₀ peptide, (B) Hydrophobic interaction of ligand molecule with LYS16, LEU17 and LYS16, (C) Hydrogen bonding interactions of ligand molecule with ASP23 and PHE20 and (D) binding of 18-7N(p₄)-18 ligand into the hydrophobic pocket of Aβ₄₀ peptide

A.



B.

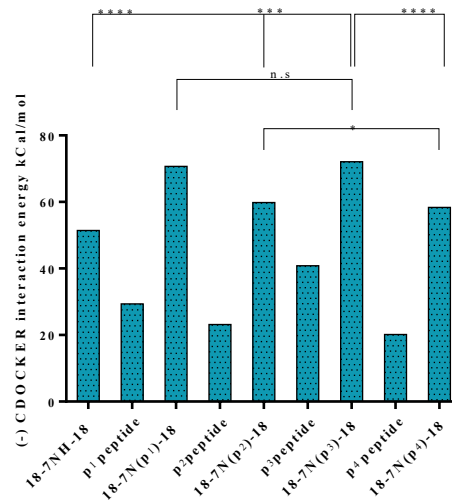


Figure 5-11 Comparative graph of (-) CDOCKER energy and (-) CDOCKER interaction energy of peptides and peptide modified gemini surfactants with A β ₄₀ peptide, (A) 18-7N(p₃)-18 ligand demonstrates significant difference (**** $p < 0.0001$ with 18-7NH-18) in (-) CDOCKER energy, (B) 18-7N(p₃)-18 and 18-7N(p₁)-18 ligands demonstrate no significant (n.s) difference in CDOCKER interaction energy, while 18-7N(p₃)-18 shows significant difference (**** $p < 0.0001$) compared with 18-7NH-18, 18-7N(p₄)-18 ligand and *** $p < 0.001$ with 18-7N(p₂)-18.

5.6 Discussion

Targeting amyloid- β aggregation in the retinal layers is a new area that has been explored in the past decade. A β is implicated in the development of neurodegenerative conditions in the eye due to the co-localization of A β with apoptotic retinal cells leading to activation of the RGC apoptosis (307). It has also been found that abnormal tau protein (AT8) accumulation occurred in the eye specimens collected from glaucoma patients with elevated IOP (301, 309). The tau protein helps to stabilize the microtubule-associated protein needed to maintain neuronal structure and integrity (324). Hyper-phosphorylated tau protein on the other hand can lead to disruption of microtubules, neuronal injury and neurodegeneration (Schematic Figure 5-2) (301). Hence, it is equally important to target the A β aggregation inhibition and disruption of the A β -fibrils in the retina to treat glaucoma effectively along with IOP lowering therapy and NTF gene therapy. It has been previously identified that amphiphilic gemini surfactants can interfere with the A β aggregation into higher order oligomers in a concentration dependent manner based on the charge interactions between the gemini surfactant and the A β ₍₁₋₄₀₎ (325). In our current study we evaluated the efficiency of the peptide modified gemini surfactants (18-7N(p₁₋₄)-18, peptides (p₁₋₄) and 18-7NH-18 to inhibit the A β aggregation and formation of higher order oligomers. Only peptide treatments p₁, p₂, p₃ and p₄ did not show any strong inhibition of the A β aggregation, while 18-7NH-18 treatment reduced the A β aggregation at 25 μ M, with strong inhibition achieved at 50 μ M. Below 25 μ M 18-7NH-18 did not reduce the aggregation, in fact the aggregation was promoted at 5 μ M and 10 μ M concentration by 18-7NH-18 (Figure 5-5 A). This could be due to the surfactant concentration being below CMC values (51.69 μ M for 18-7NH-18 as per Chapter 3, Figure 3-6) in the treatment. Another potential reason could be due to the presence of lower number of cationic charges from the 18-7NH-18 gemini surfactants compared to higher number of negative charges from the A β ₄₀ peptide. The lower charge due to low concentration (below CMC) of treatment could have helped in interacting of the surfactant monomers with the peptide and could have helped to form more ordered

β -sheets. But when the concentration of the 18-7NH-18 gemini surfactant is increased which could have been near to CMC or just below CMC the increase in the concentration will lead to increase in the total net cationic charge. This could lead to repulsion of the β -sheet structures and disrupt the oligomer structure formation. At very high concentration such as 50 μ M the surfactant inhibits the aggregation completely which could have been due to the surfactant presence above CMC or equivalent to CMC that can disrupt the aggregation by forming globular structures of A β ₄₀ by promoting the hydrophobic interactions of the alkyl tail groups and leading to formation of higher number of hydrophobic clusters leading to the inhibition of the A β ₄₀ aggregation. A similar behavior of the cationic gemini surfactants was reported previously for C₁₂C₆C₁₂Br₂ surfactants and some tetrameric cationic surfactants (325-327). Concentrations at 100 μ M inhibited the formation of the fibrils assayed by ThT fluorescence method (315). A similar behavior was observed for peptide modified compounds 18-7N(p₁₋₄)-18 in this study. The gemini surfactants were able to inhibit the aggregation of the A β ₄₀ peptide from as low as 5 μ M. 18-7N(p₁)-18, 18-7N(p₂)-18 and 18-7N(p₃)-18 inhibited A β ₄₀ peptide aggregation from as low as 5 μ M Figure 5-5 (b-d). The 18-7N(p₁)-18 and 18-7N(p₂)-18 inhibited almost 90% of the aggregation at 25 μ M while 18-7N(p₃)-18 gemini inhibits the aggregation up to 90% compared to A β ₄₀ control at a concentration of 10 μ M (Figure 5-5 C). On the other hand, 18-7N(p₄)-18 started inhibiting at 10 μ M and peak inhibition is obtained at 25 μ M. However, compared to 18-7NH-18 the peptide modified surfactants started inhibiting at lower concentrations such as 5 μ M (18-7N(p₁₋₃)-18 unlike 25 μ M for 18-7NH-18 gemini surfactant. The higher efficiency could be due to the increased cationic charge on the surfactant due to peptide conjugation leading to higher interactions of surfactant with the A β ₄₀ peptide or the stronger binding of the surfactant molecule in the hydrophobic region of the A β ₄₀ peptide which prevents the oligomer formation. Hence, the Ig-SF peptide-modified gemini surfactants can act as potential A β ₄₀ peptide aggregation inhibitors.

In Summary the 18-7N(p₃)-18 gemini surfactants showed higher A β ₄₀ aggregation inhibition compared to any other peptide modified gemini surfactants and peptides, also their higher CDOCKER and binding interaction energies (kcal/mol) show a correlation with the experimental results proving that 18-7N(p₃)-18 gemini surfactants have superior *in silico* CDOCKER and binding interaction energies compared to 18-7NH-18, and peptide-modified gemini surfactants, making them one of the ideal candidates for the development of 18-7N(p₃)-1 NPX system for gene delivery to the retina to treat glaucoma.

The results demonstrate *in vitro- in silico* correlation between the inhibition of the A β ₄₀ peptide using molecular docking studies obtained for the 18-7NH-18, 18-7N(p₁₋₄)-18 and peptides (p₁₋₄) with *in vitro* experimental data. The CDOCKER energy and binding energies from the molecular docking studies clearly demonstrate that the peptide modified gemini surfactants showed higher interaction energies and binding energies compared to the peptides themselves. Also, 18-7N(p₃)-18 showed significantly higher CDOCKER energy (****p<0.0001) compared to 18-7NH-18 and 18-7N(p₄)-18 and showed a higher CDOCKER energy (**p<0.001) compared to 18-7N(p₁)-18 and 18-7N(p₂)-18. Similarly 18-7N(p₃)-18 showed significantly higher binding energy compared to 18-7NH-18, 18-7N(p₄)-18 (****p<0.0001) and 18-7N(p₂)-18 (**p<0.001). While 18-7N(p₃)-18 and 18-7N(p₁)-18 showed no significant difference (n.s) in the binding energies. This shows the potential of 18-7N(p₃)-18 and 18-7N(p₁)-18 as lead candidates. From the *in vitro* A β ₄₀ peptide aggregation inhibition studies carried out, it is also observed that these two gemini surfactants 18-7N(p₃)-18 and 18-7N(p₁)-18 have started inhibiting the A β ₄₀ peptide aggregation at 5 μ M and 90% inhibition at 10 μ M was achieved for both the compounds. It is also evident from the results that 18-7N(p₄)-18 surfactant is the least performing surfactant from the peptide modified gemini surfactants list. These results are in correlation with the docking results obtained and show that the molecular modelling performance of the Ig-SF peptide

modified gemini surfactants (18-7N(p₁₋₄)-18) were in the following decreasing order 18-7N(p₃)-18 > 18-7N(p₁)-18 > 18-7N(p₂)-18 > 18-7N(p₄)-18. The 18-7N(p₃)-18 surfactant showed a CDOCKER energy of -86.38 and a CDOCKER interaction energy of -72.09 Kcal/mol compared to -36.16 and -51.41 respectively for 18-7NH-18 and -69.67 kcal/mol and -40.87 kcal/mol for p₃ peptide only docking demonstrating the increased energy of interaction of the 18-7N(p₃)-18 with the Aβ₄₀ peptide. The CDOCKER energy and CDOCKER interaction energy of 18-7N(p₃)-18 with the amino acids in the hydrophobic region (KLVFFA) responsible for the Aβ₄₀ peptide aggregation was higher compared other peptide modified compounds, peptides only and 18-7NH-18 gemini surfactant. Non-bonding interactions such as hydrogen bonding and hydrophobic interactions (Table 5-4 B) between alkyl groups of ligand molecule with the alkyl groups of the amino acid were few dominant interactions that might have had strong interaction with the KLVFFA region shown by molecular docking studies, leading to Aβ₄₀ peptide aggregation inhibition at the lowest concentration based on the *in vitro* aggregation inhibition studies. From the molecular docking studies data analysis, it is evident that, despite the slight lower CDOCKER energies for 18-7N(p₁)-18 compared to 18-7N(p₃)-18 and binding energies of the both the molecules was found to be similar. The *in vitro* Aβ₄₀ peptide inhibition studies for both the compounds also showed similar results, i.e. inhibiting the aggregation started at 5 μM, but the overall performance of the 18-7N(p₃)-18 was ranked better by the CDOCKER algorithm compared to 18-7N(p₁)-18 based on the number of interactions and their bond lengths which could lead to more stronger binding interactions with the Aβ₄₀ peptide.

5.7 Conclusion

Overall, in this study peptide modified amphiphilic gemini surfactants (18-7N(p₁₋₄)-18), were evaluated as potential Aβ₄₀ peptide aggregation inhibitors. *In vitro* Aβ₄₀ peptide aggregation inhibition studies showed that 18-7N(p₃)-18 and 18-7N(p₁)-18 ligands have potential to inhibit Aβ₄₀ peptide aggregation

and formation of higher order oligomers from 5 μM . For the first time the efficiency of 18 series gemini surfactant as potential $\text{A}\beta_{40}$ aggregation inhibitors was evaluated and their positive inhibition effects were reported in this study.

Also, in this study molecular docking studies were carried out to establish the *in vitro-in silico* correlation of the m-7NH-m, m-7N(p)-m (m=alkyl tail, 18C and p= IgSF peptide)gemini surfactants as $\text{A}\beta_{40}$ peptide aggregation inhibitors. The molecular docking studies clearly demonstrate the potential of 18-7N(p₃)-18 and 18-7N(p₁)-18 gemini surfactants as $\text{A}\beta_{40}$ peptide aggregation inhibitors. The docking studies have also revealed that the peptides themselves do not possess any $\text{A}\beta_{40}$ peptide aggregation inhibition efficiency compared to peptide modified amphiphilic gemini surfactants correlating the results obtained in the *in vitro* $\text{A}\beta_{40}$ peptide aggregation inhibition kinetic studies. Compared to previously published reports (317, 325) on the efficiency of amphiphilic gemini surfactants to inhibit the $\text{A}\beta_{40}$ peptide aggregation the peptide modified 18-7N(p₁₋₄)-18 gemini surfactants have shown better $\text{A}\beta_{40}$ peptide aggregation inhibition potential at 10 μM compared to 100 μM as previously reported (315). The identification of the $\text{A}\beta_{40}$ peptide oligomer inhibition potential of 18-7N(p₁₋₄)-18 could help in dual targeting of the retinal layers to target delivery of NTF genes to treat glaucoma and also to inhibit the $\text{A}\beta_{40}$ peptide aggregation that is implicated in the glaucoma pathophysiology leading to neurodegeneration and RGC apoptosis. Also, the use of molecular docking studies to correlate the *in vitro* results could help in validating molecular simulation models for carrying out high throughput screening to identify lead candidates for inhibition of $\text{A}\beta_{40}$ peptide aggregation.

5.8 Acknowledgments

The authors of this chapter would like to express their sincere thanks to Dr. Praveen Nekkar Rao Perampalli and Amy Pham at School of Pharmacy, University of Waterloo for providing unmatched

support, guidance and help with A β ₄₀ peptide aggregation inhibition kinetic studies and training to carry out molecular docking simulations at the Medicinal and Bioorganic Chemistry Lab, University of Waterloo. Ms. Amy Pham helped with the training to run the A β ₄₀ peptide aggregation inhibition kinetic studies and carried out molecular docking studies between A β ₄₀ peptide, 18-7N(p₁₋₄)-18, 18-7NH-18 and IgSF peptides only.

Chapter 6 Summary and future directions

6.1 Summary

Research presented in this thesis is an embodiment to improve gene delivery to the retina by non-viral methods using a multifunctional CAP-modified dicationic gemini surfactant pNPX system. In Chapter 3 we have improved the purity, yield and identified a simple one-pot method to synthesize m-7NH-m (m=12, 16 and 18) gemini surfactant, which acts as a parent molecule for any further functional modifications performed to improve the gene delivery to the retina. Hence, having a pure species free from any by product impurities such as DMAP or trimeric gemini surfactants is vital and their presence can prove to be detrimental for the viability of the treated cells *in vitro* and *in vivo*. In addition to the above improvement, we were also able to develop a one-pot method to synthesize bis-quaternary trimeric gemini surfactants (m-7N(m)-m) (m=12, 16 and 18)

In Chapter 4 and 5, the synthesized parent molecule (m-7NH-m) from chapter 3 was used as a building block for conjugation of selected CAPs from integrin-binding and IgSF peptide group at the amino group in the spacer (m-7N(p₁₋₅)-m, (m=C_{12, 18}). NPXs, LPXs, pNPXs and pLPXs were formulated from the parent molecules and newly synthesized peptide-functionalized gemini surfactant and subjected for TE and viability evaluation in A7 astrocyte cell lines, 3D environment using MiEye8 retinal neurospheres and *in vivo* CD1 mouse model. 18-7N(p₃)-18 pNPXs administered by IVT injection delivered tdTomato/BDNF plasmid to retinal cells and have produced higher gene expression compared other pNPXs and controls tested. EpiCorneal penetrations and interactions studies showed higher interaction for all the peptide-modified pNPXs. In summary, 18-7N(p₃)-18 pNPXs showed 2-fold higher BDNF production than 18-7N(p₁)-18 pNPXs in the treated eyes.

In Chapter 5 an exploratory study to assess the A β ₄₀ aggregation inhibition potential of the integrin-binding and IgSF peptide modified gemini surfactants using fluorescence kinetic assay demonstrated a

good inhibition potential at very low concentrations for 18-7N(p₃)-18 and 18-7N(p₁)-18 gemini surfactants compared to p₂ and p₄ peptide modified gemini surfactants. The molecular modelling studies carried out on the same have shown good correlation with the results from *in vitro* studies and exhibited better binding based on CDOCKER energy and CDOCKER interaction energy parameters with 18-7N(p₃)-18 and 18-7N(p₁)-18 gemini surfactants.

Overall, novel multifunctional IgSF peptide and integrin-binding peptide conjugated gemini NPXs provide a promising non-viral *in vivo* gene delivery approach to retinal cells and have potential to inhibit the aggregation and higher order oligomer formation with A β ₄₀, which is a highly desirable property for gemini surfactants to possess owing to the amyloid- β implications and their formation in glaucoma patients and this effect of gemini surfactants can lead to dual targeting action of the gemini NPXs in both reaching the retinal layers to deliver the gene to retinal cells in eye to treat glaucoma as mentioned in the earlier chapters and the delivered gemini surfactant NPXs can also help in amyloid- β aggregation inhibition.

6.2 Future directions

Second generation gemini surfactants (m-7NH-m) developed are used to prepare functionalized NPXs with peptide modifications to increase cell binding and potentially targeting the retina and evaluate the delivery of the therapeutic DNA *in vivo* an animal model. Various other tail lengths can be synthesized using this modified protocol and their gene delivery potential can be evaluated.

The main goal of designing the IgSF and integrin-binding peptide-functionalized gemini surfactant pNPXs is to deliver NTF genes to the retina after IVT administration to retinal cells to protect and restore the degenerating RGCs in glaucoma. Hence, further studies to determine the functionality of NPXs to provide neuroprotection will need to be carried out in glaucoma animal models. Similar conjugation studies can also be carried out with the m-7NH-m (m=12, 16) gemini surfactants and

assessed for their gene delivery efficiency. Several other CAP peptide-modified gemini surfactants could be developed and assessed for their binding ability. The actual molecular targets on retinal cells for CAP-NPXs should be elucidated in future studies keeping in mind the differences between normal and diseased retina. In this regard, the 3D neurosphere model could be useful as an *in vitro* tool to screen candidate NPXs in stressed cellular conditions and specific targeting to different retinal cells. Another area for future studies could be to study the mechanisms NPX cellular uptake, intracellular trafficking and release from the endosomes using a panel of endocytosis inhibitors. A complete cytokine array studies on pNPX treated eyes will help in identifying inflammatory markers and toxicity levels *in vivo* to avoid any later stage failures due to toxicity. *In silico* molecular docking studies of the IgSF-peptide modified gemini surfactants and target molecules can help in identifying the binding affinity and *in silico-in vitro-in vivo* correlations can be drawn from the molecular docking studies and validated with *in vitro* and *in vivo* TE and BDNF production studies.

More extensive *in vitro* inhibition studies could be carried out to identify the inhibition potential of peptide modified amphiphilic gemini surfactants. Transmission electron microscopy (TEM) imaging studies could help in visual confirmation of the A β ₄₀ peptide aggregation inhibition. Assessment of A β ₄₀ and A β ₄₂ peptide inhibition studies can help in determining the potential of gemini surfactants in inhibiting the most toxic form of A β ₄₂ peptide. Also, assessment of the A β ₄₀ peptide inhibition and toxicity studies in cell lines and *in vivo* glaucoma models with A β ₄₀ peptide aggregation could be carried out to assess the potential inhibition effects of peptide modified gemini surfactants.

Letter of copyright permission

copyright permission for Figure 1-7 B

2/11/2020

RightsLink Printable License

ELSEVIER LICENSE TERMS AND CONDITIONS

Feb 11, 2020

This Agreement between Mr. Lokesh Narsinani ("You") and Elsevier ("Elsevier") consists of your license details and the terms and conditions provided by Elsevier and Copyright Clearance Center.

License Number	4766091507210
License date	Feb 11, 2020
Licensed Content Publisher	Elsevier
Licensed Content Publication	Journal of Controlled Release
Licensed Content Title	Endocytosis of nanomedicines
Licensed Content Author	Gaurav Sahay,Daria Y. Alakhova,Alexander V. Kabanov
Licensed Content Date	Aug 3, 2010
Licensed Content Volume	145
Licensed Content Issue	3
Licensed Content Pages	14
Start Page	182
End Page	195
Type of Use	reuse in a thesis/dissertation
Portion	figures/tables/illustrations
Number of figures/tables/illustrations	2
Format	both print and electronic

<https://s100.copyright.com/AppDispatchServlet>

References

1. Zafar A, Ahmad J, Addo RT, Akhter S. Progress of controlled drug delivery systems in topical ophthalmology: focus on nano and micro drug carriers. In: Addo RT, editor. *Ocular drug delivery: advances, challenges and applications*. Cham: Springer International Publishing; 2016. p. 131-163.
2. Sasaki H, Yamamura K, Nishida K, Nakamura J, Ichikawa M. Delivery of drugs to the eye by topical application. *Progress in retinal and eye research*. 1996;15(2):583-620.
3. Mishima S, Gasset A, Klyce S, Baum J. Determination of tear volume and tear flow. *Invest Ophthalmol Vis Sci*. 1966;5(3):264-276.
4. Abelson MB, Udell IJ, Weston JH. Normal human tear pH by direct measurement. *AMA Arch Ophthalmol*. 1981;99(2):301.
5. Hughes PM, Olejnik O, Chang-Lin J-E, Wilson CG. Topical and systemic drug delivery to the posterior segments. *Advanced drug delivery reviews*. 2005;57(14):2010-2032.
6. Mishima S, Maurice DM. The oily layer of the tear film and evaporation from the corneal surface. *Exp Eye Res*. 1961;1(1):39-45.
7. Zhou L, Beuerman RW. Tear analysis in ocular surface diseases. *Progress in retinal and eye research*. 2012;31(6):527-550.
8. Gipson IK, Inatomi T. Cellular origin of mucins of the ocular surface tear film. In: *Lacrimal gland, tear film, and dry eye syndromes 2*: Springer; 1998. p. 221-227.
9. Doughty MJ, Zaman ML. Human Corneal Thickness and Its Impact on Intraocular Pressure Measures: A Review and Meta-analysis Approach. *Survey of ophthalmology*. 2000;44(5):367-408.
10. DelMonte DW, Kim T. Anatomy and physiology of the cornea. *Journal of Cataract & Refractive Surgery*. 2011;37(3):588-598.
11. Bishop P. The biochemical structure of mammalian vitreous. *Eye*. 1996;10(6):664-670.
12. Le Goff MM, Bishop PN. Adult vitreous structure and postnatal changes. *Eye*. 2008;22(10):1214-1222.
13. Zhang X, Li Q, Xiang M, Zou H, Liu B, Zhou H, Han Z, Fu Z, Zhang Z, Wang H. Bulbar conjunctival thickness measurements with optical coherence tomography in healthy chinese subjects *Investigative ophthalmology & visual science*. 2013;54(7):4705-4709.
14. Zhang W, Prausnitz MR, Edwards A. Model of transient drug diffusion across cornea. *Journal of Controlled Release*. 2004;99(2):241-258.
15. Lee TW-Y, Robinson JR. Drug delivery to the posterior segment of the eye III: the effect of parallel elimination pathway on the vitreous drug level after subconjunctival injection. *J Ocul Pharmacol Ther*. 2004;20(1):55-64.
16. Kim SH, Lutz RJ, Wang NS, Robinson MR. Transport barriers in transscleral drug delivery for retinal diseases. *Ophthalmic research*. 2007;39(5):244-254.
17. Kompella UB, Sundaram S, Raghava S, Escobar ER. Luteinizing hormone-releasing hormone agonist and transferrin functionalizations enhance nanoparticle delivery in a novel bovine ex vivo eye model. *Molecular vision*. 2006;12(134-135):1185-1198.
18. Zhang Y, Wildsoet CF. Chapter thirteen - RPE and choroid mechanisms underlying ocular growth and myopia. In: Hejtmancik JF, Nickerson JM, editors. *Progress in molecular biology and translational science*: Academic Press; 2015. p. 221-240.

19. Konno S, Akiba J, Yoshida A. Retinal thickness measurements with optical coherence tomography and the scanning retinal thickness analyzer. *Retina (Philadelphia, Pa)*. 2001;21(1):57-61.
20. Barar J, Javadzadeh AR, Omid Y. Ocular novel drug delivery: impacts of membranes and barriers. *Expert opinion on drug delivery*. 2008;5(5):567-581.
21. Hornof M, Toropainen E, Urtti A. Cell culture models of the ocular barriers. *European journal of pharmaceutics and biopharmaceutics : official journal of Arbeitsgemeinschaft fur Pharmazeutische Verfahrenstechnik eV*. 2005;60(2):207-225.
22. Edelhauser HF, Rowe-Rendleman CL, Robinson MR, Dawson DG, Chader GJ, Grossniklaus HE, Rittenhouse KD, Wilson CG, Weber DA, Kuppermann BD, Csaky KG, Olsen TW, Kompella UB, Holers VM, Hageman GS, Gilger BC, Campochiaro PA, Whitcup SM, Wong WT. Ophthalmic drug delivery systems for the treatment of retinal diseases: basic research to clinical applications. *Investigative ophthalmology & visual science*. 2010;51(11):5403-5420.
23. Chen M-S, Hou P-K, Tai T-Y, Lin BJ. Blood-Ocular Barriers. *Tzu Chi Medical Journal*. 2008;20(1):25-34.
24. Duvvuri S, Majumdar S, Mitra AK. Drug delivery to the retina: challenges and opportunities. *Expert opinion on biological therapy*. 2003;3(1):45-56.
25. Maurice D. Review: practical issues in intravitreal drug delivery. *J Ocul Pharmacol Ther*. 2001;17(4):393-401.
26. Pitkanen L, Ranta VP, Moilanen H, Urtti A. Permeability of retinal pigment epithelium: effects of permeant molecular weight and lipophilicity. *Investigative ophthalmology & visual science*. 2005;46(2):641-646.
27. Ambati J, Gragoudas ES, Miller JW, You TT, Miyamoto K, Delori FC, Adamis AP. Transscleral delivery of bioactive protein to the choroid and retina. *Investigative ophthalmology & visual science*. 2000;41(5):1186-1191.
28. Singh S, Grossniklaus H, Kang S, Edelhauser H, Ambati B, Kompella U. Intravenous transferrin, RGD peptide and dual-targeted nanoparticles enhance anti-VEGF intrareceptor gene delivery to laser-induced CNV. *Gene therapy*. 2009;16(5):645-659.
29. Russell S, Bennett J, Wellman JA, Chung DC, Yu Z-F, Tillman A, Wittes J, Pappas J, Elci O, McCague S. Efficacy and safety of voretigene neparvovec (AAV2-hRPE65v2) in patients with RPE65-mediated inherited retinal dystrophy: a randomised, controlled, open-label, phase 3 trial. *The Lancet*. 2017;390(10097):849-860.
30. Alqawlaq S, Sivak JM, Huzil JT, Ivanova MV, Flanagan JG, Beazely MA, Foldvari M. Preclinical development and ocular biodistribution of gemini-DNA nanoparticles after intravitreal and topical administration: Towards non-invasive glaucoma gene therapy. *Nanomed Nanotechnol Biol Med*. 2014;10(8):1637-1647.
31. Li HF, Petroll WM, Møller-Pedersen T, Maurer JK, Cavanagh HD, Jester JV. Epithelial and corneal thickness measurements by in vivo confocal microscopy through focusing (CMTF). *Curr Eye Res*. 1997;16(3):214-221.
32. Schaeffer HE, Krohn DL. Liposomes in topical drug delivery. *Invest Ophthalmol Vis Sci*. 1982;22(2):220-227.
33. Law SL, Huang KJ, Chiang CH. Acyclovir-containing liposomes for potential ocular delivery. Corneal penetration and absorption. *Journal of controlled release : official journal of the Controlled Release Society*. 2000;63(1-2):135-140.
34. Klang S, Siganos C, Benita S, Frucht-Pery J. Evaluation of a positively charged submicron emulsion of piroxicam on the rabbit corneum healing process following alkali burn. *J Control Release*. 1999;57(1):19-27.

35. Pitkanen L, Ruponen M, Nieminen J, Urtti A. Vitreous Is a Barrier in Nonviral Gene Transfer by Cationic Lipids and Polymers. *Pharmaceutical research*. 2003;20(4):576-583.
36. Sasaki H, Karasawa K, Hironaka K, Tahara K, Tozuka Y, Takeuchi H. Retinal drug delivery using eyedrop preparations of poly-L-lysine-modified liposomes. *European journal of pharmaceutics and biopharmaceutics : official journal of Arbeitsgemeinschaft fur Pharmazeutische Verfahrenstechnik eV*. 2013;83(3):364-369.
37. Prausnitz MR, Noonan JS. Permeability of cornea, sclera, and conjunctiva: a literature analysis for drug delivery to the eye. *Journal of pharmaceutical sciences*. 1998;87(12):1479-1488.
38. Maurice DM. The dynamics and drainage of tears. *International ophthalmology clinics*. 1973;13(1):103-118.
39. Xu J, Heys JJ, Barocas VH, Randolph TW. Permeability and diffusion in vitreous humor: implications for drug delivery. *Pharmaceutical research*. 2000;17(6):664-669.
40. Foldvari M, Chen DW, Nafissi N, Calderon D, Narsineni L, Rafiee A. Non-viral gene therapy: Gains and challenges of non-invasive administration methods. *Journal of Controlled Release*. 2016;240:165-190.
41. Quigley HA, Broman AT. The number of people with glaucoma worldwide in 2010 and 2020. *British Journal of Ophthalmology*. 2006;90(3):262-267.
42. Jonas JB, Aung T, Bourne RR, Bron AM, Ritch R, Panda-Jonas S. Glaucoma. *The Lancet*. 2017;390(10108):2183-2193.
43. Quigley HA. Glaucoma. *The Lancet*. 2011;377(9774):1367-1377.
44. Margalit E, Sada SR. Retinal and optic nerve diseases. *Artificial organs*. 2003;27(11):963-974.
45. Pease ME, McKinnon SJ, Quigley HA, Kerrigan-Baumrind LA, Zack DJ. Obstructed axonal transport of BDNF and its receptor TrkB in experimental glaucoma. *Invest Ophthalmol Vis Sci*. 2000;41(3):764-774.
46. Weber A, Harman C, Viswanathan S. Effects of optic nerve injury, glaucoma, and neuroprotection on the survival, structure, and function of ganglion cells in the mammalian retina. *The Journal of physiology*. 2008;586(18):4393-4400.
47. Wax MB, Tezel G. Neurobiology of glaucomatous optic neuropathy. *Molecular neurobiology*. 2002;26(1):45-55.
48. Howell GR, Libby RT, Jakobs TC, Smith RS, Phalan FC, Barter JW, Barbay JM, Marchant JK, Mahesh N, Porciatti V. Axons of retinal ganglion cells are insulted in the optic nerve early in DBA/2J glaucoma. *The Journal of cell biology*. 2007;179(7):1523-1537.
49. Neufeld AH, Hernandez MR, Gonzalez M. Nitric oxide synthase in the human glaucomatous optic nerve head. *Archives of ophthalmology*. 1997;115(4):497-503.
50. Farkas RH, Grosskreutz CL. Apoptosis, neuroprotection, and retinal ganglion cell death: an overview. *International ophthalmology clinics*. 2001;41(1):111-130.
51. Crish SD, Dapper JD, MacNamee SE, Balaram P, Sidorova TN, Lambert WS, Calkins DJ. Failure of axonal transport induces a spatially coincident increase in astrocyte BDNF prior to synapse loss in a central target. *Neuroscience*. 2013;229:55-70.
52. Alqawlaq S, Flanagan JG, Sivak JM. All roads lead to glaucoma: Induced retinal injury cascades contribute to a common neurodegenerative outcome. *Experimental eye research*. 2018.
53. Almasieh M, Wilson AM, Morquette B, Cueva Vargas JL, Di Polo A. The molecular basis of retinal ganglion cell death in glaucoma. *Progress in retinal and eye research*. 2012;31(2):152-181.

54. Tamm ER, Dowling JE. Astrocytes and glaucomatous neurodegeneration. *Experimental eye research*. 2017;157:1-4.
55. Neufeld AH. Microglia in the optic nerve head and the region of parapapillary chorioretinal atrophy in glaucoma. *Archives of ophthalmology*. 1999;117(8):1050-1056.
56. Murphy J, Clarke D. Target-derived neurotrophins may influence the survival of adult retinal ganglion cells when local neurotrophic support is disrupted: Implications for glaucoma. *Medical hypotheses*. 2006;67(5):1208-1212.
57. Chrysostomou V, Rezaie F, Troncone IA, Crowston JG. Oxidative stress and mitochondrial dysfunction in glaucoma. *Current Opinion in Pharmacology*. 2013;13(1):12-15.
58. Morquette JB, Di Polo A. Dendritic and synaptic protection: is it enough to save the retinal ganglion cell body and axon? *Journal of Neuro-Ophthalmology*. 2008;28(2):144-154.
59. Hernandez MR, Miao H, Lukas T. Astrocytes in glaucomatous optic neuropathy. *Progress in brain research*. 2008;173:353-373.
60. Hernandez MR. The optic nerve head in glaucoma: role of astrocytes in tissue remodeling. *Progress in retinal and eye research*. 2000;19(3):297-321.
61. Della Santina L, Ou Y. Who's lost first? Susceptibility of retinal ganglion cell types in experimental glaucoma. *Experimental eye research*. 2017;158:43-50.
62. Müller A, Hauk TG, Fischer D. Astrocyte-derived CNTF switches mature RGCs to a regenerative state following inflammatory stimulation. *Brain*. 2007;130(12):3308-3320.
63. Ma Y-T, Hsieh T, Forbes ME, Johnson JE, Frost DO. BDNF injected into the superior colliculus reduces developmental retinal ganglion cell death. *The Journal of neuroscience*. 1998;18(6):2097-2107.
64. Johnson EC, Guo Y, Cepurna WO, Morrison JC. Neurotrophin roles in retinal ganglion cell survival: Lessons from rat glaucoma models. *Experimental eye research*. 2009;88(4):808-815.
65. Cui Q. Actions of neurotrophic factors and their signaling pathways in neuronal survival and axonal regeneration. *Molecular neurobiology*. 2006;33(2):155-179.
66. Siliprandi R, Canella R, Carmignoto G. Nerve growth factor promotes functional recovery of retinal ganglion cells after ischemia. *Investigative ophthalmology & visual science*. 1993;34(12):3232-3245.
67. Colafrancesco V, Parisi V, Sposato V, Rossi S, Russo MA, Coassin M, Lambiase A, Aloe L. Ocular application of nerve growth factor protects degenerating retinal ganglion cells in a rat model of glaucoma. *Journal of glaucoma*. 2011;20(2):100-108.
68. Yan Q, Wang J, Matheson CR, Ulrich JL. Glial cell line-derived neurotrophic factor (GDNF) promotes the survival of axotomized retinal ganglion cells in adult rats: Comparison to and combination with brain-derived neurotrophic factor (BDNF). *Journal of neurobiology*. 1999;38(3):382-390.
69. Mansour-Robaey S, Clarke D, Wang Y, Bray G, Aguayo A. Effects of ocular injury and administration of brain-derived neurotrophic factor on survival and regrowth of axotomized retinal ganglion cells. *Proceedings of the National Academy of Sciences*. 1994;91(5):1632-1636.
70. Simon J, Arthur C, Fong AL, Dwyer JM, Davare M, Reese E, Obrietan K, Impey S. Mitogen- and stress-activated protein kinase 1 mediates cAMP response element-binding protein phosphorylation and activation by neurotrophins. *Journal of Neuroscience*. 2004;24(18):4324-4332.
71. Brunet A, Datta SR, Greenberg ME. Transcription-dependent and-independent control of neuronal survival by the PI3K-Akt signaling pathway. *Current opinion in neurobiology*. 2001;11(3):297-305.

72. Kimura A, Namekata K, Guo X, Harada C, Harada T. Neuroprotection, growth factors and BDNF-TrkB signalling in retinal degeneration. *International Journal of Molecular Sciences*. 2016;17(9):1584.
73. Ghaffariyeh A, Honarpisheh N, Shakiba Y, Puyan S, Chamacham T, Zahedi F, Zarrineghbal M. Brain-derived neurotrophic factor in patients with normal-tension glaucoma. *Optometry-Journal of the American Optometric Association*. 2009;80(11):635-638.
74. Harada C, Guo X, Namekata K, Kimura A, Nakamura K, Tanaka K, Parada LF, Harada T. Glia- and neuron-specific functions of TrkB signalling during retinal degeneration and regeneration. *Nat Commun*. 2011;2:189.
75. Paskowitz DM, Nune G, Yasumura D, Yang H, Bhisitkul RB, Sharma S, Matthes MT, Zarbin MA, LaVail MM, Duncan JL. BDNF Reduces the Retinal Toxicity of Verteporfin Photodynamic Therapy. *Investigative ophthalmology & visual science*. 2004;45(11):4190-4196.
76. Paskowitz DM, Donohue-Rolfe KM, Yang H, Yasumura D, Matthes MT, Hosseini K, Graybeal CM, Nune G, Zarbin MA, LaVail MM, Duncan JL. Neurotrophic Factors Minimize the Retinal Toxicity of Verteporfin Photodynamic Therapy. *Investigative ophthalmology & visual science*. 2007;48(1):430-437.
77. Spalding KL, Rush RA, Harvey AR. Target-derived and locally derived neurotrophins support retinal ganglion cell survival in the neonatal rat retina. *Journal of Neurobiology*. 2004;60(3):319-327.
78. Johnson JE, Barde Y-A, Schwab M, Thoenen H. Brain-derived neurotrophic factor supports the survival of cultured rat retinal ganglion cells. *Journal of Neuroscience*. 1986;6(10):3031-3038.
79. Foldvari M, Chen DW. The intricacies of neurotrophic factor therapy for retinal ganglion cell rescue in glaucoma: a case for gene therapy. *Neural regeneration research*. 2016;11(6):875-877.
80. Devoldere J, Peynshaert K, De Smedt SC, Remaut K. Müller cells as a target for retinal therapy. *Drug discovery today*. 2019.
81. Wang M, Wong WT. Microglia-Müller Cell Interactions in the Retina. In. New York, NY: Springer New York; 2014. p. 333-338.
82. Chen DW, Foldvari M. In vitro bioassay model for screening non-viral neurotrophic factor gene delivery systems for glaucoma treatment. *Drug Delivery and Translational Research*. 2016;6(6):676-685.
83. Boyd R, Sledge D, Boye S, Boye S, Hauswirth W, Komáromy A, Petersen-Jones S, Bartoe J. Photoreceptor-targeted gene delivery using intravitreally administered AAV vectors in dogs. *Gene therapy*. 2016;23(2):223.
84. Chu Y, Chen N, Yu H, Mu H, He B, Hua H, Wang A, Sun K. Topical ocular delivery to laser-induced choroidal neovascularization by dual internalizing RGD and TAT peptide-modified nanoparticles. *International journal of nanomedicine*. 2017;12:1353-1368.
85. Puras G, Mashal M, Zárata J, Agirre M, Ojeda E, Grijalvo S, Eritja R, Diaz-Tahoces A, Martínez Navarrete G, Avilés-Trigueros M, Fernández E, Pedraz JL. A novel cationic niosome formulation for gene delivery to the retina. *Journal of Controlled Release*. 2014;174:27-36.
86. Di Polo A, Aigner LJ, Dunn RJ, Bray GM, Aguayo AJ. Prolonged delivery of brain-derived neurotrophic factor by adenovirus-infected Müller cells temporarily rescues injured retinal ganglion cells. *Proceedings of the National Academy of Sciences*. 1998;95(7):3978-3983.
87. Sanes JR, Masland RH. The Types of Retinal Ganglion Cells: Current Status and Implications for Neuronal Classification. *Annual Review of Neuroscience*. 2015;38(1):221-246.

88. Tran NM, Shekhar K, Whitney IE, Jacobi A, Benhar I, Hong G, Yan W, Adiconis X, Arnold ME, Lee JM, Levin JZ, Lin D, Wang C, Lieber CM, Regev A, He Z, Sanes JR. Single-Cell Profiles of Retinal Ganglion Cells Differing in Resilience to Injury Reveal Neuroprotective Genes. *Neuron*. 2019;104(6):1039-1055.e1012.
89. Reiss G, Lee D, Topper J, Brubaker R. Aqueous humor flow during sleep. *Invest Ophthalmol Vis Sci*. 1984;25(6):776-778.
90. Toris CB, Gleason ML, Camras CB, Yablonski ME. Effects of brimonidine on aqueous humor dynamics in human eyes. *Archives of ophthalmology*. 1995;113(12):1514-1517.
91. Liu JH, Kripke DF, Weinreb RN. Comparison of the nocturnal effects of once-daily timolol and latanoprost on intraocular pressure. *American journal of ophthalmology*. 2004;138(3):389-395.
92. Fujita Y, Sato A, Yamashita T. Brimonidine promotes axon growth after optic nerve injury through Erk phosphorylation. *Cell Death Dis*. 2013;4:e763.
93. Semba K, Namekata K, Kimura A, Harada C, Mitamura Y, Harada T. Brimonidine prevents neurodegeneration in a mouse model of normal tension glaucoma. *Cell Death Dis*. 2014;5:e1341.
94. Mandell KJ, Kudelka MR, Wirostko B. Rho kinase inhibitors for treatment of glaucoma. *Expert Rev Ophthalmol*. 2011;6(6):611-622.
95. Kopczynski CC, Epstein DL. Emerging trabecular outflow drugs. *J Ocul Pharmacol Ther*. 2014;30(2-3):85-87.
96. Tokushige H, Waki M, Takayama Y, Tanihara H. Effects of Y-39983, a Selective Rho-Associated Protein Kinase Inhibitor, on Blood Flow in Optic Nerve Head in Rabbits and Axonal Regeneration of Retinal Ganglion Cells in Rats. *Current Eye Research*. 2011;36(10):964-970.
97. Hirata A, Inatani M, Inomata Y, Yonemura N, Kawaji T, Honjo M, Tanihara H. Y-27632, a Rho-associated protein kinase inhibitor, attenuates neuronal cell death after transient retinal ischemia. *Graefes Archive for Clinical and Experimental Ophthalmology*. 2008;246(1):51-59.
98. Lingor P, Teusch N, Schwarz K, Mueller R, Mack H, Bähr M, Mueller BK. Inhibition of Rho kinase (ROCK) increases neurite outgrowth on chondroitin sulphate proteoglycan in vitro and axonal regeneration in the adult optic nerve in vivo. *Journal of neurochemistry*. 2007;103(1):181-189.
99. Ahmed Z, Berry M, Logan A. ROCK inhibition promotes adult retinal ganglion cell neurite outgrowth only in the presence of growth promoting factors. *Molecular and Cellular Neuroscience*. 2009;42(2):128-133.
100. Koch JC, Tonges L, Barski E, Michel U, Bahr M, Lingor P. ROCK2 is a major regulator of axonal degeneration, neuronal death and axonal regeneration in the CNS. *Cell Death Dis*. 2014;5:e1225.
101. Delpace V, Ortin-Martinez A, Tsai ELS, Amin AN, Wallace V, Shoichet MS. Controlled release strategy designed for intravitreal protein delivery to the retina. *Journal of Controlled Release*. 2019;293:10-20.
102. Ginn SL, Alexander IE, Edelstein ML, Abedi MR, Wixon J. Gene therapy clinical trials worldwide to 2012 – an update. *The journal of gene medicine*. 2013;15(2):65-77.
103. Gordon K, Del AM, Sander I, Kumar A, Hamad B. Gene therapies in ophthalmic disease. In.; 2019.
104. Jay J, Murray S. Early trabeculectomy versus conventional management in primary open angle glaucoma. *British Journal of Ophthalmology*. 1988;72(12):881-889.

105. Saheb H, Ahmed IIK. Micro-invasive glaucoma surgery: current perspectives and future directions. *Current Opinion in Ophthalmology*. 2012;23(2):96-104.
106. Ahmed IIK, Katz LJ, Chang DF, Donnenfeld ED, Solomon KD, Voskanyan L, Samuelson TW. Prospective evaluation of microinvasive glaucoma surgery with trabecular microbypass stents and prostaglandin in open-angle glaucoma. *Journal of Cataract & Refractive Surgery*. 2014;40(8):1295-1300.
107. Sagawa H, Terasaki H, Nakamura M, Ichikawa M, Yata T, Tokita Y, Watanabe M. A novel ROCK inhibitor, Y-39983, promotes regeneration of crushed axons of retinal ganglion cells into the optic nerve of adult cats. *Experimental neurology*. 2007;205(1):230-240.
108. Liao JK, Seto M, Noma K. Rho kinase (ROCK) inhibitors. *Journal of cardiovascular pharmacology*. 2007;50(1):17.
109. Rao VP, Epstein DL. Rho GTPase/Rho kinase inhibition as a novel target for the treatment of glaucoma. *BioDrugs*. 2007;21(3):167-177.
110. Wang SK, Chang RT. An emerging treatment option for glaucoma: Rho kinase inhibitors. *Clinical ophthalmology (Auckland, NZ)*. 2014;8:883.
111. Rao PV, Deng P-F, Kumar J, Epstein DL. Modulation of aqueous humor outflow facility by the Rho kinase-specific inhibitor Y-27632. *Investigative ophthalmology & visual science*. 2001;42(5):1029-1037.
112. Moshirfar M, Parker L, Birdsong OC, Ronquillo YC, Hofstedt D, Shah TJ, Gomez AT, Hoopes PC, Sr. Use of Rho kinase Inhibitors in Ophthalmology: A Review of the Literature. *Med Hypothesis Discov Innov Ophthalmol*. 2018;7(3):101-111.
113. Matsuo T, Cynader M. Localization of alpha-2 adrenergic receptors in the human eye. *Ophthalmic research*. 1992;24(4):213-219.
114. Johnson TV, Bull ND, Martin KR. Neurotrophic factor delivery as a protective treatment for glaucoma. *Experimental eye research*. 2011;93(2):196-203.
115. Martinou J-C, Dubois-Dauphin M, Staple JK, Rodriguez I, Frankowski H, Missotten M, Albertini P, Talabot D, Catsicas S, Pietra C. Overexpression of BCL-2 in transgenic mice protects neurons from naturally occurring cell death and experimental ischemia. *Neuron*. 1994;13(4):1017-1030.
116. Cenni M, Bonfanti L, Martinou J, Ratto G, Strettoi E, Maffei L. Long-term survival of retinal ganglion cells following optic nerve section in adult bcl-2 transgenic mice. *The European journal of neuroscience*. 1996;8(8):1735-1745.
117. Dietz GP, Kilic E, Bähr M. Inhibition of neuronal apoptosis in vitro and in vivo using TAT-mediated protein transduction. *Molecular and Cellular Neuroscience*. 2002;21(1):29-37.
118. Jiao J, Huang X, Feit-Leithman RA, Neve RL, Snider W, Dartt DA, Chen DF. Bcl-2 enhances Ca²⁺ signaling to support the intrinsic regenerative capacity of CNS axons. *The EMBO journal*. 2005;24(5):1068-1078.
119. Stone D. Novel viral vector systems for gene therapy. *Viruses*. 2010;2(4):1002-1007.
120. Mulligan RC. The basic science of gene therapy. *Science (New York, NY)*. 1993;260(5110):926-932.
121. Naldini L. Gene therapy returns to centre stage. *Nature*. 2015;526:351.
122. Russell S, Bennett J, Wellman JA, Chung DC, Yu Z-F, Tillman A, Wittes J, Pappas J, Elci O, McCague S, Cross D, Marshall KA, Walshire J, Kehoe TL, Reichert H, Davis M, Raffini L, George LA, Hudson FP, Dingfield L, Zhu X, Haller JA, Sohn EH, Mahajan VB, Pfeifer W, Weckmann M, Johnson C, Gewaily D, Drack A, Stone E, Wachtel K, Simonelli F, Leroy BP, Wright JF, High KA, Maguire AM. Efficacy and safety of voretigene neparvovec (AAV2-

- hRPE65v2) in patients with RPE65-mediated inherited retinal dystrophy: a randomised, controlled, open-label, phase 3 trial. *The Lancet*. 2017;390(10097):849-860.
123. Ginn SL, Amaya AK, Alexander IE, Edelstein M, Abedi MR. Gene therapy clinical trials worldwide to 2017: An update. *The journal of gene medicine*. 2018;20(5):e3015.
 124. Trapani I, Auricchio A. Has retinal gene therapy come of age? From bench to bedside and back to bench. *Human Molecular Genetics*. 2019;28(R1):R108-R118.
 125. Darrow JJ. Luxturna: FDA documents reveal the value of a costly gene therapy. *Drug discovery today*. 2019.
 126. Smalley E. First AAV gene therapy poised for landmark approval. *Nature Biotechnology*. 2017;35:998.
 127. Akinc A, Maier MA, Manoharan M, Fitzgerald K, Jayaraman M, Barros S, Ansell S, Du X, Hope MJ, Madden TD, Mui BL, Semple SC, Tam YK, Ciufolini M, Witzigmann D, Kulkarni JA, van der Meel R, Cullis PR. The Onpattro story and the clinical translation of nanomedicines containing nucleic acid-based drugs. *Nature Nanotechnology*. 2019;14(12):1084-1087.
 128. de Paula Brandão PR, Titze-de-Almeida SS, Titze-de-Almeida R. Leading RNA Interference Therapeutics Part 2: Silencing Delta-Aminolevulinic Acid Synthase 1, with a Focus on Givosiran. *Molecular Diagnosis & Therapy*. 2019.
 129. Gardlík R, Pálffy R, Hodosy J, Lukács J, Turna J, Celec P. Vectors and delivery systems in gene therapy. *Medical Science Monitor Basic Research*. 2005;11(4):RA110-RA121.
 130. Templeton NS, Lasic DD. New directions in liposome gene delivery. *Molecular biotechnology*. 1999;11(2):175-180.
 131. Gupta PN, Singh P, Mishra V, Jain S, Dubey PK, Vyas SP. Topical immunization: mechanistic insight and novel delivery systems. *Indian Journal of Biotechnology*. 2004;3:9-21.
 132. Yang N. An overview of viral and nonviral delivery systems for microRNA. *International journal of pharmaceutical investigation*. 2015;5(4):179.
 133. Katare DP, Aeri V. Progress in gene therapy: A Review. *IJTPR*. 2010;1:33-41.
 134. Otsuji T, Ogata N, Takahashi K, Matsushima M, Uyama M, Kaneda Y. In vivo gene transfer into choroidal neovascularization by the HVJ liposome method. *Graefe's archive for clinical and experimental ophthalmology*. 2000;238(2):191-199.
 135. Kirby AJ, Camilleri P, Engberts JB, Feiters MC, Nolte RJ, Söderman O, Bergsma M, Bell PC, Fielden ML, García Rodríguez CL. Gemini surfactants: new synthetic vectors for gene transfection. *Angewandte Chemie International Edition*. 2003;42(13):1448-1457.
 136. Badea I, Verrall R, Baca-Estrada M, Tikoo S, Rosenberg A, Kumar P, Foldvari M. In vivo cutaneous interferon-gamma gene delivery using novel dicationic (gemini) surfactant-plasmid complexes. *The journal of gene medicine*. 2005;7(9):1200-1214.
 137. Chaum E, Hatton MP, Stein G. Polyplex mediated gene transfer into human retinal pigment epithelial cells in vitro. *Journal of cellular biochemistry*. 2000;76(1):153-160.
 138. Farjo R, Skaggs J, Quiambao AB, Cooper MJ, Naash MI. Efficient non-viral ocular gene transfer with compacted DNA nanoparticles. *PloS one*. 2006;1:e38.
 139. Puras G, Mashal M, Zarate J, Agirre M, Ojeda E, Grijalvo S, Eritja R, Diaz-Tahoces A, Martínez Navarrete G, Aviles-Trigueros M, Fernandez E, Pedraz JL. A novel cationic niosome formulation for gene delivery to the retina. *J Control Release*. 2014;174:27-36.
 140. Mashal M, Attia N, Puras G, Martínez-Navarrete G, Fernández E, Pedraz JL. Retinal gene delivery enhancement by lycopene incorporation into cationic niosomes based on DOTMA and polysorbate 60. *Journal of Controlled Release*. 2017;254:55-64.

141. Lajunen T, Hisazumi K, Kanazawa T, Okada H, Seta Y, Yliperttula M, Urtti A, Takashima Y. Topical drug delivery to retinal pigment epithelium with microfluidizer produced small liposomes. *European Journal of Pharmaceutical Sciences*. 2014;62:23-32.
142. Mitra RN, Han Z, Merwin M, Al Taai M, Conley SM, Naash MI. Synthesis and characterization of glycol chitosan DNA nanoparticles for retinal gene delivery. *ChemMedChem*. 2014;9(1):189-196.
143. Liao HW, Yau KW. In vivo gene delivery in the retina using polyethylenimine. *BioTechniques*. 2007;42(3):285-286, 288.
144. Mastorakos P, Kambhampati SP, Mishra MK, Wu T, Song E, Hanes J, Kannan RM. Hydroxyl PAMAM dendrimer-based gene vectors for transgene delivery to human retinal pigment epithelial cells. *Nanoscale*. 2015.
145. Oliveira AV, Rosa da Costa AM, Silva GA. Non-viral strategies for ocular gene delivery. *Materials Science and Engineering: C*. 2017;77:1275-1289.
146. Liu C, Jiang K, Tai L, Liu Y, Wei G, Lu W, Pan W. Facile Noninvasive Retinal Gene Delivery Enabled by Penetratin. *ACS Applied Materials & Interfaces*. 2016;8(30):19256-19267.
147. Buck J, Grossen P, Cullis PR, Huwyler J, Witzigmann D. Lipid-Based DNA Therapeutics: Hallmarks of Non-Viral Gene Delivery. *ACS Nano*. 2019;13(4):3754-3782.
148. Felgner PL, Gadek TR, Holm M, Roman R, Chan HW, Wenz M, Northrop JP, Ringold GM, Danielsen M. Lipofection: a highly efficient, lipid-mediated DNA-transfection procedure. *Proceedings of the National Academy of Sciences*. 1987;84(21):7413-7417.
149. Friend DS, Papahadjopoulos D, Debs RJ. Endocytosis and intracellular processing accompanying transfection mediated by cationic liposomes. *Biochimica et Biophysica Acta (BBA) - Biomembranes*. 1996;1278(1):41-50.
150. Alqawlaq S, Huzil JT, Ivanova MV, Foldvari M. Challenges in neuroprotective nanomedicine development: progress towards noninvasive gene therapy of glaucoma. *Nanomedicine*. 2012;7(7):1067-1083.
151. Balazs DA, Godbey W. Liposomes for use in gene delivery. *Journal of Drug Delivery*. 2011;2011:12.
152. Kawakami S, Harada A, Sakanaka K, Nishida K, Nakamura J, Sakaeda T, Ichikawa N, Nakashima M, Sasaki H. In vivo gene transfection via intravitreal injection of cationic liposome/plasmid DNA complexes in rabbits. *International Journal of Pharmaceutics*. 2004;278(2):255-262.
153. Makhlof A, Hajdu I, Badea I. Chapter 13 - Gemini surfactant-based systems for drug and gene delivery. In: Grumezescu AM, editor. *Organic Materials as Smart Nanocarriers for Drug Delivery*; William Andrew Publishing; 2018. p. 561-600.
154. Falsini S, Ristori S. Lipoplexes from non-viral cationic vectors: DOTAP-DOPE liposomes and gemini micelles. In: *Non-Viral Gene Delivery Vectors*; Springer; 2016. p. 33-43.
155. Foldvari M, Badea I, Wettig S, Verrall R, Bagonluri M. Structural characterization of novel gemini non-viral DNA delivery systems for cutaneous gene therapy. *J Exp Nanosci*. 2006;1.
156. Menger FM, Littau CA. Gemini surfactants: a new class of self-assembling molecules. *Journal of the American Chemical Society*. 1993;115(22):10083-10090.
157. Wettig SD, Wang C, Verrall RE, Foldvari M. Thermodynamic and aggregation properties of aza- and imino-substituted gemini surfactants designed for gene delivery. *Physical Chemistry Chemical Physics*. 2007;9(7):871-877.
158. Zana R. Dimeric (Gemini) Surfactants: Effect of the Spacer Group on the Association Behavior in Aqueous Solution. *Journal of colloid and interface science*. 2002;248(2):203-220.

159. Donkuru M, Wettig SD, Verrall RE, Badea I, Foldvari M. Designing pH-sensitive gemini nanoparticles for non-viral gene delivery into keratinocytes. *Journal of Materials Chemistry*. 2012;22(13):6232-6244.
160. Menger FM, Keiper JS. Gemini surfactants. *Angewandte Chemie International Edition*. 2000;39(11):1906-1920.
161. Menger FM, Mbadugha BNA. Gemini surfactants with a disaccharide spacer. *Journal of the American Chemical Society*. 2001;123(5):875-885.
162. Menger FM, Littau CA. Gemini-surfactants: synthesis and properties. *Journal of the American Chemical Society*. 1991;113(4):1451-1452.
163. Muñoz-Úbeda M, Misra SK, Barrán-Berdón AL, Datta S, Aicart-Ramos C, Castro-Hartmann P, Kondaiah P, Junquera E, Bhattacharya S, Aicart E. How Does the Spacer Length of Cationic Gemini Lipids Influence the Lipoplex Formation with Plasmid DNA? *Physicochemical and Biochemical Characterizations and their Relevance in Gene Therapy*. *Biomacromolecules*. 2012;13(12):3926-3937.
164. Obłąk E, Piecuch A, Rewak-Soroczyńska J, Paluch E. Activity of gemini quaternary ammonium salts against microorganisms. *Applied Microbiology and Biotechnology*. 2018.
165. Yadav MR, Kumar M, Murumkar PR, Hazari PP, Mishra AK. Gemini Amphiphile-Based Lipoplexes for Efficient Gene Delivery: Synthesis, Formulation Development, Characterization, Gene Transfection, and Biodistribution Studies. *ACS Omega*. 2018;3(9):11802-11816.
166. Al-Dulaymi M, Michel D, Chitanda JM, El-Aneed A, Verrall RE, Grochulski P, Badea I. Molecular Engineering as an Approach To Modulate Gene Delivery Efficiency of Peptide-Modified Gemini Surfactants. *Bioconjugate Chemistry*. 2018;29(10):3293-3308.
167. Mohammed-Saeid W, Chitanda J, Al-Dulaymi M, Verrall R, Badea I. Design and Evaluation of RGD-Modified Gemini Surfactant-Based Lipoplexes for Targeted Gene Therapy in Melanoma Model. *Pharmaceutical research*. 2017;34(9):1886-1896.
168. Cardoso AM, Morais CM, Silva SG, Marques EF, de Lima MCP, Jurado MAS. Bis-quaternary gemini surfactants as components of nonviral gene delivery systems: A comprehensive study from physicochemical properties to membrane interactions. *International Journal of Pharmaceutics*. 2014;474(1):57-69.
169. Zana R, Benraou M, Rueff R. Alkanediyl-a, w-bis (dimethyl-alkyl ammonium bromide) Surfactants. 1. Effect of the Spacer Chain Length on the CMC and Micelle Ionization Degree. *Langmuir : the ACS journal of surfaces and colloids*. 1991;7:1072-1075.
170. Luciani P, Bombelli C, Colone M, Giansanti L, Ryhänen SJ, Säily VMJ, Mancini G, Kinnunen PK. Influence of the spacer of cationic gemini amphiphiles on the hydration of lipoplexes. *Biomacromolecules*. 2007;8(6):1999-2003.
171. Wettig SD, Verrall RE, Foldvari M. Gemini surfactants: a new family of building blocks for non-viral gene delivery systems. *Current gene therapy*. 2008;8(1):9-23.
172. Elsabahy M, Badea I, Verrall R, Donkuru M, Foldvari M. Dicationic gemini nanoparticle design for gene therapy. *Organic Nanomaterials: Synthesis, Characterization, and Device Applications*. 2013:509-528.
173. Wettig SD, Badea I, Donkuru MD, Verrall RE, Foldvari M. Structural and transfection properties of amine-substituted gemini surfactant-based nanoparticles. *The journal of gene medicine*. 2007;9.
174. Badea I, Wettig S, Verrall R, Foldvari M. Topical non-invasive gene delivery using gemini nanoparticles in interferon-gamma-deficient mice. *European journal of pharmaceutics and*

- biopharmaceutics : official journal of Arbeitsgemeinschaft fur Pharmazeutische Verfahrenstechnik eV. 2007;65(3):414-422.
175. Singh J, Yang P, Michel D, Verrall RE, Foldvari M, Badea I. Amino acid-substituted gemini surfactant-based nanoparticles as safe and versatile gene delivery agents. *Current drug delivery*. 2011;8(3):299-306.
 176. Groth C, Nydén M, Holmberg K, Kanicky JR, Shah DO. Kinetics of the self-assembly of gemini surfactants. *Journal of Surfactants and Detergents*. 2004;7(3):247-255.
 177. Mondal J, Mahanthappa M, Yethiraj A. Self-Assembly of Gemini Surfactants: A Computer Simulation Study. *The Journal of Physical Chemistry B*. 2013;117(16):4254-4262.
 178. Blume G, Cevc G. Liposomes for the sustained drug release in vivo. *Biochimica et Biophysica Acta (BBA)-Biomembranes*. 1990;1029(1):91-97.
 179. Senior J, Delgado C, Fisher D, Tilcock C, Gregoriadis G. Influence of surface hydrophilicity of liposomes on their interaction with plasma protein and clearance from the circulation: studies with poly (ethylene glycol)-coated vesicles. *Biochimica et Biophysica Acta (BBA)-Biomembranes*. 1991;1062(1):77-82.
 180. Peeters L, Sanders NN, Braeckmans K, Boussery K, Van de Voorde J, De Smedt SC, Demeester J. Vitreous: a barrier to nonviral ocular gene therapy. *Invest Ophthalmol Vis Sci*. 2005;46(10):3553-3561.
 181. Wettig S, D., Badea I, Donkuru M, Verrall RE, Foldvari M. Structural and transfection properties of amine-substituted gemini surfactant-based nanoparticles. *J Gene Med*. 2007;9(8):649-658.
 182. Mayor S, Pagano RE. Pathways of clathrin-independent endocytosis. *Nature reviews Molecular cell biology*. 2007;8(8):603.
 183. Sahay G, Alakhova DY, Kabanov AV. Endocytosis of nanomedicines. *Journal of controlled release : official journal of the Controlled Release Society*. 2010;145(3):182-195.
 184. Vercauteren D, Vandenbroucke RE, Jones AT, Rejman J, Demeester J, De Smedt SC, Sanders NN, Braeckmans K. The use of inhibitors to study endocytic pathways of gene carriers: optimization and pitfalls. *Molecular therapy : the journal of the American Society of Gene Therapy*. 2010;18.
 185. Iversen T-G, Skotland T, Sandvig K. Endocytosis and intracellular transport of nanoparticles: present knowledge and need for future studies. *Nano today*. 2011;6(2):176-185.
 186. Kaplan IM, Wadia JS, Dowdy SF. Cationic TAT peptide transduction domain enters cells by macropinocytosis. *Journal of Controlled Release*. 2005;102(1):247-253.
 187. Khalil IA, Kogure K, Futaki S, Harashima H. High density of octaarginine stimulates macropinocytosis leading to efficient intracellular trafficking for gene expression. *Journal of Biological Chemistry*. 2006;281(6):3544-3551.
 188. Khalil IA, Kogure K, Akita H, Harashima H. Uptake Pathways and Subsequent Intracellular Trafficking in Nonviral Gene Delivery. *Pharmacological Reviews*. 2006;58(1):32-45.
 189. Marsh M, Helenius A. Virus Entry: Open Sesame. *Cell*. 2006;124(4):729-740.
 190. Harush-Frenkel O, Debotton N, Benita S, Altschuler Y. Targeting of nanoparticles to the clathrin-mediated endocytic pathway. *Biochemical and biophysical research communications*. 2007;353(1):26-32.
 191. Petros RA, DeSimone JM. Strategies in the design of nanoparticles for therapeutic applications. *Nature Reviews Drug Discovery*. 2010;9(8):615-627.
 192. Xiang S, Tong H, Shi Q, Fernandes JC, Jin T, Dai K, Zhang X. Uptake mechanisms of non-viral gene delivery. *Journal of Controlled Release*. 2012;158(3):371-378.

193. Oba M, Aoyagi K, Miyata K, Matsumoto Y, Itaka K, Nishiyama N, Yamasaki Y, Koyama H, Kataoka K. Polyplex micelles with cyclic RGD peptide ligands and disulfide cross-links directing to the enhanced transfection via controlled intracellular trafficking. *Molecular pharmaceutics*. 2008;5(6):1080-1092.
194. Hatakeyama H, Ito E, Akita H, Oishi M, Nagasaki Y, Futaki S, Harashima H. A pH-sensitive fusogenic peptide facilitates endosomal escape and greatly enhances the gene silencing of siRNA-containing nanoparticles in vitro and in vivo. *Journal of Controlled Release*. 2009;139(2):127-132.
195. Boussif O, Lezoualc'H F, Zanta MA, Mergny MD, Scherman D, Demeneix B, Behr JP. A versatile vector for gene and oligonucleotide transfer into cells in culture and in vivo: Polyethylenimine. *Proceedings of the National Academy of Sciences of the United States of America*. 1995;92(16):7297-7301.
196. Mochizuki S, Kanegae N, Nishina K, Kamikawa Y, Koiwai K, Masunaga H, Sakurai K. The role of the helper lipid dioleoylphosphatidylethanolamine (DOPE) for DNA transfection cooperating with a cationic lipid bearing ethylenediamine. *Biochimica et biophysica acta*. 2013;1828(2):412-418.
197. Morris MC, Deshayes S, Heitz F, Divita G. Cell-penetrating peptides: from molecular mechanisms to therapeutics. *Biology of the cell / under the auspices of the European Cell Biology Organization*. 2008;100(4):201-217.
198. Lehto T, Kurrikoff K, Langel Ü. Cell-penetrating peptides for the delivery of nucleic acids. *Expert opinion on drug delivery*. 2012;9(7):823-836.
199. Plank C, Tang MX, Wolfe AR, Szoka FC. Branched cationic peptides for gene delivery: role of type and number of cationic residues in formation and in vitro activity of DNA polyplexes. *Human gene therapy*. 1999;10(2):319-332.
200. Subia B, Reinisalo M, Dey N, Tavakoli S, Subrizi A, Ganguli M, Ruponen M. Nucleic acid delivery to differentiated retinal pigment epithelial cells using cell-penetrating peptide as a carrier. *European Journal of Pharmaceutics and Biopharmaceutics*. 2019;140:91-99.
201. Koirala A, Makkia RS, Conley SM, Cooper MJ, Naash MI. S/MAR-containing DNA nanoparticles promote persistent RPE gene expression and improvement in RPE65-associated LCA. *Human molecular genetics*. 2013;22(8):1632-1642.
202. Koirala A, Conley SM, Makkia R, Liu Z, Cooper MJ, Sparrow JR, Naash MI. Persistence of non-viral vector mediated RPE65 expression: case for viability as a gene transfer therapy for RPE-based diseases. *Journal of controlled release*. 2013;172(3):745-752.
203. Chen CW, Yeh MK, Shiau CY, Chiang CH, Lu DW. Efficient downregulation of VEGF in retinal pigment epithelial cells by integrin ligand-labeled liposome-mediated siRNA delivery. *International journal of nanomedicine*. 2013;8:2613-2627.
204. Leyton L, Schneider P, Labra CV, Rüegg C, Hetz CA, Quest AFG, Bron C. Thy-1 binds to integrin β 3 on astrocytes and triggers formation of focal contact sites. *Current Biology*. 2001;11(13):1028-1038.
205. Holliger P, Hudson PJ. Engineered antibody fragments and the rise of single domains. *Nature biotechnology*. 2005;23(9):1126-1136.
206. Nelson AL, Reichert JM. Development trends for therapeutic antibody fragments. *Nature Biotechnology*. 2009;27(4):331-337.
207. Said Hassane F, Saleh AF, Abes R, Gait MJ, Lebleu B. Cell penetrating peptides: overview and applications to the delivery of oligonucleotides. *Cellular and molecular life sciences : CMLS*. 2010;67(5):715-726.

208. Barry MA, Dower WJ, Johnston SA. Toward cell–targeting gene therapy vectors: Selection of cell–binding peptides from random peptide–presenting phage libraries. *Nature medicine*. 1996;2(3):299.
209. Rajala A, Wang Y, Zhu Y, Ranjo-Bishop M, Ma J-X, Mao C, Rajala RVS. Nanoparticle-Assisted Targeted Delivery of Eye-Specific Genes to Eyes Significantly Improves the Vision of Blind Mice In Vivo. *Nano Letters*. 2014;14(9):5257-5263.
210. Säälük P, Elmquist A, Hansen M, Padari K, Saar K, Viht K, Langel Ü, Pooga M. Protein cargo delivery properties of cell-penetrating peptides. A comparative study. *Bioconjugate chemistry*. 2004;15(6):1246-1253.
211. Vives E, Schmidt J, Pelegrin A. Cell-penetrating and cell-targeting peptides in drug delivery. *Biochimica et biophysica acta*. 2008;1786(2):126-138.
212. Liu C, Tai L, Zhang W, Wei G, Pan W, Lu W. Penetratin, a Potentially Powerful Absorption Enhancer for Noninvasive Intraocular Drug Delivery. *Molecular pharmaceutics*. 2014;11:1218-1227.
213. Midoux P, Kichler A, Boutin V, Maurizot J-C, Monsigny M. Membrane permeabilization and efficient gene transfer by a peptide containing several histidines. *Bioconjugate chemistry*. 1998;9(2):260-267.
214. Raad Md, Teunissen EA, Mastrobattista E. Peptide vectors for gene delivery: from single peptides to multifunctional peptide nanocarriers. *Nanomedicine*. 2014;9(14):2217-2232.
215. Varkouhi AK, Scholte M, Storm G, Haisma HJ. Endosomal escape pathways for delivery of biologicals. *Journal of Controlled Release*. 2011;151(3):220-228.
216. Oliveira S, van Rooy I, Kranenburg O, Storm G, Schiffelers RM. Fusogenic peptides enhance endosomal escape improving siRNA-induced silencing of oncogenes. *International journal of pharmaceutics*. 2007;331(2):211-214.
217. Lönn P, Kacsinta AD, Cui X-S, Hamil AS, Kaulich M, Gogoi K, Dowdy SF. Enhancing endosomal escape for intracellular delivery of macromolecular biologic therapeutics. *Scientific reports*. 2016;6(1):1-9.
218. Moseley GW, Roth DM, DeJesus MA, Leyton DL, Filmer RP, Pouton CW, Jans DA. Dynein light chain association sequences can facilitate nuclear protein import. *Molecular biology of the cell*. 2007;18(8):3204-3213.
219. Wang Y, Rajala A, Rajala RVS. Lipid Nanoparticles for Ocular Gene Delivery. *Journal of Functional Biomaterials*. 2015;6(2):379.
220. Ragin AD, Morgan RA, Chmielewski J. Cellular Import Mediated by Nuclear Localization Signal Peptide Sequences. *Chemistry & Biology*. 2002;9(8):943-948.
221. Tanaka K, Kanazawa T, Sugawara K, Horiuchi S, Takashima Y, Okada H. A cytoplasm-sensitive peptide vector cross-linked with dynein light chain association sequence (DLCAS) enhances gene expression. *International journal of pharmaceutics*. 2011;419(1-2):231-234.
222. Bai H, Lester GMS, Petishnok Laura C, Dean David A. Cytoplasmic transport and nuclear import of plasmid DNA. *Bioscience Reports*. 2017;37(6).
223. Pigeon L, Gonçalves C, Gosset D, Pichon C, Midoux P. An E3-14.7 K Peptide that Promotes Microtubules-Mediated Transport of Plasmid DNA Increases Polyplexes Transfection Efficiency. *Small*. 2013;9(22):3845-3851.
224. Edelman G. Cell adhesion molecules. *Science*. 1983;219(4584):450-457.
225. Quarles RH. Immunoglobulin Superfamily and the Nervous System. In. *eLS: John Wiley & Sons, Ltd; 2001. p. 1-8.*

226. D'Urso D, Brophy PJ, Staugaitis SM, Stewart Gillespie C, Frey AB, Stempak JG, Colman DR. Protein zero of peripheral nerve myelin: Biosynthesis, membrane insertion, and evidence for homotypic interaction. *Neuron*. 1990;4(3):449-460.
227. D'Urso D, Ehrhardt P, Müller HW. Peripheral Myelin Protein 22 and Protein Zero: a Novel Association in Peripheral Nervous System Myelin. *The Journal of Neuroscience*. 1999;19(9):3396-3403.
228. González-Amaro R, Sanchez-Madrid F. Cell adhesion molecules: selectins and integrins. *Critical Reviews™ in Immunology*. 1999;19(5-6).
229. Maness PF, Schachner M. Neural recognition molecules of the immunoglobulin superfamily: signaling transducers of axon guidance and neuronal migration. *Nature Neuroscience*. 2006;10:19.
230. Filla MS, Faralli JA, Peotter JL, Peters DM. The role of integrins in glaucoma. *Experimental eye research*. 2017;158:124-136.
231. Gagen D, Faralli JA, Filla MS, Peters DM. The role of integrins in the trabecular meshwork. *Journal of ocular pharmacology and therapeutics*. 2014;30(2-3):110-120.
232. Wang A-G, Yen M-Y, Hsu W-M, Fann M-J. Induction of vitronectin and integrin alphav in the retina after optic nerve injury. *Molecular vision*. 2006;12:76-84.
233. Kuppermann BD, Boyer DS, Kaiser PK, Heier JS, Campochiaro PA, Quiroz-Mercado H, Kornfield J, Karageozian L, Genead MA, Karageozian HL. Topline Results From Prospective, Double-masked, Placebo Controlled Phase 2 Clinical Study Evaluating Luminata®(ALG-1001) in Patients with Symptomatic Focal Vitreomacular Adhesion. *Investigative Ophthalmology and Visual Science*. 2016;57(12):Art. No. 1809.
234. Wang W, Lo ACY. Diabetic Retinopathy: Pathophysiology and Treatments. *International Journal of Molecular Sciences*. 2018;19(6):1816.
235. Singh SR, Grossniklaus HE, Kang SJ, Edelhauser HF, Ambati BK, Kompella UB. Intravenous transferrin, RGD peptide and dual-targeted nanoparticles enhance anti-VEGF intrareceptor gene delivery to laser-induced CNV. *Gene therapy*. 2009;16:645.
236. Yoshihara Y. Immunoglobulin Superfamily Cell Adhesion Molecules. In: Binder MD, Hirokawa N, Windhorst U, editors. *Encyclopedia of Neuroscience*. Berlin, Heidelberg: Springer Berlin Heidelberg; 2009. p. 1923-1926.
237. Tan RPA, Leshchyns'ka I, Sytnyk V. Glycosylphosphatidylinositol-Anchored Immunoglobulin Superfamily Cell Adhesion Molecules and Their Role in Neuronal Development and Synapse Regulation. *Frontiers in molecular neuroscience*. 2017;10:378-378.
238. Yang P, Singh J, Wettig S, Foldvari M, Verrall RE, Badea I. Enhanced gene expression in epithelial cells transfected with amino acid-substituted gemini nanoparticles. *European journal of pharmaceutics and biopharmaceutics : official journal of Arbeitsgemeinschaft fur Pharmazeutische Verfahrenstechnik eV*. 2010;75(3):311-320.
239. Wang X-L, Zhang X-H, Cao M, Zheng H-Z, Xiao B, Wang Y, Li M. Gemini Surfactant-Induced DNA Condensation into a Beadlike Structure. *The Journal of Physical Chemistry B*. 2009;113(8):2328-2332.
240. Sharma R, Kamal A, Abdinejad M, Mahajan RK, Kraatz H-B. Advances in the synthesis, molecular architectures and potential applications of gemini surfactants. *Advances in Colloid and Interface Science*. 2017;248:35-68.
241. Elsabahy M, Badea I, Verrall R, Donkuru M, Foldvari M. Dicationic gemini nanoparticle design for gene therapy. In: John Wiley & Sons, Inc; 2013. p. 509-528.
242. Hayashi Y. Pot economy and one-pot synthesis. *Chemical science*. 2016;7(2):866-880.

243. Raju M, Mäeorg S, Tšubrik O, Mäeorg U. Efficient solventless technique for Boc-protection of hydrazines and amines. *Arkivoc*. 2009;6:291-297.
244. Ragnarsson U, Grehn L. Novel amine chemistry based on DMAP-catalyzed acylation. *Accounts of chemical research*. 1998;31(8):494-501.
245. Zhi D, Bai Y, Yang J, Cui S, Zhao Y, Chen H, Zhang S. A review on cationic lipids with different linkers for gene delivery. *Advances in colloid and interface science*. 2018;253:117-140.
246. Pullmannová P, Funari SS, Devínsky F, Uhríková D. The DNA–DNA spacing in gemini surfactants–DOPE–DNA complexes. *Biochimica et Biophysica Acta (BBA) - Biomembranes*. 2012;1818(11):2725-2731.
247. Damen M, Groenen A, Van Dongen S, Nolte R, Scholte B, Feiters M. Transfection by cationic gemini lipids and surfactants. *MedChemComm*. 2018;9(9):1404-1425.
248. Kulkarni JA, Darjuan MM, Mercer JE, Chen S, van der Meel R, Thewalt JL, Tam YYC, Cullis PR. On the Formation and Morphology of Lipid Nanoparticles Containing Ionizable Cationic Lipids and siRNA. *ACS Nano*. 2018;12(5):4787-4795.
249. Felgner JH, Kumar R, Sridhar C, Wheeler CJ, Tsai YJ, Border R, Ramsey P, Martin M, Felgner PL. Enhanced gene delivery and mechanism studies with a novel series of cationic lipid formulations. *Journal of Biological Chemistry*. 1994;269(4):2550-2561.
250. Yin H, Kanasty RL, Eltoukhy AA, Vegas AJ, Dorkin JR, Anderson DG. Non-viral vectors for gene-based therapy. *Nature Reviews Genetics*. 2014;15(8):541-555.
251. Safinya CR. Structures of lipid–DNA complexes: supramolecular assembly and gene delivery. *Current Opinion in Structural Biology*. 2001;11(4):440-448.
252. Foldvari M, Wettig S, Badea I, Verrall R, Bagonluri M. Dicationic gemini surfactant gene delivery complexes contain cubic-lamellar mixed polymorphic phase. In: *NSTI-Nanotech*; 2006. p. 400-403.
253. Brgles M, Šantak M, Halassy B, Forcic D, Tomašić J. Influence of charge ratio of liposome/DNA complexes on their size after extrusion and transfection efficiency. *International journal of nanomedicine*. 2012;7:393.
254. Zhdanov R, Podobed O, Vlassov V. Cationic lipid–DNA complexes—lipoplexes—for gene transfer and therapy. *Bioelectrochemistry*. 2002;58(1):53-64.
255. Esumi K, Goino M, Koide Y. Adsorption and Adsolubilization by Monomeric, Dimeric, or Trimeric Quaternary Ammonium Surfactant at Silica/Water Interface. *Journal of colloid and interface science*. 1996;183(2):539-545.
256. Han Y, Wang Y. Aggregation behavior of gemini surfactants and their interaction with macromolecules in aqueous solution. *Physical Chemistry Chemical Physics*. 2011;13(6):1939-1956.
257. Liu F, Huang L. Development of non-viral vectors for systemic gene delivery. *Journal of Controlled Release*. 2002;78(1):259-266.
258. Song YK, Liu F, Chu S, Liu D. Characterization of cationic liposome-mediated gene transfer in vivo by intravenous administration. *Human gene therapy*. 1997;8(13):1585-1594.
259. Audouy S, Molema G, de Leij L, Hoekstra D. Serum as a modulator of lipoplex-mediated gene transfection: dependence of amphiphile, cell type and complex stability. *The Journal of Gene Medicine: A cross-disciplinary journal for research on the science of gene transfer and its clinical applications*. 2000;2(6):465-476.
260. Ewert KK, Zidovska A, Ahmad A, Bouxsein NF, Evans HM, McAllister CS, Samuel CE, Safinya CR. Cationic Liposome–Nucleic Acid Complexes for Gene Delivery and Silencing:

- Pathways and Mechanisms for Plasmid DNA and siRNA. In: Bielke W, Erbacher C, editors. Nucleic Acid Transfection. Berlin, Heidelberg: Springer Berlin Heidelberg; 2010. p. 191-226.
261. Taheri-Araghi S, Chen D-W, Kohandel M, Sivaloganathan S, Foldvari M. Tuning optimum transfection of gemini surfactant–phospholipid–DNA nanoparticles by validated theoretical modeling. *Nanoscale*. 2019;11(3):1037-1046.
 262. Al-Dosari MS, Gao X. Nonviral Gene Delivery: Principle, Limitations, and Recent Progress. *The AAPS journal*. 2009;11(4):671.
 263. Al-Dulaymi MA, Chitanda JM, Mohammed-Saeid W, Araghi HY, Verrall RE, Grochulski P, Badea I. Di-peptide-modified gemini surfactants as gene delivery vectors: exploring the role of the alkyl tail in their physicochemical behavior and biological activity. *The AAPS journal*. 2016;18(5):1168-1181.
 264. Almeida JA, Marques EF, Jurado AS, Pais AA. The effect of cationic gemini surfactants upon lipid membranes. An experimental and molecular dynamics simulation study. *Physical Chemistry Chemical Physics*. 2010;12(43):14462-14476.
 265. Prabha S, Arya G, Chandra R, Ahmed B, Nimesh S. Effect of size on biological properties of nanoparticles employed in gene delivery. *Artificial cells, nanomedicine, and biotechnology*. 2016;44(1):83-91.
 266. Gharagozloo M, Rafiee A, Chen DW, Foldvari M. A flow cytometric approach to study the mechanism of gene delivery to cells by gemini-lipid nanoparticles: an implication for cell membrane nanoporation. *Journal of Nanobiotechnology*. 2015;13(1):62.
 267. Elner SG, Elner VM. The integrin superfamily and the eye. *Investigative ophthalmology & visual science*. 1996;37(5):696-701.
 268. Hermosilla T, Muñoz D, Herrera-Molina R, Valdivia A, Muñoz N, Nham S-U, Schneider P, Burridge K, Quest AF, Leyton L. Direct Thy-1/ α V β 3 integrin interaction mediates neuron to astrocyte communication. *Biochimica et Biophysica Acta (BBA)-Molecular Cell Research*. 2008;1783(6):1111-1120.
 269. Jaafari MR, Foldvari M. P0 protein mediated targeting of liposomes to melanoma cells with high level of ICAM-1 expression. *Journal of drug targeting*. 1999;7(2):101-112.
 270. Foldvari M, Jaafari MR, Mezei M, Mezei C. Targeting liposomes through immunoglobulin superfamily domains: P0 protein as a model. *Drug delivery*. 1998;5(3):183-195.
 271. Foldvari M, Mezei C, Mezei M. Intracellular delivery of drugs by liposomes containing P0 glycoprotein from peripheral nerve myelin into human M21 melanoma cells. *Journal of pharmaceutical sciences*. 1991;80(11):1020-1028.
 272. Nakatani M, Shinohara Y, Takii M, Mori H, Asai N, Nishimura S, Furukawa-Hibi Y, Miyamoto Y, Nitta A. Periocular injection of in situ hydrogels containing Leu–Ile, an inducer for neurotrophic factors, promotes retinal ganglion cell survival after optic nerve injury. *Experimental eye research*. 2011;93(6):873-879.
 273. Nitta A, Nishioka H, Fukumitsu H, Furukawa Y, Sugiura H, Shen L, Furukawa S. Hydrophobic dipeptide Leu-Ile protects against neuronal death by inducing brain-derived neurotrophic factor and glial cell line-derived neurotrophic factor synthesis. *Journal of neuroscience research*. 2004;78(2):250-258.
 274. Ultsch MH, Wiesmann C, Simmons LC, Henrich J, Yang M, Reilly D, Bass SH, de Vos AM. Crystal structures of the neurotrophin-binding domain of TrkA, TrkB and TrkC. Edited by I. A. Wilson. *Journal of Molecular Biology*. 1999;290(1):149-159.
 275. Yip PM, Zhao X, Montgomery AM, Siu C-H. The Arg-Gly-Asp motif in the cell adhesion molecule L1 promotes neurite outgrowth via interaction with the α V β 3 integrin. *Molecular biology of the cell*. 1998;9(2):277-290.

276. Samatov TR, Wicklein D, Tonevitsky AG. L1CAM: Cell adhesion and more. *Progress in histochemistry and cytochemistry*. 2016;51(2):25-32.
277. Castellani V, De Angelis E, Kenwrick S, Rougon G. Cis and trans interactions of L1 with neuropilin-1 control axonal responses to semaphorin 3A. *The EMBO Journal*. 2002;21(23):6348-6357.
278. Furukawa-Hibi Y, Nitta A, Ikeda T, Morishita K, Liu W, Ibi D, Alkam T, Nabeshima T, Yamada K. The hydrophobic dipeptide Leu-Ile inhibits immobility induced by repeated forced swimming via the induction of BDNF. *Behavioural brain research*. 2011;220(2):271-280.
279. Chen D-W, Narsineni L, Foldvari M. Multipotent stem cell-derived retinal ganglion cells in 3D culture as tools for neurotrophic factor gene delivery system development. *Nanomedicine: Nanotechnology, Biology and Medicine*. 2019;21:102045.
280. Singh J, Yang P, Michel D, E Verrall R, Foldvari M, Badea I. Amino acid-substituted gemini surfactant-based nanoparticles as safe and versatile gene delivery agents. *Current drug delivery*. 2011;8(3):299-306.
281. Due-Hansen ME, Pandey SK, Christiansen E, Andersen R, Hansen SVF, Ulven T. A protocol for amide bond formation with electron deficient amines and sterically hindered substrates. *Organic & Biomolecular Chemistry*. 2016;14(2):430-433.
282. Valeur E, Bradley M. Amide bond formation: beyond the myth of coupling reagents. *Chemical Society Reviews*. 2009;38(2):606-631.
283. Vrettos EI, Sayyad N, Mavrogiannaki EM, Stylos E, Kostagianni AD, Papas S, Mavromoustakos T, Theodorou V, Tzakos AG. Unveiling and tackling guanidinium peptide coupling reagent side reactions towards the development of peptide-drug conjugates. *RSC Advances*. 2017;7(80):50519-50526.
284. Luna OF, Gomez J, Cárdenas C, Albericio F, Marshall SH, Guzmán F. Deprotection reagents in fmoc solid phase peptide synthesis: moving away from piperidine? *Molecules (Basel, Switzerland)*. 2016;21(11):1542.
285. Lin X, Zhao N, Yan P, Hu H, Xu F-J. The shape and size effects of polycation functionalized silica nanoparticles on gene transfection. *Acta Biomaterialia*. 2015;11:381-392.
286. Verma A, Stellacci F. Effect of surface properties on nanoparticle-cell interactions. *Small*. 2010;6(1):12-21.
287. Schachner M. Cell Surface Recognition and Neuron-Glia Interactions. *Annals of the New York Academy of Sciences*. 1991;633(1):105-112.
288. Jung M, Petrusch B, Stuermer CA. Axon-regenerating retinal ganglion cells in adult rats synthesize the cell adhesion molecule L1 but not TAG-1 or SC-1. *Mol Cell Neurosci*. 1997;9(2):116-131.
289. Zelina P, Avci HX, Thelen K, Pollerberg GE. The cell adhesion molecule NrCAM is crucial for growth cone behaviour and pathfinding of retinal ganglion cell axons. *Development*. 2005;132(16):3609-3618.
290. Felding-Habermann B, Silletti S, Mei F, Siu C-H, Yip PM, Brooks PC, Cheresch DA, O'Toole TE, Ginsberg MH, Montgomery AM. A single immunoglobulin-like domain of the human neural cell adhesion molecule L1 supports adhesion by multiple vascular and platelet integrins. *The Journal of cell biology*. 1997;139(6):1567-1581.
291. Foldvari M, Chen D-W. Retinal multipotent stem-cell derived "MiEye" spheroid 3D culture model for preclinical screening of non-viral gene delivery systems. *Precision Nanomedicine*. 2018;1(2):106-123.

292. Zhi Y, Lu Q, Zhang C-W, Yip HK, So K-F, Cui Q. Different optic nerve injury sites result in different responses of retinal ganglion cells to brain-derived neurotrophic factor but not neurotrophin-4/5. *Brain research*. 2005;1047(2):224-232.
293. Zhang C-W, Lu Q, You S-W, Zhi Y, Yip HK, Wu W, So K-F, Cui Q. CNTF and BDNF have similar effects on retinal ganglion cell survival but differential effects on nitric oxide synthase expression soon after optic nerve injury. *Investigative ophthalmology & visual science*. 2005;46(4):1497-1503.
294. Shen S, Wiemelt AP, McMorris FA, Barres BA. Retinal Ganglion Cells Lose Trophic Responsiveness after Axotomy. *Neuron*. 1999;23(2):285-295.
295. Castillo Jr B, Del Cerro M, Breakefield X, Frim D, Barnstable C, Dean D, Bohn M. Retinal ganglion cell survival is promoted by genetically modified astrocytes designed to secrete brain-derived neurotrophic factor (BDNF). *Brain research*. 1994;647(1):30-36.
296. Domenici L, Origlia N, Falsini B, Cerri E, Barloscio D, Fabiani C, Sansò M, Giovannini L. Rescue of retinal function by BDNF in a mouse model of glaucoma. *PloS one*. 2014;9(12).
297. Freeman EC, Weiland LM, Meng WS. Modeling the proton sponge hypothesis: examining proton sponge effectiveness for enhancing intracellular gene delivery through multiscale modeling. *J Biomater Sci Polym Ed*. 2013;24(4):398-416.
298. Jaafari MR, Foldvari M. Targeting of liposomes to melanoma cells with high levels of ICAM-1 expression through adhesive peptides from immunoglobulin domains. *Journal of pharmaceutical sciences*. 2002;91(2):396-404.
299. Jaafari MR, Foldvari M. Targeting of liposomes to human keratinocytes through adhesive peptides from immunoglobulin domains in the presence of IFN-gamma. *Drug delivery*. 2002;9(1):1-9.
300. Ramirez AI, de Hoz R, Salobar-Garcia E, Salazar JJ, Rojas B, Ajoy D, López-Cuenca I, Rojas P, Triviño A, Ramírez JM. The role of microglia in retinal neurodegeneration: alzheimer's disease, parkinson, and glaucoma. *Frontiers in Aging Neuroscience*. 2017;9(214).
301. Yan Z, Liao H, Chen H, Deng S, Jia Y, Deng C, Lin J, Ge J, Zhuo Y. Elevated intraocular pressure induces amyloid- β deposition and tauopathy in the lateral geniculate nucleus in a monkey model of glaucoma. *Investigative ophthalmology & visual science*. 2017;58(12):5434-5443.
302. Sadun AA, Bassi CJ. Optic nerve damage in Alzheimer's disease. *Ophthalmology*. 1990;97(1):9-17.
303. McKinnon SJ. Glaucoma: ocular Alzheimer's disease. *Front biosci*. 2003;8(Suppl):1140-1156.
304. Sevigny J, Chiao P, Bussière T, Weinreb PH, Williams L, Maier M, Dunstan R, Salloway S, Chen T, Ling Y. The antibody aducanumab reduces A β plaques in Alzheimer's disease. *Nature*. 2016;537(7618):50.
305. Fagan T, Strobel G. Lilliputian effect size fells phase 3 trial of solanezumab, leaving its future uncertain. In.; 2016.
306. Salt T, Nizari S, Cordeiro M, Russ H, Danysz W. Effect of the A β aggregation modulator MRZ-99030 on retinal damage in an animal model of glaucoma. *Neurotoxicity research*. 2014;26(4):440-446.
307. Guo L, Salt TE, Luong V, Wood N, Cheung W, Maass A, Ferrari G, Russo-Marie F, Sillito AM, Cheetham ME, Moss SE, Fitzke FW, Cordeiro MF. Targeting amyloid- β in glaucoma treatment. *Proceedings of the National Academy of Sciences*. 2007;104(33):13444-13449.
308. Gallego BI, Salazar JJ, de Hoz R, Rojas B, Ramírez AI, Salinas-Navarro M, Ortín-Martínez A, Valiente-Soriano FJ, Avilés-Trigueros M, Villegas-Perez MP. IOP induces upregulation of

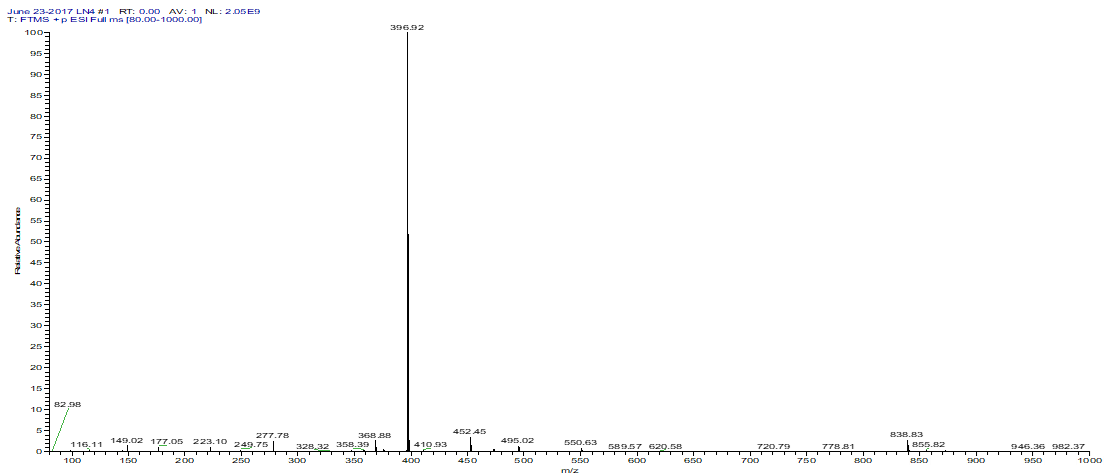
- GFAP and MHC-II and microglia reactivity in mice retina contralateral to experimental glaucoma. *Journal of Neuroinflammation*. 2012;9(1):92.
309. Gupta N, Fong J, Ang LC, Yücel YH. Retinal tau pathology in human glaucomas. *Canadian Journal of Ophthalmology*. 2008;43(1):53-60.
310. Chiasseu M, Alarcon-Martinez L, Belforte N, Quintero H, Dotigny F, Destroismaisons L, Velde CV, Panayi F, Louis C, Di Polo A. Tau accumulation in the retina promotes early neuronal dysfunction and precedes brain pathology in a mouse model of Alzheimer's disease. *Mol Neurodegeneration*. 2017;12(1):58.
311. Chiasseu M, Vargas JLC, Destroismaisons L, Velde CV, Leclerc N, Di Polo A. Tau accumulation, altered phosphorylation, and missorting promote neurodegeneration in glaucoma. *Journal of Neuroscience*. 2016;36(21):5785-5798.
312. Sisodia SS, St George-Hyslop PH. γ -Secretase, Notch, A β and Alzheimer's disease: where do the presenilins fit in? *Nature Reviews Neuroscience*. 2002;3(4):281.
313. Gazit E. Mechanisms of amyloid fibril self-assembly and inhibition. *The FEBS Journal*. 2005;272(23):5971-5978.
314. Colletier J-P, Laganowsky A, Landau M, Zhao M, Soriaga AB, Goldschmidt L, Flot D, Cascio D, Sawaya MR, Eisenberg D. Molecular basis for amyloid- β polymorphism. *Proceedings of the National Academy of Sciences*. 2011;108(41):16938-16943.
315. Wang SSS, Chen Y-T, Chou S-W. Inhibition of amyloid fibril formation of β -amyloid peptides via the amphiphilic surfactants. *Biochimica et Biophysica Acta (BBA) - Molecular Basis of Disease*. 2005;1741(3):307-313.
316. Marcinowski KJ, Shao H, Clancy EL, Zagorski MG. Solution structure model of residues 1–28 of the Amyloid β -peptide when bound to micelles. *Journal of the American Chemical Society*. 1998;120(43):11082-11091.
317. Li Y, Cao M, Wang Y. Alzheimer amyloid β (1–40) peptide: Interactions with cationic gemini and single-chain surfactants. *The Journal of Physical Chemistry B*. 2006;110(36):18040-18045.
318. Hudson SA, Ecroyd H, Kee TW, Carver JA. The thioflavin T fluorescence assay for amyloid fibril detection can be biased by the presence of exogenous compounds. *The FEBS Journal*. 2009;276(20):5960-5972.
319. Zhao D, Chen Y, Liu Q, Zhao Y, Li Y. Exploring the binding mechanism of thioflavin-T to the β -amyloid peptide by blind docking method. *Science China Chemistry*. 2012;55(1):112-117.
320. Mohamed T, Zhao X, Habib LK, Yang J, Rao PPN. Design, synthesis and structure–activity relationship (SAR) studies of 2,4-disubstituted pyrimidine derivatives: Dual activity as cholinesterase and A β -aggregation inhibitors. *Bioorganic & Medicinal Chemistry*. 2011;19(7):2269-2281.
321. Colvin MT, Silvers R, Ni QZ, Can TV, Sergeev I, Rosay M, Donovan KJ, Michael B, Wall J, Linse S, Griffin RG. Atomic Resolution Structure of Monomorphic A β 42 Amyloid Fibrils. *Journal of the American Chemical Society*. 2016;138(30):9663-9674.
322. Rao PPN, Mohamed T, Teckwani K, Tin G. Curcumin Binding to Beta Amyloid: A Computational Study. *Chemical Biology & Drug Design*. 2015;86(4):813-820.
323. Rao PPN, Du D. In Silico Strategies to Design Small Molecules to Study Beta-Amyloid Aggregation. In: Roy K, editor. *Computational Modeling of Drugs Against Alzheimer's Disease*. New York, NY: Springer New York; 2018. p. 249-261.
324. Ávila J, Lim F, Moreno F, Belmonte C, Cuellar AC. Tau function and dysfunction in neurons. *Molecular neurobiology*. 2002;25(3):213-231.

325. Cao M, Han Y, Wang J, Wang Y. Modulation of fibrillogenesis of amyloid β (1–40) peptide with cationic gemini surfactant. *The Journal of Physical Chemistry B*. 2007;111(47):13436-13443.
326. Li SD, Huang L. Gene therapy progress and prospects: non-viral gene therapy by systemic delivery. *Gene therapy*. 2006;13(18):1313-1319.
327. He C, Hou Y, Han Y, Wang Y. Disassembly of amyloid fibrils by pre-micellar and micellar aggregates of a tetrameric cationic surfactant in aqueous solution. *Langmuir : the ACS journal of surfaces and colloids*. 2011;27(8):4551-4556.
328. Bai Q, Parris RS, Burton EA. Different mechanisms regulate expression of zebrafish myelin protein zero (P0) in myelinating oligodendrocytes and its induction following axonal injury. *Journal of Biological Chemistry*. 2014;289(35):24114-24128.
329. Kupperman B. A dual-mechanism drug for vitreoretinal diseases. *Retina Today July/August*. 2015;2015:85-87.
330. Oliveira LB, Meyer CH, Kumar J, Tatebayashi M, Toth CA, Wong F, Epstein DL, McCuen II BW. RGD peptide-assisted vitrectomy to facilitate induction of a posterior vitreous detachment: a new principle in pharmacological vitreolysis. *Current Eye Research*. 2002;25(6):333-340.
331. Castellani V, Falk J, Rougon G. Semaphorin3A-induced receptor endocytosis during axon guidance responses is mediated by L1 CAM. *Molecular and Cellular Neuroscience*. 2004;26(1):89-100.
332. Friesner RA, Banks JL, Murphy RB, Halgren TA, Klicic JJ, Mainz DT, Repasky MP, Knoll EH, Shelley M, Perry JK. Glide: a new approach for rapid, accurate docking and scoring. 1. Method and assessment of docking accuracy. *Journal of Medicinal Chemistry*. 2004;47(7):1739-1749.
333. Wu G, Robertson DH, Brooks III CL, Vieth M. Detailed analysis of grid-based molecular docking: A case study of CDOCKER—A CHARMM-based MD docking algorithm. *Journal of Computational Chemistry*. 2003;24(13):1549-1562.
334. Shoichet BK, McGovern SL, Wei B, Irwin JJ. Lead discovery using molecular docking. *Current Opinion in Chemical Biology*. 2002;6(4):439-446.
335. Guedes IA, de Magalhães CS, Dardenne LE. Receptor–ligand molecular docking. *Biophysical Reviews*. 2014;6(1):75-87.
336. Kruger RP, Aurandt J, Guan K-L. Semaphorins command cells to move. *Nature Reviews Molecular Cell Biology*. 2005;6:789.
337. Wai Wong C, Dye DE, Coombe DR. The role of immunoglobulin superfamily cell adhesion molecules in cancer metastasis. *Int J Cell Biol*. 2012;2012:340296-340296.
338. Xiong JP, Stehle T, Zhang R, Joachimiak A, Frech M, Goodman SL, Arnaout MA. Crystal structure of the extracellular segment of integrin α V β 3 in complex with an Arg-Gly-Asp ligand. *Science*. 2002;296(5565):151-155.

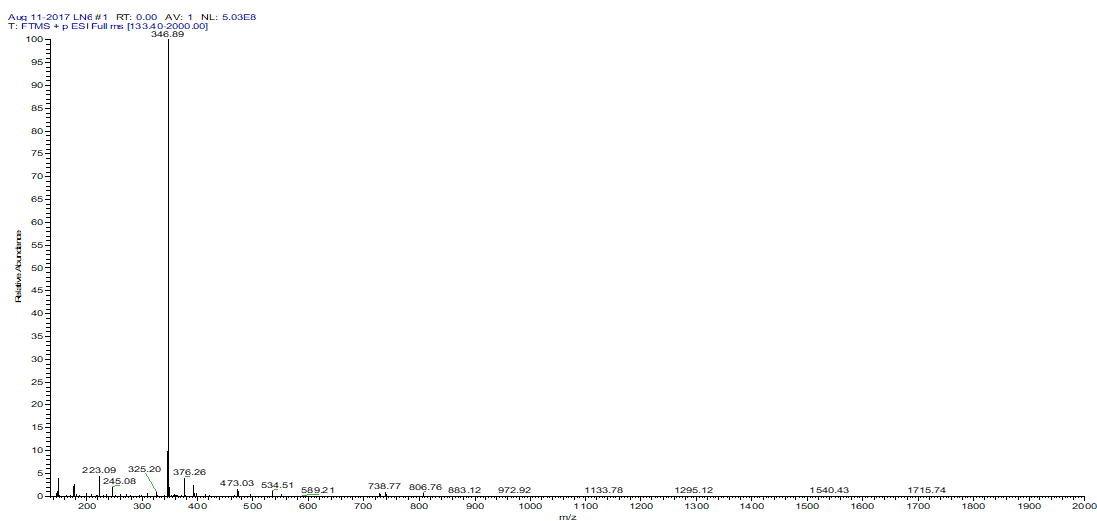
Appendices

Appendix 1 Improved synthesis and formulation design of dimeric and trimeric gemini surfactants and their evaluation as gene delivery vectors

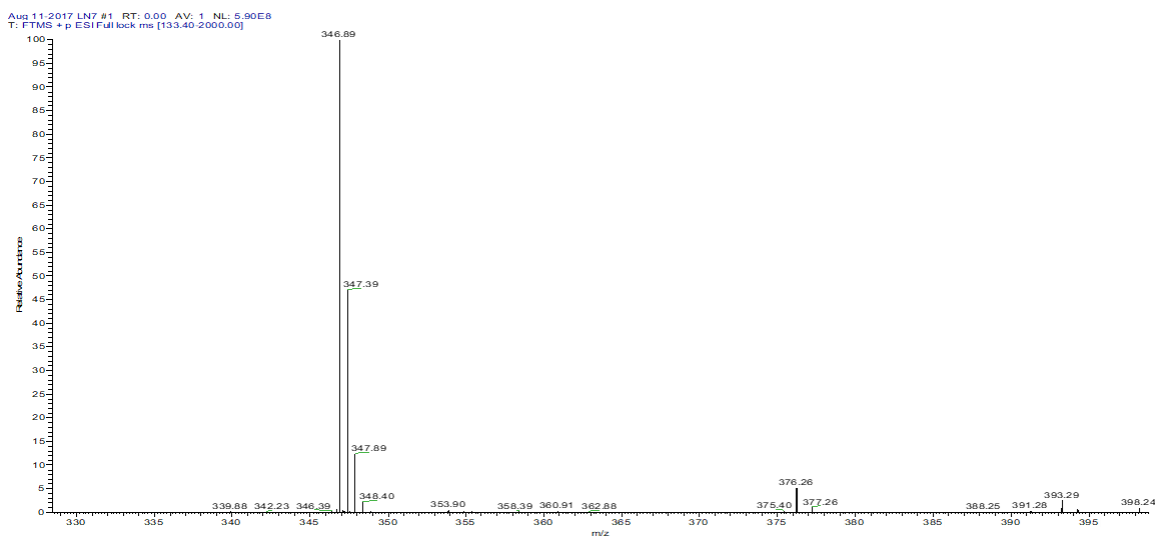
Mass spectrometry analysis of 18-7NH-18, 16-7N(16)-16 and 18-7N(18)-18 gemini surfactants, spectra's are obtained at multiple levels of synthesis and purification to confirm the obtained final product of the reaction.



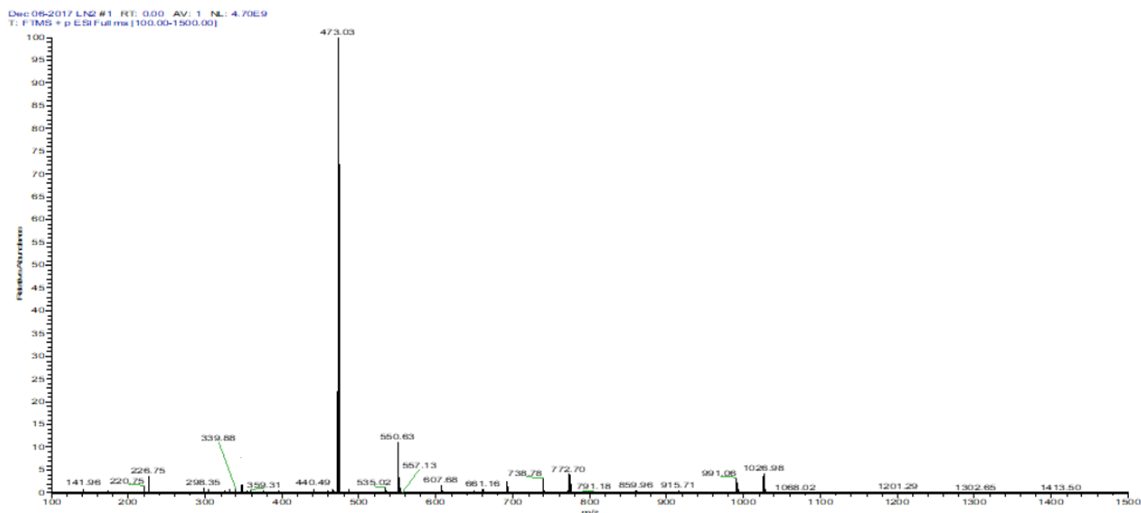
A. Mass spectra of Boc protected 18-7NH-18 before deprotection (m/z- 396.92)



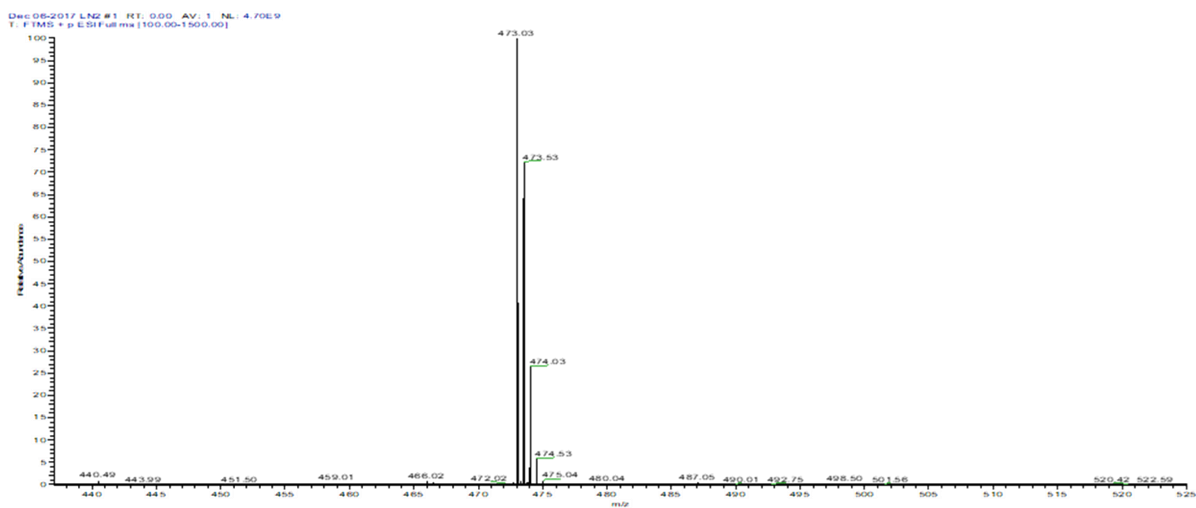
B. Mass spectra of deprotected 18-7NH-18 gemini surfactant (m/z- 346.89)



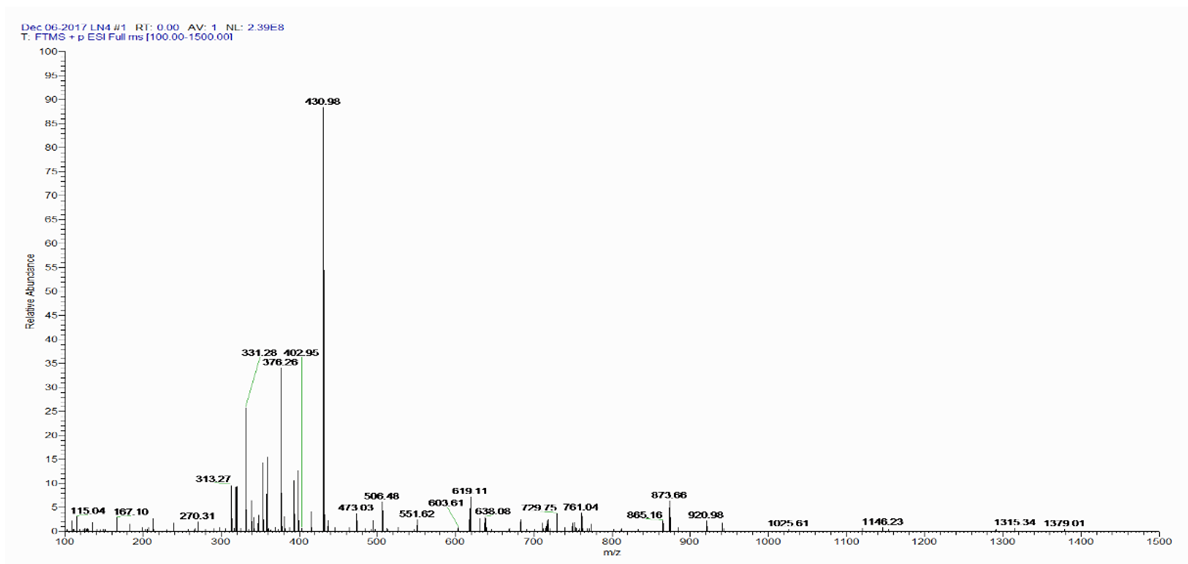
C. Mass spectra of 18-7NH-18 gemini surfactant with the split pattern of a doubly charged gemini surfactant-confirms a doubly charged dimeric bis-quaternary structure.



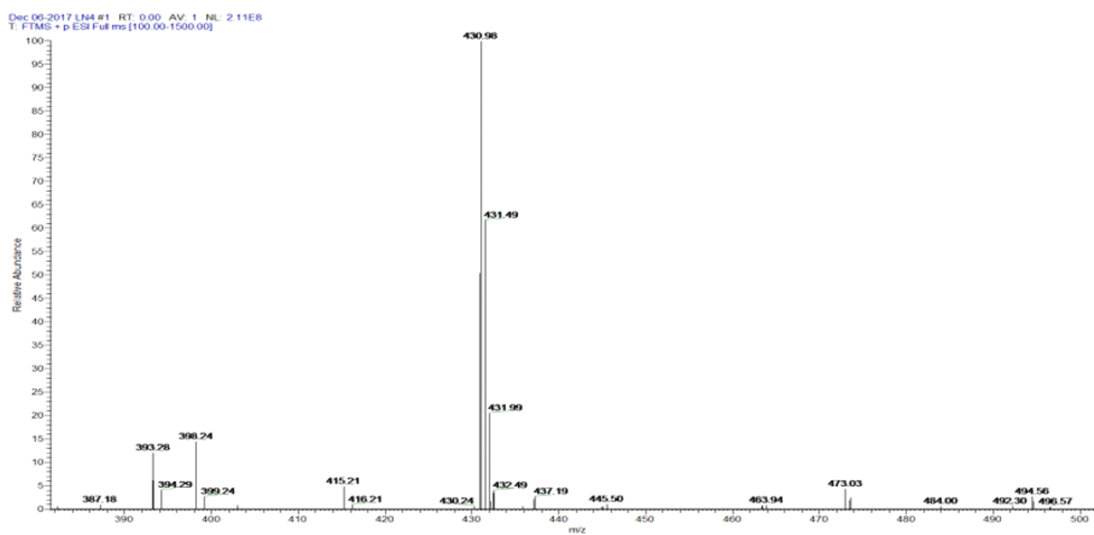
D. Mass spectra of 18-7N(18)-18 gemini surfactant (m/z- 473.03)



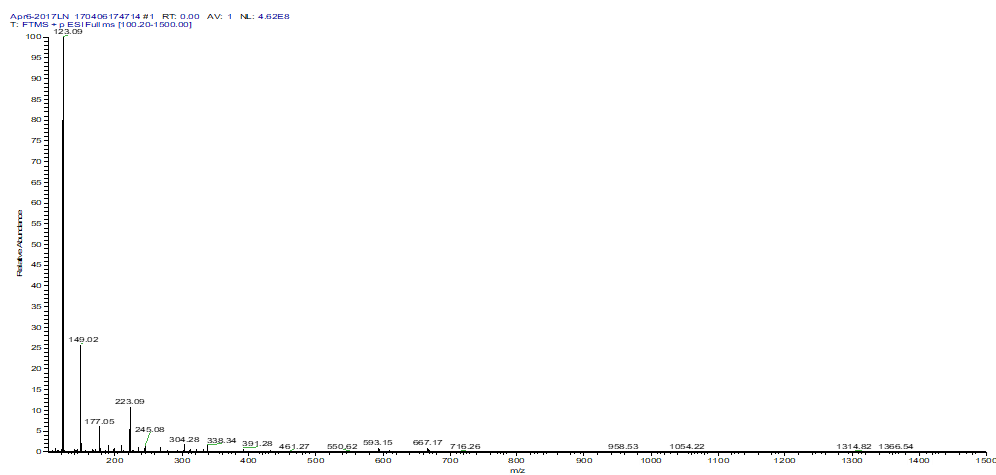
E. Mass spectra of 18-7N(18)-18 gemini surfactant with the split pattern of a doubly charged gemini surfactant-confirms a doubly charged trimeric bis-quaternary structure.



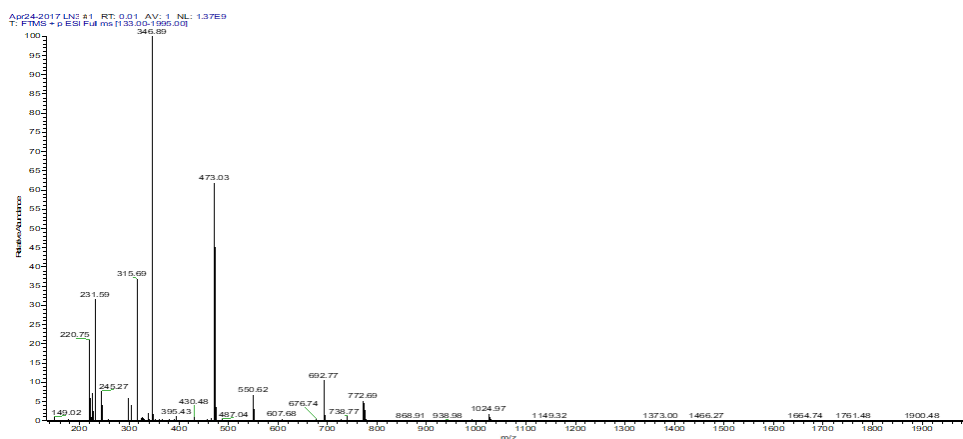
F. Mass spectra of deprotected 16-7N(16)-16 gemini surfactant (m/z- 430.98)



G. Mass spectra of 16-7N(16)-16 gemini surfactant with the split pattern of a doubly charged gemini surfactant-confirms a doubly charged trimeric bis-quaternary structure.



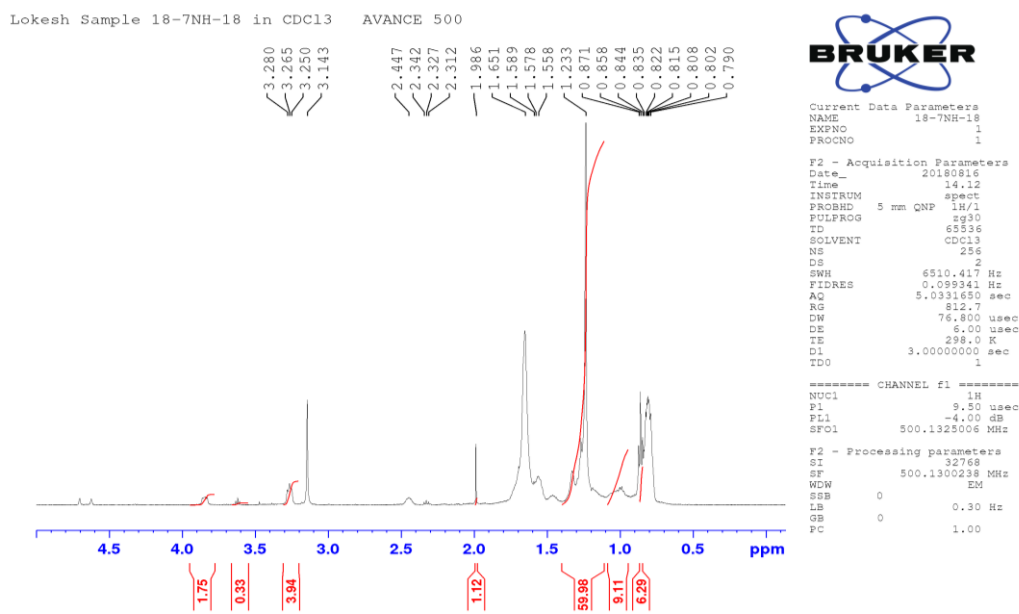
H. Gemini synthesis from published protocols and using DMAP as catalyst yields DMAP as reaction impurity and is not removed after successive recrystallizations (m/z-123.09)



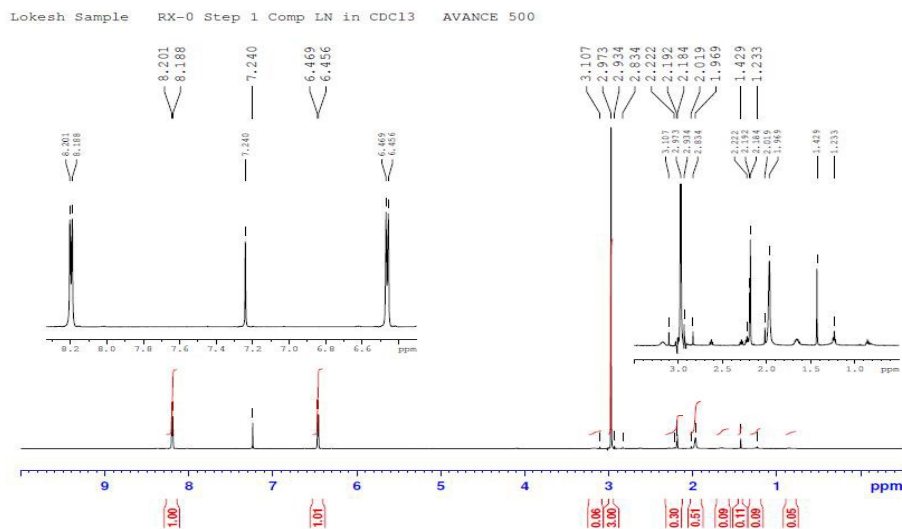
I. Presence of both dimeric and trimeric gemini surfactants at m/z 346.89 (dimeric) and m/z 473.03 (trimeric) when synthesized using published and in-house protocols.

Figure 1 Identification and characterization of gemini surfactants using mass spectrometry

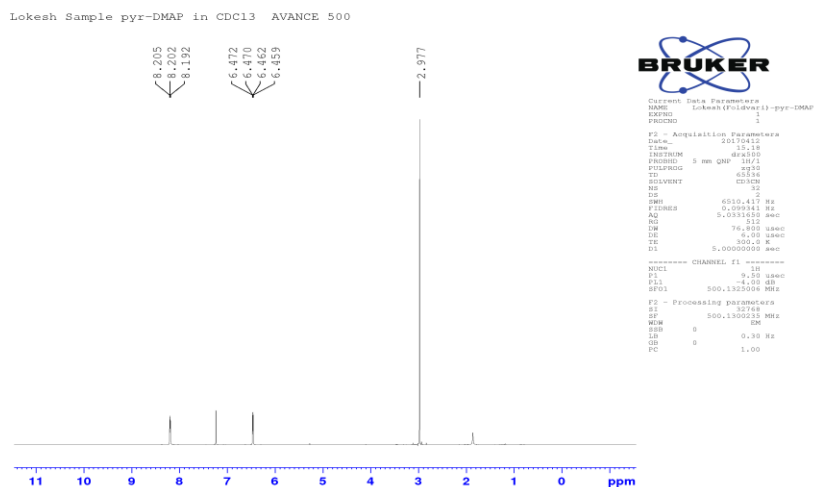
Results of 18-7NH-18 using one-pot synthesis method



A. ¹H NMR spectra of 18-7NH-18 gemini surfactant showing characteristic chemical shifts (δ ppm-0.85, 1.55, 3.28)



B. ¹H NMR spectrum of gemini synthesis as per in-house and previous published protocols containing DMAP as catalyst, presence of DMAP in final product as impurity (δ=2.9, 6.4, 8.2)



C. ¹H NMR spectrum of only DMAP to identify the chemical shifts of DMAP to compare with the final product of 18-7NH-18 made from both previous protocols and one-pot DMAP free method (δ ppm=2.9, 6.4, 8.2)

Figure 2 NMR spectroscopy analysis of purified 18-7NH-18 from old and new methods of synthesis

Surface tension and CMC determination

Below are the values of surface tension and CMC determined from Lauda TE3 automated tensiometer.

Table 1 Surface tension and surfactant concentration values for CMC determination

log C	ST (mN/m)	Surfactant conc (μM)
-1.79	69.11	0.02
-1.41	69.14	0.04
-1.21	69.68	0.06
-1.03	69.57	0.09
-0.80	69.39	0.16
-0.59	69.04	0.26
-0.38	68.99	0.42
-0.19	69.00	0.64
-0.02	68.66	0.96
0.20	68.64	1.60
0.46	68.67	2.86
0.61	68.37	4.09
0.77	68.62	5.89
0.94	68.57	8.79
1.06	68.26	11.55
1.19	66.96	15.46

1.31	66.11	20.29
1.43	63.75	26.82
1.51	62.64	32.62
1.61	60.34	40.96
1.64	56.40	43.91
1.67	54.82	46.67
1.69	52.42	49.25
1.71	48.44	51.69
1.76	46.89	57.17
1.79	46.11	61.94
1.82	46.01	66.12
1.84	45.89	69.81
1.86	45.05	73.11
1.88	45.09	76.06
1.91	45.00	81.13

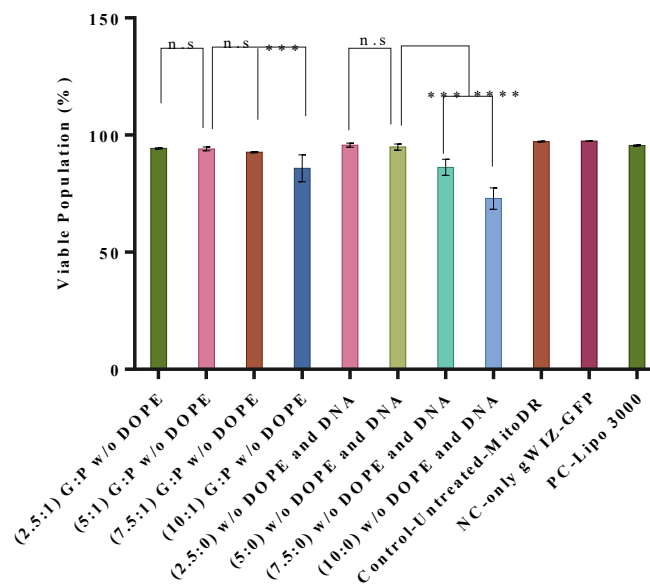


Figure 3 Effect of 18-7NH-18 (NS)-NPXs charge ratio on viability of A7 astrocytes and assessment of the effect of viability without DOPE and without DNA

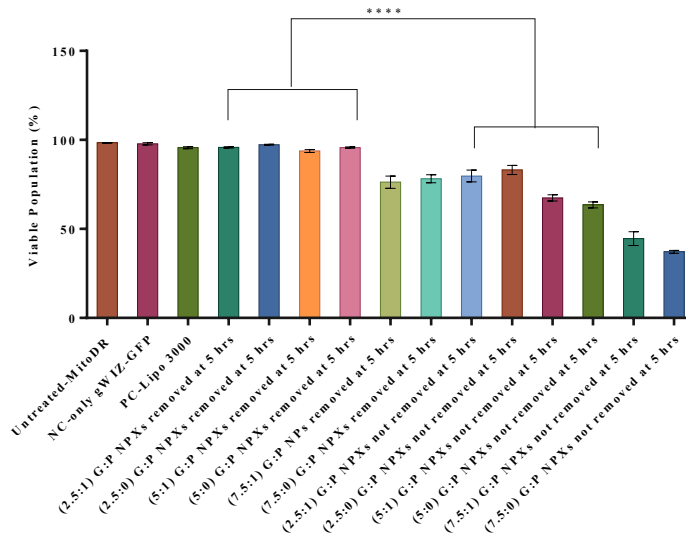


Figure 4 Viability studies for incubation and transfection assay time-point studies at 48 hrs.

Appendix 2 Development of multifunctional gemini nanoplexes for non-viral neurotrophic factor gene delivery to the retina



Figure 5 Reaction monitoring using UPLC method developed to track the changes during a peptide ligation reaction at 0, 0.5, 1 and 2 hours

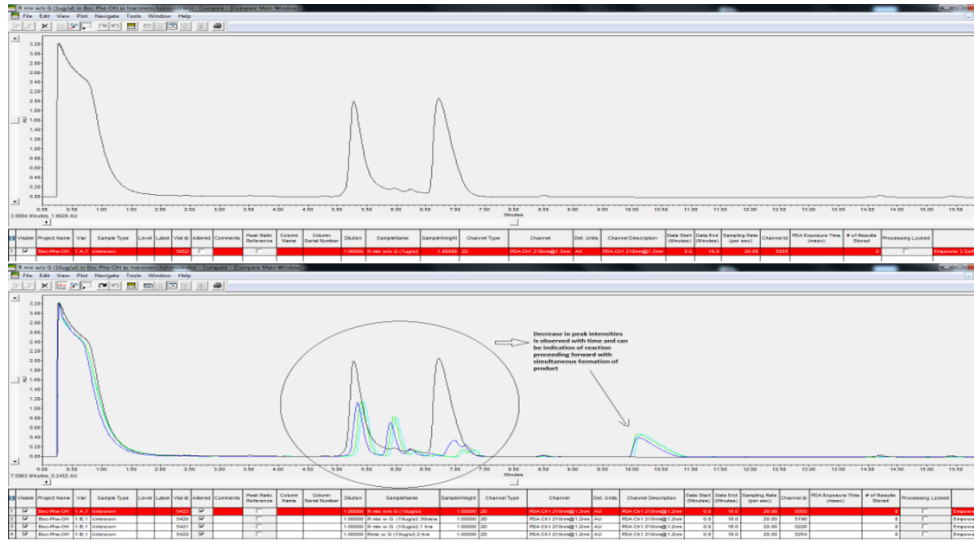


Figure 6 Reaction monitoring: graphs showing peaks before and after addition of m-7NH-m gemini surfactant into the reaction mixture

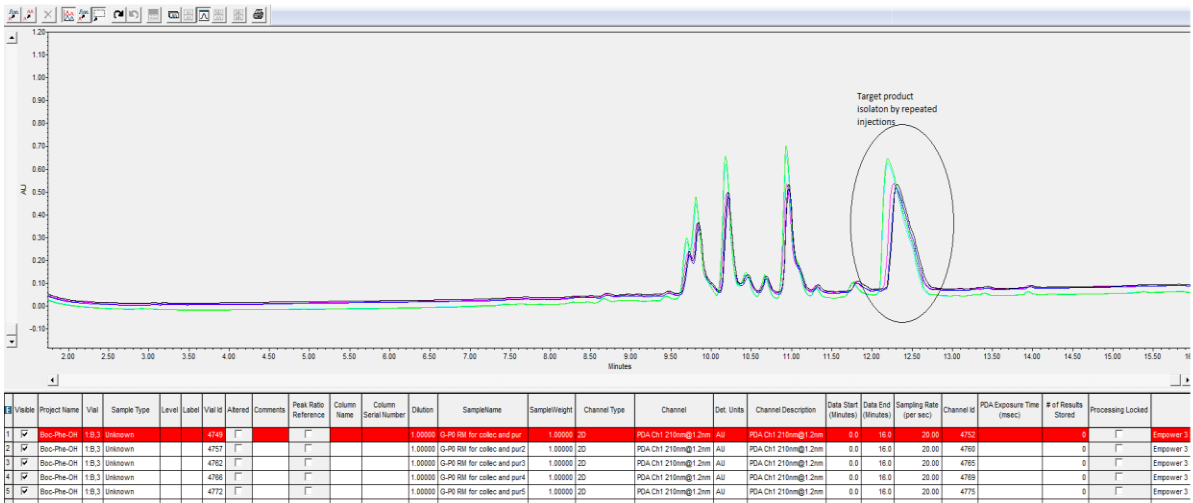


Figure 7 Pure 18-7N(p₅-protected)-18, 12-7N(p₅-protected)-12 product isolation using a semi-prep HPLC method on a C₁₈ column

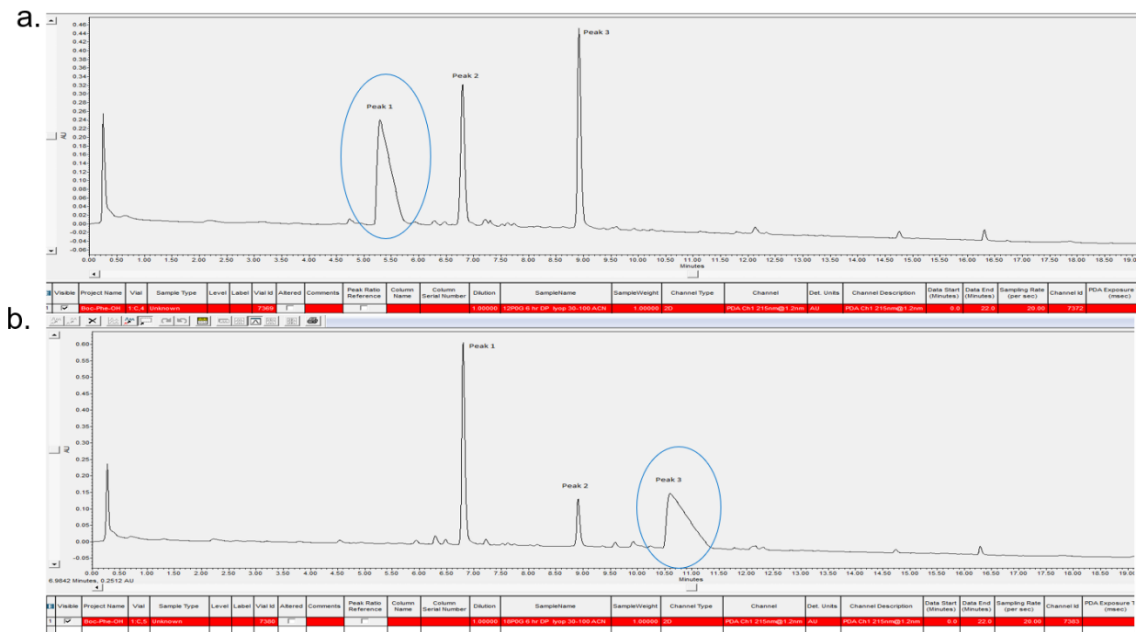


Figure 8 Deprotection reaction monitoring for (a) 12-7N(p₅)-12 and (b) 18-7N(p₅)-18-products marked with a blue circle

Table 2 Peptide-modified m-7N(p_n)-m gemini surfactants and their properties

m-7N(p _n)-m gemini surfactant (PG)	Peptide sequence	Celtek peptides code	MW of m- 7N(p _n)-m	m/z peak values (Values from Chem Draw)
12-7N(p ₅)-12	p ₅ -YTDNGTF	-NA-	1324.80	661.96, 662.46
18-7N(p ₁)-18	p ₁ - RGD	G1P1MC	1022.64	510.96, 511.46
18-7N(p ₂)-18	p ₂ - RLE	G1P2MC	1092.78	546.00, 546.05
18-7N(p ₃)-18	p ₃ - FASNKL	G1P3MC	1355.09	677.07, 677.57
18-7N(p ₄)-18	p ₄ - LI	G1P4MC	920.63	459.97, 460.47
18-7N(p ₅)-18	p ₅ - YTDNGTF	G1P5MC	1493.12	746.05, 746.55

CeltekPeptides Celtek Bioscience, LLC, 2550 Meridian Boulevard, Suite 200, Franklin, TN 37067
Tel: 615-399-7010 Fax: 615-399-7099 E-mail: psyside@celtek-bioscience.com web: www.celtek-peptides.com

Certificate of Analysis

Custom Synthetic Peptide	
Sequence: NH ₂ -R-G-D-MC	
Name: G1-P1-MC	Length: 3AA
Scale: Research	LotNo: 171213
Molecular Weight: 511	Appearance: White Powder
Requesting Purity: >95%	Requesting Weight: 200mg
Results of Analyses:	
Actual Weight: 55.0mg	
HPLC Purity: 99.46%	
Mol. Weight: 511.41	
Storage: stored at -20°C and keep dry	
The product is used for research only, not for human use	
Signature: <i>Yang Mey</i>	Date: 2018-11-25

- (a) Certificate of analysis (COA) for G1-P1-MC (18-7N(p₁)-18, MC- Parent compound (18-7NH-18), G1-P1 corresponds simply to peptide code (p₁) and MC signifies the base gemini (18-7NH-18) used to conjugate the peptide

Custom Synthetic Peptide

Sequence: NH₂-R-L-E-MC

Name: G1-P2-MC Length: 3AA

Scale: Research LotNo: 171213

Molecular Weight: 546 Appearance: White Powder

Requesting Purity: >95% Requesting Weight: 200mg

Results of Analyses:

Actual Weight: 29.5mg

HPLC Purity: 100.0%

Mol. Weight: 546.50

Storage: stored at -20°C and keep dry

The product is used for research only, not for human use

Signature: Yang Ming Date: 2018-01-04

Custom Synthetic Peptide

Sequence: NH₂-F-A-S-N-K-L-MC

Name: G1-P3-MC Length: 6AA

Scale: Research LotNo: 171221

Molecular Weight: 677 Appearance: White Powder

Requesting Purity: >95% Requesting Weight: 200mg

Results of Analyses:

Actual Weight: 40.2mg

HPLC Purity: 99.78%

Mol. Weight: 677.70

Storage: stored at -20°C and keep dry

The product is used for research only, not for human use

Signature: Yang Ming Date: 2018-01-04

(b) COA of G1-P2-MC (18-7N(p₂))-18 and (c) G1P3MC, 18-7N(p₃)-18

Custom Synthetic Peptide

Sequence: NH₂-L-I-MC

Name: G1-P4-MC Length: 2AA

Scale: Research LotNo: 171110

Molecular Weight: 460 Appearance: White Powder

Requesting Purity: >95% Requesting Weight: 200mg

Results of Analyses:

Actual Weight: 200.0mg

HPLC Purity: 99.68%

Mol. Weight: 459.96

Storage: stored at -20°C and keep dry

The product is used for research only, not for human use

Signature: Yang Ming Date: 2017-12-26

Custom Synthetic Peptide

Sequence: NH₂-Y-T-D-N-G-T-F-MC

Name: G1-P5-MC Length: 7AA

Scale: Research LotNo: 180528

Molecular Weight: 746 Appearance: White Powder

Requesting Purity: >95% Requesting Weight: 200mg

Results of Analyses:

Actual Weight: 13.6mg

HPLC Purity: 96.10%

Mol. Weight: 746.33

Storage: stored at -20°C and keep dry

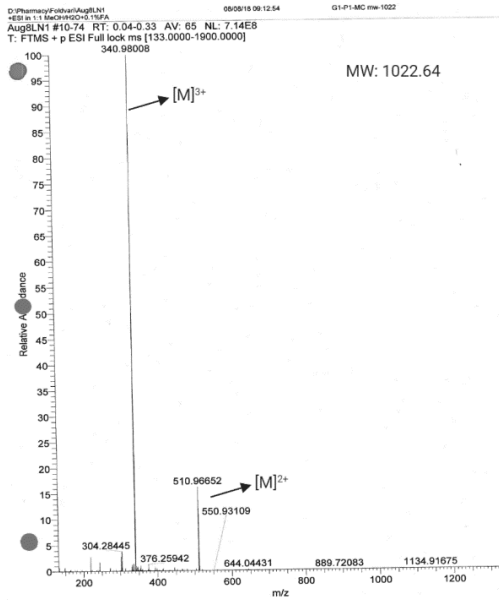
The product is used for research only, not for human use

Signature: Chen Xueying Date: 2018.07.20

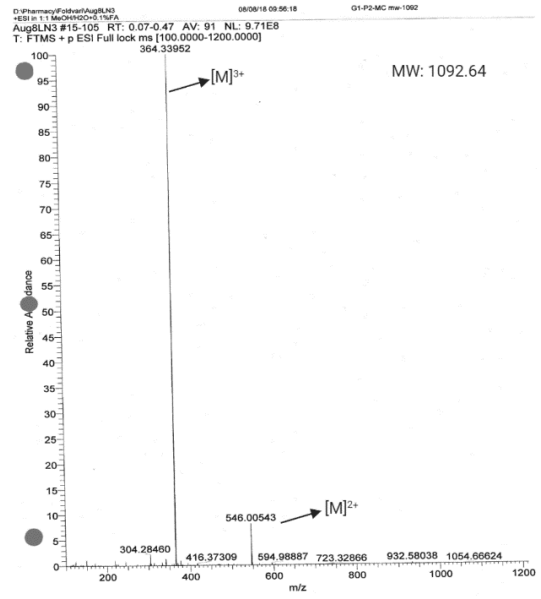
(d) COA of G1-P4-MC (18-7N(p₄))-18 and (e) G1-P5-MC (18-7N(p₅))-18

Figure 9 Certificate of analysis of peptide-modified gemini surfactants (a-e)

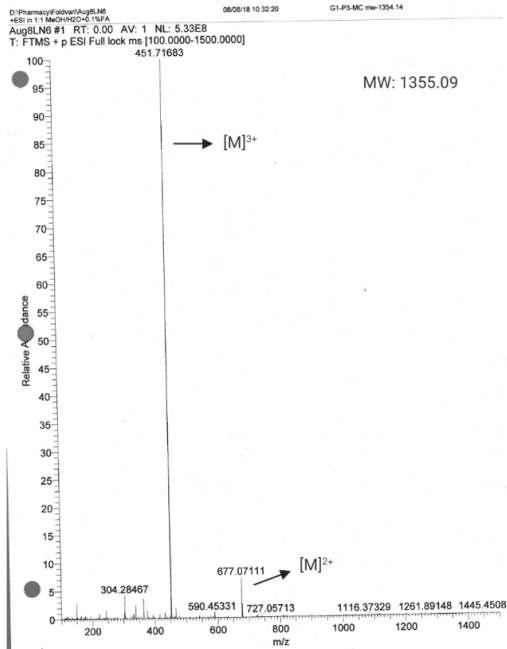
(a) 18-7N(RGD)-18



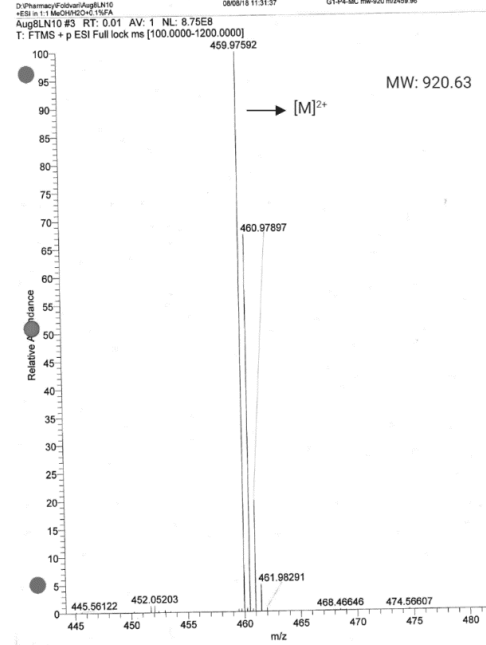
(b) 18-7N(RLE)-18



(c) 18-7N(FASNKL)-18



(d) 18-7N(LI)-18



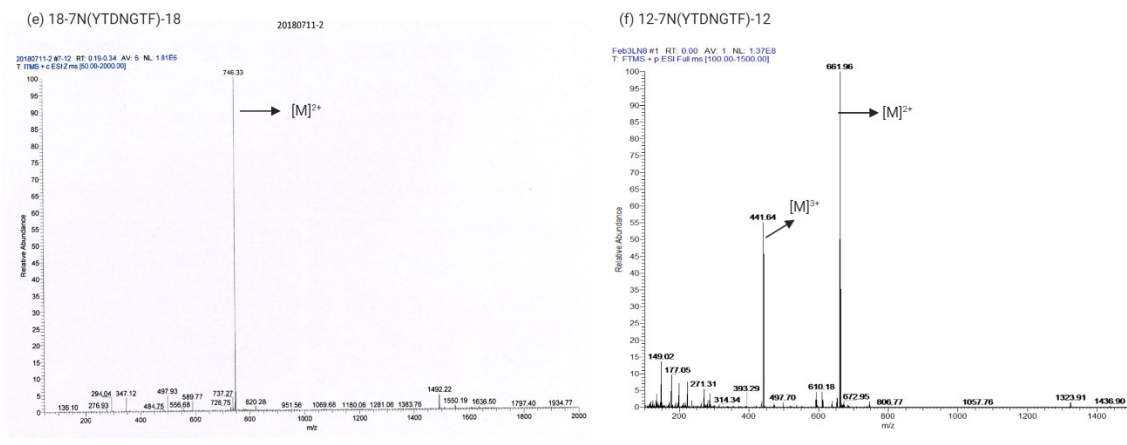
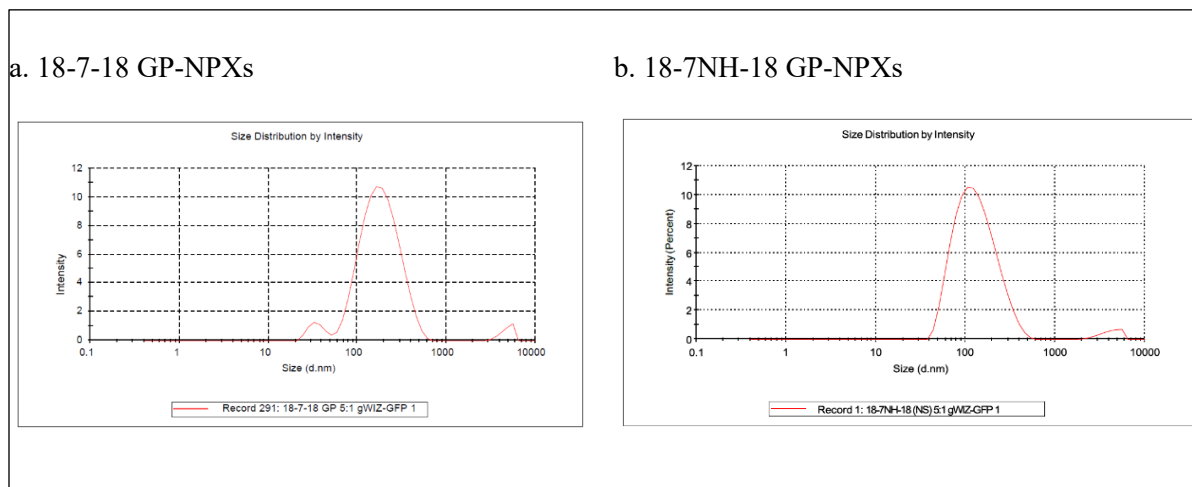
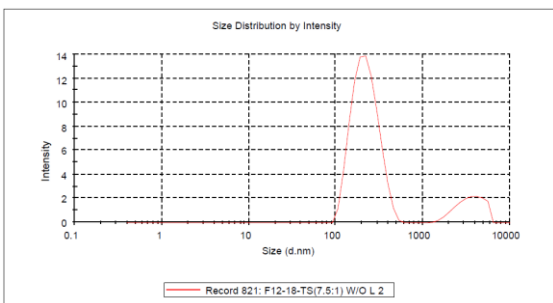


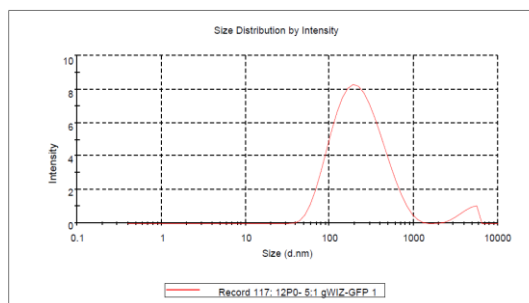
Figure 10 Peptide-modified dicationic gemini surfactants m-7N(p)-m (m=12 and 18, P= RGD, RLE, FASNKL, LI and YTDNGTF) (a-f), peaks shown in the graphs are triply charged $[M^{3+}]$ and doubly charged $[M^{2+}]$. The doubly charged peaks are characteristic peaks in the mass spectrometry from the cationic charged quaternary nitrogen's, any additional charge peaks obtained could be contributed from the peptide which is possible due to the use of 0.1% formic acid in MeOH which can form a charged species of the molecule being analyzed.



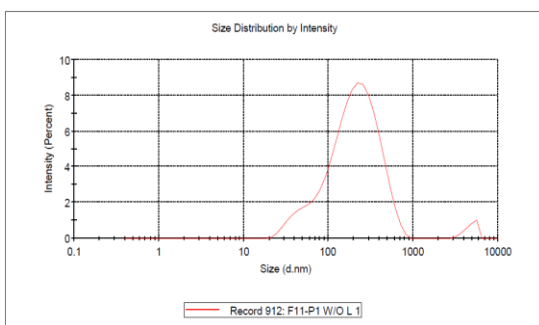
c. 18-7N(18)-18 GP-NPXs



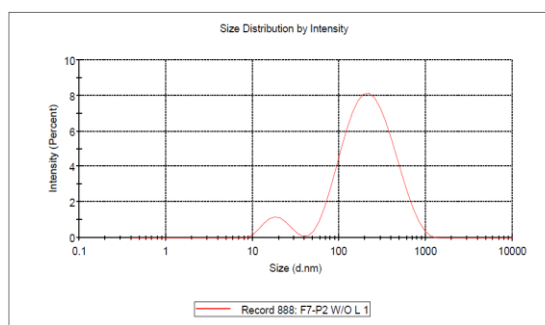
d. 12-7N(p₅)-12 pLPXs



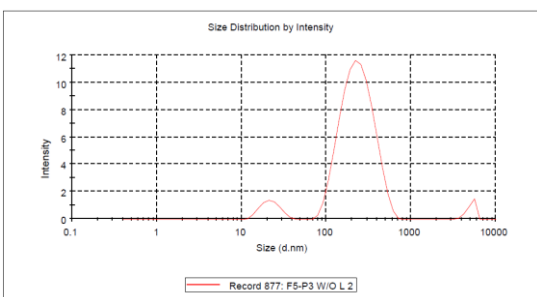
e. 18-7N(p₁)-18 pNPXs



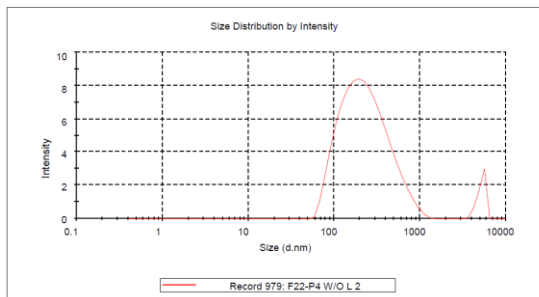
f. 18-7N(p₂)-18 pNPXs



g. 18-7N(p₃)-18 pNPXs



h. 18-7N(p₄)-18 pNPXs



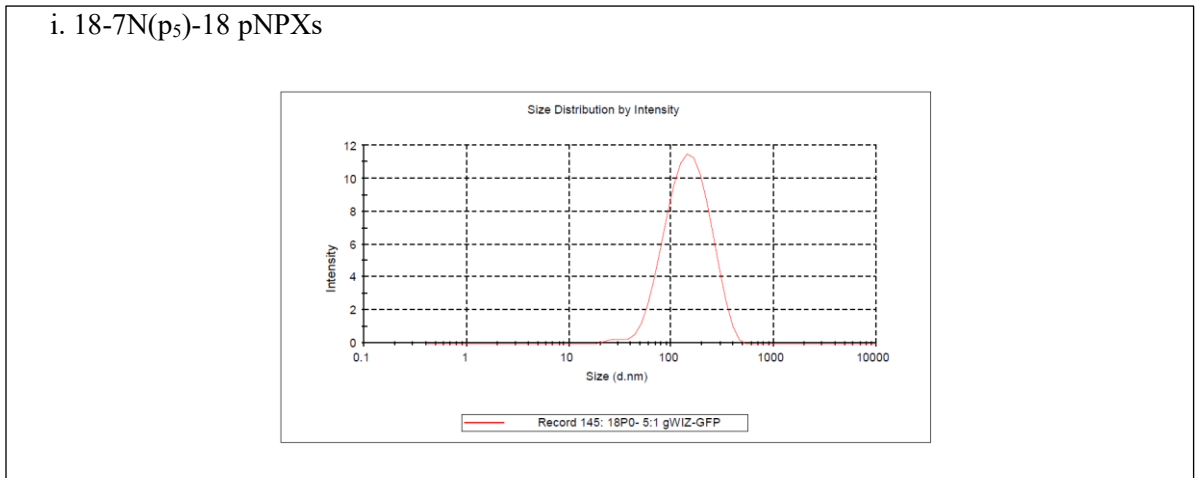


Figure 11 Particle size distribution profiles of m-7NH-m, m-7N(m)-m and m-7N(p_n)-m pNPXs (m=12 and 18, p_n=p₁₋₅) and pNPXs at 5:1 ratio of gemini:plasmid (gWIZ-GFP) obtained from DLS using Malvern ZetaSizer Nano ZS, a. 18-7-18 NPXs, b. 18-7NH-18 NPXs, c. 18-7N(18)-18 NPXs, d. 12-7N(p₅)-12 pLPXs, e. 18-7N(p₁)-18 pNPXs, f. 18-7N(p₂)-18 pNPXs, g. 18-7N(p₃)-18 pNPXs, h. 18-7N(p₄)-18 pNPXs and i. 18-7N(p₅)-18 pNPXs

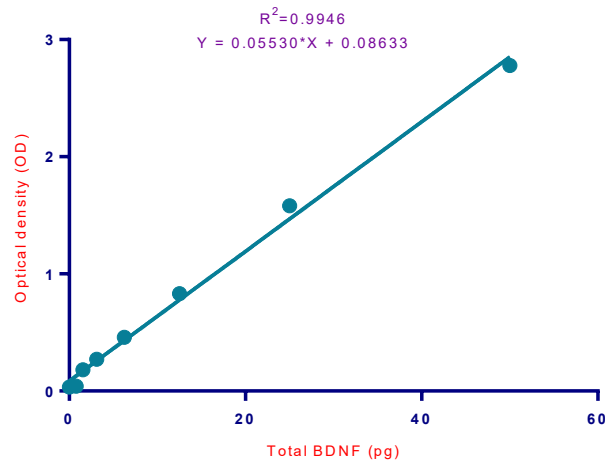


Figure 12 Standard plot for Total BDNF dilutions 15.6 pg/mL-1000 pg/mL made from BDNF standard with an R^2 value=0.9946. Unknown concentrations of the BDNF from samples analyzed were obtained from fitting the unknown values into the above standard plot

***In vivo* topical application studies of pLPXs in a CD1 mice model**

A pilot experiment was carried out to evaluate the topical delivery of gWIZ-GFP plasmid using the 18-7N(p₅)-18 pLPXs, 18-7NH-18 LPX, Lipofectamine[®] 3000 and saline controls.

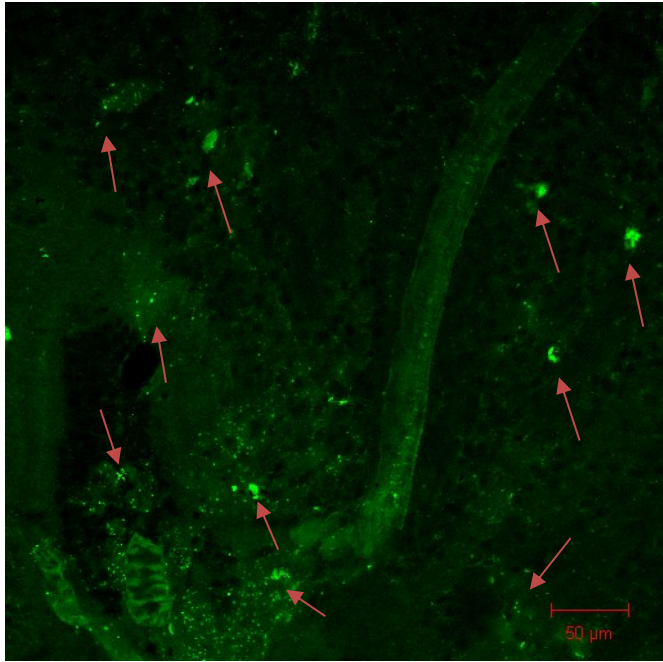
Five μL doses containing $0.5\mu\text{g}$ DNA were applied into each eye two times a day for 5 days, 6-week old male CD1[®] mice (Charles River) which were randomly assigned to three experimental groups as follows Group 1 saline control (2 mice, n=4 eyes), Group 2 with topical treatment 18-7NH-18 5:1:1 LPXs (3 mice, n=6 eyes) and Group 3 topical treatment with 18-7N(p₅)-18 5:1:1 pLPXs (3 mice, n=6 eyes).

For topical application, mice were restrained by grabbing the ventral superficial skin by hand to allow the eyes pop out to easily apply the $5\mu\text{L}$ topical doses two times a day for 5 days using a micropipette. The animals were held for 10-15 seconds before releasing them into their cages and kept busy for another 30 seconds, to avoid eye scratching and rubbing events allow the dose to spread completely in the eye. Other ophthalmic drops or ointments were not applied before or after the formulation to minimize interference with absorption of the test formulations. Animals were euthanized on Day 6, eyes were collected and placed in 4% PFA for 2 hours on a rotary shaker.

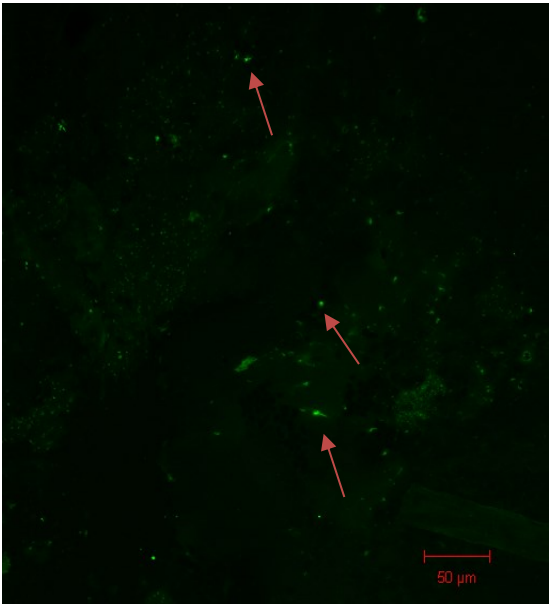
Three eyes from Group 2 and 3 and 2 eyes from Group 1 were removed for isolation of retina under a stereomicroscope and whole mounts are prepared. The remaining 3 eyes from each Group 2 and 3 and one from Group 1 were transferred to 20% sucrose solution for overnight fixation. Eyes were later embedded into cryosectioning molds using OCT medium and frozen (-20°C) till further cryosectioning using Thermo-Microm manual cryostat. The whole mount retinas isolated from the eyes from Group 2 (18-7N(p₅)-18 5:1:1 pLPXs) and Group 3 (18-7NH-18 5:1:1 LPXs) were examined for GFP expression using CLSM (Carl-Zeiss AG).

In an explorative studies, CD1 mice received $5\mu\text{L}$ doses of 18-7N(p₅)-18 7.5:1:1 pLPXs (7.5:1:1, pG:P:L) and 18-7NH-18 7.5:1:1 LPXs (7.5:1:1 ratio of G:P:L and gWIZ-GFP $0.5\mu\text{g}$ DNA/dose) twice a day for five days by topical application. The confocal microscopic examination of the isolated retinas indicated that mice treated with 18-7N(p₅)-18 7.5:1:1 pLPXs have shown good GFP expression at the

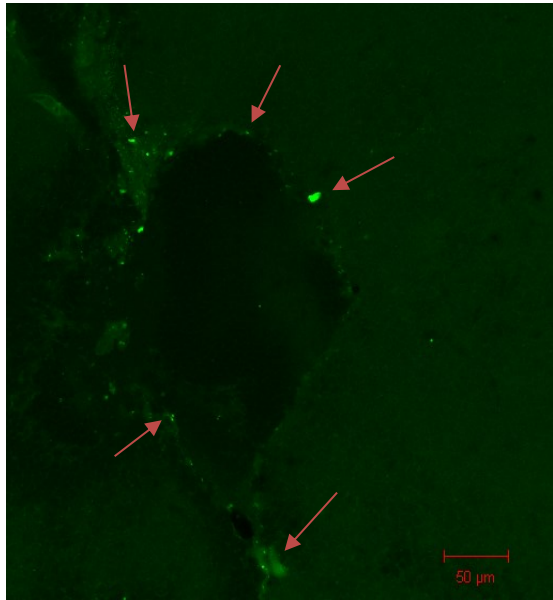
optic disc area where mostly the RGC converge to form an optic bundle, also the GFP expression was noticed in various other parts of the retina marked with red arrow heads. 18-7NH-18 7.5:1:1 LPXs treated retinas have also shown GFP expression mostly near to the optic disc area and can be seen under Appendix 2 Figure 13 F and G. Comparatively with 18-7NH-18 7.5:1:1 LPXs treated eyes, 18-7N(p₅)-18 7.5:1:1 pLPXs treated retinas have higher gene expression when observed. All the positive transfection areas were marked with red arrow heads in the images captured. Saline treated controls have not shown any autofluorescence in the retinal layers and the autofluorescence was normalized by capturing images at the same laser power and using similar gains to obtain true GFP expression data compared to controls (H and I). GFP expression was observed with both the treated retinas but the expression in 18-7NH-18 7.5:1:1 LPXs treated retina was confined mostly to the optic disc cup and was also in a lower amount compared to the 18-7N(p₅)-18 7.5:1:1 pLPXs treated retinas where the GFP expression is observed at various areas of the whole retina and has distributed in the other retinal layers. All imaged were obtained without any nuclei or cell staining, increased amount of autofluorescence in the treated retinal whole mounts has been observed. (Data is shown under below figures).



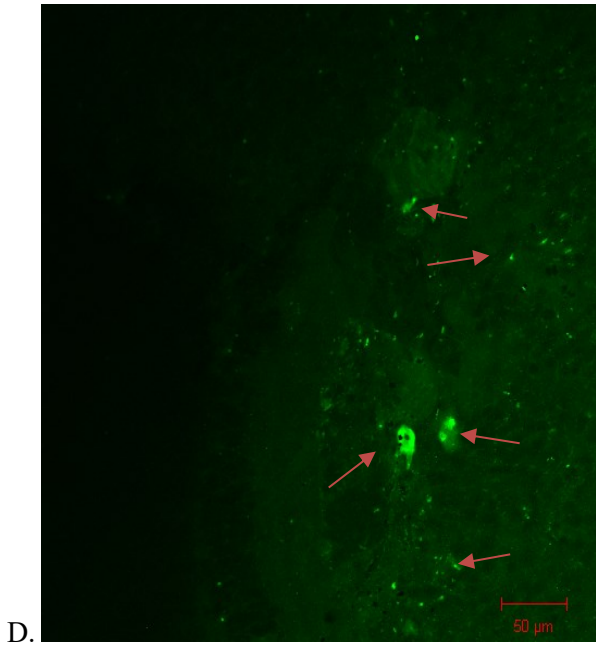
A.



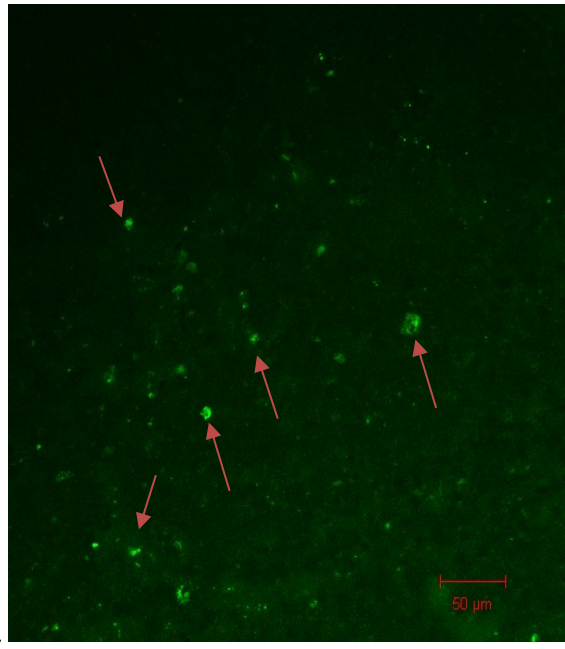
B.



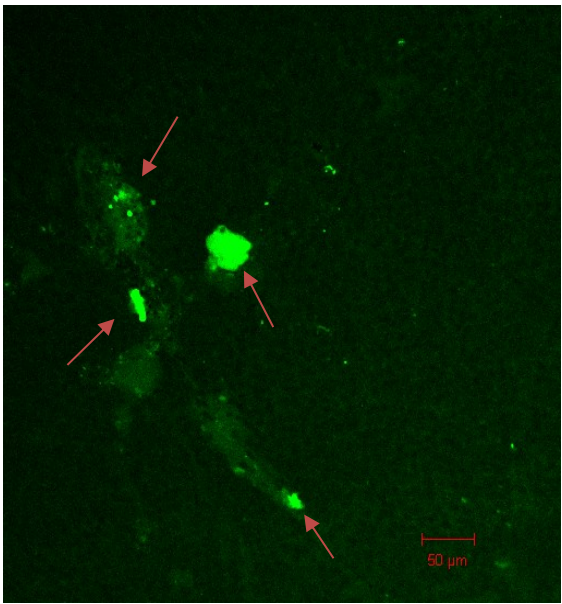
C.



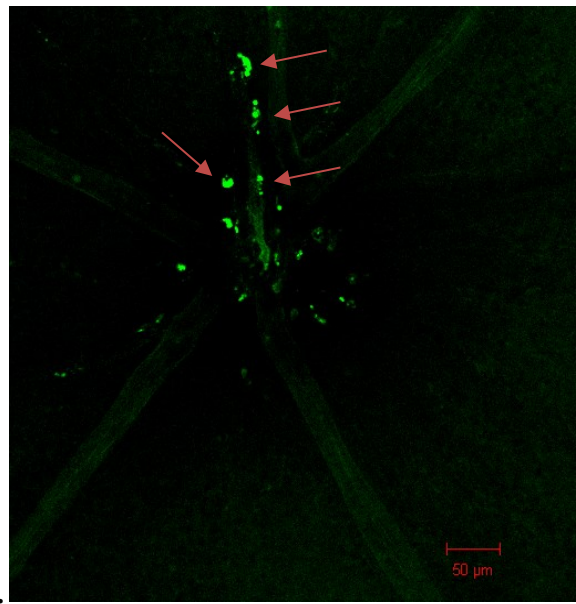
D.



E.



F.



G.

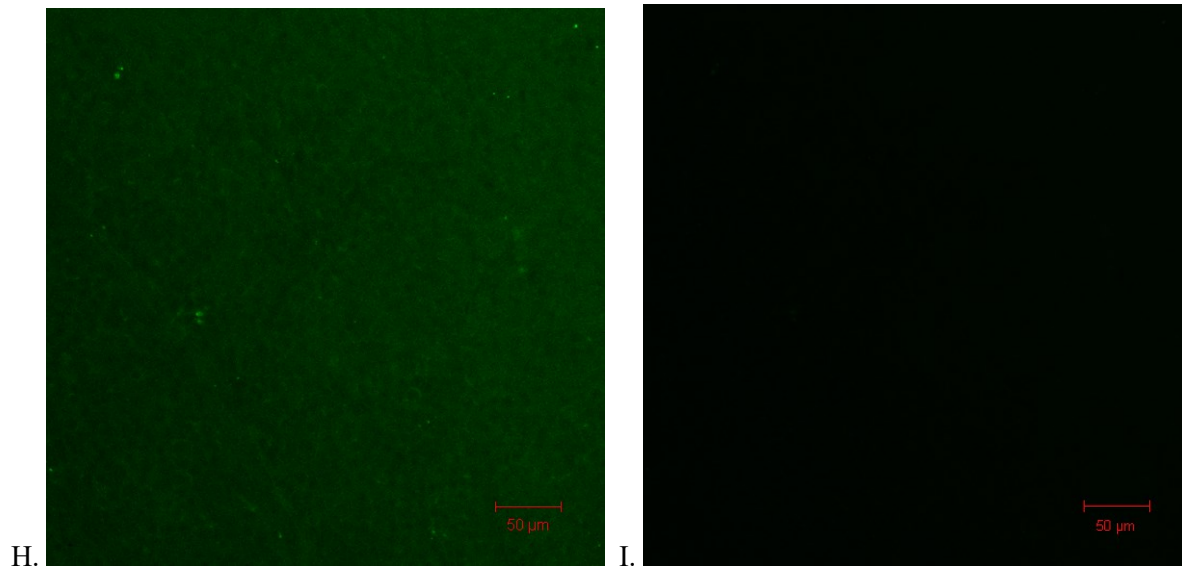


Figure 13 Evaluation of 18-7NH-18 LPXs and 18-7N(p₅)-18 pLPXs as retinal gene delivery agents after topical application in a CD1 mice model. Image A, B, C, D and E shows 18-7N(p₅)-18 LPXs treated retinas, retinal whole mount imaged using GFP channel (only few GFP expression spots were marked with red arrow heads), Image (C) shows gene expression around the optic disc area, Image (D, E) shows GFP expression on the RGC layers, Images (F, G) were treated with 18-7NH-18 LPXs retinal whole mounts imaged using GFP channel (only few GFP expression spots were marked with red arrow heads), Saline control image (H) using GFP channel at increased contrast setting to assess tissue autofluorescence, Saline control (I) imaged at a baseline contrast setting (used to image treated retinas), images did not show any autofluorescence.

Appendix 3 Assessment of IgSF-peptide modified gemini surfactants as potential cell surface binding entities to integrins and IgCAMs: An *in silico* molecular docking study- Exploratory study

Introduction

In our previous chapter we demonstrated that having a functional peptide moiety conjugated onto a gemini surfactant can improve gene delivery to retinal cells in eye. The peptide moieties are expected to improve the delivery of therapeutic genes due to improved binding with cell surface proteins bearing integrins and Ig-like domains expressed within the retinal cell population. There are many target proteins expressed in retinal cells such as integrins (230, 267), L1-CAM (276), TrKB (45, 274), while myelin protein zero (P₀) (328) is expressed during the growth and injury to the axonal structures of the RGCs. These expressed proteins help in the repair and growth of the damaged neurons and RGCs and also maintain general homeostasis of the retinal cell layers. Hence, we have identified five CAMs, such as integrin-binding (RGD, (p₁) (230, 235, 329, 330)) and IgSF-peptides such as RLE (p₂) (204), FASNKL (p₃)(276, 277, 331), LI (p₄) (272, 273) and YTDNGTF (p₅)(269-271, 328)) that can elicit homophilic and heterophilic interactions with other CAMs including Ig-like molecules. The peptides were conjugated onto 2nd generation gemini surfactant molecules and have been successfully tested to deliver therapeutic DNA to retinal cells in eye (Chapter 4).

Molecular docking studies have been used as a tool to screen ligands and chemical entities to identify their binding affinity to target proteins. Programs such as AutoDock, DOCK, FLOG, GOLD, SLIDE have been used over past decade and many new algorithms have been developed such as GLIDE (332) and CDOCKER (333). With the availability of high-resolution protein structures, identifying targets that bind with a specific peptide structure can be carried out by subjecting the peptide ligand molecule and the protein structure to the docking algorithm and ranking the ligand molecules based on their

binding affinity. This can often be adapted as a first-line technique to identify the lead targets and screen the top ligand candidates for efficiency (334). There is no doubt that the success of molecular docking studies depends on the availability of a pre-existing database; in this case databases such as proteins, nucleic acids, ligands in higher resolution can help in achieving the best target hits for ligands. Force-field based scoring functions have been developed that can be used to score the molecules based on their interaction and binding energies in docking studies (335). With the use of the molecular docking studies, the molecular confirmations of ligand binding with the protein at various active sites, charge interactions, hydrogen bonding, hydrophobic and pi-alkyl interactions can be determined.

Rationale and objective

The presence of RGD or IgSF-peptide modification on the gemini surfactant (m-7N(p₁₋₅)-m, m=C₁₈) can enhance interactions with integrins or Ig-like cell surface proteins expressed in the retinal cells of the eye. As shown in Chapter 4, NPs made from m-7N(p₁₋₅)-m improve the delivery of therapeutic DNA compared to NPs made from unmodified-gemini surfactants.

As a pilot study to explore whether molecular docking can be used to predict the binding properties of peptide-modified gemini surfactants we used peptide 1 (RGD) and 18-7N(p₁)-18 as a prototype for *in silico* molecular docking studies with its known target, 1L5G integrin protein. IgSF peptide (p₃) FASNKL and 18-7N(p₃)-18 gemini surfactant were selected from the IgSF class to identify potential cell adhesion properties with other Ig-CAMs, FASNKL peptide (L1 sequence responsible for binding with Neuropilin-1 (NP-1)) contain Ig like domains and acts like an L1-CAM mimetic. L1-CAM peptides have binding affinity to NP-1 transmembrane protein a complex of Sema 3A together and prevents endocytosis (336). The L1-CAM peptides also have affinity to bind to other Ig-like domains (homophilic adhesion-similar type of Ig-like domains) and also towards the integrins and carbohydrates (heterophilic interaction) (290, 337). Due to the non-availability of a pure crystal structure of NP-1 the

molecular docking studies were only carried out on integrin proteins (1L5G) to at least identify their binding affinity to the integrin ($\alpha\text{v}\beta\text{3}$) 1L5G.

This approach may be adapted to test large libraries of peptide modified compounds in the future.

Materials and Methods

Chem Draw 18.0 (Perkin Elmer, Santa Clara, CA, USA), BIOVIA Discovery Studio (Dassault Systems, San Diego, CA, USA), Research Collaboratory for Structural Bioinformatics (RCSB)- Protein Data Bank (PDB files)- Integrin ($\alpha\text{v}\beta\text{3}$) (1L5G), Ligands- Chem Draw structures (.sdf files) of 18-7NH-18 gemini surfactant (*N,N'*-(azanediylbis(propane-3,1-diyl))bis(*N,N*-dimethyldodecan-1-aminium) (Batch: FL18GLN-053117-RX9-001) was synthesized in-house, p₁ peptide (RGD), p₃ peptide (FASNKL), 18-7N(p₁)-18 gemini surfactant and 18-7N(p₃)-18 gemini surfactants were synthesized by Celtek peptides, TN, USA.

Molecular docking studies- binding interactions assessment of IgSF-peptides and their conjugated gemini surfactant derivatives

Based on the results in Chapter 4, the binding affinity and non-bonding interaction of two peptide modified gemini surfactants (18-7N(p₁)-18 and 18-7N(p₃)-18 and the respective peptides alone (p₁ and p₃) along with parent control 2nd generation 18-7NH-18 gemini surfactant with the integrin ($\alpha\text{v}\beta\text{3}$), PDB ID: 1L5G (338), were assessed in this part of the study. The high-resolution X-ray crystallographic structure of integrin protein ($\alpha\text{v}\beta\text{3}$) was obtained from RCSB-PDB (PDB ID:1L5G). The protein was prepared for docking by removing any already docked ligands leaving only the protein structure and minimization of energy of the 1L5G integrin protein with a steepest-descent protocol was carried out using BIOVIA Discovery Studio (Dassault Systems). Ligand molecules were sketched using Chem Draw (PerkinElmer) and imported into Discovery Studio to prepare for docking. CHARMM forcefield was applied and energy minimization was carried out using steepest descent protocol with 1000

iterations. After minimizing energy for both protein and ligand molecules, ligand-protein interaction studies were carried out by defining the active site. Ligand binding site of 75Å was selected as a large active site grid, which allows for ligand modelling all over the active sites in the 1L5G integrin protein, and the best iterations were reported. Molecular docking was carried out using the ‘receptor-ligand interactions’ module. CDOCKER algorithm was used to find the most appropriate binding sites and interactions for 18-7NH-18 gemini surfactant, p₁ peptide (RGD), p₃ peptide (FASNKL), 18-7N(p₁)-18 and 18-7N(p₃)-18 gemini surfactants. The docked ligand confirmations were ranked based on the CDOCKER energy scores. Polar and non-polar interactions were also analyzed, and all the important interactions displayed by the ligand were visualized.

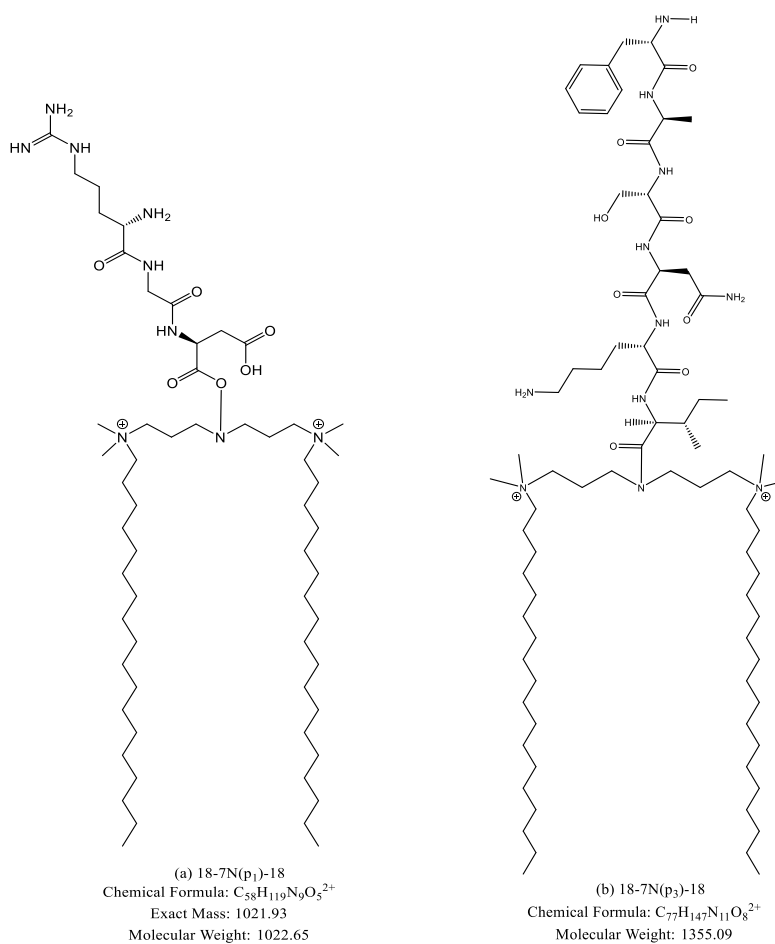
Results

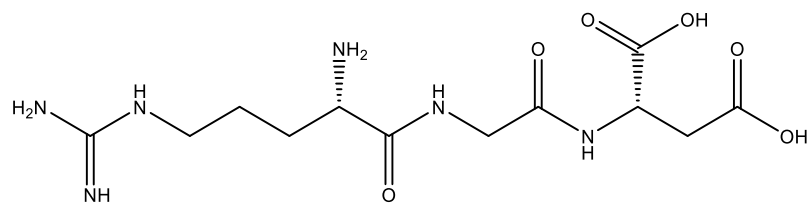
Assessment of binding affinity and interactions of IgSF-peptides (p₁ and p₃) and their conjugated gemini surfactants

Molecular docking studies of 18-7NH-18, 18-7N(p₁)-18, 18-7N(p₃)-18 gemini surfactants, p₁ and p₃ peptide ligands (Figure 14 **Figure 14** a-d) with the integrin protein ($\alpha\text{v}\beta\text{3}$) 1L5G was successfully carried out and the results obtained have shown the binding affinity of each of the ligand molecule with the integrin protein. All the non-bonding interactions of the ligand molecule with the amino acids of the integrin protein were identified and a total of 10 hits with the highest CDOCKER energy were reported. The 18-7NH-18 gemini surfactant docked on to the integrin receptor had a CDOCKER energy score of -27.95. Some of the non-bonding interaction for this ligand molecule were hydrogen bonding with Met301 (Bond length (BL): 2.76 Å), ASN332(BL): 2.88 Å) and hydrophobic interaction between alkyl groups of gemini and the ILE216 (BL: 4.93Å). Pi-alkyl interactions were also noted with HIS539 of the 1L5G integrin protein and alkyl groups of gemini surfactant (BL: 5.11 Å). The 18-7NH-18 gemini surfactant was oriented with the 1L5G integrin protein in such a way that the two alkyl tails

were placed between the α and β subunit and the interaction appeared to be mostly with the superficial amino acids and not from inside the cavity core between the α and β propeller subunits (Figure 15 **Figure 15**). The non-bonding interaction results for 18-7NH-18 docking and the interactions present were presented in Table 3.

Peptides p_1 and p_3 were also docked on to the 1L5G integrin protein, for p_1 peptide the CDOCKER energy was found to be -64.33 and CDOCKER interaction energy of -46.50 Kcal/mol.

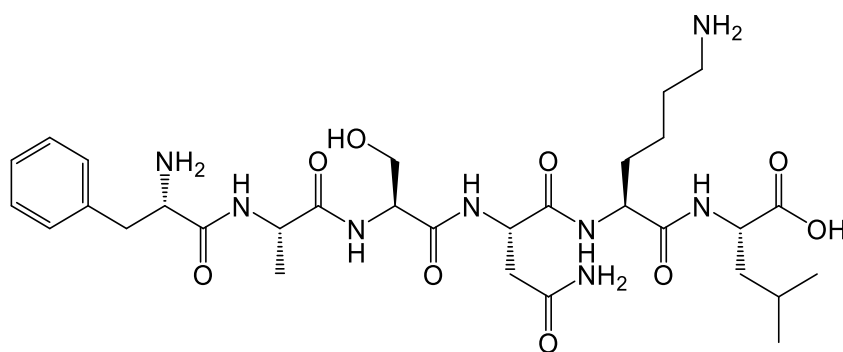




(c) p₁-RGD Peptide

Chemical Formula: C₁₂H₂₂N₆O₆

Molecular Weight: 346.34



(d) p₃-FASNKL peptide

Chemical Formula: C₃₁H₅₀N₈O₉

Molecular Weight: 678.79

Figure 14 Ligand molecules selected for docking on to 1L5G integrin protein using BIOVIA Discovery Studio with CHARMM forcefield and CDOCKER algorithm. (a) 18-7N(p₁)-18, (b) 18-7N(p₃)-18, (c) p₁ peptide (RGD) and (d) p₃ peptide (FASNKL). The 2D structures were sketched using Chem Draw.

The major non-bonding interactions were hydrogen bonding with GLN271(BL: 2.63Å), ARG303 (BL:2.71Å), GLN 314 (BL:2.52Å), ASN332 (BL:2.86), ARG 563 (BL:2.65Å), ARG303 (BL:1.75). Electrostatic interactions between H39 of p₁ peptide-ASP302 (BL:1.93Å) and O23 of p₁ peptide-LYS330 (BL:4.96) were also noted with the 1L5G integrin protein (Figure 16 c, d). All the non-bonding interactions of the p₁ peptide were shown in Table 4. CDOCKER and binding energies for 18-7NH-18 gemini surfactant docked onto 1L5G integrin protein were found to be -27.95 and -54.83 Kcal/mol, respectively.

Table 3 List of top hits and non-bonding interactions between 18-7NH-18 ligand and 1L5G integrin protein identified by docking using CDOCKER algorithm

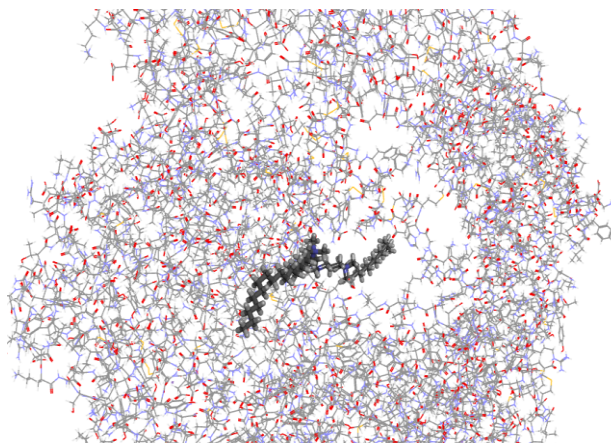
a. Top hits from docking the 18-7NH-18 ligand to 1L5G

Top hits	Peptide conformation	(-) CDOCKER energy	(-) CDOCKER interaction energy (Kcal/mol)
1	18-7NH-18_final_molecule	27.9537	54.8397
2	18-7NH-18_final_molecule	25.5525	47.6708
3	18-7NH-18_final_molecule	23.4255	58.8757
4	18-7NH-18_final_molecule	23.4225	50.8261
5	18-7NH-18_final_molecule	23.3994	50.686
6	18-7NH-18_final_molecule	23.1355	50.2547
7	18-7NH-18_final_molecule	22.8687	42.3297
8	18-7NH-18_final_molecule	22.3544	46.1682
9	18-7NH-18_final_molecule	20.4942	53.6812
10	18-7NH-18_final_molecule	20.4693	49.0691

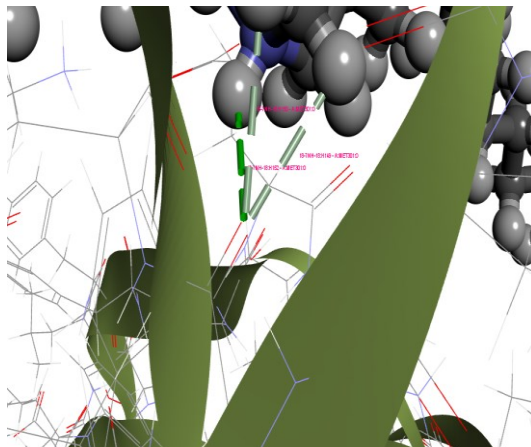
b. Non-bonding interactions between 18-7NH-18 ligand and 1L5G protein

Non-bond interactions	Bond length (Å)	Bond Type	Interaction	Donor group	Function	Acceptor group	Function
18-7NH-18:H152 - A:MET301:O	2.76	Hydrogen	Conventional Hydrogen Bond	18-7NH-18:H152	H-Donor	A:MET301:O	H-Acceptor
18-7NH-18:C29 - A:ILE216	4.93602	Hydrophobic	Alkyl	18-7NH-18:C29	Alkyl	A:ILE216	Alkyl
B:HIS539 - 18-7NH-18:C47	5.11899	Hydrophobic	Pi-Alkyl	B:HIS539	Pi-Orbitals	18-7NH-18:C47	Alkyl

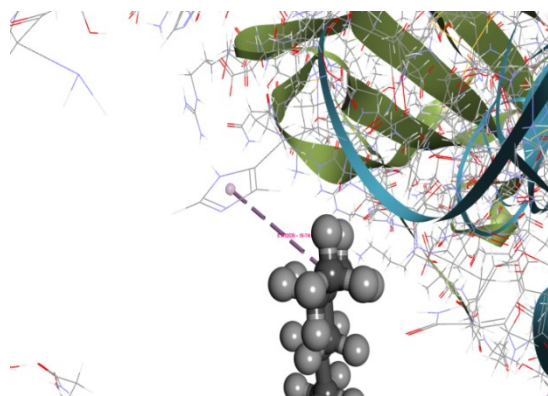
a. Docked ligand with the 1L5G protein



b. Hydrogen bonding with MET301



c. Hydrophobic Pi-Alkyl interaction with HIS539
ILE216



d. Hydrophobic Interaction-Alkyl with

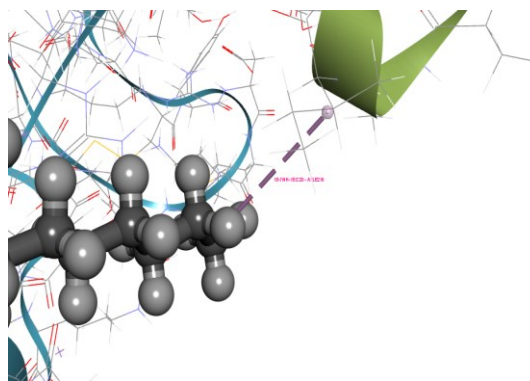


Figure 15 Docking of 18-7NH-18 ligand to 1L5G integrin protein and non-bonding interactions. a. 18-7NH-18 ligand docked between the α and β subunits, b. Hydrogen bonding interaction with MET301, c. Pi-Alkyl interaction between HIS539 and C47 of the ligand, d. Hydrophobic interaction between ILE216 and C29 of the ligand.

Table 4 List of top hits and non-bonding interactions between p₁ (RGD) peptide and 1L5G identified by docking using CDOCKER algorithm

a. Top hits from docking p₁ peptide to 1L5G protein

Top hits	Peptide conformation	(-) CDOCKER energy	(-) CDOCKER interaction energy (Kcal/mol)
1	RGD_peptide_1	64.3384	46.5078
2	RGD_peptide_1	64.2923	46.165
3	RGD_peptide_1	63.1076	45.3192
4	RGD_peptide_1	62.451	44.6273
5	RGD_peptide_1	60.3128	44.2566
6	RGD_peptide_1	60.0094	37.3512
7	RGD_peptide_1	59.6255	40.1807
8	RGD_peptide_1	56.8117	40.4812
9	RGD_peptide_1	56.6701	36.0673
10	RGD_peptide_1	56.5529	38.3077

b. Non-bonding interactions of p₁ peptide docked in to 1L5G protein

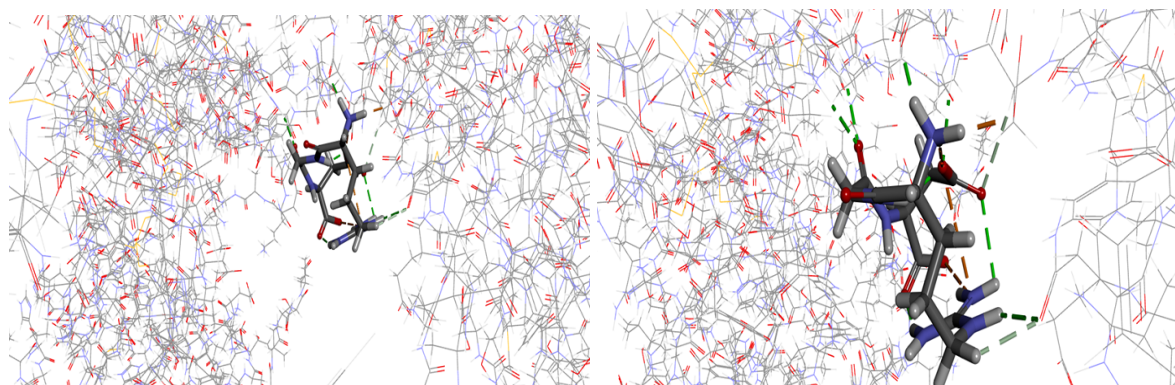
Non-bond interactions	Bond length (Å)	Bond Type	Interaction	Donor group	Function	Acceptor group	Function
RGD_peptide_1:H3 9 - A:ASP302:OD2	1.93	Hydrogen Bond;Electrostatic	Salt Bridge;Attractive Charge	RGD_peptide_1:H39	H-Donor;Positive	A:ASP302:OD2	H-Acceptor;Negative

RGD_peptide_1:H4 2 - RGD_peptide_1:O2 3	1.91	Hydrogen Bond; Electrostatic	Salt Bridge;Attrac tive Charge	RGD_peptide _1:H42	H- Donor;Po sitive	RGD_peptide_1: O23	H- Acceptor; Negative
A:LYS330:NZ - RGD_peptide_1:O2 3	4.96	Electrostatic	Attractive Charge	A:LYS330:N Z	Positive	RGD_peptide_1: O23	Negative
A:GLN271:HE22 - RGD_peptide_1:O2 4	2.63	Hydrogen Bond	Conventional Hydrogen Bond	A:GLN271:H E22	H-Donor	RGD_peptide_1: O24	H- Acceptor
A:ARG303:HE - RGD_peptide_1:O1 7	2.71	Hydrogen Bond	Conventional Hydrogen Bond	A:ARG303:H E	H-Donor	RGD_peptide_1: O17	H- Acceptor
A:GLN314:HE22 - RGD_peptide_1:O2 3	2.52	Hydrogen Bond	Conventional Hydrogen Bond	A:GLN314:H E22	H-Donor	RGD_peptide_1: O23	H- Acceptor
A:ASN332:HD22 - RGD_peptide_1:O1 3	2.86	Hydrogen Bond	Conventional Hydrogen Bond	A:ASN332:H D22	H-Donor	RGD_peptide_1: O13	H- Acceptor
B:ARG563:HH12 - RGD_peptide_1:O2	2.65	Hydrogen Bond	Conventional Hydrogen Bond	B:ARG563:H H12	H-Donor	RGD_peptide_1: O2	H- Acceptor
RGD_peptide_1:H3 8 - A:ARG303:O	1.75	Hydrogen Bond	Conventional Hydrogen Bond	RGD_peptide _1:H38	H-Donor	A:ARG303:O	H- Acceptor
RGD_peptide_1:H4 0 - A:ASN332:OD1	2.02	Hydrogen Bond	Conventional Hydrogen Bond	RGD_peptide _1:H40	H-Donor	A:ASN332:OD1	H- Acceptor

RGD_peptide_1:H4 1 - A:ASN332:OD1	2.11	Hydrogen Bond	Conventional Hydrogen Bond	RGD_peptide _1:H41	H-Donor	A:ASN332:OD1	H- Acceptor
RGD_peptide_1:H4 2 - RGD_peptide_1: O13	2.67	Hydrogen Bond	Conventional Hydrogen Bond	RGD_peptide _1:H42	H-Donor	RGD_peptide_1: O13	H- Acceptor
RGD_peptide_1:H4 3 - RGD_peptide_1: O22	1.93	Hydrogen Bond	Conventional Hydrogen Bond	RGD_peptide _1:H43	H-Donor	RGD_peptide_1: O22	H- Acceptor

a. p₁ peptide docked between α and β subunits

b. p₁ peptide interactions with 1L5G



c. Salt-bridge: attractive charge (ASP302:OD2)

d. Hydrogen-bond interactions between p₁:1L5G

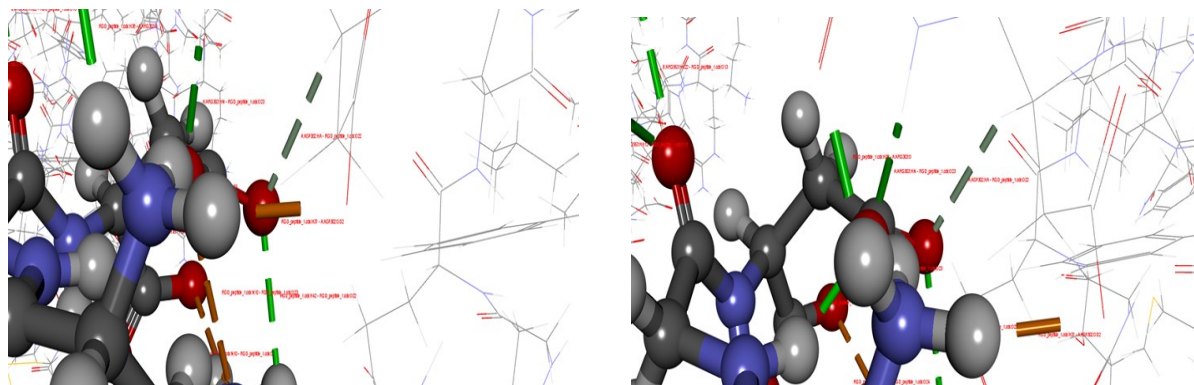


Figure 16 Docking of p₁ peptide to 1L5G integrin protein and non-bonding interactions. (A, B) p₁ peptide docked between α and β subunits of 1L5G integrin protein (C, D) Electronic and hydrogen bonding interactions between p₁ peptide and 1L5G integrin protein.

The strong binding of p₃ peptide was observed within the cavity of the integrin protein 1L5G between both the α_v and β₃ subunits (Figure 17 a, b). Electrostatic interaction between p₃ peptide (FASNKL): 1L5G receptor protein were H88-GLU270 (BL:2.91Å), N39-ASP302 (BL:4.07Å), hydrogen bonding interactions identified were ARG303-O22 (BL:2.53Å), LYS330-O29 (BL:1.87Å), H86-GLU270 (BL:1.72Å). Few other interactions were also observed such as the Pi-Sulfur interaction between MET272-Pi orbitals of p₃ peptide (BL:5.85Å) and alkyl interaction between C46-LYS330 (BL:5.07 Å). All the interactions obtained were listed under Table 5. The peptide conjugated 18-7N(p₁)-18 and 18-7N(p₃)-18 ligands were also docked on to 1L5G protein

Table 5 List of top hits and non-bonding interactions between p₃ (FASNKL) peptide and 1L5G identified by docking using CDOCKER algorithm

a. Top hits from docking p₃ peptide and 1L5G protein

Top hits	Peptide conformation	(-) CDOCKER energy	(-) CDOCKER interaction energy Kcal/mol
1	FASNKL_peptide	89.4801	59.7153

2	FASNKL_peptide	89.461	54.3412
3	FASNKL_peptide	82.3538	45.7394
4	FASNKL_peptide	81.2339	45.1971
5	FASNKL_peptide	80.7824	48.0119

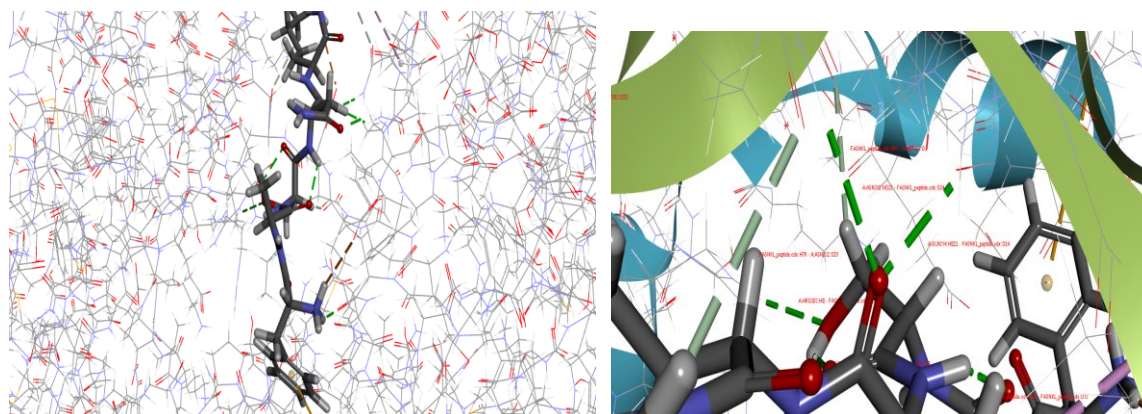
b. Non-bonding interactions between p₃ peptide and IL5G protein

Non-bond interactions	Bond length (Å)	Bond Type	Interaction	Donor group	Function	Acceptor group	Function
FASNKL_peptide:H88 - A:GLU270:OE2	2.9166	Hydrogen Bond;Electrostatic	Salt Bridge;Attractive Charge	FASNKL_peptide:H88	H-Donor;Positive	A:GLU270:OE2	H-Acceptor;Negative
FASNKL_peptide:N39 - A:ASP302:OD2	4.07733	Electrostatic	Attractive Charge	FASNKL_peptide:N39	Positive	A:ASP302:OD2	Negative
A:ARG303:HE - FASNKL_peptide:O22	2.53577	Hydrogen Bond	Conventional Hydrogen Bond	A:ARG303:HE	H-Donor	FASNKL_peptide:O22	H-Acceptor
A:GLN314:HE22 - FASNKL_peptide:O24	2.0902	Hydrogen Bond	Conventional Hydrogen Bond	A:GLN314:HE22	H-Donor	FASNKL_peptide:O24	H-Acceptor

A:LYS330:HZ2 - FASNKL_peptide:O29	1.87446	Hydrogen Bond	Conventional Hydrogen Bond	A:LYS330:HZ2	H-Donor	FASNKL_peptide:O29	H-Acceptor
A:ASN332:HD22 - FASNKL_peptide:O24	2.44996	Hydrogen Bond	Conventional Hydrogen Bond	A:ASN332:HD22	H-Donor	FASNKL_peptide:O24	H-Acceptor
FASNKL_peptide:H86 - A:GLU270:O	1.72275	Hydrogen Bond	Conventional Hydrogen Bond	FASNKL_peptide:H86	H-Donor	A:GLU270:O	H-Acceptor
A:MET272:SD - FASNKL_peptide	5.85488	Other	Pi-Sulfur	A:MET272:SD	Sulfur	FASNKL_peptide	Pi-Orbitals
FASNKL_peptide:C46 - A:LYS330	5.07907	Hydrophobic	Alkyl	FASNKL_peptide:C46	Alkyl	A:LYS330	Alkyl

a. p₃ peptide docking to 1L5G

b. H-bonding interactions between p₃:1L5G



c. Electrostatic interactions between p₃:1L5G

d. Pi-Sulfur interactions between p₃:1L5G

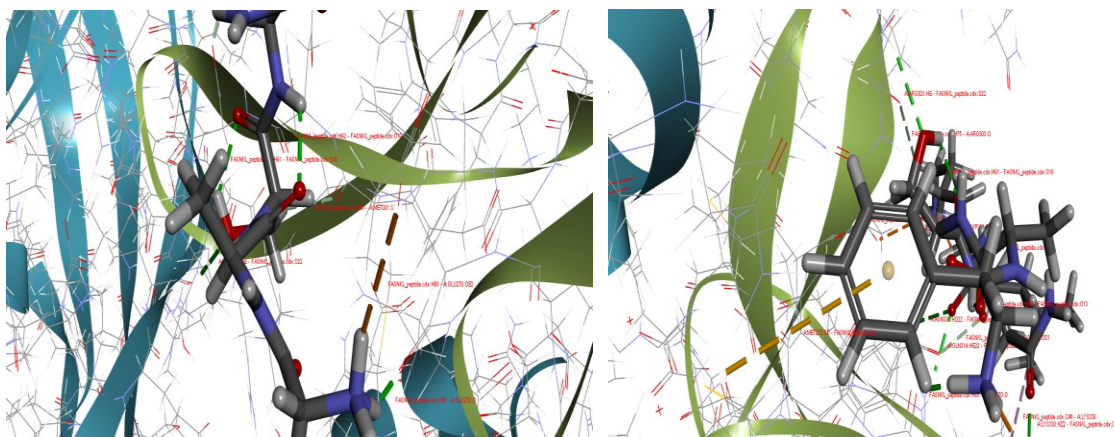


Figure 17 Docking of p₃ peptide to 1L5G integrin protein and non-bonding interactions. a. p₃ ligand molecule docked into the cavity of the $\alpha 5$ and $\beta 3$ subunits (b) Hydrogen bonding interactions of p₃:1L5G, (c) Electrostatic interactions between p₃ peptide and 1L5G and (d) Pi-Sulfur interactions between MET272 and Pi-orbitals of p₃ peptide.

Peptide conjugated gemini surfactants, 18-7N(p₁)-18 and 18-7N(p₃)-18, were also evaluated to identify their potential binding affinity towards 1L5G integrin protein. Docking studies demonstrate stronger binding affinity of 18-7N(p₁)-18 compared to p₁ peptide or 18-7NH-18. The CDOCKER energy of the best hit was found to be -83.02 Kcal/mol with a CDOCKER interaction energy value of -80.77 Kcal/mol. Hydrogen bonding was found to be the dominant binding interaction obtained from 18-7N(p₁)-18 docking on to 1L5G protein. Complete list of non-bonding interactions that arise from the 18-7N(p₁)-18 ligand docking onto the 1L5G integrin protein are listed in Table 6. These are hydrogen bonding between ligand: proteins such as O60:ARG303 (BL:2.92 Å), O68:ARG303 (BL:2.47 Å), O68:ARG303-HH21 (BL:2.00 Å), H186:GLU270 (BL:2.79), H188: GLU270 (BL:2.29 Å), and H128:ASN332-OD1 (BL:2.44 Å) (Figure 18).

Table 6 List of top hits and non-bonding interactions between 18-7N(p₁)-18 gemini surfactant and 1L5G integrin protein identified by docking using CDOCKER algorithm

a. Top hits from docking 18-7N(p₁)-18 ligand to 1L5G integrin protein

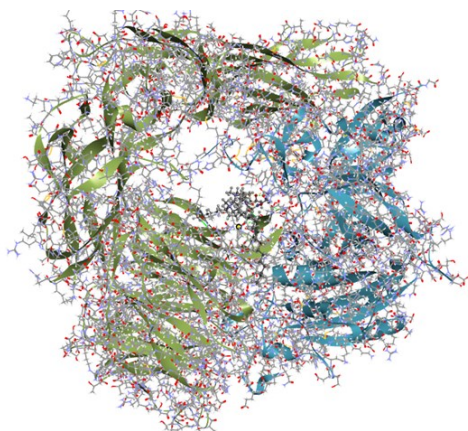
Top hits	Peptide conformation	(-) CDOCKER energy	(-) CDOCKER interaction energy Kcal/mol
1	18-7N(p ₁)-18	83.024	80.7795
2	18-7N(p ₁)-18	75.5032	69.3201
3	18-7N(p ₁)-18	65.9547	57.6342
4	18-7N(p ₁)-18	65.8202	78.2045
5	18-7N(p ₁)-18	65.3899	80.313
6	18-7N(p ₁)-18	63.6058	82.9474
7	18-7N(p ₁)-18	63.574	67.8352
8	18-7N(p ₁)-18	63.1893	69.9844
9	18-7N(p ₁)-18	62.3711	68.0847
10	18-7N(p ₁)-18	62.0203	62.9072

b. Non-bonding interactions between 18-7N(p₁)-18 ligand and 1L5G protein

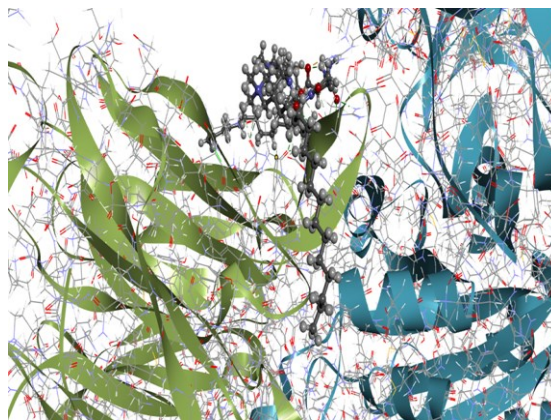
Non-bond interactions	Bond length (Å)	Bond Type	Interaction	Donor group	Function	Acceptor group	Function
A:ARG303:HN - 18-7N(RGD)-18_final_molecule:O60	2.92486	Hydrogen Bond	Conventional Hydrogen Bond	A:ARG303:HN	H-Donor	18-7N(RGD)-18_final_molecule:O60	H-Acceptor

A:ARG303:HE - 18-7N(RGD)- 18_final_molecule:O68	2.47255	Hydrogen Bond	Conventional Hydrogen Bond	A:ARG303:HE	H-Donor	18-7N(RGD)- 18_final_molecule:O68	H-Acceptor
A:ARG303:HH21 - 18-7N(RGD)- 18_final_molecule:O68	2.00892	Hydrogen Bond	Conventional Hydrogen Bond	A:ARG303:HH21	H-Donor	18-7N(RGD)- 18_final_molecule:O68	H-Acceptor
18-7N(RGD)- 18_final_molecule:H186 - A:GLU270:O	2.7953	Hydrogen Bond	Conventional Hydrogen Bond	18-7N(RGD)- 18_final_molecule:H186	H-Donor	A:GLU270:O	H-Acceptor
18-7N(RGD)- 18_final_molecule:H188 - A:GLU270:O	2.29769	Hydrogen Bond	Conventional Hydrogen Bond	18-7N(RGD)- 18_final_molecule:H188	H-Donor	A:GLU270:O	H-Acceptor

a. Docking of 18-7N(p₁)-18 ligand with 1L5



b. Alkyl tail interactions 18-7N(p₁)-18:1L5G



c. Hydrogen bonding H186:GLU270

d. Hydrogen bonding O60: ASP302, ARG303

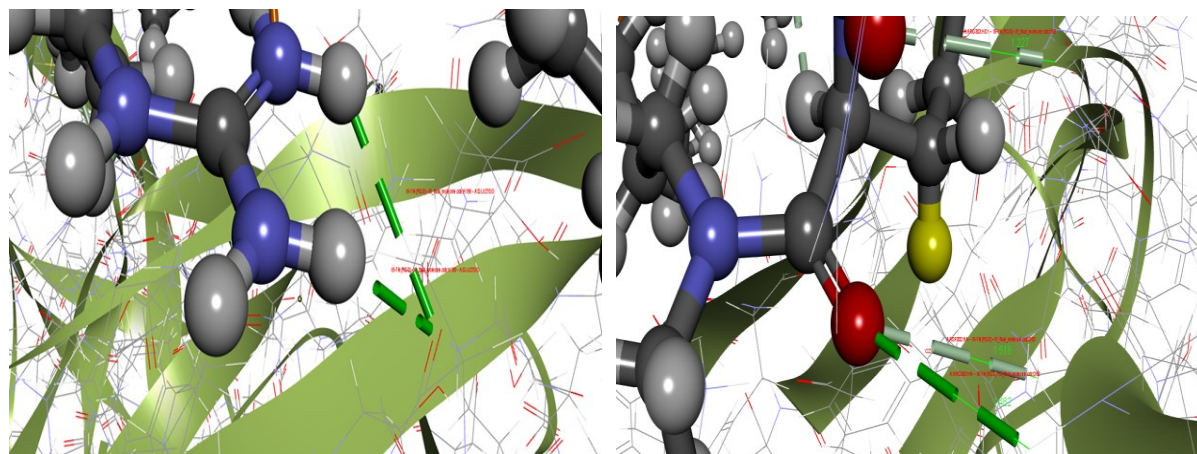


Figure 18 Docking of 18-7N(p₁)-18 gemini surfactant to 1L5G integrin protein and non-bonding interactions. a. 18-7N(p₁)-18 ligand molecule docked into the cavity of the α 5 and β 3 subunits and alkyl tails positioned over the subunits b. Alkyl tail interactions of 18-7N(p₁)-18:1L5G, c. Hydrogen bonding interactions between 18-7N(p₁)-18 and 1L5G (H186:GLU270), d. Hydrogen bonding interactions between 18-7N(p₁)-18 O60:1L5G-ASP302 and ARG303.

Docking studies for the 18-7N(p₃)-18 demonstrated stronger binding affinity compared to p₃ peptide and 18-7NH-18. The CDOCKER energy of the top hit was found to be -92.82 Kcal/mol with a CDOCKER interaction energy value of -100.116 Kcal/mol. Comparatively, CDOCKER energy and CDOCKER interaction energy of p₃ peptide were -89.48 –and 59.71 Kcal/mol, respectively. (Table 7a). Among non-bonding interactions, hydrogen bonding was predominant in the 18-7N(p₃)-18 docking, with some electrostatic and hydrophobic interactions also present (Figure 19). Electrostatic attractive interactions were found to be between (Ligand: Protein) N-GLU335 (BL:4.94 Å) and N-ASP302 (BL:5.26 Å). Alkyl hydrophobic interaction was identified between C-ARG303 (BL:4.27 Å). All other interaction were mostly hydrogen bonding between hydrogens of the ligand and oxygens of the amino acid of the 1L5G integrin protein with lower bond length between H-PHE334 (BL:1.80 Å), H-ASP302 (BL:2.01 Å) and H-GLY333 (BL:2.26 Å) all the other hydrogen bonding interactions were shown under (Table 7b).

Table 7 List of top hits and non-bonding interactions between 18-7N(p₃)-18 gemini surfactant and 1L5G integrin protein identified by docking using CDOCKER algorithm

a. Top hits for 18-7N(p₃)-18 gemini surfactant docking to 1L5G integrin protein

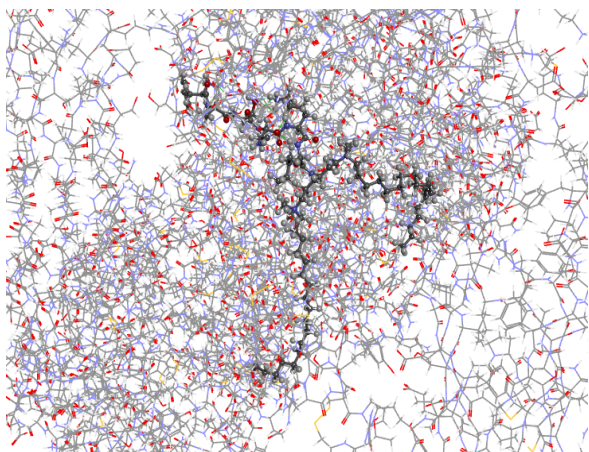
Top hits	Peptide conformation	(-) CDOCKER energy	(-) CDOCKER interaction energy Kcal/mol
1	18-7N(FASNKL)-18	92.82	100.11
2	18-7N(FASNKL)-18	90.39	103.39
3	18-7N(FASNKL)-18	87.45	94.37
4	18-7N(FASNKL)-18	77.88	82.310

b. Non-bonding interactions between 18-7N(p₃)-18 ligand and 1L5G integrin protein

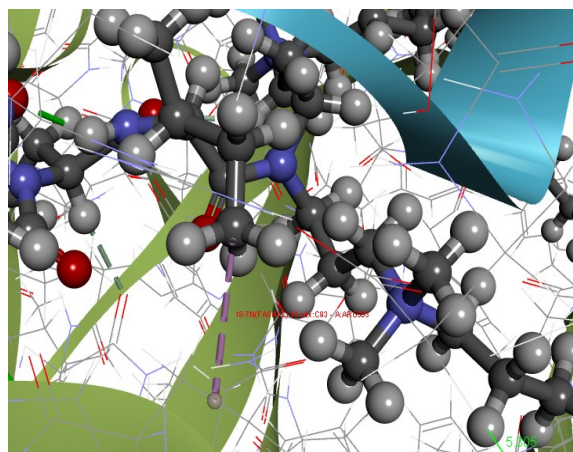
Non-bond interactions	Bond length (Å)	Bond Type	Interaction	Donor group	Function	Acceptor group	Function
18-7N(FASNKL)-18:N52 - A:GLU335:OE2	4.94	Electrostatic	Attractive Charge	18-7N(FASNKL)-18:N52	Positive	A:GLU335:OE2	Negative
18-7N(FASNKL)-18:N84 - A:ASP302:OD2	5.26	Electrostatic	Attractive Charge	18-7N(FASNKL)-18:N84	Positive	A:ASP302:OD2	Negative

18-7N(FASNKL)-18:H234 - A:PHE334:O	1.80	Hydrogen Bond	Conventional Hydrogen Bond	18-7N(FASNKL)-18:H234	H-Donor	A:PHE334:O	H-Acceptor
18-7N(FASNKL)-18:H238 - A:ASP302:OD2	2.013	Hydrogen Bond	Conventional Hydrogen Bond	18-7N(FASNKL)-18:H238	H-Donor	A:ASP302:OD2	H-Acceptor
18-7N(FASNKL)-18:H242 - A:GLY333:O	2.26	Hydrogen Bond	Conventional Hydrogen Bond	18-7N(FASNKL)-18:H242	H-Donor	A:GLY333:O	H-Acceptor
18-7N(FASNKL)-18:H243 - A:ASN332:O	2.48	Hydrogen Bond	Conventional Hydrogen Bond	18-7N(FASNKL)-18:H243	H-Donor	A:ASN332:O	H-Acceptor
18-7N(FASNKL)-18:H243 - A:GLY333:O	2.39	Hydrogen Bond	Conventional Hydrogen Bond	18-7N(FASNKL)-18:H243	H-Donor	A:GLY333:O	H-Acceptor
18-7N(FASNKL)-18:C93 - A:ARG303	4.27	Hydrophobic	Alkyl	18-7N(FASNKL)-18:C93	Alkyl	A:ARG303	Alkyl

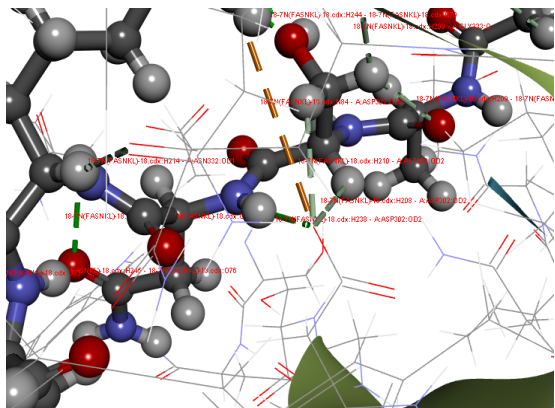
a. Docking of 18-7N(p₃)-18 with 1L5G



b. Hydrophobic interactions between C-ARG303



c. Electrostatic interactions N84-ASP302



d. Hydrogen bonding interactions

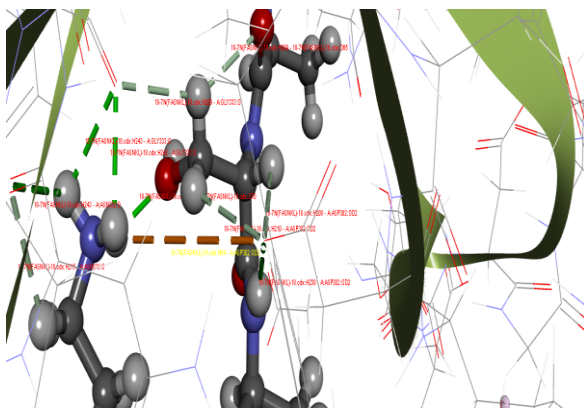


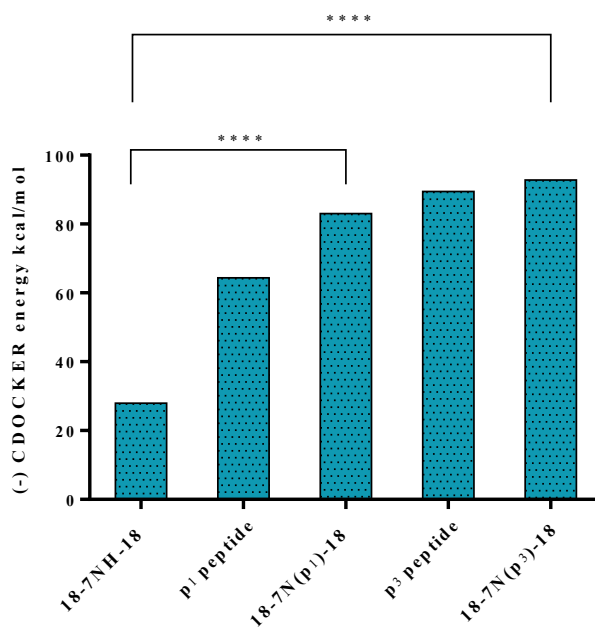
Figure 19 Docking of 18-7N(p₃)-18 gemini surfactant to 1L5G integrin protein and non-bonding interactions obtained. a. Docking of 18-7N(p₃)-18 with 1L5G, b. Hydrophobic interaction between alkyl tail and ARG303, c. Electrostatic interaction between N-ASP302 and the nitrogens N52 and N84 and d. Hydrogen bonding interactions.

Comparative analysis of the CDOCKER energies and binding energies showed that the 18-7N(p₃)-18 ligand molecules have shown significantly higher CDOCKER energy and CDOCKER interaction energy (-92.82 and -100.11 Kcal/mol, respectively) (***)*p*<0.0001, compared to 18-7NH-18 (-27.95

and -54.83 Kcal/mol, respectively). Also, the p₃ peptide had similar CDOCKER energy to 18-7N(p₃)-18 (-89.48) while the CDOCKER interaction energy was found to be -59.71 Kcal/mol.

Similarly, docking 18-7N(p₁)-18 ligand onto the 1L5G integrin protein produced a top with a CDOCKER energy of -83.02 and CDOCKER interaction energy of -80.77 Kcal/mol, which are significantly higher (****p<0.0001) compared to unconjugated 18-7NH-18 gemini surfactant ligand (-27.95 and -54.83 Kcal/mol, respectively) (Figure 20 a, b).

a.



b.

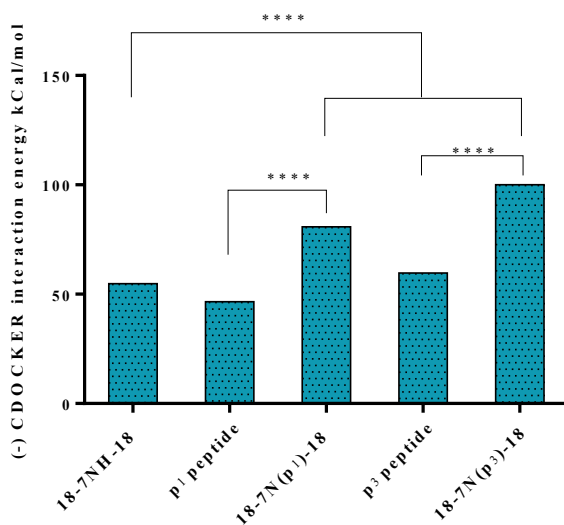


Figure 20 Comparative analysis of (-) CDOCKER energy and (-) CDOCKER interaction energy from molecular docking studies. a. comparative analysis of (-) CDOCKER energies of 18-7NH-18, p₁ peptide, 18-7N(p₁)-18, p₃ peptide and 18-7N(p₃)-18 ligands. 18-7N(p₃)-18, 18-7N(p₁)-18 demonstrated significantly higher CDOCKER energies compared to 18-7NH-18 and their respective peptides p₃ and p₁ peptide (****p<0.0001), b. comparative analysis of (-) binding energies of 18-7NH-18, p₁, p₃ peptides, 18-7N(p₁)-18 and 18-7N(p₃)-18 gemini surfactants, 18-7N(p₃)-18 and 18-7N(p₁)-18 ligands demonstrate a significant difference (****p<0.0001) compared to 18-7NH-18 and their respective peptides p₃ peptide and p₁ peptide (****p<0.0001).

Discussion

Molecular docking studies are a vital tool in drug target identification, screening and in identifying ligands with suitable binding affinities to target proteins. With the availability of high resolution X-ray crystallographic structures of proteins, and various molecular docking algorithms such as CDOCKER (Biovia Discovery Studio) (333), Libdock (Biovia Discovery Studio), GLIDE (Schrodinger) (332) were developed to simulate and optimize the binding interactions. In previous chapters we have demonstrated

the *in vitro* and *in vivo* TE of pNPXs made from selected ligands such as 18-7N(p₃)-18, 18-7N(p₁)-18 and 18-7NH-18.

The improvement in the TE was clearly evident with the pNPXs prepared from peptide modified gemini surfactants. p₁ peptide (RGD) is known to exhibit interaction with the integrin ($\alpha\text{v}\beta\text{3}$). Hence RGD peptide is conjugated on to 18-7NH-18 gemini surfactant to provide the specificity of binding with integrin protein that are highly expressed in the retinal layers of the eye. From the *in vitro* and *in vivo* results, it has been identified that p₁ peptide modified gemini surfactant has shown positive TE. Similarly, p₃ peptide (FASNKL) from IgSF sequences has been identified to improve the cell adhesion of the p₃ peptide sequence with the IgSF cell surface proteins such as L1-CAMs, it has to be noted in this study due to the lack of L1-CAMs protein x-ray crystallographic structures, we used integrin ($\alpha\text{v}\beta\text{3}$) PDB ID:1L5G to assess the interactions for 18-7N(p₃)-18 gemini surfactant as well along with 18-7N(p₁)-18. It has been reported that p₃ peptide is able to bind with integrin ($\alpha\text{v}\beta\text{3}$)(276). To better understand the interaction and adhesion of peptide modified ligands with cell surface integrin proteins and the possible mechanisms involved, *in silico* docking studies were carried out on parent molecule 18-7NH-18, p₁ peptide, p₃ peptide, 18-7N(p₁)-18 and 18-7N(p₃)-18. Docking studies for all the above ligands listed were carried out using CDOCKER algorithm using a grid-based molecular docking method that utilizes CHARMM forcefield. In this method the receptor is held rigid and the ligands were docked and are allowed to be flexible. The algorithm has generated the top hits for each of the ligand molecule docked on to the 1L5G protein and were ranked based on their interactions and CDOCKER energy was used as parameter by the software to rank the top 10 hits. The top hits and the interactions of all the 5 ligand molecules docked on to 1L5G have shown comparatively that 18-7N(p₃)-18 gemini surfactant ligand has the highest CDOCKER energy -92.82 kcal/mol with a CDOCKER interaction energy value of -100.116 kcal/mol obtained by docking compared to -27.95 kcal/mol and -89.48

kcal/mol CDOCKER energy and CDOCKER interaction energy of -54.83 kcal/mol and -59.71 kcal/mol for 18-7NH-18 and p₃ peptide respectively. Similarly, 18-7N(p₁)-18 showed a CDOCKER energy of -83.04 kcal/mol with the CDOCKER interaction energy of -80.77 kcal/mol compared to CDOCKER energy of -64.33 kcal/mol and a CDOCKER interaction energy of -46.50 kcal/mol for p₃ peptide.

The 18-7N(p₃)-18 gemini surfactant has shown hydrogen bonding interactions as major contributors of the interaction energies and other interactions such as electrostatic and hydrophobic interactions also contributed to the strong binding affinity to the protein. CDOCKER energy acts as a marker for the overall performance of binding of the 18-7N(p₃)-18 with the 1L5G integrin protein. The higher negative value represents stronger bond that is difficult to disrupt. The results clearly demonstrate that 18-7N(p₃)- possess the highest CDOCKER energy compared to any other ligand docked in this study, CDOCKER energies and binding energies for unmodified 18-7NH-18 gemini surfactant ligand indicate 5-fold and 2-fold higher binding affinity with values -27.95 kcal/mol and -54.83 kcal/mol, respectively. Similarly, 18-7N(p₁)-18 showed higher CDOCKER energy and CDOCKER interaction energy compared to 18-7NH-18 and p₁ peptide. These results demonstrate that the gemini surfactant without peptide modification does not possess higher interaction ability with the cell surface proteins, conjugation of peptides to gemini surfactants helped in retaining the interaction ability of the peptides with the integrin receptors and the superiority of the 18-7N(p₁)-18 and 18-7N(p₃)-18 compared to their unconjugated gemini and only peptides has been established. The *in silico* docking studies also helped in identifying the potential interaction involved in the binding and adhesion interactions of ligands with the 1L5G protein.

Conclusion

The molecular docking studies has shown that the p₃ peptide modified gemini surfactant (18-7N(p₃)-18 showed the highest CDOCKER and CDOCKER interaction energy compared to p₃ peptide and 18-

7NH-18 gemini surfactant similarly 18-7N(p₁)-18 showed higher CDOCKER energy compared to p₁ peptide and 18-7NH-18 gemini surfactant which is a non-conjugated form of gemini surfactant. These results demonstrate their superiority over the other peptide modified gemini surfactant molecules. The 5-fold increase in the CDOCKER energy and 2-fold increase in the CDOCKER interaction energy of the 18-7N(p₃)-18 and 3-fold, 1.5 fold increase in CDOCKER energy and CDOCKER interaction energy for 18-7N(p₁)-18 compared to 18-7NH-18 gemini surfactant shows the advantage of RGD peptide and IgSF-peptide conjugation with 2nd generation parent gemini surfactant 18-7NH-18 to improve binding and cell adhesion with their respective proteins such as integrins.

Performing the docking studies of the p₃ peptide and peptide modified compounds on a Ig-CAM protein would have made the results more interesting to identify the behavior of a IgSF peptide in interacting with an IgCAM protein, which could have provided more realistic conclusion on the obtained data. Despite non-availability of a workable IgCAM protein, this study has shown that molecular docking studies can be used to identify binding interactions between peptide ligands and target proteins and can be used as a tool for high throughput screening of peptide functionalized delivery systems.

This study also helps in drawing the *in vitro*- *in vivo*- *in silico* correlation to confirm if the results obtained both *in vitro* and *in vivo* on the 18-7N(p₃)-18 gemini pNPXs are repetitive and dependent on the peptide modifications performed on the surfactant and that the results are mere reflection of their molecular interactions leading to their eventual adhesion with the cell surface proteins. This study also reiterates the importance of *in silico* molecular modelling software in identifying the binding affinities and interactions of the peptide ligand with the target proteins and it can be used as a screening tool to identify potential peptides and peptide modified molecules to improve the delivery of therapeutic molecules to the target cells expressing various surface proteins.

Future directions

The screening carried out is completely an *in silico* based screening that depends mostly on the already available data from the protein data base and the algorithms that were developed to simulate the binding of ligand molecules to the active binding sites of the protein to identify their affinity to the target protein. But an *in vitro* or *in vivo* demonstration of the binding affinities can be more of a real reflection of the actual results. Despite having the *in silico* results clearly showing the lead compound and interactions with the protein, one should not always completely rely on the *in silico* results to confirm their binding affinity and interaction with the protein instead an *in vitro* receptor blocking assay, a binding assay can help in confirming the results from an *in silico* study. Hence, an *in vitro* binding assay or the receptor blocking studies will need to be carried out to support the findings and inferences made with the *in vitro*, *in vivo* transfection studies and *in silico* molecular docking studies to make a strong and validated method for future peptide modifications to improve TE and their evaluation.

Also, another major important aspect that need to be focused on is developing the NPX and nanoparticle ligand systems, instead of docking a simple ligand molecule. There is an unmet need in building physiologic based models such as bilayer models, surface and transmembrane receptor models that can dynamically mimic all the physiologic conditions that these ligand systems get exposed to and challenge the molecules by performing the dockings which can provide with more realistic data and lead compounds that can behave similarly close to *in vivo* conditions.

Acknowledgements

The authors of this chapter would like to express their sincere thanks to Dr. Praveen Nekkar Rao Perampalli and Amy Pharm at School of Pharmacy, University of Waterloo for providing unmatched support, guidance and training to carry out molecular docking simulations at the Medicinal and Bioorganic Chemistry Lab, University of Waterloo.

Appendix 4 Investigation of amphiphilic gemini surfactants and peptide-modified gemini surfactants as potential Amyloid- β_{1-40} self-aggregation inhibitors

Table 8 Top hits for 18-7NH-18 ligand with A β_{40} peptide

Top Hit	(-) CDOCKER energy	(-) CDOCKER interaction energy kcal/mol
1	36.16	51.41
2	34.83	54.59
3	32.87	48.48
4	32.73	44.34
5	32.58	49.71
6	31.43	46.26
7	31.02	52.44
8	30.20	52.86
9	29.27	46.21
10	29.15	46.17

Table 9 Top hits of 18-7N(p₁)-18 and Non-bonding interactions of p₁ peptide with 2LMN

a. Top hits of 18-7N(p₁)-18 docked on to 2LMN peptide

Top Hit	(-) CDOCKER energy	(-) CDOCKER interaction energy kcal/mol
1	60.57	70.69

2	59.78	51.76
3	58.71	55.99
4	56.60	53.49
5	56.03	55.39
6	55.69	55.08
7	54.61	61.44
8	54.35	58.32
9	54.09	53.34
10	53.62	59.10

b. Non-bonding interactions of p₁ peptide docked with 2LMN peptide

Non-bond interactions	Bond length (Å)	Bond Type	Interaction	Donor group	Function	Acceptor group	Function
A:VAL18:HN - P1_peptide.sdf:O22	1.94	Hydrogen Bond	Conventional Hydrogen Bond	A:VAL18:HN	H-Donor	P1_peptide.sdf:O22	H-Acceptor
P1_peptide.sdf:H25 - B:LEU34:O	2.04	Hydrogen Bond	Conventional Hydrogen Bond	P1_peptide.sdf:H25	H-Donor	B:LEU34:O	H-Acceptor
P1_peptide.sdf:H34 - A:PHE20:O	2.80	Hydrogen Bond	Conventional Hydrogen Bond	P1_peptide.sdf:H34	H-Donor	A:PHE20:O	H-Acceptor
P1_peptide.sdf:H35 - A:VAL18:O	2.94	Hydrogen Bond	Conventional Hydrogen Bond	P1_peptide.sdf:H35	H-Donor	A:VAL18:O	H-Acceptor
P1_peptide.sdf:H35 - P1_peptide.sdf:O24	2.07	Hydrogen Bond	Conventional Hydrogen Bond	P1_peptide.sdf:H35	H-Donor	P1_peptide.sdf:O24	H-Acceptor

P1_peptide.sdf:H36 - A:PHE20:O	1.91	Hydrogen Bond	Conventional Hydrogen Bond	P1_peptide. sdf:H36	H-Donor	A:PHE20:O	H- Acceptor
P1_peptide.sdf:H45 - A:LYS16:O	2.42	Hydrogen Bond	Conventional Hydrogen Bond	P1_peptide. sdf:H45	H-Donor	A:LYS16:O	H- Acceptor

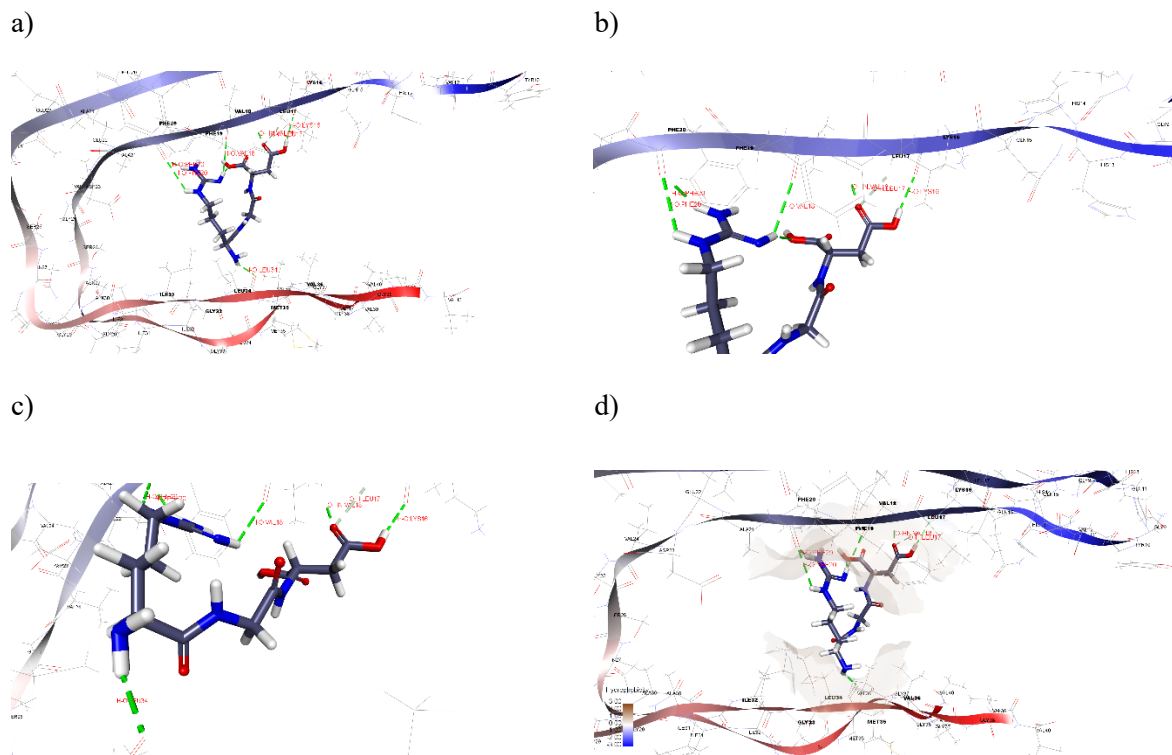


Figure 21 Non-bonding interactions between p₁ peptide and Aβ₄₀ peptide, (a) Interaction of p₁ peptide with the 2LMN peptide, (b, c) hydrogen bonding interactions p₁ peptide with VAL18, ASP23 and LEU34, (d) binding of peptide into the hydrophobic pocket of the Aβ₄₀ peptide

Table 10 Top hits of 18-7N(p₂)-18 and Non-bonding interactions of p₂ peptide with 2LMNa. Top hits of 18-7N(p₂)-18 with 2LMN

Top Hit	(-) CDOCKER energy	(-) CDOCKER interaction energy Kcal/mol
1	63.36	59.86
2	62.45	74.87
3	61.82	58.43
4	61.09	64.15
5	59.57	62.30
6	59.17	66.39
7	56.81	54.19
8	56.13	49.23
9	55.74	54.98
10	55.60	48.69

b. Non-bonding interactions of p₂ peptide with 2LMN

Non-bond interactions	Bond length (Å)	Bond Type	Interaction	Donor group	Function	Acceptor group	Function
P2_Peptide.sdf:H35 - A:VAL18:O	2.52	Hydrogen Bond	Conventional Hydrogen Bond	P2_Peptide. sdf:H35	H-Donor	A:VAL18:O	H- Acceptor
P2_Peptide.sdf:H36 - A:VAL18:O	2.34	Hydrogen Bond	Conventional Hydrogen Bond	P2_Peptide. sdf:H36	H-Donor	A:VAL18:O	H- Acceptor

P2_Peptide.sdf:H43 - A:ASP23:OD1	2.77	Hydrogen Bond	Conventional Hydrogen Bond	P2_Peptide. sdf:H43	H-Donor	A:ASP23:OD1	H- Acceptor
P2_Peptide.sdf:H44 - A:VAL18:O	2.60	Hydrogen Bond	Conventional Hydrogen Bond	P2_Peptide. sdf:H44	H-Donor	A:VAL18:O	H- Acceptor
P2_Peptide.sdf:H46 - B:LEU34:O	2.06	Hydrogen Bond	Conventional Hydrogen Bond	P2_Peptide. sdf:H46	H-Donor	B:LEU34:O	H- Acceptor

Table 11 Top hits of 18-7N(p₃)-18 and Non-bonding interactions of p₃ peptide with 2LMN

a. Top hits of 18-7N(p₃)-18 with 2LMN

Top Hit	(-) CDOCKER energy	(-) CDOCKER interaction energy Kcal/mol
1	86.38	72.09
2	85.94	64.96
3	80.53	60.85
4	79.10	59.58
5	77.91	58.47
6	77.73	53.70
7	77.43	66.86
8	76.46	59.58
9	76.41	58.12
10	76.22	58.86

b. Non-bonding interactions of p₃ peptide with 2LMN

Non-bond interactions	Bond length (Å)	Bond Type	Interaction	Donor group	Function	Acceptor group	Function
A:VAL18:HN - P3_peptide.sdf:O2	2.26	Hydrogen Bond	Conventional Hydrogen Bond	A:VAL18:HN	H-Donor	P3_peptide.sdf:O2	H-Acceptor
P3_peptide.sdf:H64 - A:VAL18:O	2.78	Hydrogen Bond	Conventional Hydrogen Bond	P3_peptide.sdf:H64	H-Donor	A:VAL18:O	H-Acceptor
P3_peptide.sdf:H74 - B:LEU34:O	2.31	Hydrogen Bond	Conventional Hydrogen Bond	P3_peptide.sdf:H74	H-Donor	B:LEU34:O	H-Acceptor
P3_peptide.sdf:H85 - A:PHE19	3.14	Hydrogen Bond	Pi-Donor Hydrogen Bond	P3_peptide.sdf:H85	H-Donor	A:PHE19	Pi-Orbitals
P3_peptide.sdf:C46 - B:LEU34	4.56	Hydrophobic	Alkyl	P3_peptide.sdf:C46	Alkyl	B:LEU34	Alkyl
P3_peptide.sdf - A:LEU17	4.90	Hydrophobic	Pi-Alkyl	P3_peptide.sdf	Pi-Orbitals	A:LEU17	Alkyl

Table 12 Top hits of 18-7N(p₄)-18 and Non-bonding interactions of p₄ peptide with 2LMN

a. Top hits of 18-7N(p₄)-18 docked with 2LMN peptide

Top Hit	(-) CDOCKER energy	(-) CDOCKER interaction energy Kcal/mol
1	42.47	58.3
2	40.88	63.51
3	38.05	50.48
4	37.08	59.41
5	36.23	53.77
6	35.48	48.93

7	34.86	52.54
8	34.33	50.59
9	33.99	45.78
10	33.98	51.60

b. Non-bonding interactions of p₄ peptide docked with 2LMN peptide

Non-bond interactions	Bond length (Å)	Bond Type	Interaction	Donor group	Function	Acceptor group	Function
B:LEU34:HN - P4_peptide.sdf:O10	2.11	Hydrogen Bond	Conventional Hydrogen Bond	B:LEU34:HN	H-Donor	P4_peptide.sdf: O10	H-Acceptor
P4_peptide.sdf:H19 - B:LEU34:O	1.93	Hydrogen Bond	Conventional Hydrogen Bond	P4_peptide.sd f:H19	H-Donor	B:LEU34:O	H-Acceptor
P4_peptide.sdf:H30 - B:LEU34:O	2.19	Hydrogen Bond	Conventional Hydrogen Bond	P4_peptide.sd f:H30	H-Donor	B:LEU34:O	H-Acceptor
P4_peptide.sdf:C16 - B:LEU34	4.39	Hydrophobic	Alkyl	P4_peptide.sd f:C16	Alkyl	B:LEU34	Alkyl